British Geological Survey

National seismic hazard maps for the UK: 2020 update

Multi Hazards and Resilience

Open Report OR/20/053

BRITISH GEOLOGICAL SURVEY

MULTI HAZARDS AND RESILIENCE PROGRAMME

OPEN REPORT OR/20/053

National seismic hazard maps for the UK: 2020 update

I Mosca, S Sargeant, B Baptie, RMW Musson and T Pharaoh

Keywords

Seismic hazard, UK, earthquake catalogue, ground motion.

Bibliographical reference

MOSCA, I, S SARGEANT, S, BAPTIE, B, MUSSON, RMW AND PHARAOH, T 2020. National seismic hazard maps for the UK: 2020 update. *British Geological Survey Open Report*, OR/20/053. 138pp.

Keyworth, Nottingham British Geological Survey 2020

BRITISH GEOLOGICAL SURVEY

The full range of our publications is available from BGS shops at Nottingham, Edinburgh, London and Cardiff (Welsh publications only) see contact details below or shop online at www.geologyshop.com

The London Information Office also maintains a reference collection of BGS publications, including maps, for consultation.

We publish an annual catalogue of our maps and other publications; this catalogue is available online or from any of the BGS shops.

The British Geological Survey carries out the geological survey of Great Britain and Northern Ireland (the latter as an agency service for the government of Northern Ireland), and of the surrounding continental shelf, as well as basic research projects. It also undertakes programmes of technical aid in geology in developing countries.

The British Geological Survey is a component body of UK Research and Innovation.

British Geological Survey offices

Nicker Hill, Keyworth,
Nottingham NG12 5GG

Tel 0115 936 3100

BGS Central Enquiries Desk

Tel 0115 936 3143
email enquiries@bgs.ac.uk

BGS Sales

Tel 0115 936 3241
email sales@bgs.ac.uk

The Lyell Centre, Research Avenue South,
Edinburgh EH14 4AP

Tel 0131 667 1000
email scotsales@bgs.ac.uk

Natural History Museum, Cromwell Road,
London SW7 5BD

Tel 020 7589 4090
Tel 020 7942 5344/45
email bgslondon@bgs.ac.uk

Cardiff University, Main Building, Park Place,
Cardiff CF10 3AT

Tel 029 2167 4280

Maclean Building, Crowmarsh Gifford,
Wallingford OX10 8BB

Tel 01491 838800

Geological Survey of Northern Ireland, Department of Enterprise, Trade & Investment, Dundonald House, Upper Newtownards Road, Ballymiscaw,
Belfast, BT4 3SB

Tel 01232 666595
www.bgs.ac.uk/gsni/

Natural Environment Research Council, Polaris House, North Star Avenue, Swindon SN2 1EU

Tel 01793 411500 Fax 01793 411501
www.nerc.ac.uk

UK Research and Innovation, Polaris House,
Swindon SN2 1FL

Tel 01793 444000
www.ukri.org

Website www.bgs.ac.uk
Shop online at www.geologyshop.com

Foreword

This report is the published product of a study by the British Geological Survey (BGS) to update the national seismic hazard maps for the UK. This is to take account of advances in seismic hazard methodology since the last seismic hazard maps were developed by Musson and Sargeant (2007) and present the results in a format that will be compatible with the future Eurocode 8 revisions.

Acknowledgements

This work has benefitted from the knowledge and experience of a large number of people. We are very grateful to the experts who have been supporting this work: Guillermo Aldama-Bustos, John Douglas, Ben Edwards, Peter Stafford, Fleur Strasser and Iain Tromans. We are also very grateful for the support and input of the members of the BSI National Committee B/525/8 Structures in Seismic Regions and Edmund Booth, Ziggy Lubkowski and Tim Allmark in particular, and members of the ONR Review Panel for their helpful reviews of an earlier draft of the report.

From BGS, we thank Davie Galloway for his assistance in developing and checking the earthquake catalogue, and Margarita Segou for useful discussions on the catalogue analysis. Maarten Krabbendam and Graham Leslie have provided guidance on matters relating to the seismotectonics of the UK, and we are grateful to Richard Luckett, Margarita Segou, Ciaran Beggan, Ekbal Hussain and David Kerridge for internally reviewing the report.

This work is supported by the British Geological Survey and the Institution of Civil Engineers.

Contents

FIGURES

TABLES

List of abbreviations

AB06	Atkinson and Boore (2006)
ASK14	Abrahamson et al. (2014)
AKK14	Akkar et al. (2014)
ASCR	Active shallow crustal regions
BSSA14	Boore et al. (2014)
BGS	British Geological Survey
BIIS	British Irish Ice Sheet
BIN14	Bindi et al. (2014)
CAU15	Cauzzi et al. (2015)
CB14	Campbell and Bozorgnia (2014)
CG	Central Graben
CSB	Caledonides of Southern Britain
CSFZ	Church Stretton Fault Zone
CT	Charnwood Terrane
CY14	Chiou and Youngs (2014)
EC8	Eurocode 8
EDR	Euclidian distance-based ranking
EPRI	Electric Power Research Institute
ESHM13	2013 European seismic hazard model
FAS	Fourier amplitude spectrum
FCAT-17	2017 earthquake catalogue for France (Manchuel et al., 2018)
FMD	Frequency-magnitude distribution
GGF	Great Glen Fault
GSHAP	Global Seismic Hazard Map
GIA	Glacio-Isostatic Adjustment
GM	Geometric mean
GMC	Ground motion characterisation
GMPE	Ground motion prediction equation
GT	Grampian Terrane
HBF	Highland Boundary Fault
HEM	hybrid-empirical method
HPC	Hinkley Point C
HT	Hebridean Terrane
IRVT	Inverse random-vibration theory
ISC	International Seismological Centre
KiK-Net	Kiban-Kyoshin Network
KOT16	Kotha et al. (2016)

LGM	Last Glacial Maximum
LLH	The log-likelihood
LLT	Leinster-Lakesman Terrane
LSZ	Lleyn Shear Zone
mb	Body wave magnitude
MDE	Modified Euclidian distance
ML	Malvern Lineament
ML	Local magnitude
Mmax	Maximum magnitude
MS07	Musson and Sargeant (2007)
MSFZ	Menai Strait Fault System
MT	Monian Terrane
MTZ	Moine Thrust Zone
MVT	Midland Valley Terrane
Mw	Moment magnitude
NGA	Next Generation Attenuation
NGA-West 2	Next Generation of Ground-Motion Attenuation Models for the western US
NHT	Northern Highlands Terrane
OIT	Outer Isles Thrust
ONR	Office for Nuclear Regulation
PGA	Peak ground acceleration
PML	Penalised maximum likelihood
PSHA	Probabilistic seismic hazard analysis
QWL	Quarter Wavelength
RIET13	Rietbrock et al. (2013)
Rjb	Joyner-Boore distance
RotD050	non-redundant rotation angles
RS	Response spectra
RVT	Random-vibration theory
SA	Spectral acceleration
SCR	Stable continental regions
SHARE	Seismic hazard harmonisation in Europe
SSC	Seismic source characterisation
SSHAC	Senior Seismic Hazard Analysis Committee
SUF	Southern Uplands Fault
SUT	Southern Uplands Terrane
UHS	Uniform Hazard Spectra
UK	United Kingdom
VF	Variscan Front

VG	Viking Graben
VRZ	Variscide Rhenohercynian Zone
WT	Wrekin Terrane
WUS	Western United States

Summary

This report presents the development of the new national seismic hazard maps for the UK using a Monte Carlo-based approach. The new maps have been developed to update the advice currently given in the BSI Published Document PD6698 - Recommendations for the design of structures for earthquake resistance to BS EN 1998. The work done by the BGS team in this study has been informed at key stages by external experts who have provided advice or acted as informal reviewers (see Acknowledgements for details).

The analysis is based on a composite earthquake catalogue consisting of data from the BGS catalogue, the International Seismological Centre (ISC) online database and the earthquake catalogue of Manchuel et al. (2018) for France. A thorough assessment of the completeness of the catalogue has been undertaken. The source zone model is based on the model used by Woessner et al. (2015) for the Seismic Hazard Harmonisation in Europe (SHARE) project with some modifications. Earthquake recurrence statistics have been calculated for this model and catalogue, and the validity of the source model has been tested against the observed seismicity. The ground motion characterisation model uses the multi-GMPE model of Tromans et al. (2019) and Vs-κ_0 adjustments have been determined for these GMPEs.

The new seismic hazard maps cover the region between 49°N - 61°N and 8.5°W - 2°E and the calculations have been made at individual points spaced at 0.125° in latitude and 0.25° in longitude. The maps show peak ground acceleration (PGA) and spectral acceleration (SA) at 0.2 s and 1.0 s for 5% damping on rock (Vs30 = 800 m/s) as a proportion of g and for return periods of 95, 475, 1100 and 2475 years (these are the return periods that were requested by Panel 7 of the B/525/8 committee on Structures in Seismic Regions). Although no longer cited in the revised Eurocode 8 (EC8; CEN, 2004), including PGA in this study allows for comparison with Musson and Sargeant (2007). Uniform hazard spectra have also been calculated for four sites across the UK (Cardiff, Edinburgh, London and Dover) and a disaggregation of the hazard for these sites has also been undertaken.

The key modifications with respect to the last national seismic hazard maps developed by Musson and Sargeant (2007) are:

1. The earthquake catalogue has been extended (it now ends on 31 August 2018) and the earthquake catalogue for France of Manchuel et al. (2018) has been used to augment the UK data for the southernmost part of the model. Data from the ISC catalogue have been also included for offshore areas such as the North Sea.
2. All magnitudes have been converted to Mw (moment magnitude) where required using the relation of Grünthal et al. (2009). This is an update of Grünthal and Wahlström (2003), which was used by Musson and Sargeant (2007).
3. The completeness of the earthquake catalogue has been assessed using a different approach.
4. The seismic source characterisation model has been modified, including the zone geometry and assessment of the maximum magnitude.
5. The earthquake recurrence parameters for the source model have been calculated using the updated catalogue and revised assessment of completeness.
6. A new ground motion characterisation model that accounts for advances in ground motion modelling since 2007 has been used.
7. The model now includes the Shetland Islands.

For a return period of 475 years, the PGA hazard is lower than 0.04 g for much of the UK, with some exceptions: in most of Wales and North Central England, the hazard exceeds 0.04 g, reaching 0.05 g in the England-Wales border region and 0.09 g in North Wales. A similar spatial pattern in the hazard is observed at 0.2 s with the highest hazard in North Wales (0.16 g) and the variations are more pronounced. At 1.0 s, the hazard is less than 0.02 g and there is little variation across the UK.

For a return period of 1100 years, we observe a similar spatial variation with the highest hazard again in Wales (up to 0.09 g in the England-Wales border and 0.16 g around North Wales), North Central England, and western Scotland (up to 0.06 g). However, the south-eastern tip of England now shows slightly higher hazard relative to the surrounding area (up to 0.04 g). Again, this spatial variation is similar but more pronounced for 0.2 s SA where the hazard reaches a maximum of 0.29 g in North Wales. There is much less variation at 1.0 s but the England-Wales border and North Wales region are where the hazard is highest (up to 0.04 g).

For 2475 years, the Channel Islands, North Wales, the England-Wales border through to North Central England and the Lake District, and NW Scotland are the areas of highest hazard for PGA and 0.2 s SA. The highest hazard values (up to 0.25 g for PGA and 0.47 g for 0.2 s SA) are observed in North Wales.

Although this study and MS07 use different earthquake catalogues, assessments of completeness, seismic source models, and ground motion characterisation models, the two models are not markedly different and the resulting maps for PGA are similar in terms of spatial distribution of the hazard. However, there are small differences in the results. This study shows slightly higher PGA values in North Wales, North Central England, and NW Scotland, and lower PGA values around Comrie, South Wales, and Midlands than found by MS07.

It is important to note that these seismic hazard maps are not a substitute for site-specific hazard assessment and high-consequence-of-failure installations (designated CC4-Highest in the new edition of EN1990, 2002) in particular. The user must take responsibility for checking that use of the results contained in this report is appropriate for the case in question.

All of the input data and elements of the model described in this report will be freely available from www.earthquakes.bgs.ac.uk as will the output files. The computer code can be made available on request to ukeqs@bgs.ac.uk.

1 Introduction

The most recent seismic hazard maps developed specifically for the UK were produced by Musson and Sargeant (2007; hereafter referred to as MS07). These maps show peak ground acceleration (PGA) on bedrock for return periods of 475 and 2500 years. They indicate that the PGA hazard is low in global terms, as one would expect in a low seismicity region like the UK. For a 475 year return period, the map shows that values are less than 0.02 g for most of the UK and Northern Ireland and slightly higher in North and South Wales (up to 0.08 g and 0.06 g, respectively). For 2500 years, PGA hazard is still low over much of the country (less than 0.08 g) with higher values seen around Comrie in central Scotland (up to 0.12 g), South Wales (up to 0.12 g), and in North Wales (up to 0.18 g).

Two factors have prompted the revision of the hazard maps for the UK. Firstly, it is commonly understood that probabilistic seismic hazard assessments require updates from time to time as new data, better-constrained models and advances in the methodology become available (Frankel, 1995; Grünthal et al., 2018). Since 2007, there have been significant advances particularly with respect to how ground motion and its uncertainties are modelled. Secondly, updated maps are required to update the advice currently given in the BSI Published Document PD6698 - Recommendations for the design of structures for earthquake resistance to BS EN 1998 (E. Booth, *pers. comm*.).

Furthermore, since the 2007 maps were published, there have been a number of projects that have assessed seismic hazard in the UK and it is reasonable to revisit the 2007 national seismic hazard model in light of these. Earthquake hazard has been assessed for the UK region as part of the SHARE (Seismic Hazard Harmonisation in Europe) project (Woessner et al., 2015). There have also been a number of site-specific probabilistic seismic hazard assessments carried out for the development of new nuclear power plants (e.g. Tromans et al., 2019; Villani et al., 2020a) undertaken in connection with the British Government's Nuclear Industrial Strategy (BIS, 2013). The aim of the work presented in this report is therefore to make use of the advances that have been made by these recent projects (and others elsewhere) to develop a new set of seismic hazard maps for the UK.

1.1 PROJECT IMPLEMENTATION

The approach taken in this study has been developed through informal consultation with potential users of the map and various experts in seismic hazard assessment from outside the project team. Engineers from the B/525/8 committee on Structures in Seismic Regions (the committee responsible for the UK input to EC8) have provided guidance on the design requirements for the seismic hazard maps so that they can be used to update the advice currently given in the BSI Published Document PD6698 - Recommendations for the design of structures for earthquake resistance to BS EN 1998.

We sought to bring in the views of experts from outside the project team as the ground motion characterisation (GMC) model was developed and to do this, a meeting of the members of the project team and four external experts was held on 27 September 2018. The external experts were Dr Guillermo Aldama-Bustos, Dr John Douglas, Dr Ben Edwards and Dr Fleur Strasser. The objectives of the meeting were to discuss what the experts considered to be the key ground motion issues that needed to be accounted for in the development of the maps and to come to a shared view through an open discussion about how the GMC model should be developed (this is discussed further in Section 6). The discussion at the meeting was written up in a short report. These experts provided

further advice and technical support as the GMC model and Vs- κ_0 adjustments were implemented.

Two other external experts (Dr Peter Stafford and Dr Iain Tromans) have also provided informal feedback on brief progress reports that were prepared at key stages in the project (the development of the source zone model and the GMC model). We did not respond to these comments formally but their feedback helped us to develop our approach. Further comprehensive reviews of the first draft of this report were received by these experts and a number of others from industry and academia (10 in total). Each of the reviewers' comments has been responded to directly and all the necessary revisions made. This document contains the final version of the report.

All of the input data and elements of the model described in this report will be freely available from www.earthquakes.bgs.ac.uk as will the output files. The computer code can be made available on request to ukeqs@bgs.ac.uk.

1.2 KEY MODIFICATIONS WITH RESPECT TO MS07

These are the key differences compared with the model used for the previous maps developed by MS07:

1. The earthquake catalogue has been extended (it now ends on 31 August 2018) and the earthquake catalogue for France of Manchuel et al. (2018) has been used to augment the UK data for the southernmost part of the model. Data from the ISC catalogue have been also included for offshore areas such as the North Sea.
2. All magnitudes have been converted to Mw (moment magnitude) where required using the relation of Grünthal et al. (2009). This is an update of Grünthal and Wahlström (2003), which was used by Musson and Sargeant (2007).
3. The completeness of the earthquake catalogue has been assessed using a different approach.
4. The seismic source characterisation model has been modified, including the zone geometry and assessment of the maximum magnitude.
5. The earthquake recurrence parameters for the seismic source model have been calculated using the updated catalogue and revised assessment of completeness.
6. A new GMC model that accounts for advances in ground motion modelling since 2007 has been used.
7. The model now includes the Shetland Islands.

The basic hazard parameters in the revised EC8 are S_α and S_β and PGA is no longer cited. S_α is the 5% damped spectral period at the peak of the spectrum on rock and S_β is the 'long period' spectral acceleration on rock, with 1.0 s being the required value of the associated period (E. Booth, *pers. comm*.). The main output from this work is a set of national seismic hazard maps (for return periods of 95, 475, 1100 and 2475 years) based on the new model that depict spectral acceleration (SA) at 0.2 s and 1.0 s for 5% damping, and for a single rock site condition (Vs30 = 800 m/s) across the study area. The PGA hazard has also been assessed in order to compare the results with MS07.

2 Methodology

We use a probabilistic approach to assess the hazard (for background see MS07; Cornell, 1968; Reiter, 1990; McGuire, 2004). This combines seismological, geological and geophysical data to produce a probabilistic description of expected ground shaking that may occur at a site and consists of four steps that are illustrated in the schematics in Figure 1:

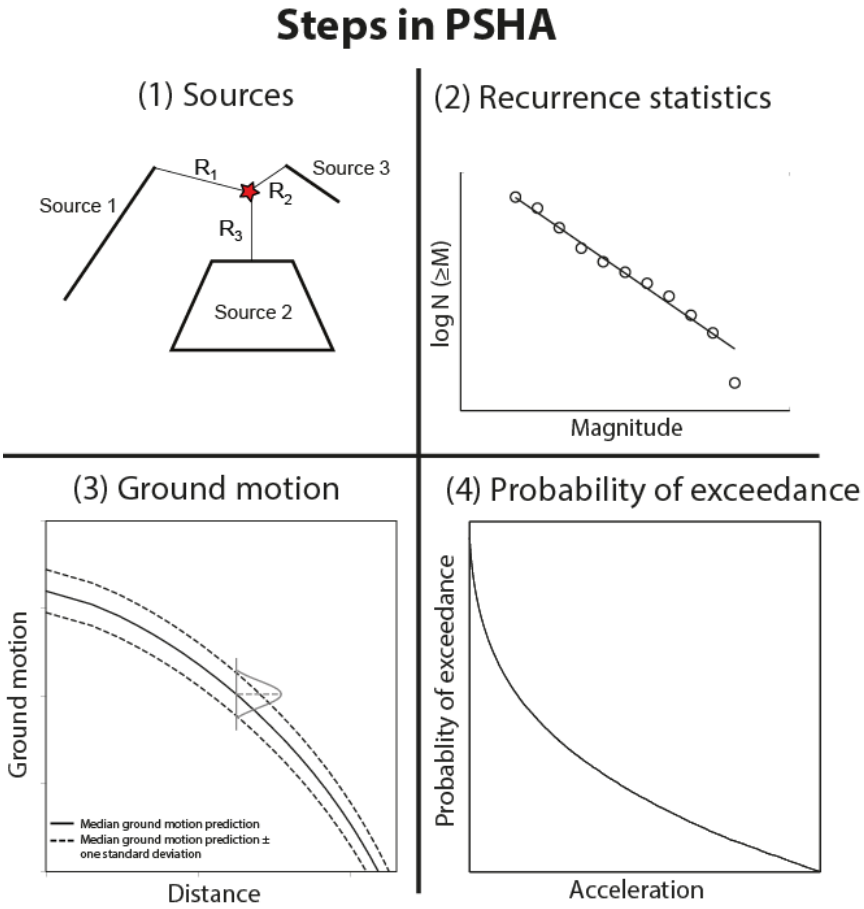

Figure 1: Schematic description of the main steps of PSHA, following Reiter (1990). In Box 1, R is the source-to-site distance and the red star indicates the site. The grey probability distribution in Box 3 describes the median prediction and the aleatory variability of the ground motion. The return period is the inverse of the annual probability of exceedance.

Step 1: Define seismic sources based on knowledge of the tectonics, geology and seismicity of the study area. In theory, such a model may contain both areal sources, areas in which the seismicity is assumed to have a distribution of homogeneous sources, and faults sources, specific faults or fault zones that are known to be active. There is an assumption that each seismic source behaves in a consistent way with regard to producing earthquakes and therefore seismicity has an equal probability of occurring anywhere within the source from a geographic perspective. A collection of seismic sources makes up the seismic source model.

Step 2: Quantify the rate of earthquake occurrence for each seismic source zone using the Gutenberg-Richter frequency-magnitude law (Gutenberg and Richter, 1954) that is commonly expressed as

$$\log_{10} N = a - b\,M \tag{1}$$

where *N* is the number of earthquakes above a given magnitude *M*. The constant *a*, is a function of the total number of earthquakes in the sample and is known as the activity rate. This is commonly normalised over a period of time, such as a year. The constant *b* gives the relative number of events of different magnitudes and is commonly referred to as the *b*-value. In general, *b*-values are close to unity. This means that for each unit increase in magnitude, the number of earthquakes reduces tenfold.

Step 3: Characterise the 'earthquake effect' (Reiter, 1990, p184). This is generally expressed in terms of some instrumental ground motion measure or seismic intensity.

Step 4: Estimate the hazard at the site(s) by analytically integrating the models for the location and size of potential future earthquakes (Steps 1 and 2) with predictions of the potential shaking intensity caused by these future earthquakes (Step 3), including the associated uncertainty in each. This is expressed as the probability that a particular ground motion level will be exceeded within a certain period of time. This approach to PSHA is often referred as to Cornell-McGuire PSHA.

The output from Steps 1 and 2 is the seismic source characterisation (SSC) model. The SSC model describes the spatial and temporal distribution of earthquakes of different magnitudes in a specific region. The GMC model is developed in Step 3 and describes the value(s) of the ground motion parameter of interest at the site from all possible earthquake scenarios. For maps, the seismic hazard is computed for a grid of 'sites' and the results are contoured.

One of the challenges for any probabilistic seismic hazard assessment is how to manage the incomplete knowledge of the underlying geological and seismological processes that contribute to the hazard. Modern PSHA studies incorporate the epistemic uncertainties, i.e. uncertainties due to our lack of knowledge regarding the earthquake process, using the logic tree formalism (Kulkarni et al., 1984; McGuire, 2004). Following the SSHAC (Senior Seismic Hazard Analysis Committee) guidelines, the SSC and GMC models are usually expressed as logic trees that capture the centre, body and range of the technically defensible interpretations of the models (Budnitz et al., 1997; USNRC, 2012). The centre of the distribution is the best estimate of the resulting interpretations, the body describes the shape of the distribution around the best estimate, and the range captures the tails of the distribution (USNRC, 2012). The likelihood of fully capturing the uncertainty in SSC and GMC models is achieved by including alternative models and parameters in the logic tree where weights are assigned to each branch using expert judgement that reflects the relative confidence in the models and parameters (Coppersmith and Bommer, 2012).

As in MS07, in this study, the hazard is computed using Monte Carlo simulation to generate artificial catalogues based on the SSC model (e.g., Musson, 1999, 2000a; Hong and Goda, 2006; Assatourians and Atkinson, 2013). This method uses random numbers to sample from the different probability distributions in the SSC model. Since the SSC model is assumed to completely describe the way in which earthquakes occur in a region, each of the artificial earthquake catalogues represents a version of what could occur in the next 50 or 100 years, based on what has previously been observed. From the direct observation of the effects of a very large number of simulations, probabilities can be easily calculated. This method allows epistemic uncertainties in the input parameters to be dealt with in a very transparent way - parameters can be entered as probability distribution functions with observed means and standard deviations. A different value can be sampled from the distribution for each simulation. The approach consists of the following steps (Musson, 1999, 2000a):

1. Generate a synthetic earthquake catalogue of N years in length.
2. For each event in this catalogue, simulate the ground motion at the site using the GMC model.
3. Note the highest ground motion value obtained in each year.
4. Repeat steps (1)-(3) R times, such that R× N is at least 10^3 times greater than the return period of interest. Thus, if one were concerned about hazard with the annual probability of 10^{-4}, one could use 100,000 catalogues of 100 years or 200,000 of 50 years that gives a total of 10,000,000 years of simulated data. This would be sufficient to resolve the hazard accurately for a 10,000 year return period.
5. In this example, one now has 10,000,000 values for the annual maximum ground motion for the site. To find the ground motion that has an annual frequency of being exceeded of 1 in 10,000, simply sort the values in order of decreasing severity and pick the 1001st value. This has been exceeded 1,000 times out of 10,000,000 and therefore has a 1 in 10,000 probability.

This process is summarised in Figure 2.

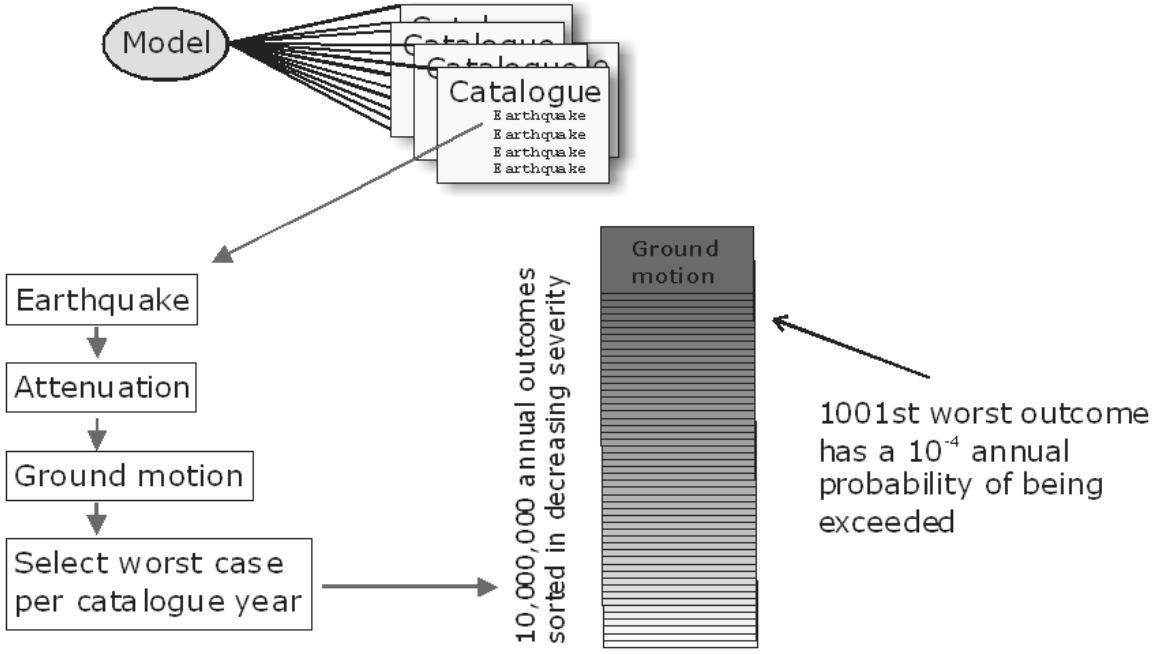

Figure 2: The elements of the Monte Carlo simulation approach to probabilistic seismic hazard assessment (from Musson, 2000).

Monte Carlo-based PSHA and Cornell-McGuire type approach to PSHA are completely compatible with each other and produce the same output given the same initial model, although their processes are different (Musson, 2012a; Mosca, 2019). However, Monte Carlo-based PSHA has several advantages. First, it is very flexible and can be adapted easily. Second, the process is transparent and therefore it is very easy to halt the simulation process at any point and examine the simulated data. For example, the synthetic catalogues can be inspected to see if the model is reproducing key features of the data. It is also easy to determine which simulated earthquakes are causing high ground motions. All that said, while the Monte Carlo approach is an efficient way to

assess the hazard in low seismicity areas like the UK, it can be computationally intensive for high seismicity regions.

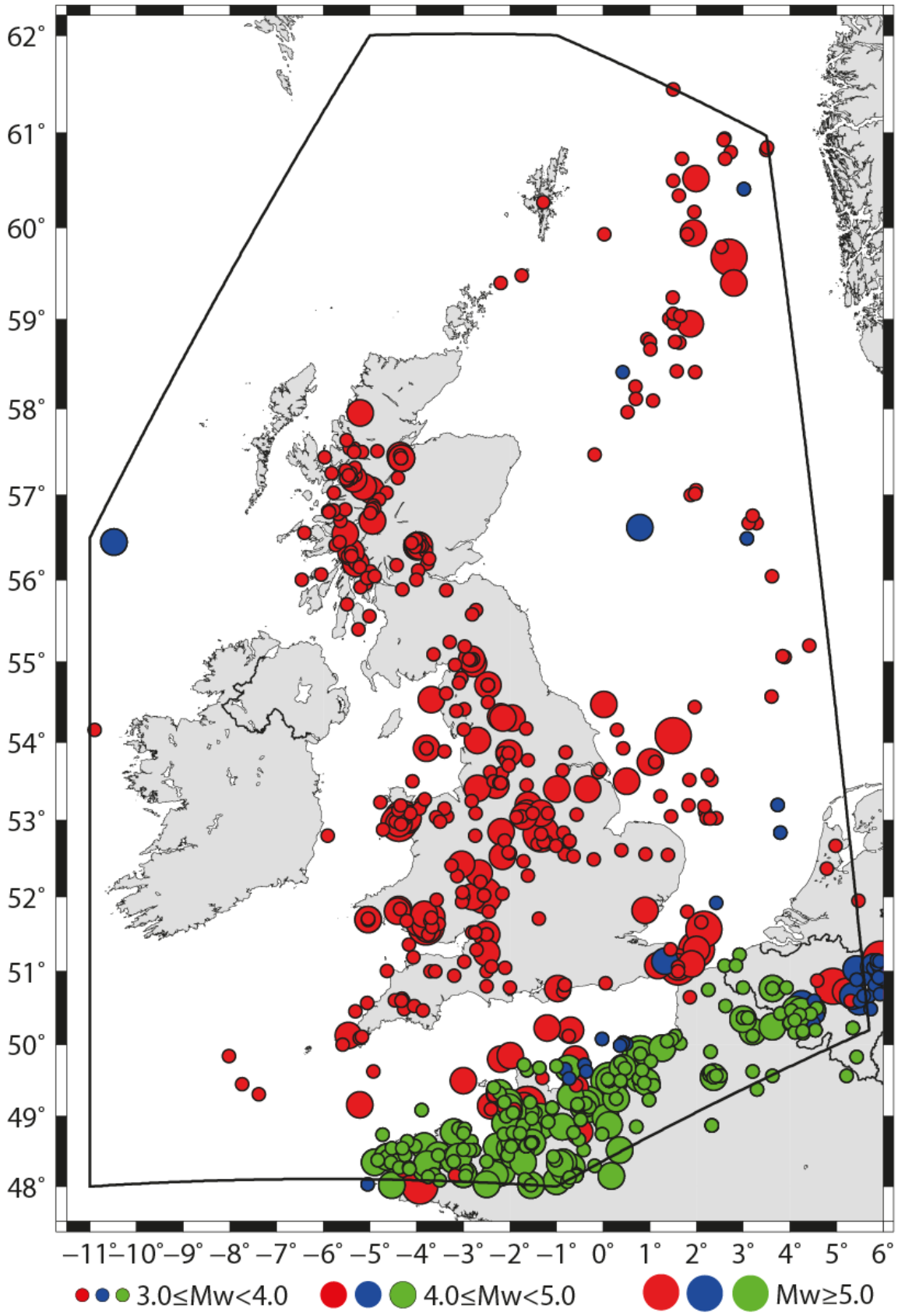

Figure 3: The distribution of earthquakes in the composite catalogue used in this study (Mw ≥ 3.0). Red, blue, and green circles are events from the BGS catalogue, the ISC

database, and the catalogue of Manchuel et al. (2018), respectively. The black polygon delineates the boundaries of the study area.

3 Earthquake catalogue

3.1 DATA SOURCES

The earthquake catalogue used in this study covers the polygon in Figure 3. It comes from three sources that have been merged: the British Geological Survey (BGS) catalogue, the ISC online database and the French earthquake catalogue of Manchuel et al. (2018), referred to as FCAT-17.

The BGS catalogue contains historical (pre-1970) and instrumental data. The primary source of data for earthquakes before 1970 is the catalogue of Musson (1994, along with subsequent updates), which is based on historical reports of earthquake effects. The original scope of Musson (1994) was to include all events with local magnitude (ML) ≥ 4.0 between 1700 and 1969 and, as far as possible, all events onshore that were larger than 3.0 ML. For earlier periods only events that appeared to be larger than 4 ML were included. Subsequent updates have been expanding this range on a regional basis, both in terms of adding smaller events and estimating parameters where possible for pre-1700 earthquakes. The catalogue is therefore markedly more comprehensive for some areas (e.g. SW England and South Wales) than for others (e.g. the English Midlands). The first earthquake in the BGS catalogue for the UK is an event on 25 July 1122 in SW England. This is the earliest event for which the magnitude (4.0 Mw) and location have been estimated albeit with considerable uncertainty. Earlier events are known (e.g. in 974) but are impossible to parameterise, since nothing is known about them apart from the year they occurred.

For 1970 to the present, the primary source of data for this study is the annual bulletins of earthquake activity published by BGS (e.g. Burton and Neilson, 1980; Turbitt, 1985; Galloway et al., 2013). These contain event origin times, locations and local magnitudes determined from instrumental recordings made on the UK seismic monitoring network (e.g. Baptie, 2012). Instrumental monitoring of earthquakes in the UK started in 1969 when a local seismic network consisting of seven stations (LOWNET) was deployed in Central Scotland (Crampin et al., 1970). The seismic network gradually expanded through the 1980s and 1990s reaching a peak in the late 1990s, with over 140 stations. Since then, the number of stations has been reduced and the network currently consists of 100, mostly broadband, seismograph stations located across the UK, roughly half of which are permanent. The way the network configuration has changed over time and the impact of this on detection thresholds across the UK is shown in Figure 4.

As well as tectonic earthquakes, seismicity induced by coal mining in central-northern England, South Wales, and Scotland has also been recorded (e.g. Westbrook et al., 1980; Redmayne, 1988; Bishop et al., 1994; Verdon et al., 2018) often by dense local networks of sensors installed to study these events in detail. Wilson et al. (2015) suggest that perhaps as much as 20% of all earthquakes in the instrumental catalogue may be related to coal-mining. The number of coal mining events fell throughout the 1990s as the industry declined and there are now very few such events. The magnitudes of coal mining events in the UK have tended to be small with a maximum observed magnitude of 3.1 ML (Redmayne, 1988). These mining-induced events have been identified based on their temporal and spatial proximity to known mining operations (Baptie et al., 2016) and removed from the catalogue used in this study. It is possible that there are larger pre-instrumental mining-related events in the catalogue that have not been identified but it is impossible to discriminate between these and tectonic events.

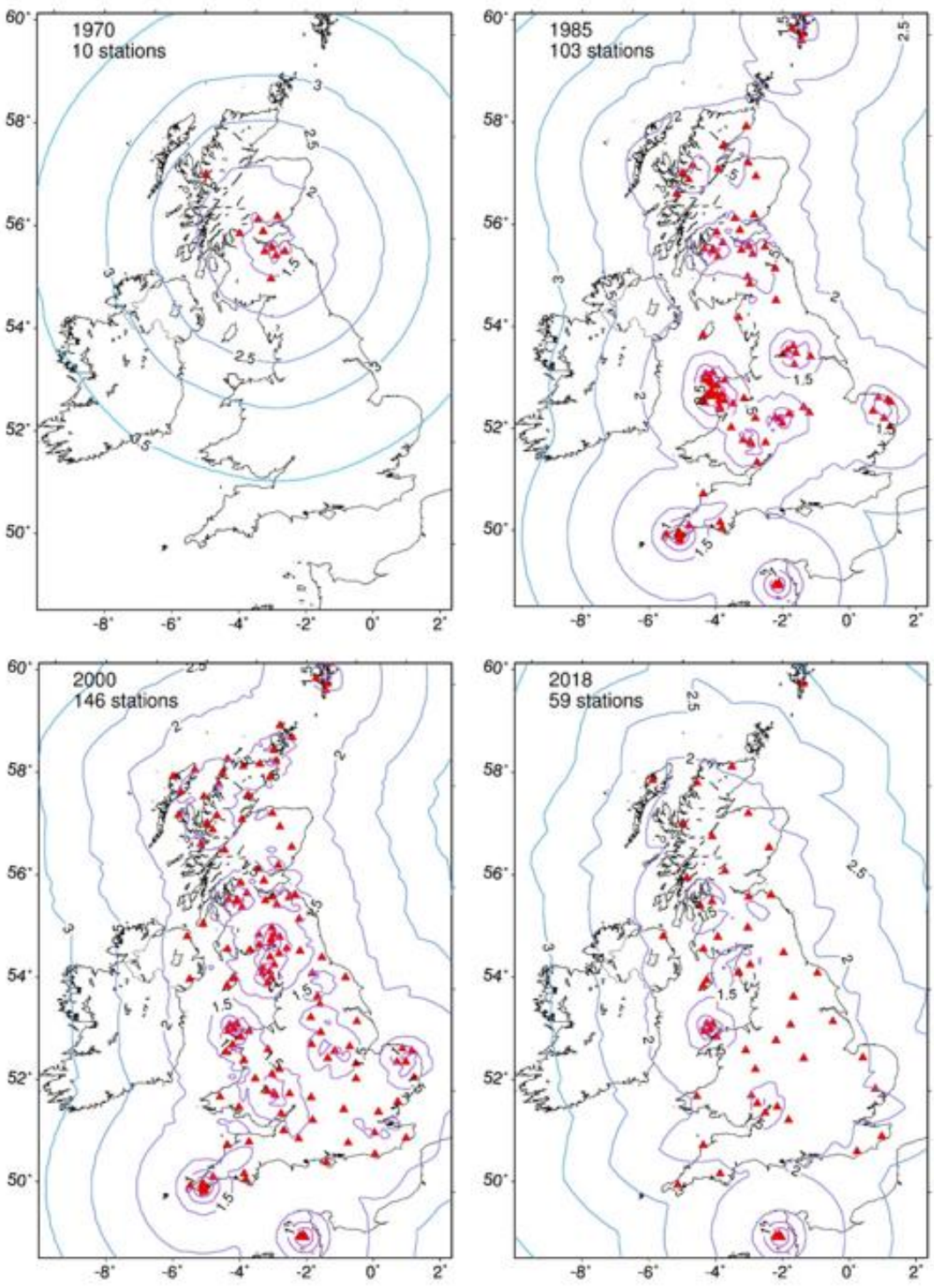

Figure 4: Development of the monitoring network since the 1970s. Red triangles show operational stations. The contours show the magnitude of earthquake that can be detected at different points across the region. A signal in excess of three times the background noise needs to be recorded at three or more stations in order for an earthquake to be detected. A background noise level of 4 nm is assumed at all stations.

The UK data have been supplemented by information from the ISC online database and FCAT-17. The ISC online database contains data from 1904 to the present and is based

on bulletin data collected from 515 seismological agencies around the world (http://www.isc.ac.uk/). Each earthquake is characterised by an origin time, epicentre coordinates, focal depth and any magnitude estimated by the agencies that detected the event (i.e. surface wave magnitude Ms, body wave magnitude mb, and Mw). Data from the ISC catalogue for the area 48-62° N and 11°W-6°E have been used in this study. FCAT-17 is a parametric earthquake catalogue that merges the historical and instrumental catalogues for metropolitan France (Manchuel et al., 2018). Here, we have included data for the area 6°W-6°E and 48.0-51.5°N.

To merge the catalogues, we used the following hierarchy where there were duplicate events (events with similar locations and original times, which were identified manually). The BGS determinations were given priority across the study area because these were considered to be the most well-constrained for the region, then the ISC estimates and then the entries in FCAT-17. The composite catalogue starts in 842 AD (an event in FCAT-17) and ends on 31 August 2018. It contains 683 earthquakes of 3.0 Mw and above for which the date (day, month and year) is known. Most of the data are from the BGS catalogue (403 events). The ISC data (42 events) improve the completeness of the catalogue for the North Sea and the English Channel, and FCAT-17 improves the completeness in northern France and Belgium (238 events of Mw ≥ 3).

While Mw is the preferred magnitude scale for seismic hazard assessment, earthquake size in the BGS catalogue is traditionally expressed in terms of ML. We have therefore converted ML to Mw for these events using the relation of Grünthal et al. (2009). This is a revised version of Grünthal and Wahlström (2003), which was the conversion relation used by MS07. The dataset used by Grünthal and Wahlström (2003) is from an area that covers much of mid and southern Germany, Austria, Switzerland and the Czech Republic, with Grünthal et al. (2009) adding further events from several Balkan countries, Finland, France and Italy. Neither includes any original Mw determinations for UK earthquakes. However, the Mw values calculated using Grünthal et al. (2009) do compare relatively well with measured Mw for the UK (see Figure 5) although unfortunately, there are very few data for earthquakes larger than 4.0 ML to extend the comparison to larger magnitudes. Edwards et al. (2008) and Sargeant and Ottemöller (2009) have proposed linear relations specifically for the UK but these have also been limited by the fact that most of the available data are from small events and are therefore not constrained at moderate to high magnitudes. Consequently, Grünthal et al. (2009) is preferred here. It has also been used recently in site-specific PSHA for nuclear power plants in the UK (Tromans et al., 2019; Villani et al., 2020a). All the references to moment magnitudes (Mw) for UK events in the rest of this report are converted from local magnitude (ML) determinations using the equation of Grünthal et al. (2009), unless stated otherwise.

The magnitudes associated with earthquakes in the ISC database are measured using various scales, including body wave magnitude (mb). To homogenise the earthquake catalogue in terms of Mw, the various magnitude scales were converted to Mw using the equations of Grünthal et al. (2009). The earthquake magnitudes in FCAT-17 are given in terms of Mw (Manchuel et al., 2018) and we have not gone back to the original sources on which FCAT-17 is based so these values are imported directly. Manchuel et al. (2018) compare the Mw estimates in FCAT-17 with those in the SHARE European Earthquake Catalogue (AD1000-2006). They find no particular bias in the catalogue estimates but note that there is a large scatter in the data for low-to-moderate (< 4.5 Mw) earthquakes (see Figure 11 in Manchuel et al., 2018).

We have not accounted for either uncertainty in either the original magnitudes in each catalogue or the variability in the magnitude conversion in the analysis that follows. There are multiple sources of uncertainty in the final determinations of Mw. The first is the uncertainty in the original magnitude and the second is related to the conversion from the original magnitude to Mw. The uncertainty in ML is not assessed for either historical or instrumentally recorded events in the BGS earthquake catalogue. For historical events,

estimating uncertainty is not straightforward because the ML determinations for historical earthquakes are based on macroseismic intensity data, which is an additional source of uncertainty in the final Mw estimates for these events. Furthermore, uncertainties associated with original magnitudes in the ISC database are not given. Musson (2012b) demonstrates that care should be taken when the magnitude uncertainties are accounted for in the recurrence statistics, especially when an earthquake catalogue merges many sources and contains more than one original magnitude scale in order to avoid over- or underestimating the activity rate and the *b*-value in the area under consideration. However, it is clear that a robust and homogeneous assessment of the magnitude uncertainty for earthquake catalogues would be preferable in future.

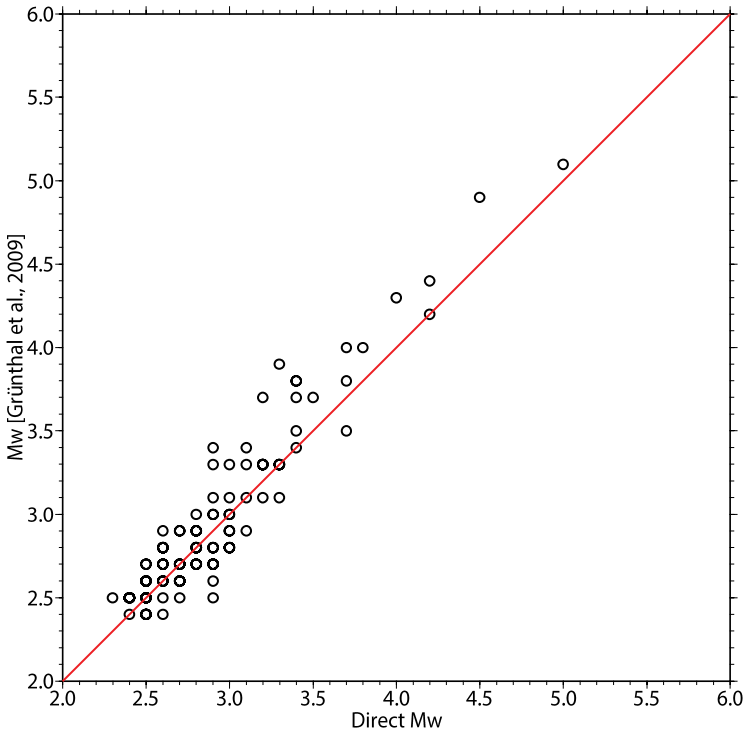

Figure 5: Comparison between measured Mw for UK earthquakes for which estimates are available and the Mw estimates converted from ML using Grünthal et al. (2009).

3.2 CATALOGUE ANALYSIS

3.2.1 Declustering the catalogue

Most seismic hazard estimations are based on the assumption that the occurrence of an earthquake is independent of the occurrence of any other, i.e. the probability of the occurrence of an earthquake in a given period of time follows a Poisson distribution. Therefore we remove dependent earthquakes (i.e. foreshocks and aftershocks) from the catalogue prior to further analysis. There have been seismic hazard studies that consider time-dependent events (e.g. Marzocchi and Taroni, 2014; Allen et al., 2015) but there is no established procedure to do so in PSHA yet. It may be useful to explore the role of time-dependent events in PSHA in future.

There are a number of ways to decluster the earthquake catalogue. MS07 remove dependent events manually. However, given the need for the process to be transparent and reproducible, in this study, we use the windowing method of Burkhard and Grünthal (2009), which is based on the approach of Grünthal (1985). This uses magnitude

dependent time and space windows calibrated for the earthquake catalogue in Central Europe. We did not test the effect of changing the window parameters. Visual inspection of the results showed that in a few cases (e.g. the 11 March and 23 April 1877 earthquakes in Mull, the Torridon earthquake sequence between August 1934 and May 1936, and the Kintail earthquake sequence in Western Scotland between 1974 and 1975), the Burkhard and Grünthal (2009) window parameters failed to identify aftershocks correctly because of the location uncertainties. In these cases, the dependent events were removed by hand.

Figure 6 shows the cumulative and annual number of earthquakes of 3.0 Mw and above in the catalogue before and after declustering. After declustering, the total number of mainshocks of Mw ≥ 3 is 547 (out of 683 events of 3 Mw and above). Note the marked increase in the number of events once instrumental monitoring begins in 1969/70.

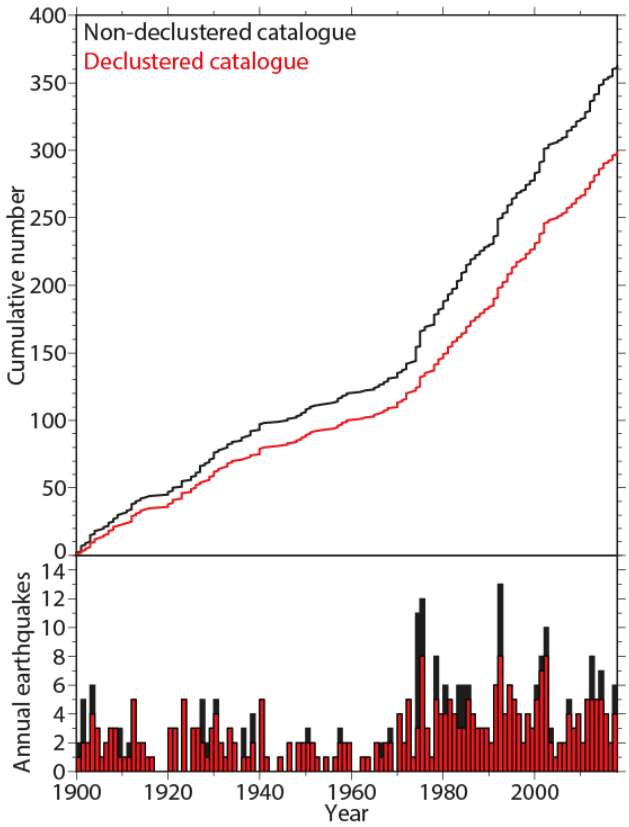

Figure 6: Cumulative number (top panel) and annual number (bottom panel) of earthquakes with Mw ≥ 3.0 before and after the declustering analysis as a function of time from 1900 to 2018.

We tested whether the declustered catalogue exhibits temporal Poisson behaviour using the chi-square test (e.g. Luen and Stark, 2012). The chi-square test determines whether there is a statistically significant difference between the expected (E_i) and observed (O_i) frequencies:

$$\chi^2 = \frac{\sum_{i=1}^{N}(O_i - E_i)^2}{E_i} \qquad (2)$$

where N is the number of classes. It is not straightforward to test the Poisson hypothesis of the declustered catalogue when the completeness of the catalogue varies over time.

As a result, the test was carried out on the mainshocks of Mw ≥ 4.0 since 1750 because the completeness of this subset of the catalogue is constant between 1750 and 2018 (see below). In this case, we divided the time window between 1750 and 2018 into bins of 10 years and counted the number of earthquakes of Mw ≥ 4.0 falling within each bin. Then, we counted the total number of bins containing 0, 1, 2, 3, etc. earthquakes (the observed frequencies), and compared them with the frequencies that would be expected if the occurrence of earthquakes were Poissonian. We found that $\chi^2 = 6.34$ for the declustered catalogue. The upper-tail critical value at 95% confidence for a χ^2 distribution with 9 degrees of freedom is 16.92, therefore we cannot reject the null hypothesis that the earthquake distribution is Poissonian. The number of degrees of freedom is given by $N - p - 1$, where N=11 is the largest number of bins, and p=1 is the mean of the Poisson distribution estimated from the data.

3.2.2 Catalogue completeness

After removing the foreshocks and aftershocks, one also needs to know the extent to which the record of mainshocks in an earthquake catalogue is complete. Especially for the historical period, some earthquakes may not be present in the catalogue because no record of them survives to the present day. Normally, completeness improves with time (i.e. it is generally better nearer the present day) and with magnitude (i.e. it is better for larger earthquakes). The completeness magnitude, Mc, is defined as the lowest magnitude at which (approximately) 100% of the earthquakes in a space-time volume are detected (Rydelek and Sacks, 1989). Mc will vary with time and is usually low for recent seismicity where instrumental recordings are available and gets progressively higher further back in time.

We assessed Mc for the composite catalogue (i.e. the BGS, ISC and FCAT-17 catalogues; see Table 1). For earthquakes of 4.0 Mw and above, we use the determination of MS07, which is based on the detailed investigation of documented historical earthquakes by Musson (2007). General understanding of the completeness of the historical catalogue for the UK has not changed since MS07 so this remains appropriate. For earthquakes of 3.0 Mw and above, the level of completeness for the UK is determined by the level of instrumental monitoring by BGS in the region. Modelled detection capability of the UK network at different times (e.g. Galloway, 2019; Figure 4) suggests that in the 1970s there were parts of mainland Britain where the detection threshold exceeded 3.5 ML (3.3 Mw). This suggests that the assessment of completeness by MS07 for earthquakes smaller than 4.0 Mw might be slightly over-optimistic. However, by 1985 the network was capable of detecting events with a magnitude of 2.0 ML (2.0 Mw) or above across nearly all of mainland Britain (Figure 4). Note that this modelling does not take into account the possible failure of individual monitoring stations and the impact of this on the detection capability. With this in mind, we assume that the instrumental catalogue for the UK and the English Channel is complete for magnitudes of 3.0 Mw and above from 1975 to present.

We have assumed that the completeness of FCAT-17 is the same as for the BGS catalogue for the UK mainland. The completeness assessment of Drouet et al. (2020), was not available when the analysis of the earthquake catalogue for this study was done in 2018. Drouet et al. (2020) estimate that FCAT-17 is complete since 1950 for Mw ≥ 3.0, whereas we estimate it to be complete for Mw ≥ 3.0 since 1975. We assume that the composite catalogue is complete from 1750 for Mw ≥ 4.0, whereas Drouet et al. (2020) assess the completeness for earthquakes of 4.0 Mw and above to start in 1850. This indicates that assuming the completeness of FCAT-17 is the same as for the BGS catalogue may result in a small part of the incomplete portion of FCAT-17 being included in the computation of the recurrence statistics (five events of 4.0-4.5 Mw between 1750 and 1850 in northern France).

Mc	*UK*	*Mc*	*North Sea*
3.0	1975	3.7	1970
4.0	1750	4.1	1890
4.5	1700	4.7	1800
5.0	1650	5.5	1700
5.5	1650		
6.0	1650		
6.5	1000		

Table 1: Completeness values for the composite catalogue. The completeness analysis for the North Sea is from Woessner et al. (2015).

There are numerous catalogue-based techniques to assess completeness. For example, Wiemer and Wyss (2000) use both the maximum value of the first derivative of frequency-magnitude distribution (FMD) as Goodness-of-Fit test, which calculates Mc by comparing the observed FMD with synthetic ones. Cao and Gao (2002) determine Mc from *b*-value stability, while Woessner and Wiemer (2005) use an Entire Magnitude Range approach to assess Mc. However, Roberts et al. (2015) determine that at least 200 events above Mc are needed to assess the completeness of the earthquake catalogue statistically. This means that these methods will not produce a statistically meaningful result for the composite catalogue, which contains only 147 events.

In order to examine the validity of our assessment of completeness, we have compared the recurrence statistics calculated for the entire catalogue, the pre-1975 portion (i.e. dominated by pre-instrumental data) and the post-1975 catalogue portion (instrumental data only) for the UK region using the completeness estimates in the 'UK' column in Table 1. The UK region is considered here to be 49°N - 59°N, 7°W-3°E. Our assumption is that if the completeness estimates are valid, the activity rate and *b* values for the different catalogue variants will be roughly the same.

To determine the activity rate and *b*-value in the FMD, we use a penalised maximum likelihood procedure (Johnston et al., 1994). A detailed description of this approach is given in Section 5.3. The results of this test are shown in Figure 7. They show that the activity rates are similar for the different catalogue variants although the activity rate is slightly lower for the pre-1975 portion compared with the post-1975 portion (although still within the uncertainty). The *b*-values of the three catalogues are very similar. These results suggest that the proposed completeness thresholds in Table 1 are appropriate and that each catalogue variant contains roughly the same proportion of larger and smaller events. We did a similar test for the completeness thresholds determined by MS07 (see Table 2 and Figure 8). This shows that the difference between the activity rates and *b* values determined for the three catalogue portions is larger suggesting that using the completeness estimates used in MS07 may result in incomplete parts of the catalogue being used in the FMD calculation (Figure 8).

In the North Sea region, there is a severe lack of data before the 1970s because only a few seismometers were operating in the northern UK and Norway (Figure 9). For this region, we use the completeness analysis for Northern Europe undertaken by Woessner et al. (2015). According to this, the catalogue can be considered to be complete for 3.7 Mw and above since 1970 (Table 1). This seems to be in agreement with the break-in slope in the cumulative number of earthquakes at around 1970 in the top panel of Figure 9. Certainly, from the cumulative and annual numbers of earthquakes of Mw ≥ 3.0 in

Figure 9, the catalogue is not complete for 3.0 Mw and above since 1970 in the North Sea, as assessed by MS07.

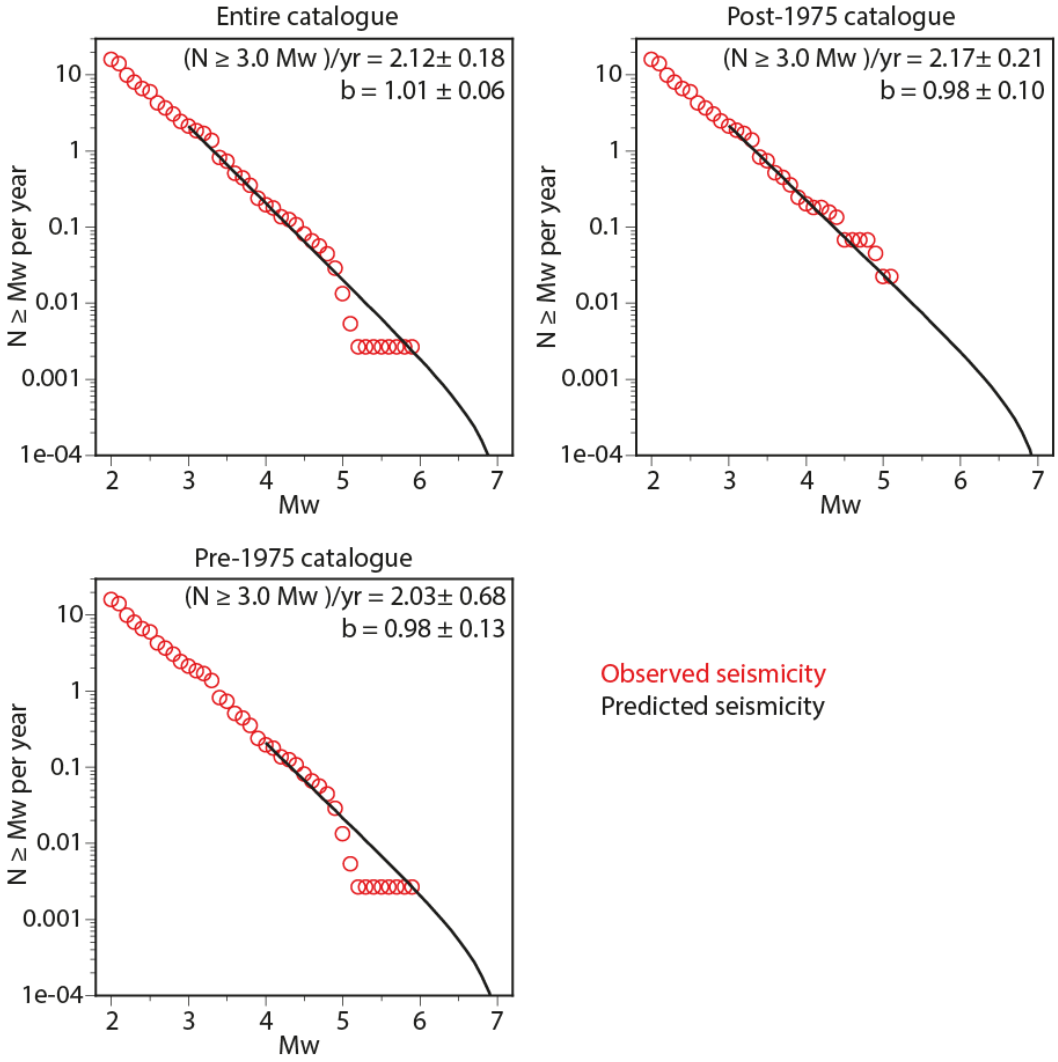

Figure 7: FMD calculated for the UK region using the completeness values in Table 1. The red circles are based on the observed FMD and the black line shows the Gutenberg-Richter model for the parameters given on the graph. The values of N (≥3.0 Mw)/yr and *b* are given with their standard errors.

Mc	UK	SE England	Dogger Bank	Viking Graben
3.0	1970	1970	1970	1970
3.5	1850	1850	1970	1970
4.0	1750	1750	1850	1970
4.5	1700	1700	1750	1900
5.0	1650	1650	1650	1900
5.5	1650	1300	1650	1900
6.0	1650	1300	1650	1900
6.5	1000	1000	1000	1700

Table 2: Catalogue completeness determined by MS07.

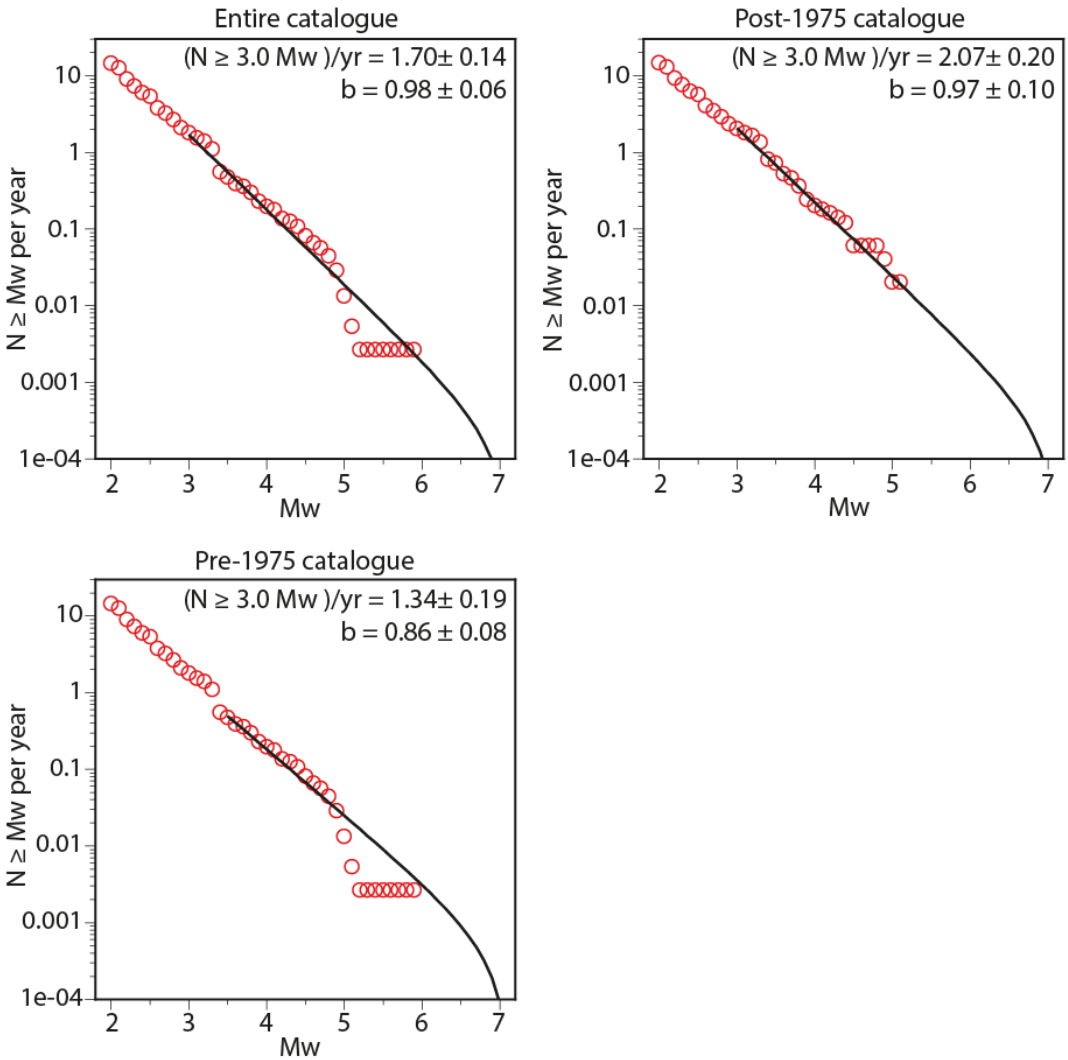

Figure 8: FMD for the UK region using the Mc values in MS07 (Table 2). Symbols are as in Figure 7.

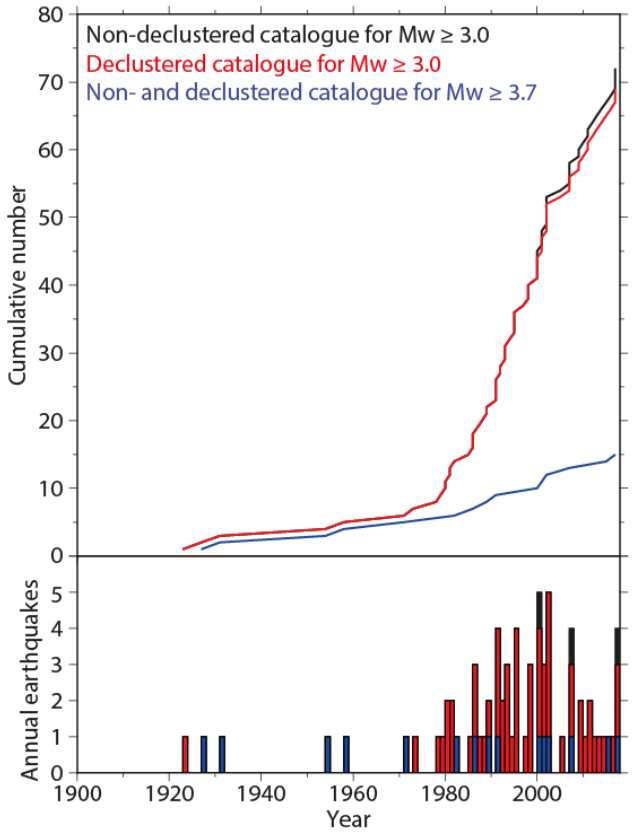

Figure 9: Cumulative number (top panel) and annual number (bottom panel) of earthquakes before and after the declustering analysis as a function of time from 1900 to 2018 in the North Sea.

4 Tectonics and seismicity of the British Isles

The UK lies on the northwest part of the Eurasian plate and at the northeast margin of the North Atlantic Ocean (Figure 10). The nearest plate boundary lies approximately 1,500 km to the northwest where the formation of new oceanic crust at the Mid-Atlantic ridge has resulted in a divergent plate boundary and significant earthquake activity. Around 2,000 km south, the collision between Africa and Eurasia has resulted in a diffuse plate boundary with intense earthquake activity throughout Greece, Italy and, to a lesser extent, North Africa. This activity extends North through Italy and Greece and into the Alps. The deformation arising from the collision between the African and European plates results in compression, commonly referred to as “Alpine compression”, that is generally directed in a north-south direction. The northeast margin of the North Atlantic Ocean is passive and is characterised by low levels of seismic activity in comparison to other passive margins around the world.

As a result of this geographic position, the UK is characterised by low levels of earthquake activity (e.g. Musson, 2012c). Evidence for this comes from observations of earthquake activity dating back several hundred years, which suggests that although there are many accounts of earthquakes felt by people, damaging earthquakes are rare.

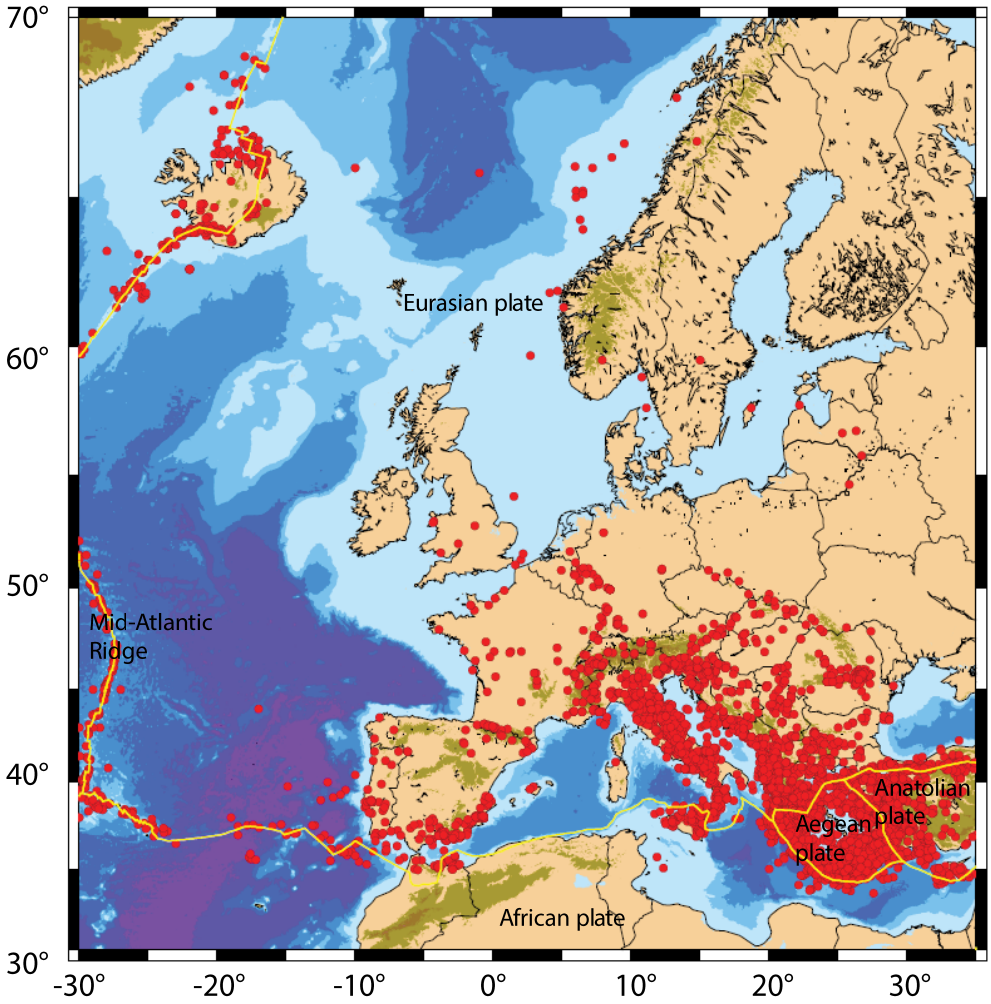

Figure 10: Distribution of earthquakes of Mw ≥ 5 across Europe. The earthquake data for the UK are from the catalogue used in this study. The seismicity data for the rest of Europe are from the catalogue developed in the SHARE project (Woessner et al., 2015). The topography is from the global model ETOPO1 (Amante and Eakins, 2009). Plate boundaries are indicated by solid yellow lines.

4.1 CRUSTAL STRUCTURE AND FAULTING

The continental crust of the British Isles was formed by the amalgamation of several faults bounded structural blocks or terranes of either Precambrian or lower Palaeozoic age (Bluck et al. 1992), during a complex geological history consisting of multiple episodes of deformation (Woodcock and Strachan, 2012). These terranes are bounded by major fault systems with evidence of long reactivation histories. Figure 11a shows both the terranes and the major bounding faults. The present configuration of these terranes is the result of a series of tectonic processes related to two major events: the Caledonian Orogeny (460-420 Ma), and the later Variscan Orogeny (290 Ma) and has remained relatively unchanged since then. The former is a result of the collision between Baltica, Avalonia and Laurentia, and other fragments of Gondwana following the closure of Iapetus Ocean (Woodcock and Strachan, 2012). The latter led to the formation of the supercontinent of Pangaea (Ziegler, 1990) in Permian time. Rifting of this supercontinent led to the opening of the Tethys Ocean, the rifting of the North Sea (Triassic to Jurassic time) and eventually the opening of the North Atlantic (Palaeogene). These tectonic episodes have resulted in a complex system of faults across Britain and Ireland in which

many of the principal structures are approximately NE-trending faults that were formed during the Caledonian orogeny (Figure 11b).

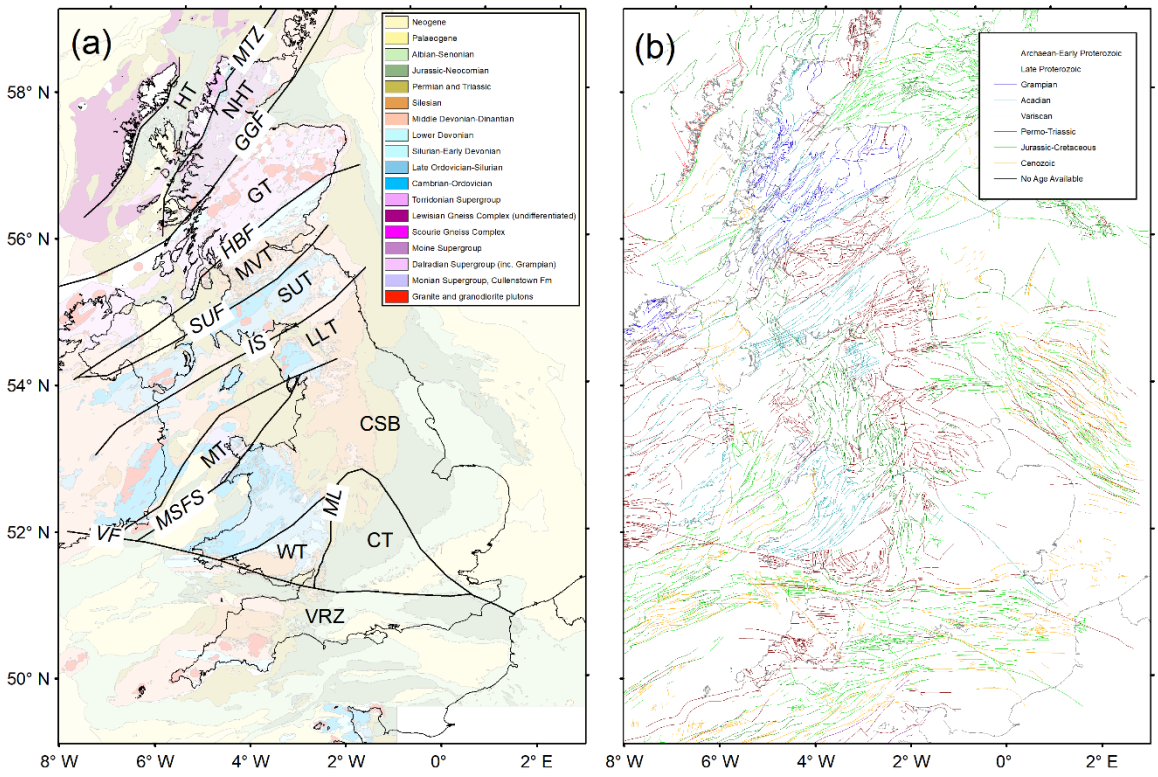

Figure 11. (a) Tectonic terrane map of the British Isles after Woodcock and Strachan (2012) and Bluck et al. (1992) superimposed on a simplified solid geology. The terranes are labelled as follows: Caledonides of Southern Britain (CSB); Charnwood Terrane (CT); Grampian Terrane (CHGT); Hebridean Terrane (HT); Leinster-Lakesman Terrane (LLT); Midland Valley Terrane (MVT); Monian Terrane (MT); Northern Highlands Terrane (NHT); Southern Uplands Terrane (SUT); Variscide Rhenohercynian Zone (VRZ); and, Wrekin Terrane (WT). Major faults/fault systems corresponding to terrane boundaries are abbreviated as follows: Moine Thrust (MTZ); Great Glen Fault (GGF); Highland Boundary Fault (HBF); Iapetus Suture (IS); Southern Uplands Fault (SUF); Menai Strait Fault System (MSFS); Malvern Lineament (ML); and, Variscan Front (VF). (b) Observed faults from the tectonic maps of the UK (Pharaoh et al, 1996). Faults are coloured by age.

The region north of the Iapetus Suture (Figure 11a) comprises various terranes associated with the margin of Laurentia (Bluck et al., 1992; Woodcock and Strachan, 2012), with crustal formation ages ranging from Archaean (Hebridean and Northern Highlands terranes) to Palaeoproterozoic (Rhinns and Grampian terranes), Mesoproterozoic (Midland Valley Terrane) and Ordovician (Southern Uplands Terrane). The boundaries between these terranes are sharply defined by the Great Glen Fault, the Highland Boundary Fault and the Southern Uplands Fault, all with a NE-SW Caledonian trend. These structures have also been the locus of later deformation, including Carboniferous rifting, which involved N-S extension during the Lower Carboniferous with the formation of NE-SW trending normal faults along the site of pre-existing Caledonian structures such as the Highland Boundary Fault, Southern Uplands Fault and the Iapetus suture (Bluck et al., 1992; Worthington and Walsh, 2011). Recent work shows that these faults were subsequently reactivated during the Palaeocene and Oligocene as strike-slip

faults arising from approximately N-S directed Alpine compression (Cooper et al., 2012), with sinistral strike-slip displacements of up to 2km on NE-trending faults The presence of long-lived faults which are susceptible to reactivation within diverse tectonic regimes, could therefore have a profound effect on crustal stress distributions.

The central UK, south of the Iapetus Suture and north of the Variscan Front, (Figure 11) comprises Neoproterozoic and Ordovician crustal terranes accreted to the margin of Gondwana and Avalonia during late Precambrian and Ordovician orogenic episodes and juxtaposed with the Laurentian terranes following the closure of the Iapetus Ocean in Silurian time. The same Caledonian structural trend is also clear throughout the Iapetus Suture Zone, extending into northern Wales and the West Midlands. In Eastern England, a NW-SE structural trend more likely reflects the late Ordovician collision of Avalonia with Baltica (Pharaoh, 2018).

The boundary between the Neoproterozoic subduction-related magmatic complexes of the wedge-shaped Midlands Microcraton (Charnwood and Wrekin terranes) and the juvenile Ordovician crust to North is concealed by the overlying sediment cover but is apparent on both magnetic and gravity anomaly maps. Pharaoh (2019) suggests that the Malvern Lineament forms the boundary between the Charnwood and Wrekin terranes (see Figure 11a). South of the Variscan Front, the crust was strongly affected by the Variscan Orogeny in late Carboniferous time. Commercial seismic reflection data reveal WNW-ESE and W-E trending Mesozoic basins developed by extensional reactivation in the hanging-walls of Variscan thrusts throughout the upper crust.

During the Jurassic and Cretaceous, Pangea began to split apart. The associated opening of the Atlantic caused crustal extension in the British Isles, forming large rift basins throughout the mainland and North Sea. Although these rift basins were formed by subsidence, the British Isles have experienced up to 3 km (locally) of uplift and exhumation. A possible cause of this is thought to be underplating of buoyant igneous material due to the North Atlantic opening over the Icelandic plume (Brodie and White 1994; Nadin et al. 1995, 1997; Bijwaard and Spakman 1999; Kirstein and Timmerman 2000; Foulger 2002; Bott and Bott 2004; Anell et al. 2009). However, Hillis et al. (2008) argue that the crust has been modified by contractional deformation which has caused some of the observed Cenozoic uplifts.

4.2 SEISMOTECTONICS

While earthquake activity in the UK is generally understood to result from the reactivation of existing faults by present-day deformation, the nature of crustal strain field and its relation to the observed distribution of earthquake activity in the British Isles is still not clearly understood. This is partly a result of the very low strain results, which are likely to require long time series of geodetic data in order to resolve these. Across the British Isles and the surrounding region, tectonic stresses generated at the Mid-Atlantic ridge due to forces acting perpendicular to the spreading ridge, as well as stresses resulting from the collision of Africa with Europe are expected to result in a uniform stress field with approximately northwest-southeast compression and northeast-southwest tension (e.g. Gölke and Coblentz, 1996; Heidbach et al., 2016). This stress field will result in the tectonic loading of existing fault structures.

However, during the Quaternary the British Isles were affected by repeated glaciations. The last glacial period reached its maximum extent around 29,000-27,000 years ago at the Last Glacial Maximum (LGM) when the British Irish Ice Sheet (BIIS) covered large parts of Britain and all of Ireland. Glacio-Isostatic Adjustment (GIA) of the crust has been on-going since the BIIS retreated from its LGM position (e.g. Lambeck, 1993; Shennan et al., 2006). As a result, it has been suggested that GIA may play a significant role in the seismicity of the region.

For example, Muir-Wood (2000) suggests that post-glacial rebound is likely to be the dominant influence on current crustal strain rates over much of northern Europe, resulting in a strain field that comprises of a radial component of extension over the rebound dome and contraction over the surrounding forebulge. Main et al. (1999) also suggest that the observed neotectonic uplift combined with a direction of maximum (regional) stress deduced from earthquake focal mechanisms supports the theory that deformation is dominated by glacio-isostatic recovery. Muir-Wood (2000) also argues that the interaction between the GIA strain field, and the pre-existing tectonic strain field, will cause areas of constructive and destructive interference, according to the pre-existing stress state (whether extensional, strike-slip or compressional). In the British Isles, this model predicts that the seismic components of the rebound dome should lie in the northeast and southwest quadrants. The northwest and southeast quadrants of the forebulge should also show seismic activity. However, the model fails to account for the lack of seismicity in the expected forebulge to the northwest.

To fully resolve the question of how each of these two strain fields influences current seismicity and strain accumulation is likely to require long term geodetic observations from permanent GPS stations in order to better characterise the strain fields for both these processes. However, currently, it remains unclear which is the primary factor explaining the observed nature and distribution of seismicity.

Earthquake focal mechanisms provide both fault geometries and principal stress directions that can be used to help constrain our understanding of the driving forces of current deformation. Figure 12 shows both earthquake activity superimposed on mapped tectonic faults (a) and published focal mechanisms for selected earthquakes in the UK (b) determined by various authors including King (1980), Turbitt et al. (1985), Trodd et al. (1985), Heyburn et al. (2005), Baptie et al. (2005), Ottemöller et al. (2009) and Baptie (2010). Focal mechanisms show mainly strike-slip faulting that suggests north-south to northwest-southeast compression and east-west to northeast-southwest tension (Baptie, 2010). In Scotland, the strike of left lateral mechanisms is consistent with left-lateral loading of major structures such as the Great Glen Fault or the Highland Boundary Fault that strike northeast-southwest as a result of north-south compression. In England and Wales, focal mechanisms predominantly show either right-lateral east-west fault planes or left-lateral north-south planes. These orientations appear consistent with tectonic loading from first-order plate motions that results in northwest-southeast compression and northeast-southwest tension and is supported by other stress data (e.g. Heidbach et al., 2016)

No earthquake in the UK in the historical or instrumental record has ever produced unambiguous evidence of a surface rupture (see ONR Expert Panel on Natural Hazards, 2018, and references therein). Typical fault rupture dimensions estimated for the largest instrumentally recorded British earthquakes appear to be of the order of 1-2 km (Baptie, 2010). As a result, it is difficult to accurately associate earthquakes with specific faults, particularly at depth, where the fault distributions and orientations are unclear. Conversely, seismicity may be associated with unmapped faults whose spatial extent and orientation is unknown. This leads to considerable epistemic uncertainty in our understanding of active faults across the region.

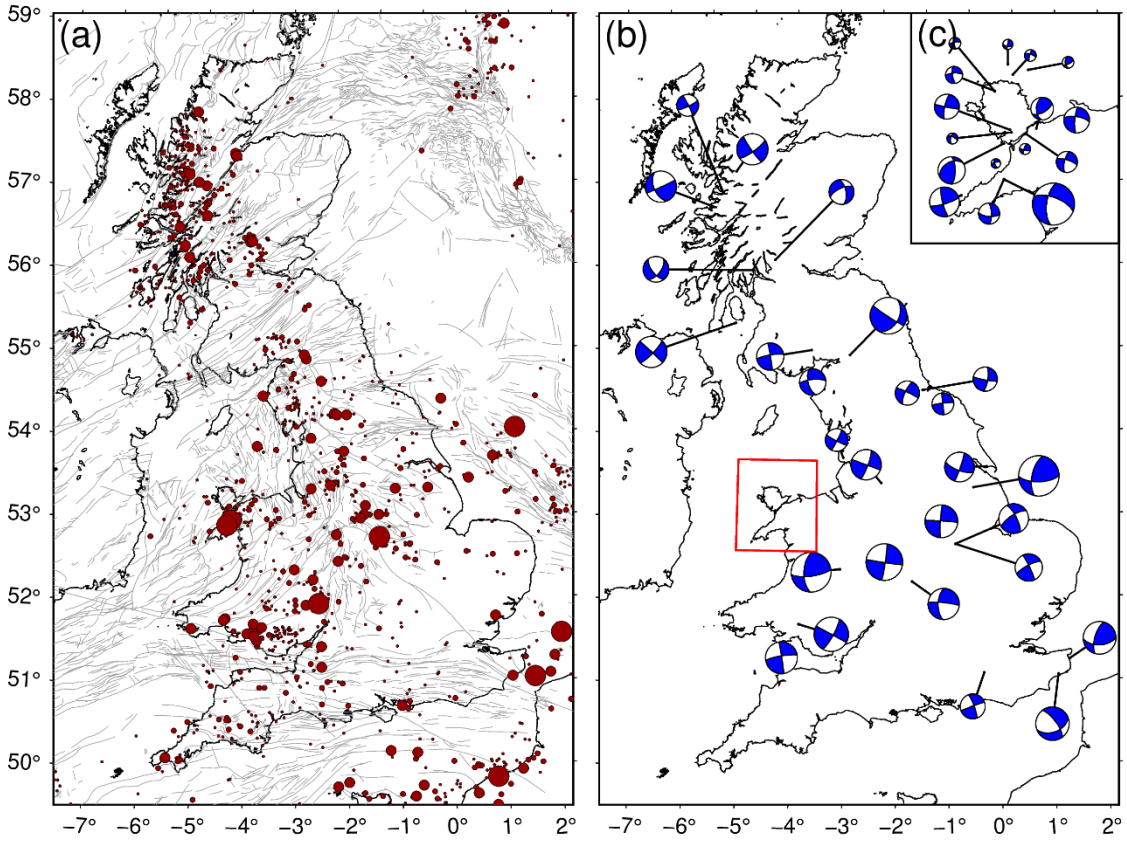

Figure 12: (a) Faults (grey lines) from the tectonic map of the UK (Pharaoh et al., 1996) along with earthquakes in the catalogue used for this study (red circles scaled by magnitude). (b) Earthquake focal mechanisms for selected earthquakes (e.g. Baptie, 2010). (c) Focal mechanisms in North Wales in the region shown by the red rectangle in (b). Blue and white quadrants show area of compression and dilatation.

A number of authors have attempted to relate specific earthquakes to known faults using interpretation of focal mechanisms and alignment of hypocentres in aftershock sequences. Assumpção (1981) shows that focal mechanisms for events in the Kintail earthquake sequence in northwest Scotland have strike-slip focal mechanisms that suggest that they may be associated with the northeast-southwest striking Strathconon Fault. Ottemöller and Thomas (2007) suggest that a sequence of earthquakes observed near Aberfolye in 2003 may have been caused by reactivation of a fault within the Highland Boundary Fault Zone. More generally, Baptie et al. (2017) suggest that earthquake activity in northwest Scotland may be the result of reactivation of a number of favourably oriented, steeply dipping fault systems, again due to deformation associated with first-order plate motions.

Chadwick et al. (1996) examined the relationship between major fault structures and seismicity, finding that while in some cases seismicity is observed in both the hanging-wall and foot-wall blocks of major dipping structures, or close to vertical structures, in other cases it is not. As a result, they conclude that any relationship between earthquakes and these structures appears more complex than a simple reactivation mechanism would produce. For example, the north-northeast trending Outer Isles Thrust is one of the largest and clearest deep crustal structures in the UK and dips gently to the east-southeast, however, it does not appear to be seismically active. By contrast, there is seismicity in both the hanging-wall and foot-wall blocks along parts of the northwest

dipping Highland Boundary Fault. Similarly, there is significant seismicity in the hanging-wall block of the north-northwest dipping Iapetus Thrust (e.g. at the intersection with the Pennine Fault) and both the hanging-wall and foot-wall blocks of the northwest dipping Lleyn Shear Zone.

Considerable seismicity also appears to be associated with faults within the Welsh Borderland Fault System, which separates the northwest margin of the Midlands Microcraton from the Welsh Caledonides. These faults include the northeast-trending Church Stretton Fault Zone along with other sub-parallel, related faults such as the Pontesford-Linley Fault. For example, the Bishop's Castle earthquake is believed to be associated with the Church Stretton Fault (Ritchie et al., 1990), although uncertainties in both estimated depth and fault geometry make it difficult to assess if the hypocentre lies in the hanging-wall or foot-wall block.

The west-northwest trending Variscan Front Thrust marks the northern edge of the Variscan Orogenic Belt and is clearly visible on seismic reflections and refraction profiles from southern Ireland to northern France. The Variscan Front Thrust dips south and there are considerable variations in seismicity along its length. For example, significant historical seismicity has occurred close to the Variscan Front Thrust in both south Wales and the Dover Straits, whereas in southern Ireland and central southern England there is very little recorded activity. Chadwick et al (1996) suggest that areas of seismicity may correspond to intersections between the Variscan Front Thrust and northwest-trending near-vertical transcurrent faults.

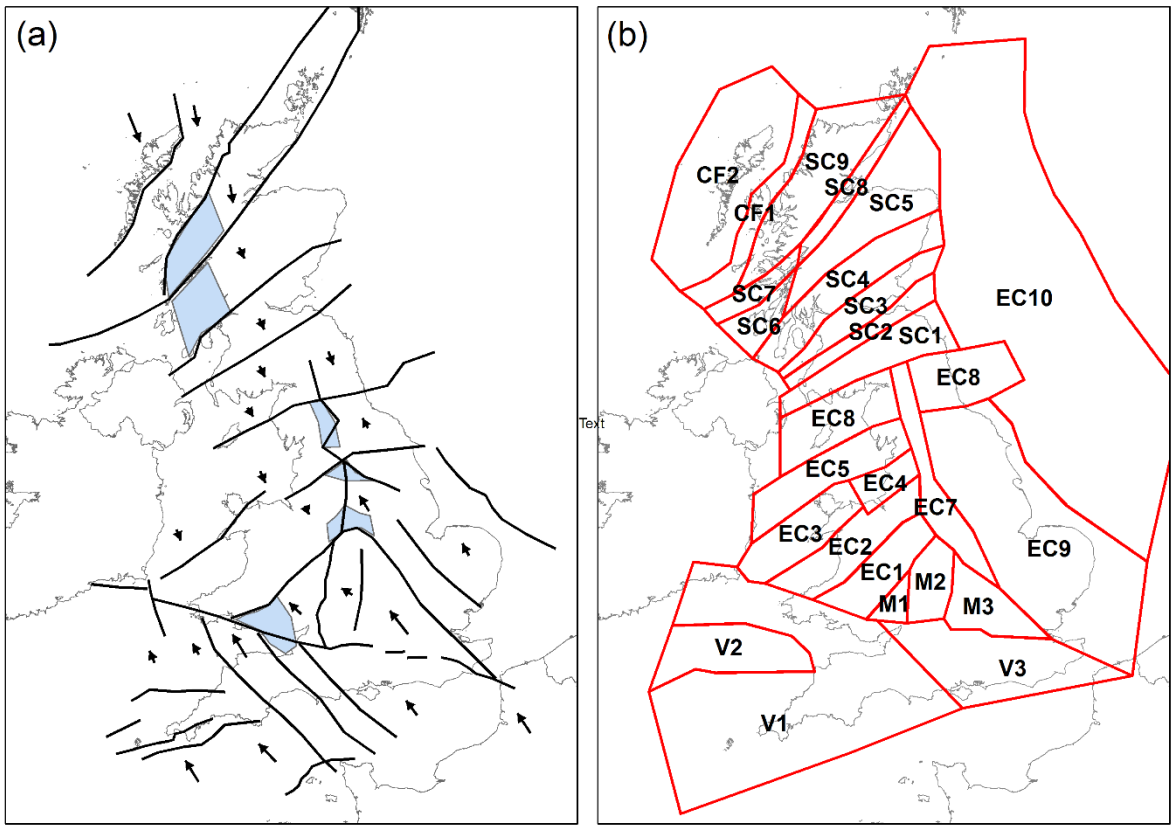

Figure 13. (a) Schematic map of kinematic interactions between upper crustal structural block (Chadwick et al., 1996). Arrows show directions of relative motion. Blue shades zones show apical areas between converging major faults (b) Generalised seismotectonic zones related to the principal upper crustal faults and shear zones.

Chadwick et al. (1996) compare crustal blocks and faults inferred from seismic reflection, potential field and structural data for the UK with earthquake activity, suggesting that most earthquakes are a consequence of minor interactions and adjustments ('jostling') between upper crustal blocks (Figure 13a) that is driven primarily by first-order plate motions rather than by post-glacial uplift. They also observe enhanced seismicity associated with the apical areas between converging major faults and, in particular, with the intersections of major faults, where several upper crustal blocks interact. This model is used to divide the UK into a set of seismotectonic zones (Figure 13b), each with uniform structural characteristics and associated seismicity.

Other authors have suggested the earthquake activity in the British Isles is driven by processes other than large-scale plate tectonics or GIA. Goes et al. (2000) used seismic tomography to identify an anomalous low-velocity region in the Upper Mantle under much of mainland Britain that extends down to at least 200 km. Bott and Bott (2004) argue this low-density upper mantle is the main cause of the Cenozoic uplift and exhumation and that earthquake activity is driven by tensional loading stress in all directions and bending stresses associated with the upper-crustal flexuring accompanying uplift. Their numerical modelling suggests a dominant pattern of NW–SE maximum compressive stress, NE–SW tension, and an intermediate vertical principal stress. In this stress regime, strike-slip events might predominate, but existing planes of weakness would also allow thrust events resulting from NW–SE compression and normal events from NE–SW tension to occur. However, while some earthquakes do overlie the low-velocity anomaly, there are many that fall outside this zone and the predominantly strike-slip mechanisms can be explained by stresses from first-order plate motions.

Arrowsmith et al. (2005) also used seismic tomography to map the upper mantle low-velocity zone with a greater resolution, showing significant seismic velocity anomalies at depths of 50–250 km. Arrowsmith et al. (2005) suggest that this anomaly results from thermal upwelling in the asthenosphere related to the Iceland plume. They also note the correspondence between the edges of the low-velocity anomaly and the locations of earthquakes across Britain. However, this is not fully supported by the observed distribution of earthquakes.

4.3 SEISMICITY OF THE BRITISH ISLES

There are relatively strong variations in the spatial distribution of seismicity throughout the British Isles (Baptie, 2010). Earthquake activity occurs in a north-south band along the length of Britain, mainly along the western flank. This band gets wider moving south. The northeast of Britain, the northwest Atlantic margin and Ireland all show an absence of notable seismicity. The earthquake band on mainland Britain cuts across the geological terrane boundaries (Figure 14) and activity is not confined to either particular structural blocks or boundaries between the blocks.

The geographical distribution of instrumentally recorded earthquakes from 1970 to present generally follows the distribution of historical seismicity over the last 300 years (Musson, 2007). However, historical evidence shows that significant earthquakes have occurred in the Dover Straits, SW Wales and around Inverness in NE Scotland, where there has been relatively little instrumentally recorded seismicity. For example, there is considerable evidence for damaging earthquakes in the Dover Straits over the last 1000 years such as an earthquake in 1580 with an estimated magnitude 5.8 ML (García-Moreno et al., 2015).

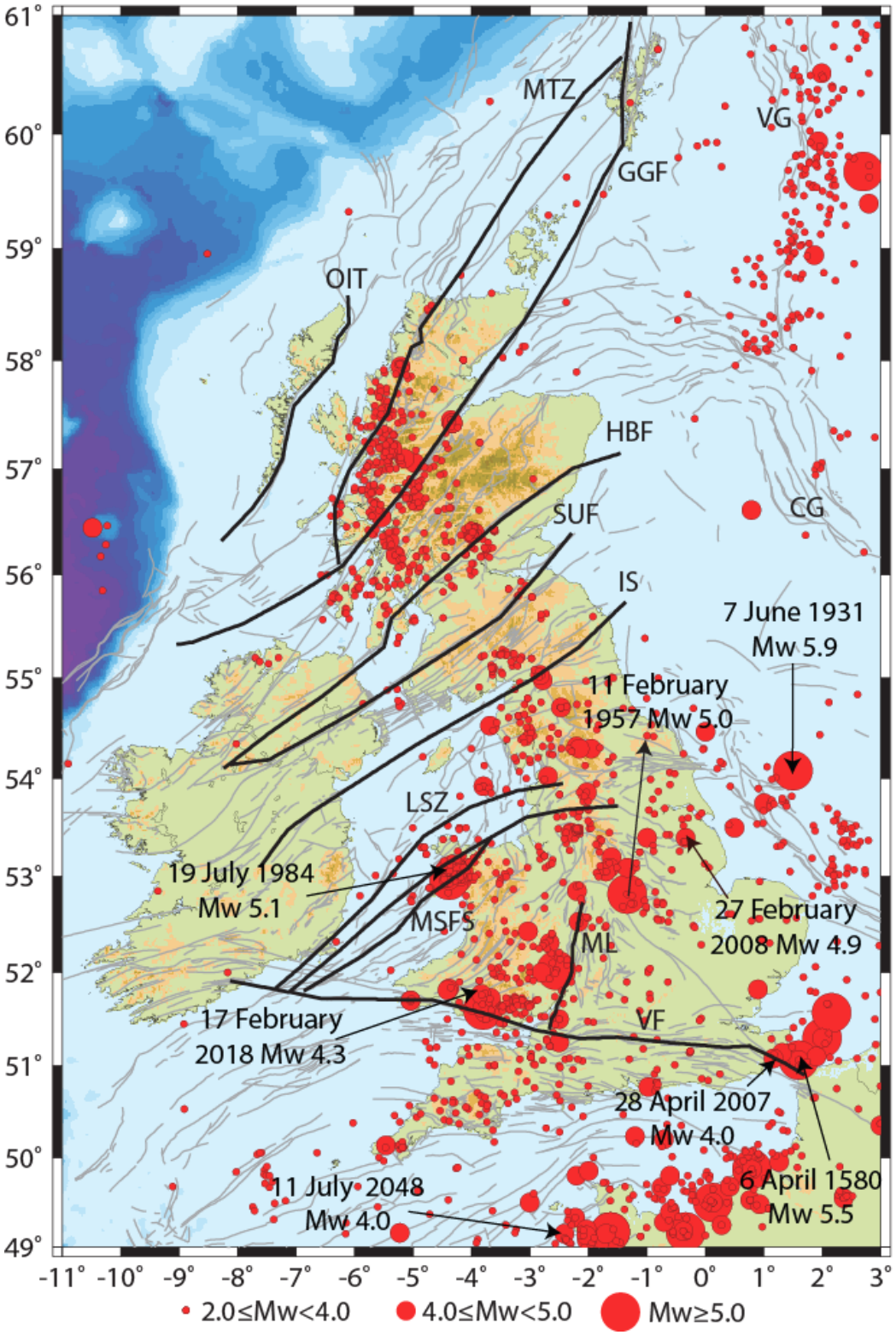

Figure 14: Seismotectonic map for the British Isles region. Topography data are from the global model ETOPO1 (Amante and Eakins, 2009). Bold black lines are major features (OIT=Outer Isles Thrust, MTZ=Moine Thrust Zone, LSZ=Lleyn Shear Zone). VG and CG are the Viking Graben and Central Graben, respectively. See Figure 11 for the labels of the other tectonic structures. Grey lines are major mapped lineaments (after Pharaoh et al., 1996).

The largest instrumentally recorded earthquake in the UK catalogue occurred on 7 June 1931 (5.9 Mw) in the Dogger Bank area of the North Sea (Neilson et al., 1984). Musson (2015) discusses the potential for larger events that may have affected the UK in historical times, but their magnitudes are uncertain. For example, in the BGS catalogue, there is an earthquake in 1275 (for which there are reports of damage to houses and buildings in many places in England) that probably had a magnitude of at least 6.0 Mw. Melville et al. (1996) posit that an earthquake in the Dover Straits in 1382 must have had a magnitude of at least 6.0 Mw. For further discussion, see Musson (2015). The largest onshore earthquake in the UK since 1970 occurred on 19 July 1984 near Yr Eifl on the Lleyn Peninsula in north-west Wales and had a magnitude of 5.4 ML (see discussion in Section 4.2.6)

There have been three moderate magnitude (Mw ≥ 4.0) earthquakes since the end of 2007: the 4.9 Mw Market Rasen earthquake on 27 February 2008; the 4.0 Mw Jersey earthquake on 11 July 2014; and the 4.3 Mw Cwmllynfell earthquake on 17 February 2018 (see discussion below).

The hypocentral depths of the earthquakes in the UK catalogue are distributed throughout the crust between depths of 0 and 30 km rather than centred on a specific value (Figure 15). This suggests a relatively broad seismogenic zone. However, it should be noted that the uncertainties in the focal depths for instrumentally recorded depths can exceed ±10 km. Similarly, the catalogue does not contain uncertainties for the depths of historical earthquakes. These may exceed typical depth uncertainties for instrumentally recorded events. In the following sections, we discuss specific regions in more detail with respect to their structure and seismicity.

4.3.1 English Channel

The Ouessant-Alderney Fault Zone marks the structural boundary between the Palaeozoic Cornubian Ridge in the northern side of the English Channel and the Precambrian Armorican Massif on the southern side of the Channel. It seems that levels of seismicity are higher in the southern area, especially close to the Cotentin Peninsula and the Channel Islands. Generally speaking, present-day seismicity in this region is diffusely distributed with magnitudes less than 4.5 Mw. Historically, relatively large earthquakes have occurred in this region such as an event on 30 July 1926 (5.1 Mw) to the east of Jersey (e.g. Lagarde et al., 2003). The most recent earthquake in the English Channel occurred on 11 July 2014, 15 km west of Jersey. Its magnitude was estimated to be 4.0 Mw (4.3 ML). It was felt on Jersey and weakly on the south coast of England but no damage was reported.

4.3.2 Southern UK

The southern UK, which we define here as the area south of the WNW-ESE trending Variscan Front, is a relatively low seismicity region with few earthquakes greater than 4.0 Mw. The Variscan NW-SE trending dextral strike-slip Sticklepath-Lustleigh Fault is the most prominent (i.e. visible, mappable) of a series of NW-SE trending late-Variscan Faults (the Watchet-Cothelstone Fault is another). These structures do not appear to be favourably oriented for re-activation based on the findings of Baptie (2010).

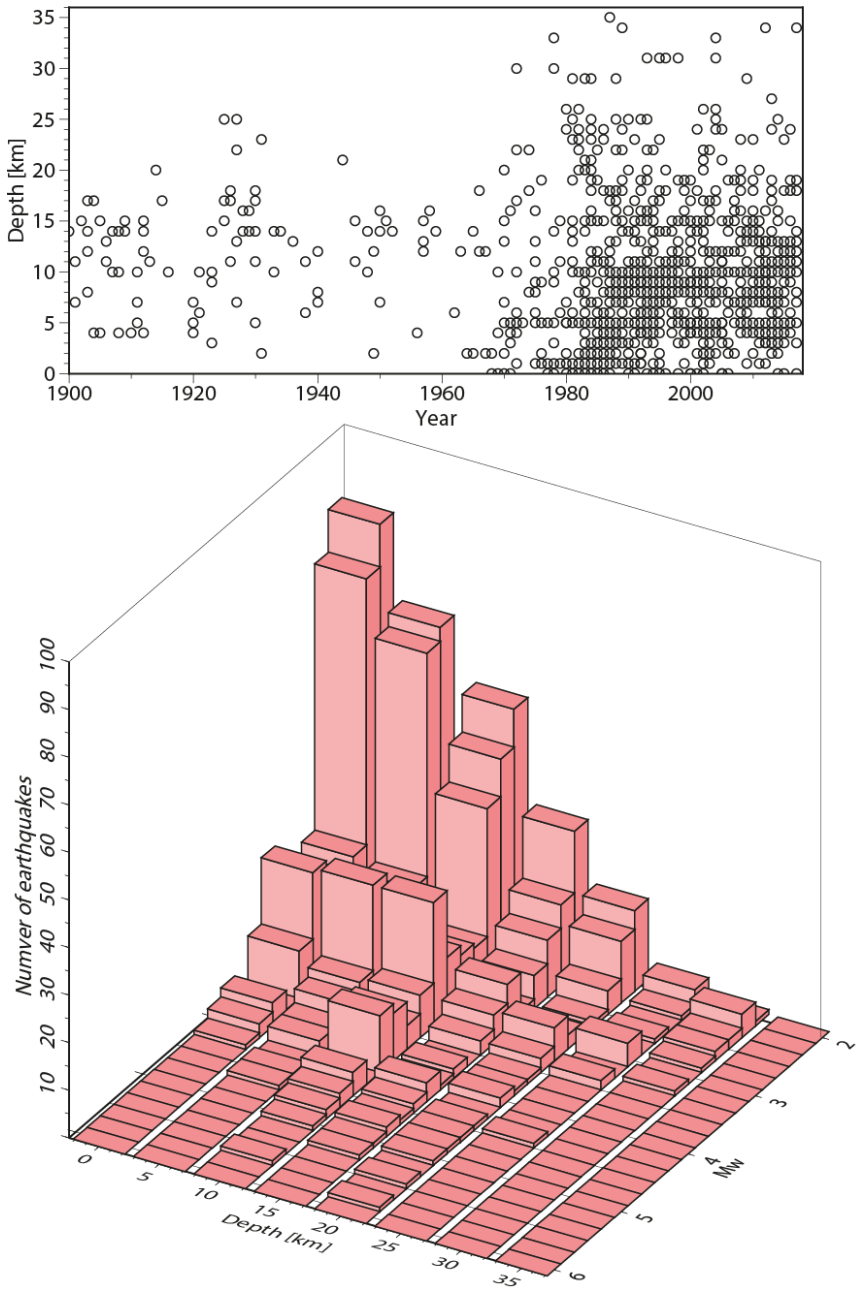

Figure 15 (a) Depth estimates in the composite catalogue (i.e. BGS, ISC and FCAT-17) from 1900 to 2018 plotted over time and (b) 3D histogram showing the distribution of earthquakes (Mw ≥ 2) with respect to magnitude and depth.

4.3.3 Dover Straits

There have been several large (≥ 5 Mw) historical earthquakes in the Dover Straits, e.g. in 1382 (~6.0 Mw) and 1580 (5.5 Mw). The magnitudes of these events are associated with large uncertainties. For example, Camelbeeck et al. (2007) estimated a moment magnitude of 6 Mw for the 1580 earthquake. Garcia-Moreno et al. (2015) investigated the correlation between seismicity and tectonics in the Dover Straits focussing on the Sangatte Fault, which is part of the North Artois Shear Zone that runs through the Dover Straits from Sangatte in northeast France to Folkestone in southeast England. This fault is thought to be the probable source of the 1580 earthquake (Camelbeeck et al., 2007)

and may be associated with two other moderate magnitude earthquakes in 1776 (3.8 Mw) and the Folkestone earthquake on 28 April 2007 (4.0 Mw).

4.3.4 Eastern England and Southern North Sea

Much of eastern England (south of the Scottish Borders) is characterised by relatively low levels of seismicity both onshore and offshore. There is an increase in seismic activity south of 54.5°N. Offshore, the seismicity in the southern North Sea seems to follow a NW-SE trending distribution but this may not reflect the real locations of these events because of the large uncertainties associated with the locations of historical events. The largest earthquake in the Southern North Sea is also the largest instrumentally recorded earthquake in the UK catalogue (7 June 1931 earthquake on Dogger Bank). The other significant earthquake occurred on 27 February 2008. Its epicentre was located 4 km north of the town of Market Rasen in Lincolnshire, and the local magnitude was estimated to be 5.2 ML. This is the largest to occur in the UK since the 1984 earthquake on the Lleyn Peninsula. Ottemöller and Sargeant (2010) estimate Mw to be 4.5 ± 0.1 from modelling displacement spectra from data recorded on stations in the UK, Belgium and the Netherlands. This is slightly lower than predicted using the relation of Grünthal et al. (2009; 4.9 Mw) but comparable to estimates from regional moment tensors (e.g. 4.6 Mw determined by Istituto Nazionale di Geofisica e Vulcanologia, Pondrelli et al., 2011). This earthquake was relatively deep (~20 km) and had a high stress drop (344±136 bar) (Ottemöller and Sargeant, 2010), which may account for the difference between Mw and ML.

4.3.5 Midland Platform

The Midland Platform is characterised by relatively low seismicity in the Anglo-Brabant Massif (to the east of the Malvern Lineament, see Figure 11a) and higher levels of seismicity in the Welsh Massif to the west of this structure.

The largest earthquake in the Anglo-Brabant Massif occurred on 11 February 1957 approximately 10 km SE of Derby (5.0 Mw). It was felt over the whole of the English Midlands down to villages close to Exeter and caused damage to chimneys and roofs in the Derby-Nottingham-Loughborough area and relays were tripped at several power stations (Musson, 1994). A few people were injured by falling masonry. There was also damage to Blackbrook Reservoir about 10 km from the epicentre (Musson, 1994).

South Wales has experienced a number of moderate magnitude, damaging earthquakes in the last 300 years. For example in 1727 (4.9 Mw), 1775 (4.8 Mw) and 1906 (4.9 Mw) - see Musson (2007). These earthquakes were felt strongly over a wide area and caused some damage (Musson, 1994). The 1906 earthquake was one of the most damaging earthquakes in the twentieth century and resulted in two injuries in Swansea where the damage was considerable (Musson, 1994). More recently, a damaging earthquake occurred 18 km NNE of Swansea on 17 February 2018. This had a moment magnitude of 4.0±0.2 Mw calculated from source displacement spectra (4.6 ML). The focal mechanism of this event may suggest that the seismicity in the Welsh Massif is the result of reactivation of a number of favourably oriented, steeply dipping faults by deformation associated with first-order plate motions (Baptie et al., 2018). Baptie et al. (2018) find that the recorded peak ground accelerations for this earthquake are significantly higher than those predicted by different GMPEs that might be appropriate for use in the UK such as Akkar et al. (2014a), Campbell and Bozorgnia (2014) and Chiou and Youngs (2014).

4.3.6 North Wales

North Wales is one of the most seismically active areas of mainland Britain, with a relatively high number of earthquakes of Mw ≥ 4.0 having been observed compared to other parts of the UK. Most of these occurred on the Lleyn Peninsula, at the northwest

edge of Snowdonia, e.g. 1534 (4.2 Mw), 1690 (4.9 Mw), 1852 (5 Mw), 1903 (4.6 Mw) and 1940 (4.4 Mw). The largest earthquake in the Lleyn Peninsula was the 1984 earthquake (5.1 Mw), which was felt widely in the UK and parts of Ireland with many reports of minor damage (Turbitt et al., 1985). It was relatively deep (20 km) which limited the amount of damage (Trodd et al., 1985). The earthquake was followed by a significant aftershock sequence of several hundred earthquakes, the largest of which had a magnitude of 3.7 Mw (Marrow and Walker, 1988).

4.2.7 Northern England

Strong earthquake activity is localised along the Pennines, from the Peak District to the Scottish Borders, and in the Lake District. The largest earthquake in the Lake District occurred on 11 August 1786 (4.7 Mw), just off the Cumberland coast near Whitehaven (Musson, 1994). The proximity of the epicentre to the Lake District Boundary Fault has led to the suggestion that the earthquake was caused by movement on this fault (Musson, 1994). However, the large uncertainty in the epicentre and the lack of any information on the mechanism of this event, means that this is highly uncertain (Musson, 1994). The largest seismicity in the Pennines is around Wensleydale (4.5 Mw) and Derbyshire (4.7 Mw), southeast of the Peak District.

4.3.7 Scotland

Seismicity in and around Scotland is strongly localised to an area bounded approximately by Dunoon and Ullapool (south to north) and Mull to Perth (west to east). There is almost no recorded seismicity anywhere west, north or east of this area until the Viking and Central Grabens to the east. The seismic activity here appears to be associated with steeply dipping fault systems that strike approximately NE-SW or NW-SE (e.g. the Highland Boundary Fault Zone, the Great Glen Fault Zone, the Strathconon Fault, the Kinlochhourn Fault and the Loch Maree Fault). These are therefore favourably oriented with respect to the expected stress regime, as confirmed by the focal mechanisms of earthquakes that occurred in Scotland (Baptie, 2010).

The magnitude 4.9 Mw Argyll earthquake in 1880 is the largest known Scottish earthquake and was felt along the west coast of Scotland, east as far as Perthshire and throughout the Hebrides. Earthquakes with magnitudes of 4.8 and 4.7 Mw occurred in Inverness in 1816 and 1901. The 1901 earthquake was felt over much of Scotland and caused substantial amounts of minor damage in Inverness, including falling chimneys and masonry. The earthquake was followed by an aftershock sequence that lasted some months. The Inverness earthquakes are located close to the Great Glen Fault and it seems possible that they were caused by reactivation of structures within this fault zone.

Comrie, on the Highland Boundary Fault, experienced earthquake swarms (sequences of earthquakes clustered in time and space without a clear distinction of mainshock and aftershocks) between 1788 and 1801, and again between 1839 and 1846. The largest event in this sequence was a 4.5 Mw (4.8 ML) event in 1839. The magnitude 4.1 Mw Kintail earthquake in 1974 is the largest instrumentally recorded earthquake in the catalogue. This was the largest in a swarm of over 20 events that occurred over several months.

4.3.8 Ireland and adjacent offshore area

Ireland is characterised by very low levels of seismic activity in comparison to mainland Britain. The historical seismicity of Ireland has been studied by a number of researchers including Davison (1924) and Richardson (1975) and a review of published data confirms that earthquake activity is very low. Historical accounts, which are as good as other parts of mainland Britain, reveal only 26 events in the period 1500 to 1970, which can be deemed credible. Half of these accounts can be attributed to moderate earthquakes that

occurred in the western part of mainland Britain. The other thirteen events occurred in Ireland and the immediate offshore area. All of these have low intensities suggesting that these were small earthquakes.

Almost all the instrumental seismicity lies in areas where historical earthquakes have occurred; mainly in Wicklow and the Irish Sea; Wexford, Waterford and Cork on the south coast of Ireland and, Donegal in the north. The exception to this is the magnitude 3.7 Mw (4.0 ML) earthquake off the coast of Mayo in 2012, which is the largest Irish event in the catalogue. Nearly all the seismic activity in Ireland, both instrumental and historical, is concentrated around the coast and there is an almost complete absence of seismicity inland.

4.3.9 Viking Graben and Central Graben

The distribution of seismicity in the central and northern North Sea delineates the trend of the Viking and Central Grabens (Figure 14). This is more apparent for the Viking Graben, which is the most seismically active area in Northern Europe, and therefore seismicity rates are higher. There has been at least one significant earthquake in the Viking Graben (1879), which was large enough to be felt weakly on both sides of the North Sea, in Norway and the Shetlands. Musson (1989) proposes that a poorly documented but possibly significant earthquake in 1508 also originated here, although there is no macroseismic data available from Norway that might support this. The Central Graben is much less active, and prior to modern instrumental monitoring, there were no earthquakes reported here.

5 Seismic source characterisation model

In PSHA methodology, the SSC model refers to the numerical representation of all possible earthquake sources, describing where and how often earthquakes occur in terms of inter-event time and magnitude-frequency in a specific region (e.g. Reiter, 1990). The study area (defined as the region in which earthquakes might have significance for a particular location) is divided into a series of seismic sources (zones or faults) where the seismic activity in each source zone is considered to be of homogeneous earthquake potential, and earthquakes have an equal chance of occurring at any point in the source (e.g. Reiter, 1990).

A general problem that arises in all studies of this kind is whether it is more appropriate to model individual faults as sources or to merge them into zones, which may be considered aggregates of similar faults. Any fault that is a uniquely controlling feature, or is such that the hazard at the site is dependent on the geometry or dip of the fault, will generally be treated as an individual source if sufficient information is available to define it. It is not common practice in the UK for source models used in regional PSHA studies (e.g. SHWP, 1993; MS07) and sometimes in site-specific studies (e.g. Musson et al, 2001; Tromans et al. 2019; Villani et al., 2020a) to include fault sources, though they have to be considered. Although some earthquake activity appears to be spatially associated with large scale fault structures (e.g. Chadwick et al, 1996; Baptie et al, 2017), it is difficult to conclusively relate specific earthquakes to motion on particular fault structures because of uncertainties in both earthquake locations and the faults themselves. As a result, there is considerable epistemic uncertainty associated with any rupture scenario. In addition, using a zonation approach allows potentially buried, and therefore unknown, fault structures to be accounted for in the source zone model.

Each zone in the SSC model is defined by the following parameters:

i) The geometry of the zone
ii) The Gutenberg-Richter FMD

iii) The maximum magnitude
iv) The depth distribution
v) The expected orientations of faulting (which can be random) and the fault types (i.e. thrust, normal, strike-slip, oblique).

Uncertainties in these parameters can be expressed using a logic tree formalism (see following sections).

The parameters above are used to model each event in a simulated catalogue as a finite fault rupture in a very simple way. First, the hypocentre of a synthetic earthquake of a specific magnitude is generated in a source zone and is assumed to be located at the centre of a fault rupture. The length of the rupture is then calculated from the event magnitude using Leonard (2014) and its orientation is selected from the logic tree (see Subsection 5.5) to determine the coordinates of the two endpoints of the rupture. We assume that the zone boundaries are permeable and therefore the endpoints of the rupture can extend outside the source zone boundaries. Down-dip rupture width is computed by assuming that the fault rupture has an aspect ratio (i.e. the ratio between the length of the rupture along the strike of the fault and the down-dip rupture width) of 1.0. Ruptures are constrained to stop at 33 km, which we assume to be the bottom of the seismogenic zone in the study area. However, none of the GMPEs in the GMC include width as an independent variable and so this simplification does not affect the results. Although the modelled rupture scenario for the source zones is a highly simplified representation of what could happen, it is unlikely to have a significant impact on the overall results since the hazard in the UK is dominated by small-to-moderate earthquakes. However, where it could become an issue is for the very largest earthquakes being considered, which will have bigger ruptures but even then, because of their low frequency of occurrence in the study area we expect the impact on the results to be minimal, especially for the return periods considered here.

5.1 GEOMETRY OF THE SOURCE MODEL

We use a single source model that is based on current understanding of the main structural domains and distribution of seismicity in the UK. This is shown in Figure 16a. The zone geometry used in this study can be considered to be the next stage in the development of a UK seismic source model that started with work on the GSHAP (Global Seismic Hazard Map) project in the early 1990s (Grünthal et al. 1999). Later iterations have been influenced by a study of the seismotectonics of the UK of Chadwick et al. (1996). The seismic source model used by MS07 (Figure 17a), which is based on Chadwick et al. (1996), included modifications to achieve a better agreement with the distribution of seismicity in the region. The source model was developed further for the 2013 European Seismic Hazard Model (ESHM13; Woessner et al., 2015) as shown in Figure 17b. While the location of the major crustal discontinuities and terrane boundaries in the UK shown in Figure 11a are relatively well-known, the inter-relationship between these regional-scale structures and other complementary but not necessarily parallel faults within the terranes is less well-understood (G. Leslie*, pers. comm*.). Given the uncertainty regarding the behaviour and location of seismogenic structures in the UK region, source models for the UK are associated with significant epistemic uncertainty, including the one used in this study, which is described below.

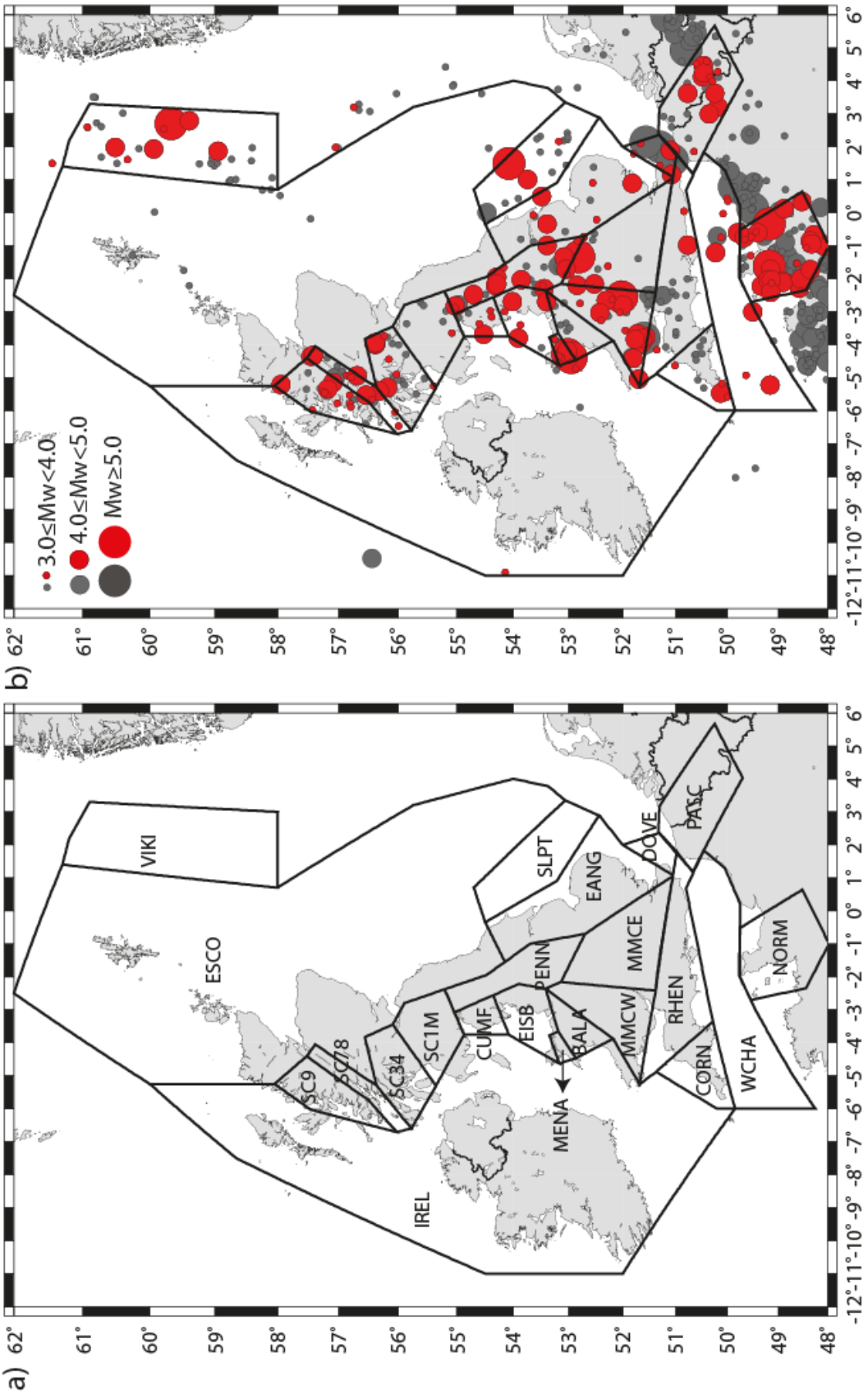

Figure 16: (a) The SSC model developed for this study with zone names; (b) the SSC model plotted along with mainshocks of Mw ≥ 3.0 for the whole catalogue (grey circles) and within the completeness thresholds in Table 1 (red circles).

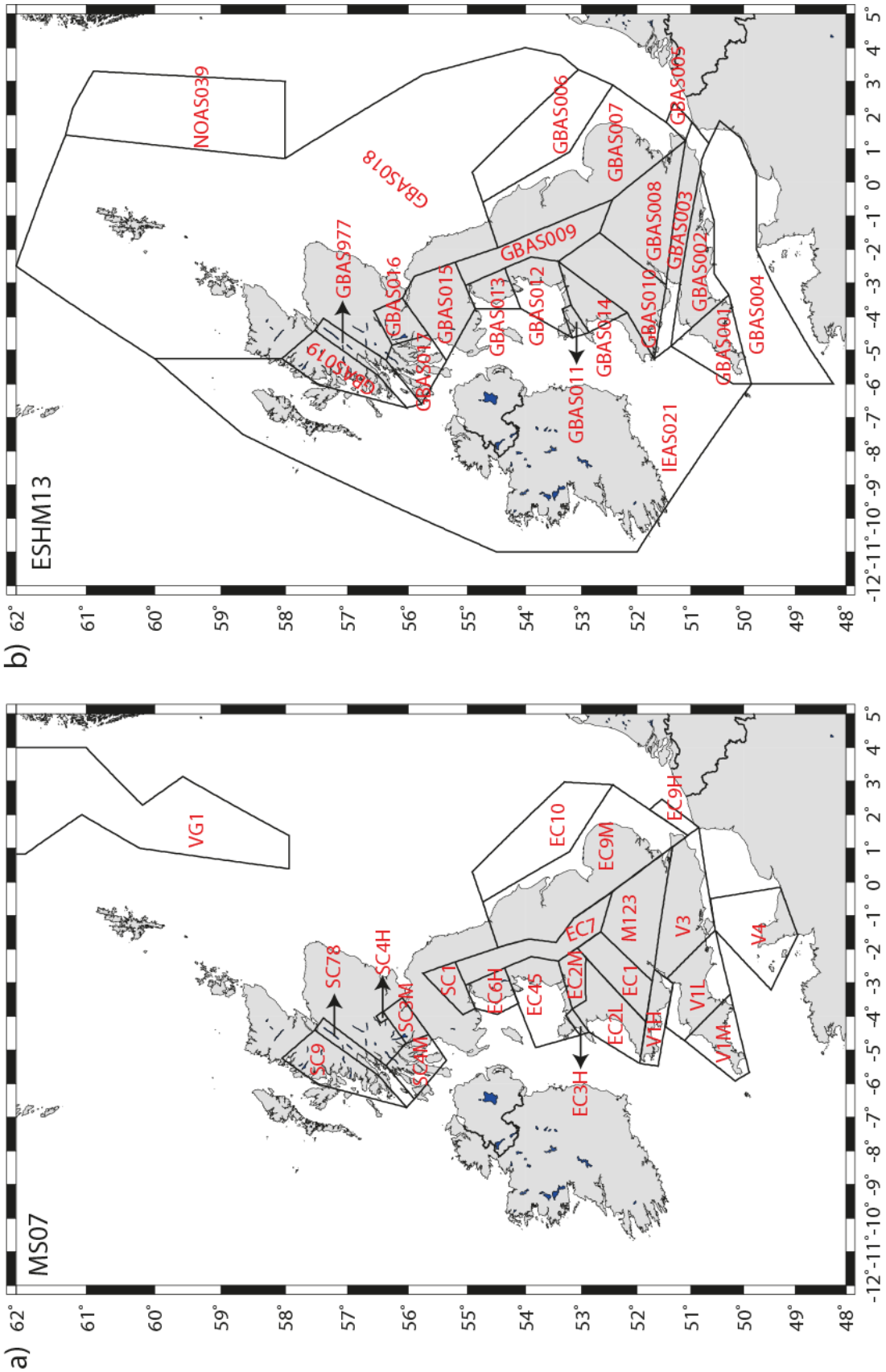

Figure 17: a) Source zone model developed by MS07; and b) source zone model for ESHM13 (Woessner et al., 2015).

The zonation for this study is based on the ESHM13 zone boundaries but we have made some modifications, which are described below (see also Section 4.2). This zonation broadly aligns with the seismotectonic blocks and zones shown in Figure 11. However, one may ask to what extent this zonation takes account of the vertical distribution of crustal structures and therefore reflects the true 'structural grain' of the UK (G. Leslie, *pers. comm.*). What is clear is that the relationship between the distribution of earthquakes and the consensus-view of the broad scale UK tectonic framework is not straightforward. Further research is required to better understand this and would potentially result in other models that are significantly different from the one used here.

An alternative approach would be to use a zoneless (zone-free, smoothed) model as has been done in other recent national seismic hazard studies e.g. for Switzerland by Wiemer et al. (2015), Germany by Grünthal et al. (2018), and France by Drouet et al. (2020). The zoneless approach is based on smoothed epicentral locations of past seismicity using smoothing kernel functions that are spatial probability density functions (e.g. Beauval et al., 2006; Zechar and Jordan, 2020 for more details). The advantage of this approach is that it removes the need to define the geometry of the individual source zones (and associated uncertainties) and to make assumptions of homogeneous seismicity within the zones. However, the zoneless approach introduces inherent uncertainties related to the definition of the kernel function used to smooth the observed seismicity and relies on the observed catalogue, which has a limited temporal duration, being an accurate reflection of the long-term hazard in a low-seismicity region like the UK. Zoneless models also incorporate uncertainties in earthquake locations and magnitudes. However, since our catalogue does not include these, this limits the applicability of the approach. Beauval et al. (2006), Drouet et al. (2020), and Villani et al. (2020b) show that a zoneless source model results in lower hazard results than if a zonation source model is used. Furthermore, in the SSC logic tree for the Swiss, German and French maps, the zoneless source model used is associated with a lower weight than the zonation source model. If a low weighting were given to a zoneless model in the SSC logic tree for the UK maps, it would probably result in little change to the final hazard estimates. However, once the location and magnitude uncertainties of the UK observed catalogue are comprehensively assessed, the use of the zoneless approach as an alternative to a zonation model should be considered in the future development of the UK seismic hazard model.

The SSC model developed for this study consists of 22 source zones and is shown in Figure 16a.

WCHA – The English Channel is included in a single zone of high seismic activity. This is based on GBAS004 of the ESHM13 but the boundary that runs along the south coast of England has been simplified because there is not really any evidence to support a more detailed geometry. The southern boundary of WCHA corresponds to the Ouessant-Alderney Fault Zone.

RHEN – The region south of Variscan Front is modelled as a single zone because there is insufficient evidence (geological, tectonic, earthquake activity) for dividing it into two source zones as in the ESHAM13 (GBAS002 and GBAS003).

MMCW/MMCE – These zones are based on zones GBAS010 and GBAS008 in the ESHM13. The boundaries between GBAS010 and GBAS008 have been modified to reflect the discussions in Pharaoh (2018) (see PENN, MMCE and MMCW on Figure 16a). MMCW corresponds to the Welsh Massif and is characterised by high seismic activity. The low seismicity zone MMCE corresponds to the Anglo-Brabant Massif.

DOVE – This zone covers the Dover Straits. It includes the revised location of the 1382 earthquake and the 1580 event. The zone's southern and eastern boundaries are based on GBSS005 of the ESHM13 but the size of the zone has been increased to account for the recent work by Garcia-Moreno et al. (2015). This suggests that the Sangatte Fault, which runs through the Dover Straits to Sangatte (northeast France) to south-east

England is the probable source of the 1580 earthquake (Camelbeeck et al., 2007) and the 2007 Folkestone earthquake (Ottemöller et al., 2009) too. Therefore, this zone has been extended slightly to the west to include the 2007 event and north to include the 1382 event. Note that the northern boundary is drawn only so that the 1382 event is included and there is no structural argument for doing this based on current knowledge. However, given the potentially large uncertainty associated with the location of this event, it is possible that it is associated with a structure in the North Artois Shear Zone of which the Sangatte fault is a part.

EANG – This source zone is based on GBAS007 of the ESHM13. It is similar to the EC9M zone in MS07, except for the northern boundary. The more southerly position of the northern boundary of EANG relative to GBAS007 reflects the fact that the Flamborough Head Fault Zone provides a more appropriate northern boundary for this zone because it is a major structure in this area.

SLPT – Similarly to EANG, the northern boundary of the zone SLPT now corresponds to the Flamborough Head Fault Zone; otherwise it is unchanged with respect to the ESHM13 (zone GBAS006).

PENN – This is based on zone GBAS009 of the ESHM13 but the southern part of zone has been made slightly wider so that it follows the topography of the Pennines in North Central England.

SC34 – GBAS016 and GBAS017 of the ESHM13 have been merged to form zone SC34. The seismicity appears to be homogeneous in this zone and there is no strong evidence for a structural boundary to divide it into two zones as in the ESHM13.

ESCO - This low seismicity source zone includes Eastern Scotland and the offshore area in the North Sea east to Scotland, covering the area defined by zone GBAS977 in the ESHM13.

IREL – This is also a low seismicity source zone that includes Ireland, the Irish Sea, and the Celtic Sea.

VIKI – The Viking Graben is included in the source model as a single zone due to its high levels of seismicity. We included this area in the source model because of its proximity to the eastern coast of Scotland and the Shetlands.

NORM and PASC –The zone NORM includes the Channel Islands and the high seismicity in Normandy, and the zone PASC covers the Belgium-Pas de Calais region. It is to be expected that seismicity in northern France and Belgium has some marginal impact on the hazard in Southern England. However, since the purpose of this project is not to calculate hazard on the continent, seismicity across the English Channel was treated in a simplified fashion, adequate for the purpose of assessing UK hazard only.

The other zones (SC1M, SC78, SC9, CUMF, EISB, MENA, BALA, and CORN) are the same as the zones in the source zone model for ESHM13 maps (see Figure 17b).

It is a basic assumption in PSHA that an earthquake has an equal probability of occurring anywhere within a source zone, i.e. events are not clustered. Here, this is tested using nearest neighbour analysis. This method computes the ratio between the average of the shortest distances between earthquakes' locations with the average expected distance between events in a source zone. If the nearest neighbour ratio is close to zero, the distribution of the events in the zone is clustered; if the ratio is between 0.5 and 1.5, the earthquake distribution is uniform (a ratio of 1 indicates a perfectly random distribution); and values of the ratio around 2 indicate that the seismicity in the zone is random (Davis, 1986). The results of the nearest neighbour analysis on the SSC model show that the seismicity in almost all the zones is uniformly distributed (the ratio is between 0.82 and 1.44), except for zone DOVE for which the seismicity is randomly distributed (the nearest neighbour ratio is 1.67).

Note that we are only considering clustering of epicentres rather than the clustering of hypocentres due to the large epistemic uncertainties on the depth estimates for earthquakes in the catalogue.

5.2 MAXIMUM MAGNITUDE

Maximum magnitude (Mmax) describes the size of the largest possible earthquake in the region under investigation. This is often highly uncertain, although, in a broad sense the maximum magnitude is limited by fault length because any large earthquake requires a sufficiently large structure or system of interacting structures to host it. However, defining Mmax in intraplate regions (i.e. in the plate interior, away from the boundaries) is particularly challenging (Holschneider et al., 2011, 2014). This is because the recurrence interval of large earthquakes is of the order of several hundreds to thousands of years due to the low rate of deformation and therefore far exceeds the relatively short duration of any earthquake catalogue based on historical data. As a result, it is quite possible that the largest possible earthquake may not be have been observed.

The UK historical earthquake catalogue includes two earthquakes with magnitudes greater than or equal to 6.0 Mw: a magnitude 6.2 Mw events in the Dover Straits in 1382; and a magnitude 6.0 Mw event in South Wales in 1275. Significant uncertainties are likely to be associated with both the locations and the magnitudes of these events as a result of the time before present (Musson, 2015). The largest earthquake for which a magnitude can be estimated reliably is the Dogger Bank event that occurred on 7 June 1931 (5.9 Mw). Earthquakes of Mw ≥ 6.0 have occurred in analogous tectonic regions. For example, the three principal earthquakes in the 1811-1812 New Madrid sequence had magnitudes of around 7 Mw (6.7 Mw, 6.5 Mw and 6.8 Mw for the 16 December 1811, 23 January 1812 and 7 February 1812 earthquakes, respectively; Hough and Page, 2011), the 1886 Charleston earthquake in South Carolina (7.3 ± 0.3 Mw; Johnston, 1996), the 1941 Meeberrie earthquake in Western Australia (7.2 ML; Johnston et al., 1994), and the 1356 Basel earthquake in Switzerland (6.6 ± 0.5 Mw). The Basel event is the largest earthquake ever recorded in north-west Europe (Fäh et al., 2011).

There is no standard procedure for determining Mmax for a PSHA (for a review, see Wheeler, 2009; and Meletti et al., 2009). In terms of estimates of maximum magnitude for the UK, Main et al. (1999) calculate a tectonic moment release rate for the seismogenic part of the lithosphere using a flexural-plate model for glacio-isostatic recovery and compare this with the observed seismic moment release rate. These two moment release rates are then used to estimate maximum magnitudes by applying the Gutenberg-Richter law. They find maximum magnitudes of 6.3 and 7.5 ML from seismic and tectonic moment release, respectively. As the latter value assumes 100 per cent seismic efficiency, Main et al. (1999) suggest that the actual maximum magnitude will lie closer to the lower value. MS07 used a weighted maximum magnitude distribution for onshore areas (between 5.5 - 6.5 Mw, with the highest weighting on magnitude 6 Mw) and offshore areas (6.0-6.5 Mw with the highest weighting again on 6.0 Mw). This is based on those authors' judgement of what might be possible in the region using observations from analogous regions where the largest earthquakes have happened in the UK region (mostly offshore).

Meletti et al. (2009) adopt the Electric Power Research Institute (EPRI) statistical approach (see Johnston et al., 1994) to determine the Mmax distribution for ESHM13 in areas of low seismicity. The starting point for the EPRI method is information from an analysis of the global dataset of seismicity for stable continental regions in Johnston et al. (1994). Then, this is updated with local information available for the study area using a Bayesian approach. In this way, the lack of large earthquakes in the study area is compensated for by observations from analogous tectonic regions (Meletti et al., 2009). Table 3 shows the Mmax distribution for low-to-moderate seismicity regions, including the UK, determined by Meletti et al. (2009). We use these values in this study for all zones.

The magnitudes in the distribution are higher than those used by MS07 for two reasons. First, the different choice of approach (statistical vs expert judgement) and second, new information on the occurrence of earthquakes greater than 6.0 Mw (such as the 1275 South Wales earthquake; see Musson, 2015) becoming available since 2007.

Mmax	*Weight*
6.5	0.5
6.7	0.2
6.9	0.2
7.1	0.1

Table 3: Distribution of the Mmax values and the weights assigned to each in the SSC model (after Woessner et al., 2015).

Known structures such as the Great Glen Fault and the Highland Boundary Fault are long enough to accommodate earthquakes with magnitudes greater than 7.0, and also have associated seismic activity, however, none of these earthquakes are larger than 5.0 Mw. There are also examples from elsewhere where large earthquakes have resulted from a collection of relatively small ruptures. For example, various faulting scenarios have been posited for the New Madrid earthquakes involving rupture on two fault segments between roughly 30 to 70 km long (Johnston and Schweig, 1996).

5.3 RECURRENCE STATISTICS

The relationship between the magnitude and number of earthquakes in a given region and time period generally can be expressed by the Gutenberg-Richter FMD (equation 1; Gutenberg and Richter, 1954). The most common variation of the Gutenberg-Richter FMD is the truncated version where the range of earthquake magnitudes is limited by a lower and upper bound (equation 3, Cornell and Vanmarcke, 1969):

$$N \geq M = 10^{a(Mmin)} \frac{e^{-\beta(M-Mmin)} - e^{-\beta(Mmax-Mmin)}}{1 - e^{-\beta(Mmax-Mmin)}} \qquad (3)$$

where $\beta = b * \ln(10)$, Mmin is the minimum magnitude and Mmax is the maximum magnitude.

Determining the activity rate, *a,* and *b*-value for individual sources tends not to be straightforward in low seismicity areas. When the number of events is small, the uncertainty in the *b*-value is high. Therefore, it is desirable to be able to maximise the information provided by different time windows of the catalogue that have different magnitude completeness thresholds (Weichert, 1980). The penalised maximum likelihood (PML) procedure described in Johnston et al. (1994) is one way to do this. It accounts for different time windows of the catalogue completeness, the uncertainty in *a* and *b* (while also taking into account the correlation between them), and a weighted prior constraining the *b*-value when there are too few earthquakes in the source zone for a reliable estimate to be made. The *b*-value is introduced as a penalty function for which the weight can be specified. The weight and the deviation of estimated b from prior b-value are then factored into the likelihood function to produce the penalised likelihood function. The estimated *b*-value is conditioned by the prior *b*-value as the weight increases and the number of events in the zones decreases. The results from the PML method are

expressed by a 5×5 matrix of possible values for *a* and *b*, determining 25 triplets of activity rate, *b*-value and their weight.

Zone	*N*	*Mmax[obs]*	*Mw [mean]*	*(N≥ 3.0 Mw)/yr*	*b-value*	*Area (km²)*
CORN	4	4.1	3.6	0.06 ± 0.03	1.03 ± 0.10	15474
RHEN	3	4.4	3.7	0.05 ± 0.03	1.00 ± 0.01	35023
WCHA	9	4.8	3.9	0.13 ± 0.04	0.99 ± 0.09	59037
DOVE	4	4.6	3.8	0.06 ± 0.03	1.00 ± 0.10	4870
SLPT	3	5.9	4.8	0.17 ± 0.10	0.97 ± 0.10	25100
EANG	7	4.9	3.9	0.11 ± 0.04	0.99 ±0.09	43698
MMCE	5	5.0	4.2	0.07 ± 0.03	0.96 ± 0.09	29878
PENN	16	4.6	4.0	0.23 ± 0.06	0.94 ± 0.09	16508
MMCW1	7	4.5	3.5	0.12 ± 0.05	1.01 ± 0.10	20047
MMCW2	10	5.0	4.8	1.12 ± 0.52	1.02 ± 0.10	20047
MENA1	4	4.4	3.4	0.07 ± 0.03	1.01 ± 0.10	1678
MENA2	3	5.1	4.9	0.33 ± 0.22	1.00 ± 0.10	1678
EISB	5	4.7	3.9	0.08 ± 0.03	0.99 ± 0.09	12116
CUMF	4	4.7	3.6	0.06 ± 0.03	1.02 ± 0.10	5384
BALA	0	-	-	0.0037	1.00	7445
SC1M	1	3.3	3.3	0.02 ± 0.02	1.01 ± 0.10	14046
SC34	8	4.9	3.8	0.12 ± 0.04	1.00 ± 0.09	13729
SC78	12	4.8	3.8	0.18 ± 0.05	0.99 ± 0.09	6489
SC9	11	4.5	3.6	0.17 ± 0.05	1.04 ± 0.09	11848
ESCO	0	-	-	0.15	1.00	297185
IREL	2	3.7	3.6	0.03 ± 0.02	1.01 ± 0.10	293319
VIKI	8	5.4	4.3	0.47 ± 0.19	1.01 ± 0.09	42083
NORM	29	5.2	4.2	0.37 ± 0.07	0.86 ± 0.08	33004
PASC	13	4.7	3.8	0.19 ± 0.05	1.00 ± 0.08	29123

Table 4: Recurrence statistics for each zone. *N*: number of earthquakes in the zone within the completeness periods in Table 1, *Mmax [obs]*: maximum observed magnitude, *Mw [mean]*: mean magnitude, *(N ≥ 3.0 Mw)/yr*: number of earthquakes greater than or equal to 3.0 Mw per year, and *b*-value of the individual source zones of the seismic model, *Area*: area of zone in km^2.

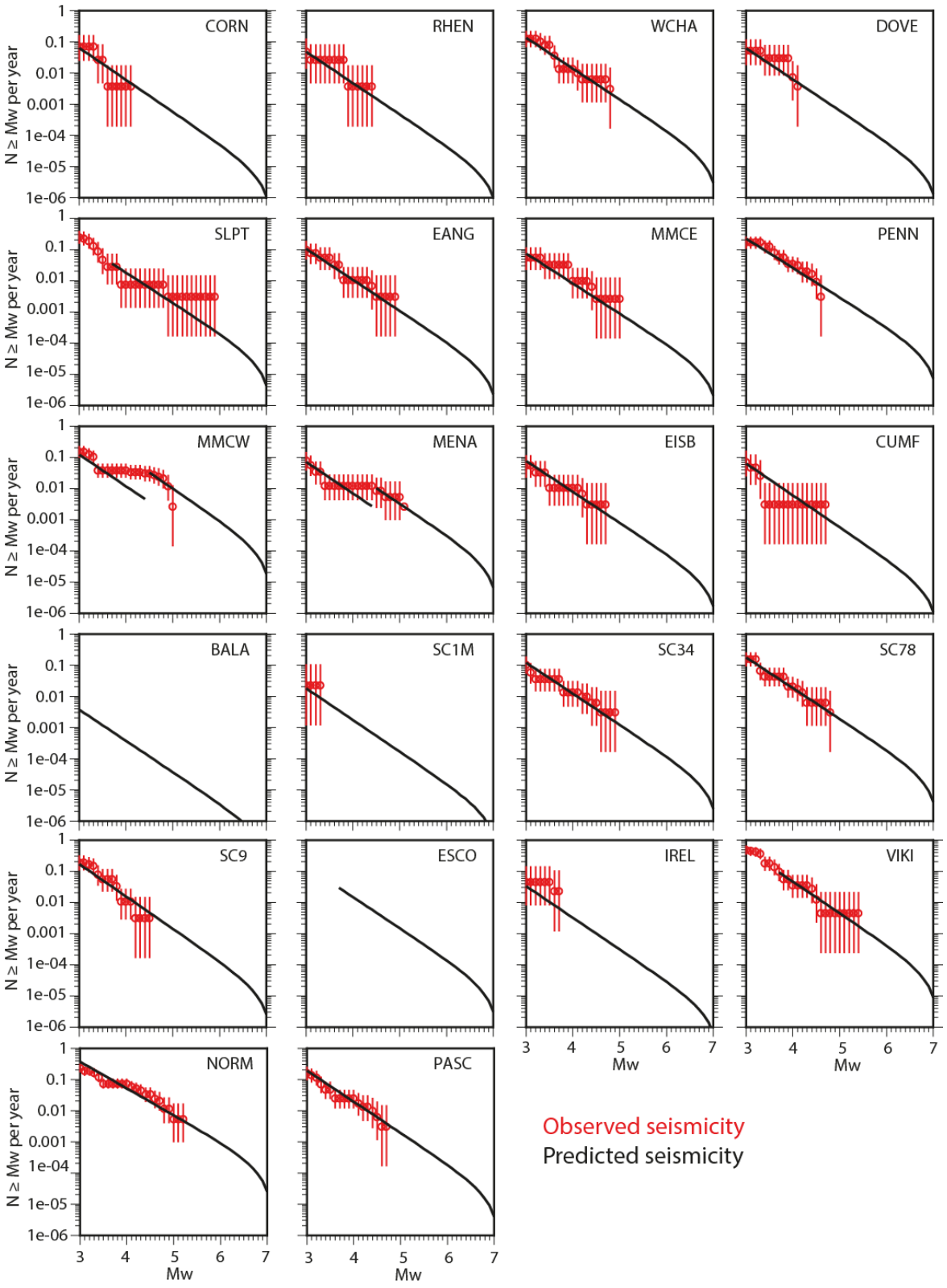

Figure 18: FMD for each of the zones in the source model. Note that N ≥ Mw per year was estimated for each source zone.

We applied the PML method to each zone in the source model using the results of the completeness analysis in Table 1. The minimum magnitude for the recurrence

calculations is 3.0 Mw. For the maximum magnitude (Mmax in Equation 3) we used a value of 7.1. This is the largest value in the Mmax distribution in the source model used for the hazard calculations (see Table 3). However, the choice for this is not critical for the results because Mmax has little influence on the estimation of the activity rates and *b*-values of the source model (Musson, 2012b). We use the *b*-value determined in Section 3.2.2 (1.0) as the prior for this analysis with a weight of 100% applied in all zones even if the anticipated catalogue completeness is different. A 100% weight for the prior b-value indicates that the b-value is forced to be the prior b-value if there are few earthquakes in the zone; otherwise, the estimated b-value is slightly adjusted to the events in the zone.

The recurrence statistics determined for each of the zones in the source model are shown in Table 4 and Figure 18. The errors quoted on the activity rate and *b*-values (also in Figures 7 and 8) are the standard deviations of the 25 triplets for each parameter. As explained in Section 3.1, we did not apply the standard error for individual magnitude estimates. The length of the error bars in Figure 18 is inversely proportional to the number of observations above a certain magnitude in the catalogue for that zone. This gives a general indication of the uncertainties in the long-term recurrence rate for that magnitude. The sum of the ($N \geq 3.0$ Mw)/yr estimates for the individual zones in the UK region (excluding VIKI and NORM) is ($N \geq 3.0$ Mw)/yr = 2.07 and therefore approximately equal to ($N \geq 3.0$ Mw)/yr derived for the region between 49.9°N and 59.0°N and 7.0°W and 3.0°E (see Figure 7), which covers most of the same area (($N \geq 3.0$ Mw)/yr = 2.12 ± 0.18). This consistency gives some confidence in the ($N \geq 3.0$ Mw)/yr estimates for individual zones. For zones SLPT, ESCO and VIKI we used the results of the completeness analysis for the North Sea. Although ESCO also includes eastern Scotland, all the earthquakes recorded in this zone have occurred offshore. For this reason, we consider it to be more appropriate to adopt the completeness estimates for the North Sea for this zone.

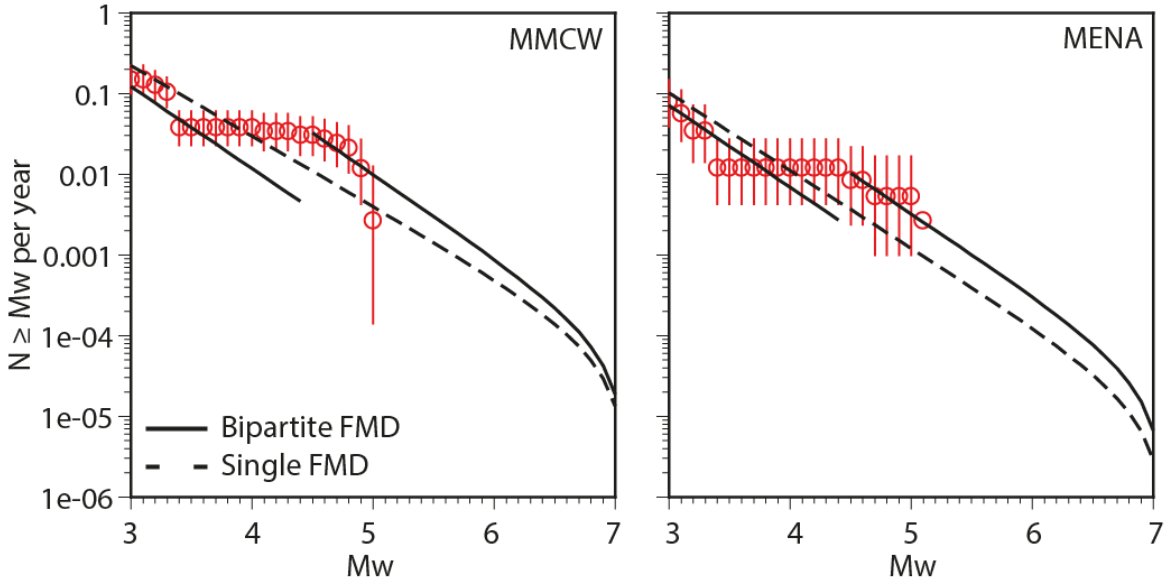

Figure 19: Magnitude-frequency recurrence for the source zones MMCW and MENA using the bipartite FMD (solid lines) and the single FMD (dashed lines).

Musson (2011) shows that the activity rate should be dependent on the area of the zone and independent of completeness periods when the zone contains no earthquakes. He proposes as a working hypothesis that these zones experience earthquakes with Mw ≥ 4 at one-tenth the average rate for the low seismicity regions of Central and Northern Europe, that is (N ≥ 4.0 Mw)/yr = 0.05 per 10^6 km^2. In this study, we applied this approach

to the zones BALA and ESCO, which contain no earthquakes within the completeness thresholds. For these, the *b*-value is also fixed to be the chosen prior determined in Section 3.2.2, i.e. 1.0. Zone SC1M contains one earthquake in the complete part of the catalogue. Applying the penalised maximum likelihood method here gives ($N \geq 3.0$ Mw)/yr = 0.02 but there are obviously significant uncertainties associated with this estimate.

The seismicity in zones MMCW in Mid and South Wales and MENA in North Wales shows a "hump" in the observed seismicity around 4.5 Mw with more earthquakes of Mw ≥ 4.5 than are predicted by the Gutenberg-Richter FMD between 3.0-5.0 Mw. This "semi-characteristic" behaviour of the seismicity in these regions was first observed by MS07, and later by Tromans et al. (2019) and Villani et al. (2020a). It can be explained by the presence of a 'bipartite FMD' (see Musson, 2015). This means that the seismicity of MMCW and MENA can be modelled as two populations of earthquakes. The first is a population of "normal" earthquakes represented by the levels of seismicity in the range Mw 3.0 to 4.5 (MMCW1 and MENA1 in Table 4). The second population consists of earthquakes in the range Mw 4.5 to 7.1 (MMCW2 and MENA2 in Table 4). The *b*-value is very similar for the two populations of earthquakes identified in MMCW and MENA. Any attempt to model the seismicity by a single FMD was found inevitably to underestimate the number of earthquakes around 4.5-5.0 Mw, a hazard-critical range for the UK (Figure 19).

Musson (2015) argues that the possibility of the two apparent populations being due to catalogue completeness issues is not credible and some 'statistical fluke' so improbable as to be discounted. However, this behaviour is at odds with widely observed exponential relationship between magnitude and frequency of occurrence in higher seismicity regions, which have higher quality catalogues, and also with the UK average. In this study we make a pragmatic decision to use the bipartite FMD as it fits the data in these two zones and reduces the possibility of underestimating the number of earthquakes of Mw ≥ 4.5 in North and South Wales (Figure 19; see also discussion in Section 8.2), however, this requires further study to fully explore the effects of magnitude uncertainties and catalogue completeness.

To determine which factors have the greatest influence on the recurrence statistics estimated for each of the source zones, we calculated the recurrence statistics for the source zones using four different combinations of catalogues and assessments of completeness:

1. The catalogue and completeness assessment used by MS07;
2. The catalogue used by MS07 and the completeness estimates in Table 1;
3. The catalogue developed for this study and the completeness assessment of MS07;
4. The catalogue developed for this study and the completeness estimates in Table 1.

The test results are shown in Figure 20. Zones NORM and PASC are not included because the catalogue used by MS07 is not complete in those regions. In general, the differences are not large and can be explained by two factors. Firstly, the magnitude conversion equations of Grünthal et al. (2009) used in the catalogue developed for this study give slightly higher Mw values than Grünthal and Wahlström (2003) used by MS07. This has a small effect on all zones. Secondly, the number of earthquakes is higher for some zones, which means that the recurrence statistics for these are better constrained. This is most evident for zones RHEN, WCHA, CUMF, and SC78. The more conservative completeness analysis results in different activity rates for zones SLPT, ESCO, BALA and IREL.

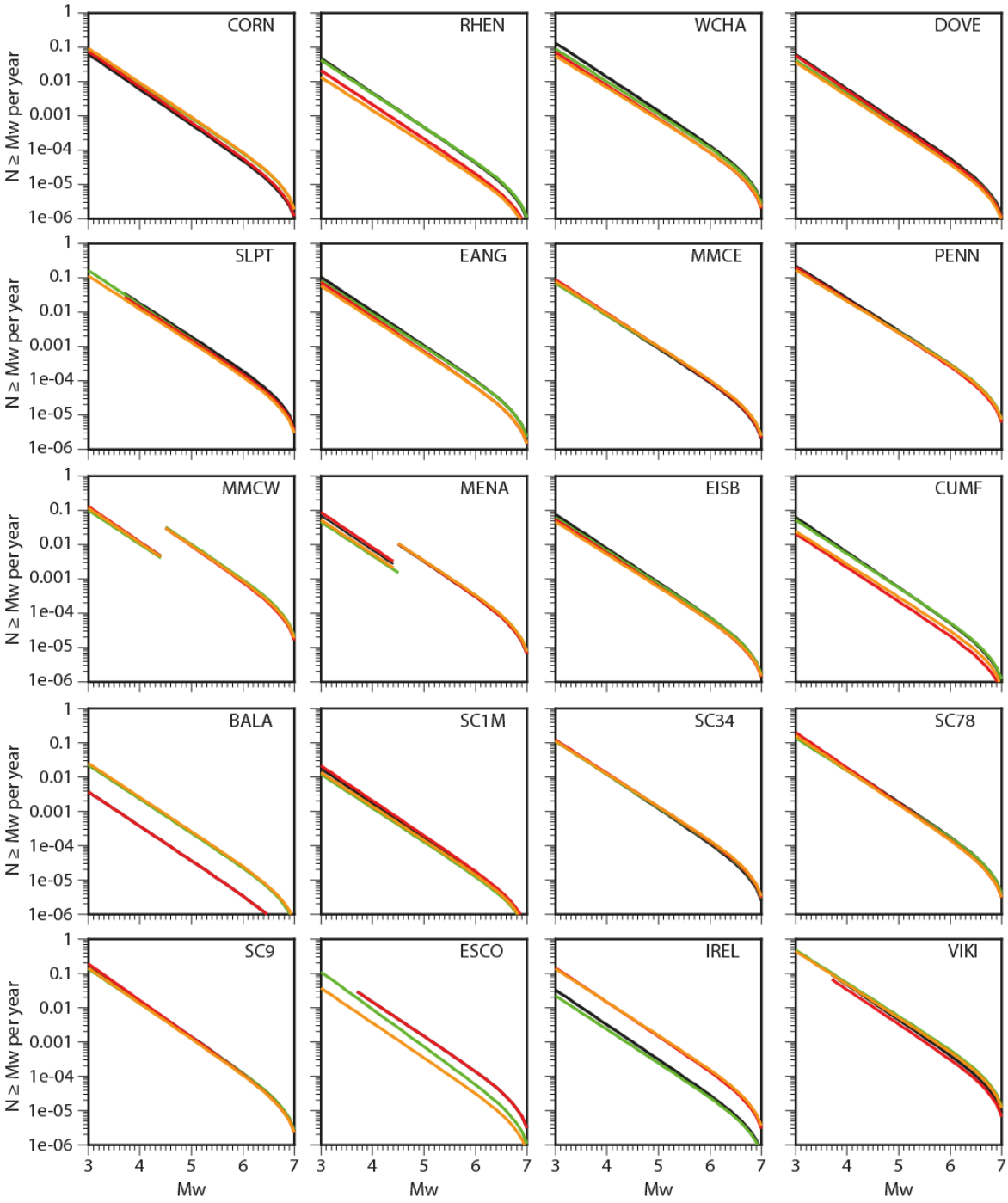

Figure 20: FMD for four tests of the source model in Figure 16a: the 2007 catalogue and the completeness in MS07 (orange lines); the 2007 catalogue and the completeness estimates in Table 1 (red lines); the updated catalogue and the completeness in MS07 (green lines); and the updated catalogue and the completeness estimates in Table 1 (black lines).

5.3.1 Validation of the source model

We used the method of Musson and Winter (2012) to assess whether the source model produces seismicity that is consistent with what has been observed. If the seismic source

model is well defined, the observed earthquake catalogue will be a credible member of the set of synthetic catalogues derived using the source model (Musson and Winter, 2012).

We generated 5000 synthetic catalogues using the SSC model. Each catalogue is 268 years long (the time period over which the observed catalogue is assessed to be complete for events of 4 Mw and above) with a variable number of earthquakes Mw ≥ 4 in that 268 year period. Each synthetic catalogue is fully described by the number of earthquakes and the mean magnitude because the former is related to the (N>=3 Mw)/yr and the latter to the *b*-value. By comparing the distribution of the number of earthquakes and the mean magnitude of each of the synthetic catalogues with the observed catalogue, the extent to which the source model is an adequate representation of the observed seismicity can be assessed visually (see Figure 21). If the observed catalogue lies outside the distribution (i.e. the shaded area in Figures 21 and 22), then the source model is not an adequate representation of observed seismicity and will lead to unreliable estimates of the hazard. As can be seen in Figure 21, the observed catalogue falls comfortably within the distribution, suggesting that the source model is well defined.

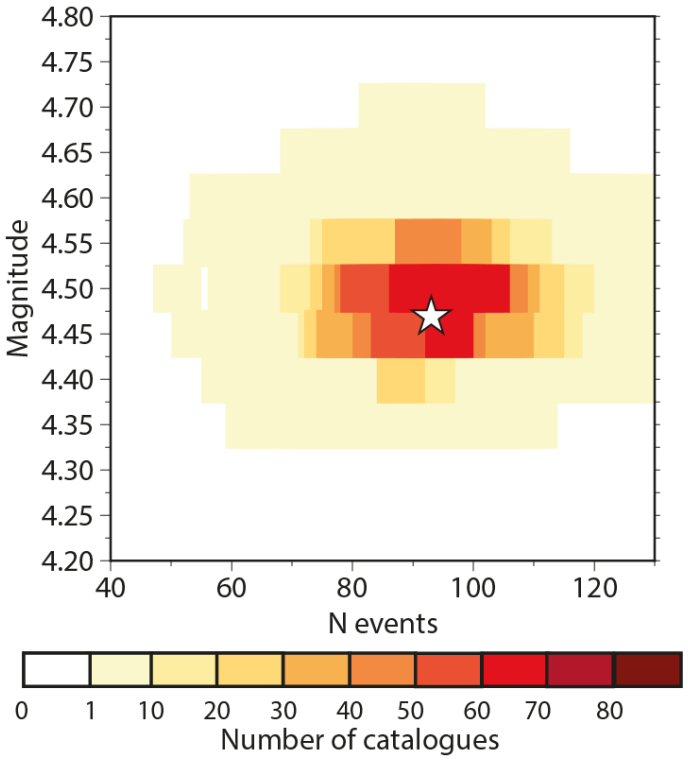

Figure 21: Distribution of the synthetic catalogues (each described in terms of the number of events and the mean magnitude). The star denotes the observed catalogue of mainshocks (described in terms of the number of events and the mean magnitude of earthquakes of Mw ≥ 4 since 1750).

We also applied this test to zones MENA and MMCW to determine whether considering the seismicity as consisting of two distinct populations of earthquakes was appropriate (Figure 22). Using a bipartite FMD, the observed mainshocks for these two zones fall more comfortably within the distribution of 5000 synthetic catalogues derived from MENA and MMCW (bottom panel in Figure 22) than if the seismicity in either zone is considered to have a single population of events (top panel in Figure 22). Figures 21 and 22

therefore show that our source model is probably an adequate representation of observed seismicity.

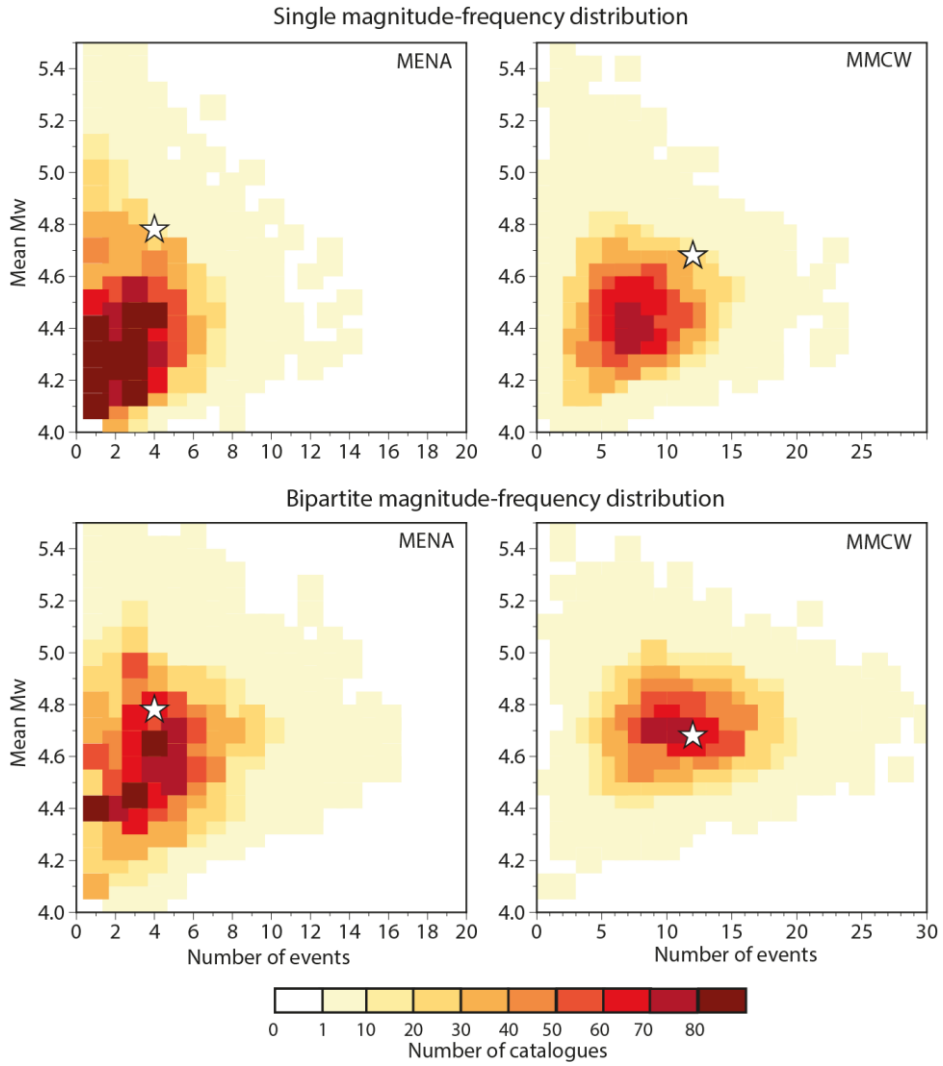

Figure 22: Distribution of the synthetic catalogues (each described in terms of the number of events and the mean magnitude) for zones MENA (on the left) and MMCW (on the right). The star indicates the observed catalogue of mainshocks (in terms of the number of events and the mean magnitude of seismicity Mw≥4 since 1750).

Depth (km)	*Weight*
5	0.1
10	0.25
15	0.4
20	0.25

Table 5: Depth distribution used in the model (after Musson and Sargeant, 2007).

5.4 DEPTH DISTRIBUTION

We use the depth distribution determined by MS07 because the general understanding of the distribution of the hypocentral depths of British earthquakes has not changed since that report was published. In MS07, the earthquakes are considered to occur between 5 and 20 km, with a modal depth of 15 km (see Table 5 for details).

See Section 4.3 for further discussion on the hypocentral depths of British earthquakes.

5.5 FAULTING

Each zone in the model has a weighted distribution of possible styles and orientations of faulting associated with it. Given the stress conditions in the UK, it is assumed here that future significant earthquakes are most likely to be strike-slip events with either north-south or east-west focal mechanisms and these orientations are equally weighted in the model. This is consistent with what has been observed predominantly for larger events in the last 30 years of UK seismicity (Baptie, 2010, see Figure 12b).

The size of each rupture is computed using the magnitude of each simulated event. In this study, we use the magnitude-length scaling relation of Leonard (2014) for earthquakes on strike-slip faults in stable continental regions. This is based on data from a relatively small dataset (ten strike-slip earthquakes between 2.6-6.5 Mw). The seismogenic thickness of a region will limit the potential width of a large strike-slip earthquake (e.g. Leonard, 2014; Stafford, 2014). Relatively well-constrained depths for events like the Lleyn Peninsula (1984) and Market Rasen (2008) earthquakes are around 20 km, which suggests that the thickness of the seismogenic zone in the UK is probably at least 20 km (the depth to the Moho is up to at least 35 km in some places).

6 Ground motion characterisation model

The ground motion characterisation (GMC) model describes the value(s) of the ground motion parameter of interest at the site from all possible earthquake scenarios. Its choice is one of the most challenging aspects of seismic hazard studies because the hazard estimates are strongly affected by the GMC model, both in terms of estimated median prediction and the aleatory uncertainty, i.e. the random variability.

The traditional way to capture the epistemic uncertainties in a GMC model is to use multiple GMPEs (ground motion prediction equations) in a logic tree that captures the centre, body, and range of technically defensible interpretations (Budnitz et al., 1997; Atkinson et al., 2014). Each GMPE is assigned a weight defined by data-driven approaches and/or expert judgements (e.g. Delavaud et al., 2012). The set of branches at the same node should be mutually exclusive and collectively exhaustive (Budnitz et al., 1997; USNRC, 2012). Care is required in the design of the logic tree, especially with regard to what should be included and what should be left out. Bommer and Scherbaum (2008) argue that because the alternative models selected to populate the ground motion logic tree are often derived from the same dataset, they do not fully capture the epistemic uncertainty in the median prediction of the GMC model.

A multi-GMPE approach was used by MS07 with the GMPEs of Campbell and Bozorgnia (2006) and Bommer et al. (2007) equally weighted. More recently in the UK, the multi-GMPE logic tree approach has been used in the GMC model of Tromans et al. (2019), which was developed for the new nuclear site at Hinkley Point C (HPC) in Somerset (see Table 6). This consists of five GMPEs, which represent a range of tectonic environments: stable continental regions (SCR; Atkinson and Boore, 2006, 2011), active shallow crustal regions (ASCR; Cauzzi et al., 2015; Bindi et al., 2014; and Boore et al., 2014), and the

UK (the stochastic model of Rietbrock et al., 2013). The weights given to each model by Tromans et al. (2019) were based on expert judgement assessment because the results from comparing the GMPEs to the available ground motion data were not conclusive (Table 6). Tromans et al. (2019) assign a low weight (0.1) to the stochastic GMPEs of Atkinson and Boore (2006, 2011) and Rietbrock et al. (2013) because these models are poorly constrained at short distances. The GMPE of Boore et al. (2014) and Bindi et al. (2014) are given the highest weight (0.3) because of their good performance in statistical tests in a shortlist of 12 GMPEs considered to be possible candidates for use in the HPC PSHA. The GMPE of Cauzzi et al. (2015) is given a lower weight (0.2) because it performs less well than that of Boore et al. (2014) and Bindi et al. (2014) (for further information, see Tromans et al., 2019).

GMPE	*Weight*
Atkinson and Boore (2006, 2011)	0.1
Bindi et al. (2014)	0.3
Boore et al. (2014)	0.3
Cauzzi et al. (2015)	0.2
Rietbrock et al. (2013)	0.1

Table 6: Logic tree for the median prediction of the GMC model developed for the site-specific PSHA for the Hinkley Point C (Tromans et al., 2019) and also used in this study.

In the last five years, the backbone approach has emerged as a way to capture the epistemic uncertainties in the median prediction of the GMC model. It is based on the selection of one or more GMPEs, which is referred to as the ‘backbone model’. The median predictions of the backbone model are then scaled up and down to capture the epistemic uncertainties in the median ground motion (see Atkinson et al., 2014; Goulet et al., 2017; Douglas, 2018). Douglas (2018) develops the backbone approach for a regional scale. The GMPE of Kotha et al. (2016) is the backbone and is scaled up and down to account for variations in average stress drop, anelastic attenuation and the statistical uncertainty in the regression-based models using the European strong motion dataset. These scaling factors can be adjusted for a specific target region by using ground motion observations from that region.

During the ground motion modelling workshop that was convened for this study in September 2018, both the more traditional multi-GMPE logic tree approach (the model of Tromans et al., 2019 given in Table 6) and the backbone approach of Douglas (2018) were discussed as possible ways to characterise ground motion. Testing the backbone approach of Douglas (2018) was considered to be the appropriate first step by the group because this method is more transparent in terms of tracking how the epistemic uncertainties in the GMPEs propagate into the hazard. However, the scaling approach requires sufficient data to calibrate the backbone model to the region of interest. This calibration in regions where there are few strong ground motion observations, like the UK, is difficult. Additionally, the scaling factors in Douglas (2018) have been computed for PGA and a spectral period of 1.0 s but not for 0.2 s, which is required for the revised version of Eurocode 8. Therefore, the project team decided that the multi-GMPE model of Tromans et al. (2019) was preferable. This decision is consistent with the findings in Villani et al. (2019) who investigate the suitability of recent GMPEs for use in the UK and conclude that the multi-GMPE logic tree approach is probably best given the lack of strong motion data for UK earthquakes of Mw > 4.5.

GMPE	Code	Region	Max Period [s]	Definition of ground motion	Magnitude range [Mw]	Distance range [km]
Atkinson and Boore (2006, 2011)	AB06	North-East US	5.0	GM	3.5-8.0	0-1000
Rietbrock et al. (2013)	RIET13	UK	5.0	GM	3.0-7.0	0-300
Abrahamson et al. (2014)	ASK14	Worldwide ASCR	10.0	RotD050	3.0-8.5	0-300
Boore et al. (2014)	BSSA14	Worldwide ASCR	10.0	RotD050	3.0-8.5	0-400
Campbell and Bozorgnia (2014)	CB14	Worldwide ASCR	10.0	RotD050	3.3-8.5	0-300
Chiou and Youngs (2014)	CY14	Worldwide ASCR	10.0	RotD050	3.5-8.5	0-300
Akkar et al. (2014a)	AKK14	Europe, Middle East ASCR	4.0	RotD050	4.0-7.6	0-200
Bindi et al. (2014)	BIN14	Europe, Middle East, ASCR	3.0	GM	4.0-7.6	0-300
Cauzzi et al. (2015)	CAU15	Worldwide ASCR	10.0	GM	4.5-7.9	0-150
Kotha et al. (2016)	KOT16	Europe, Middle East ASCR	4.0	GM	4.0-7.6	0-200

Table 7: The GMPEs used in the comparison with the UK strong motion data. GM = geometric mean of two horizontal components. RotD050 = 50th percentile of the response spectra over all non-redundant rotation angles.

To confirm whether the GMC model of Tromans et al. (2019) was an appropriate choice for the UK seismic hazard maps, we compared the ground motion predictions made using a number of GMPEs, including those used by Tromans et al. (2019), with PGA, 0.2 s and 1.0 s SA observations from a set of UK earthquakes recorded at distances between 0-400 km. This was to determine whether other GMPEs might be a better choice for the UK. The GMPEs that were used in the comparison are listed in Table 7. Besides those used by Tromans et al. (2019), we tested Abrahamson et al. (2014), Akkar et al. (2014a), Campbell and Bozorgnia et al. (2014), Chiou and Youngs (2014) and Kotha et al. (2016).

All of these relations are for active shallow continental regimes and were selected because they meet the criteria of Cotton et al. (2006) and Bommer et al. (2010) and are often used for site-specific PSHA in the UK (e.g. Tromans et al., 2019; Villani et al., 2020a). We tested the GMPE of Kotha et al. (2016) with and without the regional term that is estimated for Italy, Turkey and "Others", i.e. all the other countries in Europe and Middle East contributing to the RESORCE strong motion database (Akkar et al., 2014b).

The GMPEs of Abrahamson et al. (2014), Boore et al. (2014), Campbell and Bozorgnia (2014), and Chiou and Youngs (2014) are all expressed as the 50th percentile of the response spectra over all non-redundant rotation angles (RotD050) whereas the other GMPEs are expressed as the geometric mean of the two orthogonal horizontal components (GM). We treated RotD50 as the same as GM because the predicted ground motions from the definition of the GM and RotD50 do not differ from each other (Beyer and Bommer, 2006; Kale and Akkar, 2013).

The UK ground motion dataset consists of observations from 10 earthquakes between 3.4 and 5.0 Mw (see Table 8). There are 150 PGA observations, 107 for 0.2 s SA and 45 for 1.0 s SA (defined as the geometric mean of the two orthogonal horizontal components of ground motion). Figure 23 shows the distribution of the observations in terms of magnitude and distance. Although the UK data fall outside the range of applicability of many GMPEs in terms of magnitude and distance (e.g. Akkar et al., 2014a; Cauzzi et al., 2015; and Kotha et al., 2016; see Table 7), we did not exclude these GMPEs from the comparison because PSHA studies often have to extrapolate GMPEs outside of their range of applicability (Kale and Akkar, 2013) and the comparison is still instructive.

Date	*Lat [°N]*	*Lon [°E]*	*Depth [km]*	*ML*	*Mw*	*Location*
22/09/2002	52.53	-2.16	14	4.7	4.4	Dudley
28/04/2007	51.08	1.17	5	4.3	4.0	Folkestone
27/02/2008	53.40	-0.33	18	5.2	4.9	Market Rasen
28/04/2009	54.16	-2.99	10	3.7	3.4	Ulverstone
14/07/2011	50.12	-0.74	10	3.9	3.6	English Channel
29/05/2013	52.88	-4.72	11	3.8	3.5	Lleyn Peninsula
20/02/2014	51.36	-4.16	4	4.1	3.8	Bristol Channel
11/07/2014	49.15	-2.41	12	4.3	4.0	Jersey
22/05/2015	51.30	1.44	12	4.2	3.9	Ramsgate
17/02/2018	51.77	-3.83	8	4.6	4.3	Cwmllynfell

Table 8: Earthquakes in the UK strong motion dataset.

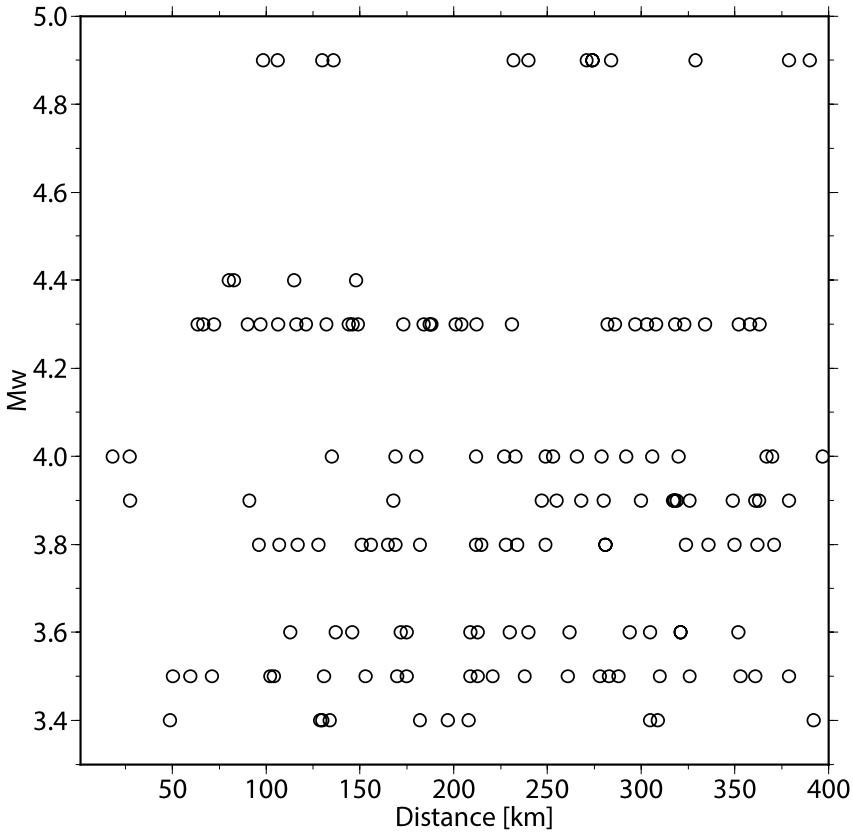

Figure 23: Distribution of the UK ground motion data in terms of distance and magnitude (for distances up to 400 km).

We visually compared the set of chosen GMPEs and the UK ground motion dataset for PGA (Figure 24), 0.2 s and 1.0 s SA (Appendix 1). For the sake of brevity, we only show the comparison for the GMPEs used in the hazard calculations that follow but the statistical analysis (residuals, likelihood analysis and the Euclidian distance-based ranking method) are shown in Figures 25 and 26 for the full range of GMPEs. The ground motion curves were computed for a rock site (Vs30= 800 m/s), a strike-slip faulting mechanism and a hypocentral depth of 10 km. In general, the GMPEs for ASCR seem to underestimate the UK data and the GMPE of Atkinson and Boore (2006, 2011) over-predicts the data (Figure 24). This is the case whether or not a Vs-κ_0 adjustment is applied.

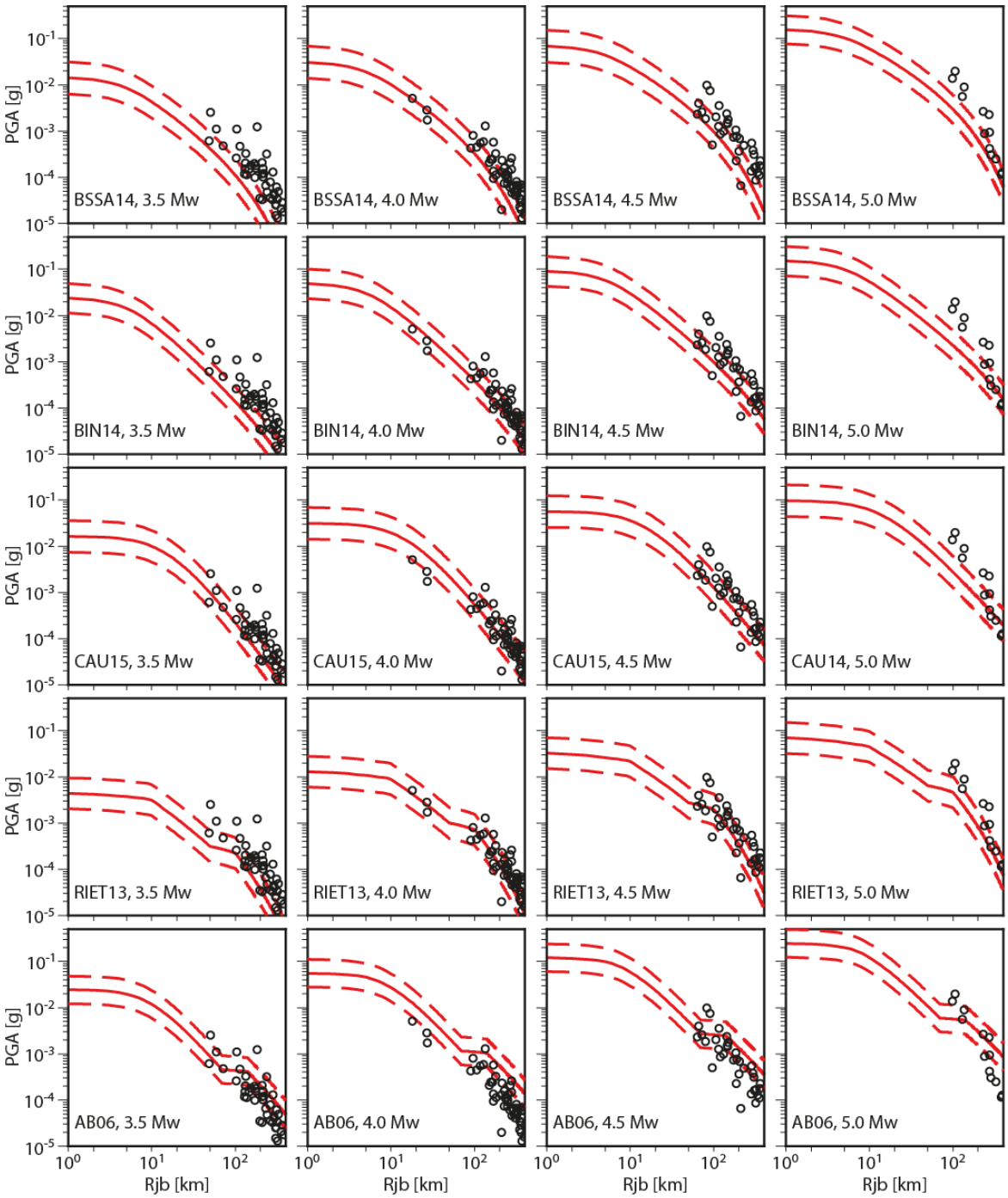

Figure 24: Comparison of the ground motion curves from a set of GMPEs and the UK strong motion data for PGA. The solid red lines describe the median prediction of the GMPEs; and the dashed red lines describe the median prediction ± one sigma.

6.1 COMPARISON WITH UK GROUND MOTION OBSERVATIONS

We also carried out some statistical tests in order to make a more objective assessment of the suitability of a particular GMPE. We used various statistical methods, i.e. residual analysis, the log-likelihood method of Scherbaum et al. (2009), and the Euclidian Distance-based Ranking method of Kale and Akkar (2013).

In the residual analysis, the normalised residual is:

$$Residual = \frac{[\ln(GM_{obs}) - \ln(GM_{th})\,]}{\sigma_{GMth}} \quad (4)$$

where GM_{obs} and GM_{th} are the observed and predicted ground motion at a spectral period and σ_{GMth} is the total standard deviation of the GMPE. Ideally, the residual should be zero indicating that the observed and predicted ground motion match exactly. If the residual is positive, the GMPE underestimates the ground motion whereas if the residual is negative, the GMPE is overestimating ground motion. The residual analysis also allows us to determine the bias in the mean residual and to check the trend of the residuals as functions of magnitude and distance. The results of the residual analysis are shown in Figure 25 for PGA and Appendix 1 for 0.2 s and 1.0 s SA. Figure 25 shows that all of the GMPEs tend to underestimate the UK data, except for the model of Atkinson and Boore (2006, 2011) that clearly overestimates the ground motion.

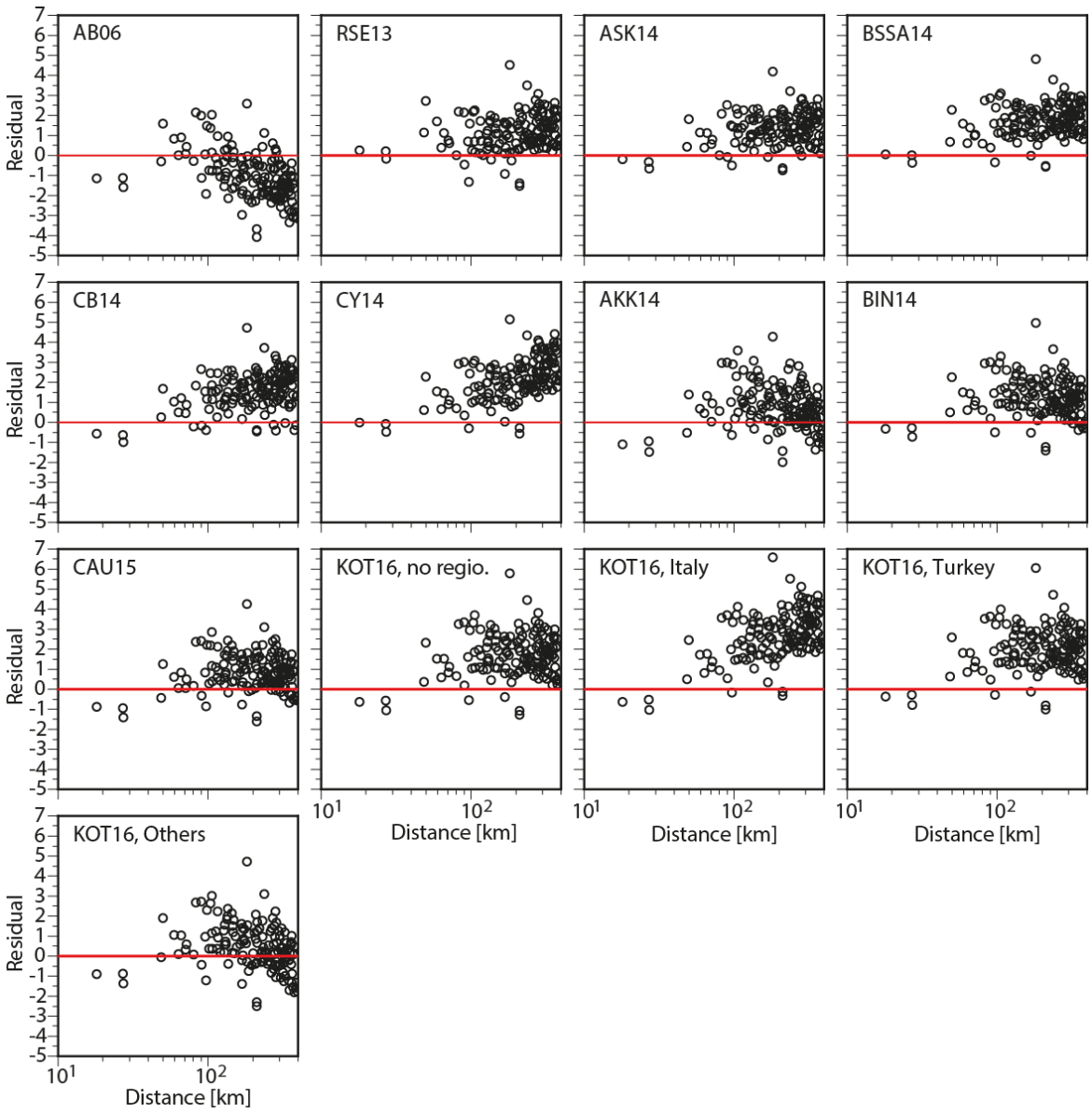

Figure 25: Model residuals between the UK strong motion data and the predictions for a set of GMPEs for PGA. The red line describes the ideal case, i.e. when the residuals are zero.

The log-likelihood (LLH) parameter in the method of Scherbaum et al. (2009) is:

$$LLH(g,x) = -\frac{1}{N}\sum_{i=1}^{N}\log_2\big(g(x_i)\big) \quad (5)$$

where x_i is the i-th empirical datum, $g(x_i)$ is the probability density function from a specific GMPE to predict the observation x_i. The smaller the LLH, the better the performance of the GMPE for a particular ground motion dataset. Kale and Akkar (2013) argue that the LLH approach of Scherbaum et al. (2009) may favour GMPEs with large aleatory uncertainty and therefore the hazard estimates may be over-conservative for low annual frequencies of exceedance (Restrepo-Velez and Bommer, 2003).

To overcome this, Kale and Akkar (2013) propose an approach based on the Euclidian distance. The main outcomes of this approach are the parameters MDE (Modified Euclidian distance), $k^{0.5}$, and EDR (Euclidian distance-based ranking). The first evaluates the effect of the standard deviation of the GMPE with the observed ground motion dataset. The parameter $k^{0.5}$ evaluates the median prediction of the GMPE for the observed dataset. The overall effect of these two parameters is given by EDR. The reader is referred to as Kale and Akkar (2013) for full details of the EDR approach.

Figure 26 displays the results of the log-likelihood and the EDR method for PGA, 0.2 s, 1.0 s SA, and the average over these three measures for the ten GMPEs in Table 7. The values of LLH, MDE, $k^{0.5}$, and EDR for 1.0 s SA (green circles in Figure 26) are smaller than those for PGA and 0.2 s SA because they are computed for fewer data (45 observations for 1.0 s SA against 150 for PGA and 107 for 0.2 s SA), which are not sufficient for significant statistics. The overall performance of the GMPEs is very similar for the same spectral period, except in a few cases, such as the LLH value of the GMPE of Kotha et al. (2016) for Italy. This suggests that the statistical methods are unable to assess the predictive model performance of the selected GMPEs for the strong motion dataset in the UK and provide only a qualitative indication of the GMPE performance. This is because this dataset is too small to rank the GMPEs in a more quantitative way. This conclusion was also highlighted in Tromans et al. (2019).

We adopt the GMC model of Tromans et al. (2019) for this work (Table 6). It agrees with the recommendations for the definition of the GMC model in Villani et al. (2019) who suggest using one GMPE among Boore et al. (2014), Campbell and Bozorgnia (2014) and Chiou and Youngs (2014), together with the GMPE of Bindi et al. (2014), Cauzzi et al. (2015), and the stochastic model of Rietbrock and Edwards (2019). For this work, we use the stochastic model of Rietbrock et al. (2013) rather than the updated model of Rietbrock and Edwards (2019) because the latter was not available when we started to test the existing GMPEs against the UK strong motion data in 2018.

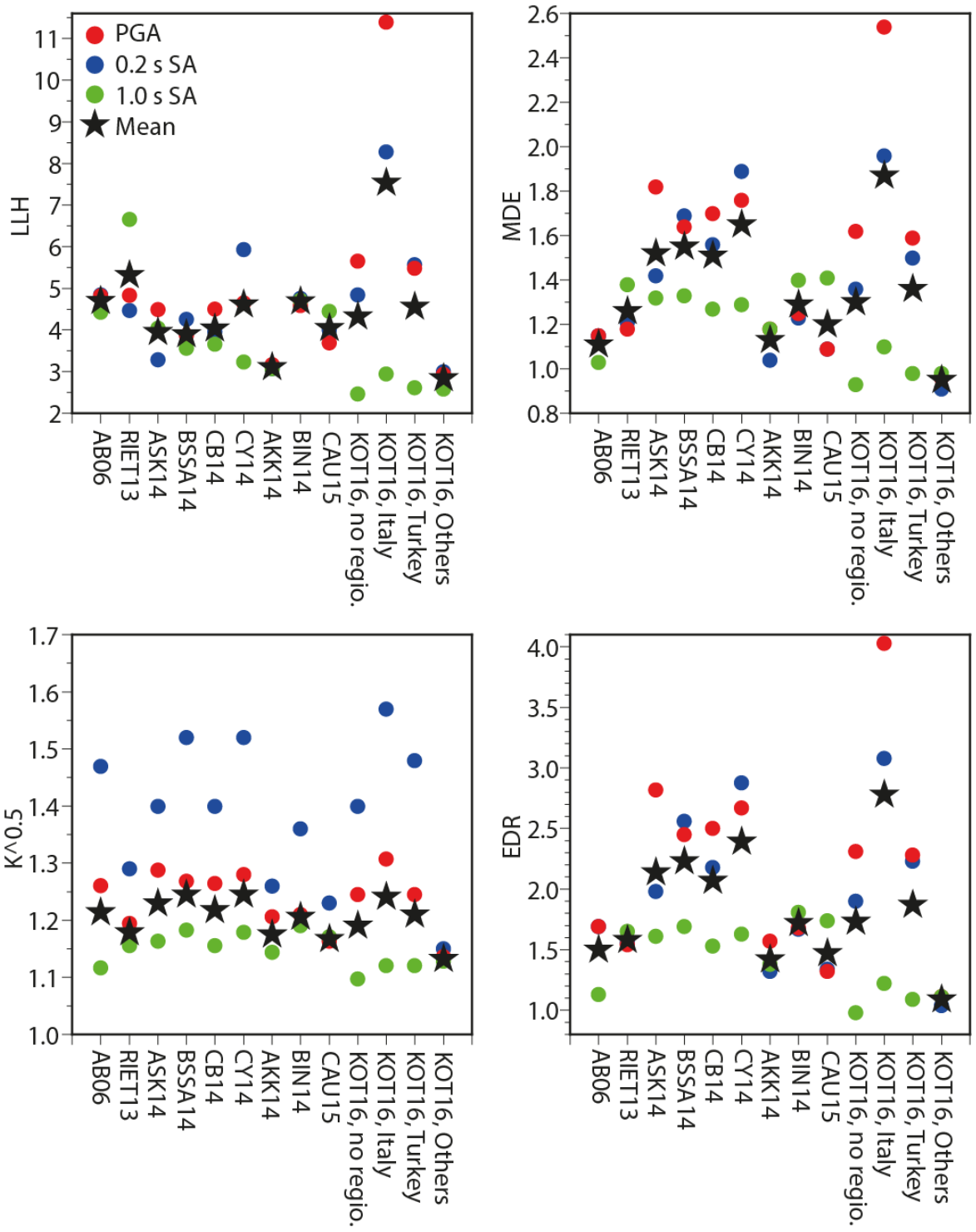

Figure 26: LLH, MDE, $k^{0.5}$, and EDR values as a function of the GMPEs in Table 7 for PGA (red circles), 0.2 s SA (blue circles), 1.0 s SA (green circles), and the average over these three (black stars).

6.2 SOIL CONDITIONS

We assume a rock site condition with a time-averaged shear wave velocity for the top 30 m (Vs30) of 800 m/s. 800 m/s marks the transition from subsoil class A (unweathered rock with high strength, Vs >800 m/s) to class B (moderately weathered rock with lower strength, 350 m/s < Vs < 800 m/s) in EC8 (CEN, 2004) and is required in the forthcoming revision. This is an idealised rock site with well-specified conditions rather than indicative of the actual site conditions at a particular location. This should be borne in mind when interpreting the maps presented in Section 7.

6.3 VS-K_0 ADJUSTMENT

GMPEs used for estimating earthquake ground motions are usually based on empirical data from regions where there are large numbers of recordings. As a result, these GMPEs represent the site conditions of the specific region, or regions, for which they were derived. Ideally, when applying a GMPE from a given host region to a specific target site or region, in this case, the UK, the GMPE should be adjusted to account for differences between the host and the target (Douglas and Edwards, 2016). This process is often referred to as Vs-κ_0 (or host-to-target) adjustment since it needs to account for both the effects of elastic amplification due to shear wave velocity structure and near-surface attenuation at a site.

Anderson and Hough (1984) modelled the high-frequency decay of the Fourier amplitude spectrum (FAS) of earthquake ground motions as

$$a(f) = A_0 exp(-\pi\kappa f) \tag{6}$$

where the parameter kappa (κ) controls the high-frequency decay of the FAS of the ground motion. The term κ_0 is commonly used to represent the attenuation of shear waves at a given site as a result of the physical properties of the near-surface rocks and soils.

Campbell (2003) proposed a hybrid-empirical method (HEM) to make host-to-target adjustments using random-vibration theory (RVT) (Cartwright and Longuet-Higgins, 1956). However, this method requires information about source and path specific parameters, such as stress drop and attenuation, in both the host and target regions. Al Atik et al. (2014) developed a method based on inverse RVT (IRVT; Gasparini and Vanmarcke, 1976) to transform the response spectrum calculated using a given GMPE (RS_{GMPE}) into a compatible FAS (FAS_{GMPE}). The host-to-target adjustments are applied to the FAS before recalculating response spectra using the RVT approach. This method requires no assumptions about source or path specific model parameters for the host and target sites. Additionally, working in the Fourier domain has the advantage that adjustments are independent of the input motion.

Following Edwards et al. (2016), the frequency-dependent adjustment function is given by

$$C_{FAS,V_s-\kappa_0}(f) = \frac{A_{target}(f)}{A_{host}(f)} e^{-\pi f(\kappa_{0,target}-\kappa_{0,host})} \approx \frac{FAS_{target}}{FAS_{GMPE}}(f) \tag{7}$$

where A describes the velocity-dependent amplification and κ_0 describes the attenuation in the host and target regions. The period-dependent adjustment to the response spectra is then given by

$$C_{PSA,V_s-\kappa_0}(T) = \frac{RS_{target}}{RS_{GMPE}}(T) \tag{8}$$

Typically, these adjustments are calculated for a number of different earthquake scenarios for a given site.

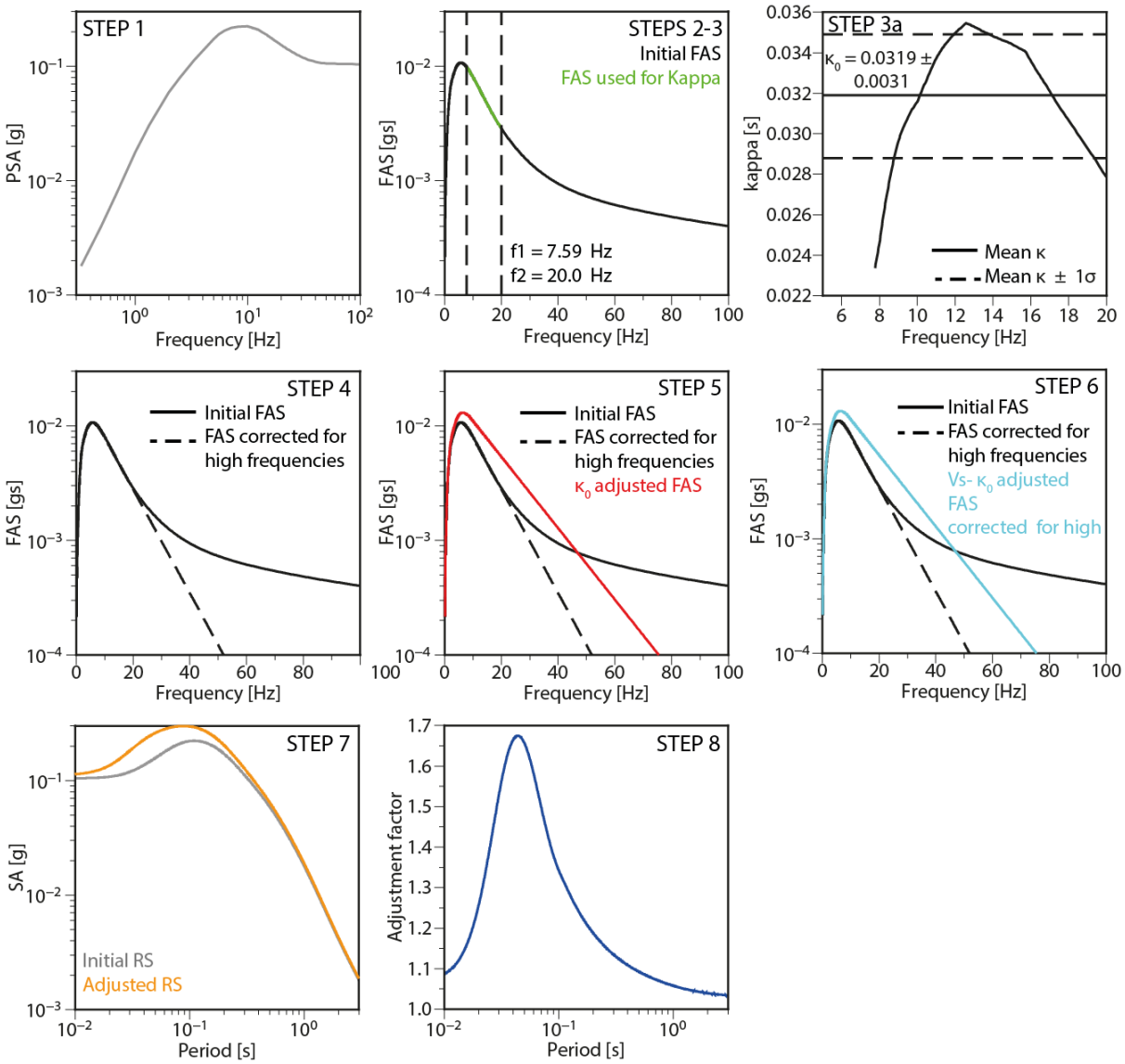

Figure 27: Example of the IRVT for the GMPE of Boore et al. (2014). We used an earthquake scenario of 5.0 Mw, Rjb of 5.0 km, 10 km focal depth, strike-slip faulting and Vs30 = 800 m/s. After Al Atik et al (2014).

6.3.1 Methodology

Here we follow the approach of Al Atik et al. (2014), using IRVT to compute $\kappa_{0,host}$ values and adjustment factors from the response spectra for each GMPE in the GMC model for a number of different earthquake scenarios. This approach is also used to determine Vs-κ_0 corrections for the GMPEs used in the Swiss National Seismic Hazard Maps (Edwards et al., 2016) and for the recent probabilistic seismic hazard assessment for HPC (Tromans et al, 2019).

We used the Quarter Wavelength (QWL) method of Boore (2003) to estimate frequency-dependent site amplification factors for specific Vs profiles for both the target and host. The Vs profiles were either derived from applicable values of Vs30 using the approach of Cotton et al. (2006) or provided by the developer of the stochastic models. We implemented the QWL method using the software provided as part of the *SMSIM* software package (Boore, 2005).

Figure 27 shows how we implement the approach to scale the GMPE of Boore et al. (2014) to a target κ_0 of 0.027 s and Vs30= 800 m/s for the scenario of a magnitude 5.0 Mw earthquake at a Joyner-Boore distance (Rjb) of 5.0 km. The approach can be broken down into the following steps:

1) Compute the response spectra from the GMPE for the selected earthquake scenario and site conditions (i.e. rock site conditions).

2) Convert the response spectra into Fourier amplitude spectra using IRVT. Here, we use the Python software *pyRVT* (Kottke, 2020), which is based on the *Strata* computer program (Kottke and Rathje, 2008) to invert each acceleration response spectrum to a compatible FAS. This uses signal durations defined by a simple regional model.

3) Host κ_0 is computed from the slope in the high-frequency part of the corrected FAS spectra by fitting the Anderson and Hough (1984) κ function in a given frequency range. The lower and upper limits of this frequency range, f_1 and f_2 (green line in Figure 27), are picked by visual inspection to ensure that the natural logarithm of the FAS as a function of the frequency is linear within this frequency range. Al Atik et al. (2014) suggests that f_2 should be smaller than 35 Hz, i.e. the frequency limit of the West United States (WUS) model. PNNL (2014) suggest that f_2 should not exceed 20 Hz for WUS. Here, we use f_2 = 20 Hz, while f_1 equals the frequency for the maximum value of the FAS plus 2 Hz. These frequency limits generally allow us to consider the largest acceptable portion of the corrected FAS to estimate the host κ_0 value. The κ_0 value is the average of the first derivatives of $ln[a(f)]$ between f_1 and f_2 and divided by $-\pi$ (step 3a).

4) If $\kappa_{0,host}$ is greater than $\kappa_{0,target}$ and the frequency is higher than f_1, the FAS is replaced by a straight line fit to the FAS slope between f_1 and f_2 (black dashed line in Figure 27). This step avoids having an increase in the FAS at high frequencies when the kappa corrections are applied.

5) The FAS is multiplied by $exp[-\pi f (\kappa_{0,target} - \kappa_{0,host})]$ where f is the frequency (red line in Figure 27) to obtain the κ adjusted FAS.

6) To adjust the FAS to the target Vs profile, the FAS is multiplied by the ratio between the target-to-host site amplification factors computed using the QWL method (cyan solid line in Figure 27).

7) The Vs-κ_0 scaled FAS is converted into response spectra using RVT (orange line in Figure 27).

8) The Vs-κ_0 adjustment factors are computed dividing the Vs-κ_0 scaled FAS by the initial GMPE response spectra.

We successfully tested our methodology by calculating Vs -κ_0 adjustments for the GMPEs used in the HPC GMC model and comparing these with those calculated by Tromans et al (2019) using the same target and host Vs profiles and the same target κ_0 value of 0.0197 s. Figure 28 shows input response spectra for each GMPE for a scenario earthquake with magnitude 5.0 Mw at a distance of 30 km, uncorrected and corrected Fourier amplitude spectra, and calculated Vs -κ_0 adjustments. Details of the target and host Vs profiles and the target κ_0 value can be found in Tromans et al. (2019). A comparison of Figure 28d with Figure 7 in Tromans et al (2019) suggests that our results show good agreement with those of Tromans et al (2019), with only small differences in the adjustments. This test helps provide some assurance of the methodology that we use for the calculation of the adjustments for a generic UK target.

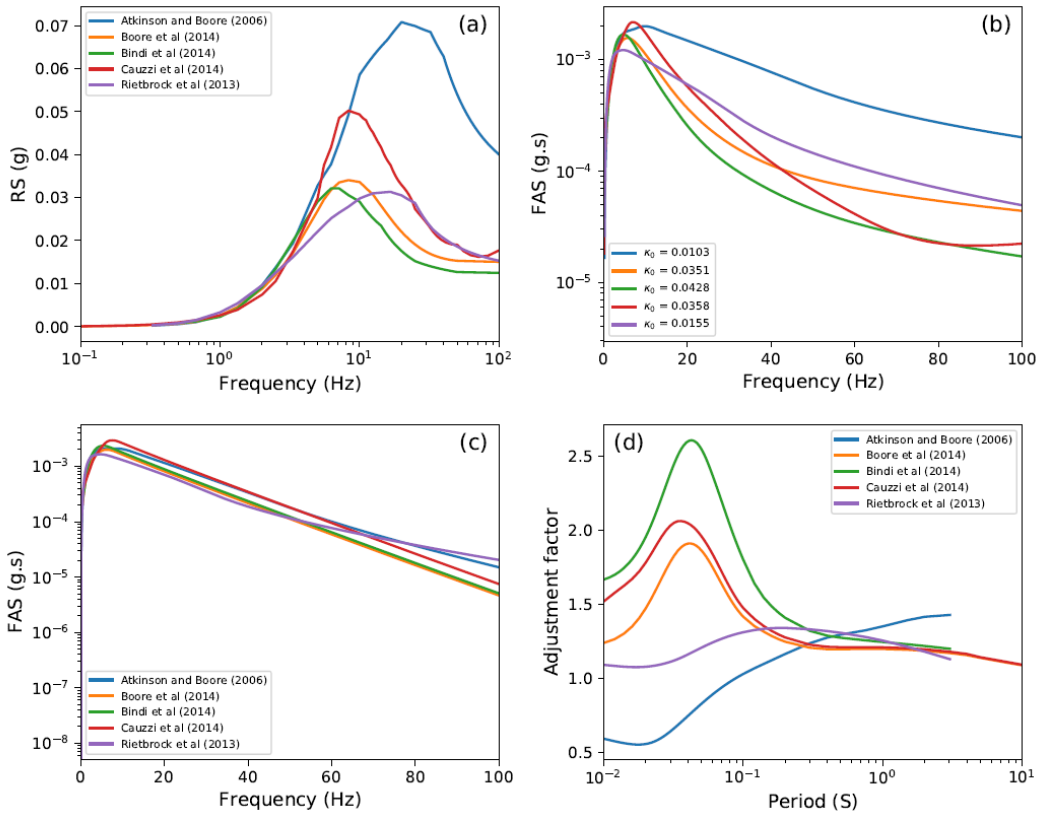

Figure 28: Vs -κ_0 adjustments for the GMPEs used in the HPC ground motion model. (a) Response spectra for each GMPE for a magnitude 5.0 Mw earthquake at 30 km. (b) Compatible FAS for each response spectrum. (c) FAS corrected for Vs and κ_0. (d) Calculated Vs -κ_0 adjustments.

6.3.2 Input parameters

The target Vs30 is 800 m/s across the whole of the UK (see Section 6.2). We use this to estimate the target κ_0 from the empirical relationship between Vs30 and κ_0 derived by Van Houtte et al. (2011). This uses a large number of measurements from both the KiK-net (Kiban-Kyoshin Network; https://www.kyoshin.bosai.go.jp/) and the NGA (Next Generation of Attenuation) database (Power et al., 2008). For our chosen value of Vs30 = 800 m/s, we estimate a value for κ of 0.027 s. We use the standard deviation of 0.55 in $ln(\kappa_0)$ (Van Houtte et al., 2011) to estimate lower and upper bounds for κ_0 of 0.016 and 0.047 s, respectively. This allows us to account for epistemic uncertainty in κ_0, though we do not include any uncertainty in the target Vs30. The three values of κ_0 (0.027, 0.016, and 0.047 s) are assigned weights of 0.6, 0.2, and 0.2 following a three-point approximation to a normal distribution (Miller and Rice, 1983). The best-estimate of κ_0 = 0.027 s is within one standard deviation of the value estimated by Villani et al. (2019), κ_0 = 0.030 s, for rock site conditions (760 ≤ Vs30 ≤ 1100 m/s) using the recordings of ground motions from sites across the UK.

We use the equations specified by Cotton et al. (2006) to derive a generic Vs profile given a value of Vs30. This provides a smooth velocity profile, where the velocities at specific depths are interpolated from the generic models of Boore and Joyner (1997). Between these depths, the velocities are represented by a power law model. The resulting Vs

profile derived for the UK target Vs30 of 800 m/s is shown in Figure 29a. We also use a host Vs30 of 800 m/s for the three empirical GMPEs, Boore et al. (2014), Bindi et al. (2014) and Cauzzi et al. (2015). This eliminates any amplification differences due to the Vs by using the same Vs profile for both host and target. The Vs profile for the GMPE of Rietbrock et al. (2013) is a generic Vs profile for the UK given by Booth et al. (2001). This Vs profile is also shown in Figure 29a.

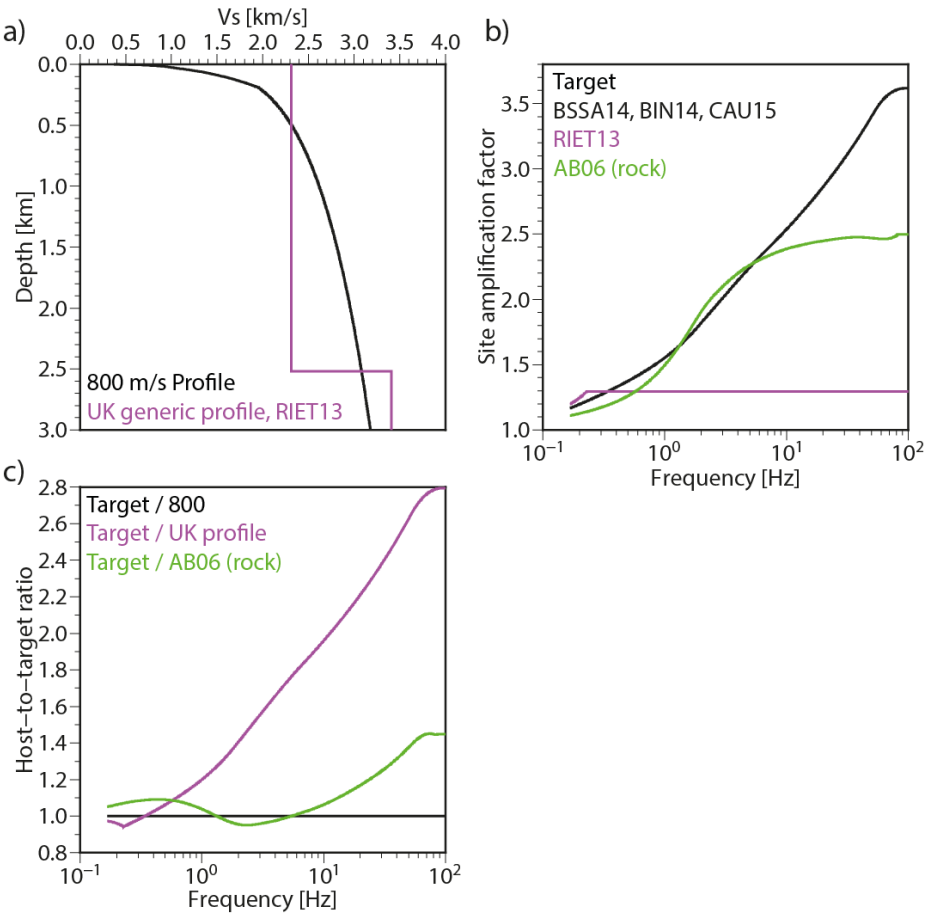

Figure 29: (a) Target and host Vs profiles used for specific GMPEs. (b) Target and host site amplification factors used for each GMPE. (c) Host-to target amplification ratios.

We then apply the QWL method (Boore, 2003) to estimate frequency-dependent site amplification factors for the target velocity profile and the Booth et al. (2001) model. Amplification factors for Atkinson and Boore (2006) are provided by the authors. The amplification factors for all three are shown in Figure 29b as a function of frequency. Figure 29c shows the host-target amplification ratios used for correcting each FAS.

Response spectra are calculated using each GMPE for a number of different earthquake scenarios with different magnitude and distance combinations. These scenarios were selected based on the preliminary disaggregation of the hazard at four sites (Cardiff, Dover, Edinburgh and London), each of which is located in regions with different levels of hazard. The controlling scenarios for the hazard at these sites are listed in Table 9 as functions of magnitude and distance (see Section 7.4 for details on the disaggregation approach). Since the Vs-κ_0 adjustment factors are more important at short distances (≤ 20 km) and high frequencies (> 10 Hz; Al Atik et al., 2014), we selected nine earthquake scenarios based on the disaggregation analysis in the high frequency range: Mw = 4.0,

5.0, and 6.0, and Rjb = 5, 15, and 25 km. The final Vs-κ_0 adjustment for the GMPE is the average from all nine scenarios.

	Short Periods		*Long periods*	
Site	*475 yr*	*2475 yr*	*475 yr*	*2475 yr*
Cardiff	4.5 ≤ Mw < 4.7, 5 ≤ Rjb < 15 km	4.5 ≤ Mw < 4.7, Rjb < 5 km	5.3 ≤ Mw < 5.5, 25 ≤ Rjb < 35 km	5.3 ≤ Mw < 5.7, 5 ≤ Rjb < 25 km
Dover	Mw < 4.1, 5 ≤ Rjb < 15 km	4.3 ≤ Mw < 4.5, Rjb < 5 km	4.9 ≤ Mw < 5.1, 25 ≤ Rjb < 35 km	4.7 ≤ Mw < 4.9, Rjb < 5 km
Edinburgh	4.5 ≤ Mw < 4.7, 45 ≤ Rjb < 55 km	4.9 ≤ Mw < 5.1, 25 ≤ Rjb < 35 km	5.7 ≤ Mw < 5.9, 135 ≤ Rjb < 145 km	5.7 ≤ Mw < 5.9, 135 ≤ Rjb < 145 km
London	4.3 ≤ Mw < 4.5, 25 ≤ Rjb < 35 km	4.3 ≤ Mw < 4.7, 5 ≤ Rjb < 25 km	5.9 ≤ Mw < 6.1, 235 ≤ Rjb < 245 km	5.9 ≤ Mw < 6.1, 225 ≤ Rjb < 235 km

Table 9: Earthquake scenarios identified from the preliminary disaggregation analysis (i.e. without Vs -κ_0 adjustment) at four sites in the UK.

6.3.3 Results

Figure 30 shows the calculated Vs – κ_0 adjustment factors as a function of the period for each of the five GMPEs in the GMC model. These are the average values of all nine scenarios. Calculated adjustments for both the median value and the upper and lower limits in our target κ_0 are shown. The average $\kappa_{0,host}$ values calculated using IRVT for the five selected GMPEs are shown in Table 10. For the three empirical GMPEs (Bindi et al, 2014; Boore et al., 2014; and Cauzzi et al., 2015), the average $\kappa_{0,host}$ values are all similar (~0.350-0.375 s), slightly greater than our target κ_0 value of 0.027 s. The average $\kappa_{0,host}$ values for the two stochastic GMPE's (Atkinson and Boore, 2006; Rietbrock et al., 2013) are both smaller than the target κ_0 value.

GMPE	*$\kappa_{0,host}$ [s]*
Boore et al. (2014)	0.0374 ± 0.0048
Bindi et al. (2014)	0.0375 ± 0.0057
Cauzzi et al. (2015)	0.0347 ± 0.0035
Rietbrock et al. (2013)	0.0102 ± 0.0027
Atkinson et al. (2006)	0.0164 ± 0.0027

Table 10: Average $\kappa_{0,host}$ values for the five GMPEs in the ground motion model.

Overall, we find that the calculated adjustment factors for PGA for the GMPEs in the ground motion model vary between approximately 0.65 and 1.25 for the median target κ_0 value of 0.027 s (Figure 30). Calculated values of the adjustments for a $\kappa_{0,target}$ value of 0.027 s for all five GMPEs converge to approximately 1.0 at longer periods. The

adjustments for all three empirical GMPEs (Bindi et al, 2014; Boore et al., 2014; and Cauzzi et al, 2015) have a similar form, with a peak at 0.05 s and values that decrease at longer periods. The maximum adjustment factor for Boore et al. (2014) and Bindi et al. (2014) is approximately 1.4 - 1.5. For Cauzzi et al (2015), the maximum adjustment factor is approximately 1.2. Applying these host-target adjustments will result in slight increases in the spectral response at periods less than around 1 s. This is consistent with the calculated values for the host κ_0 for these three GMPEs, which are all larger than those for the target rather than elastic amplification, since the host and target Vs30 are relatively similar.

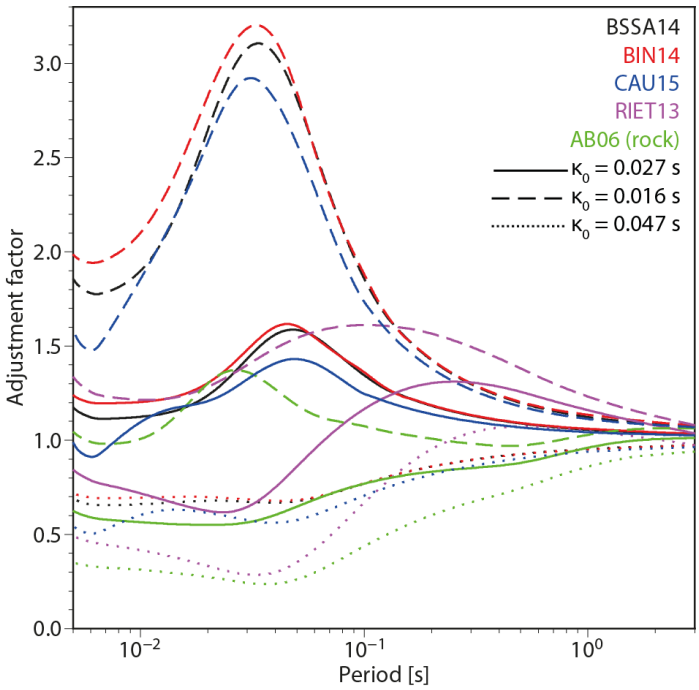

Figure 30: Vs – κ_0 adjustment factors for the GMPEs in the ground motion model. The solid lines show adjustments for the median target κ_0 value, while the dotted and dashed lines show the calculated adjustments for the lower and upper limits of our target κ_0.

We observe notable differences in the period dependent adjustments for the two stochastic GMPEs (Rietbrock et al., 2013; Atkinson and Boore, 2006) with both of these resulting in a small decrease in the original spectral level at the shortest periods. This may be a result of differences in both elastic amplification and κ_0 for the host and target. Specifically, the adjustments for Atkinson and Boore (2006) shows a quite different form, with values of less than 1.0 at periods of less than 1.0 s, resulting a decrease in spectral response at these periods. The adjustment factors for Rietbrock et al. (2013) are also less than 1.0 for periods of less than 0.08 s, but are larger than 1.0 at longer periods, increasing to a peak at approximately 0.2 s before decreasing to around 1.0 at periods of more than 1.0 s.

The calculated adjustments for upper and lower target κ_0 allow us, to some extent, to assess the effect of epistemic uncertainty in our choice of target κ_0 on the results. The adjustments for the lower $\kappa_{0,target}$ value of 0.016 s are consistently larger than those for the $\kappa_{0,target}$ value of 0.027 s, and are greater than 1.0 for all five GMPEs all most periods. Conversely, adjustments for the upper $\kappa_{0,target}$ value of 0.047 s are less than 1.0 for all the GMPEs.

Table 11 shows the adjustment factors for PGA, 0.2 s and 1.0 s only. The reader can read the adjustment factors applied to the other spectral accelerations from Figure 30 and the file containing all the adjustment factors will be made available from the project website (www.earthquakes.bgs.ac.uk). The adjustments for PGA for Boore et al. (2014), Bindi et al. (2014), and Cauzzi et al. (2015) for a $\kappa_{0,target}$ value of 0.027 s are slightly greater than one, indicating a scaling increase. At periods of 0.2 s and 1.0 s, the values decrease to closer to 1.0. For Rietbrock et al. (2013), the PGA adjustment is slightly lower than 1.0 a $\kappa_{0,target}$ value of 0.027 s, but is larger than 1.0 at periods of 0.2 and 1.0 s. Similarly, for Atkinson and Boore (2006), the PGA adjustment is 0.63 and 0.83 and 0.96 for the two longer periods.

	κ_0= 0.027			*κ_0= 0.016*			*κ_0= 0.047*		
GMPE	*PGA*	*0.2 s*	*1.0 s*	*PGA*	*0.2 s*	*1.0 s*	*PGA*	*0.2 s*	*1.0 s*
Boore et al. (2014)	1.18	1.18	1.06	1.86	1.43	1.12	0.69	0.86	0.95
Bindi et al. (2014)	1.24	1.19	1.06	1.99	1.43	1.14	0.72	0.86	0.95
Cauzzi et al. (2015)	0.99	1.14	1.04	1.60	1.38	1.11	0.55	0.82	0.94
Rietbrock et al. (2013)	0.84	1.30	1.16	1.34	1.57	1.23	0.49	0.95	1.05
Atkinson et al. (2006)	0.63	0.83	0.96	1.05	1.01	1.03	0.35	0.60	0.86

Table 11: Vs- κ_0 adjustment factors for PGA and 0.2 and 1.0 s and the GMPEs of the GMC model.

Figure 31 shows the adjustment factors calculated for each GMPE and each scenario earthquake using a target κ_0 value of 0.027 s. This allows us to assess how the adjustments vary with scenarios. We also observe some differences between individual GMPEs for given scenarios. For example, at the shortest periods, the largest adjustments for both Boore et al. (2014) and Bindi et al. (2014) are for smaller magnitudes, regardless of distance. The higher magnitude scenarios result in lower adjustments. For Cauzzi et al. (2015), the results for different scenarios show only minor variations, although the lower magnitude scenarios appear to result in lower adjustments.

In the case of the two stochastic GMPEs, the larger magnitude scenarios also generally require less adjustment at the shortest periods, although distance also plays a role, with larger distance also contributing to a reduction in the required adjustment.

At periods of greater than around 0.07 s, the results are independent of scenario except for Atkinson and Boore (2006). In the latter case, the results for the magnitude 4.0 scenarios diverge from those for the larger magnitude events at around 0.6 s.

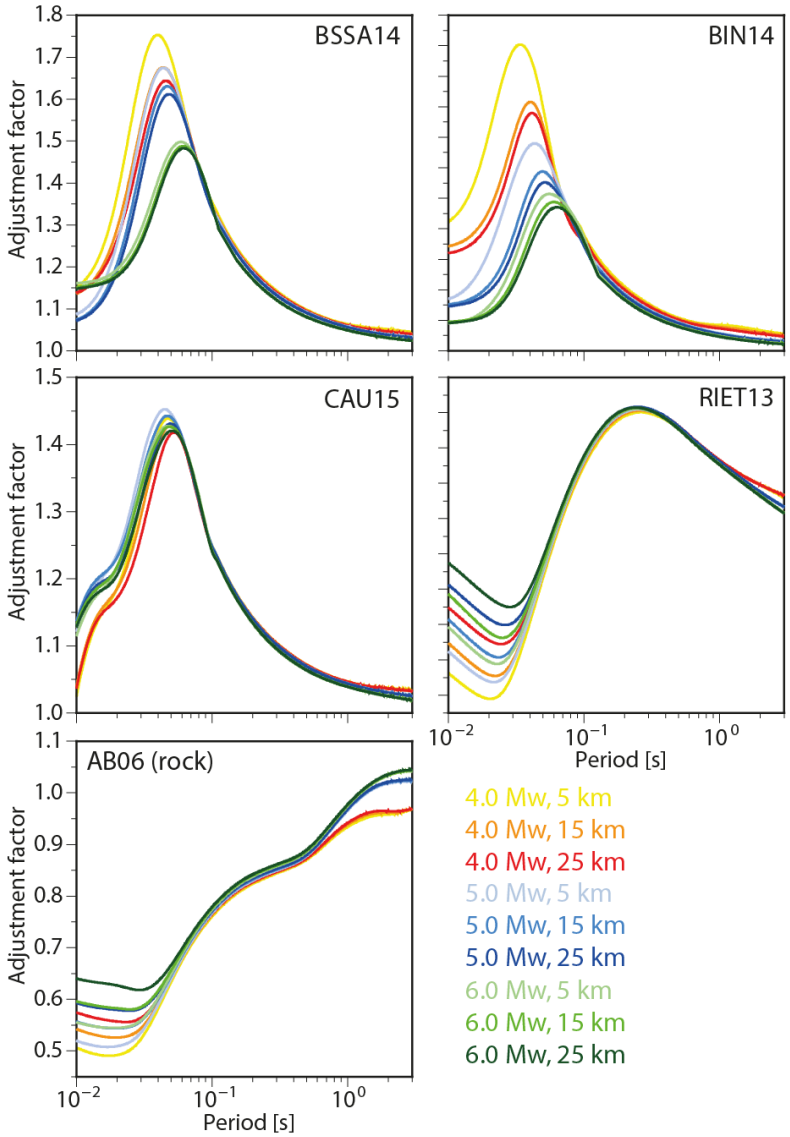

Figure 31: Adjustment factors calculated for each GMPE and each scenario earthquake using a target κ_0 value of 0.027 s.

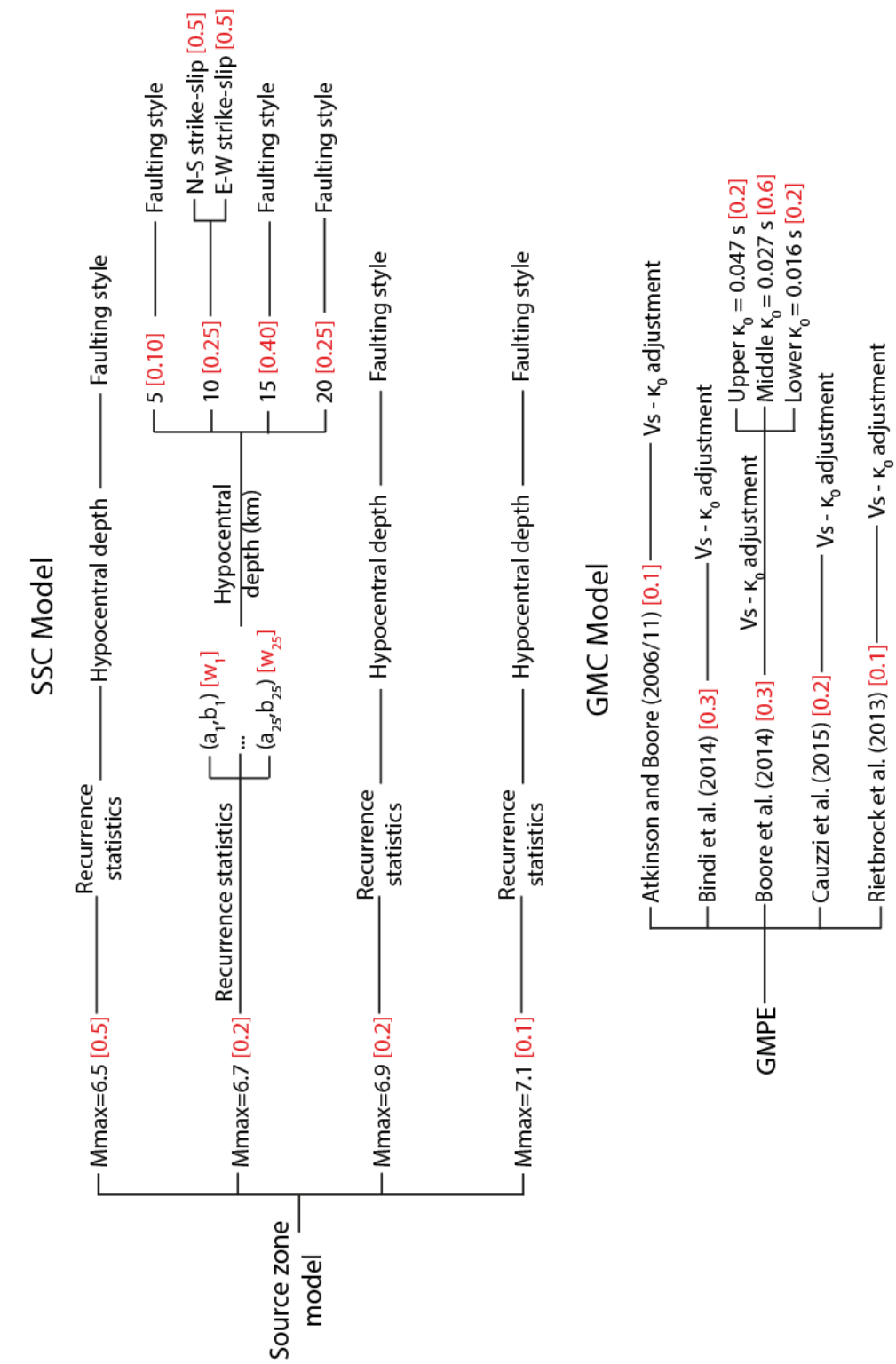

Figure 32: SSC and GMC logic tree for the UK hazard maps.

7 Hazard calculations

Figure 32 shows the SSC and GMC logic trees used for the hazard calculations. Using the Monte Carlo-based approach of Musson (2000, 2012a) encoded in the FORTRAN software M3C, we simulated 100,000 earthquake catalogues, each 100 years long. This means simulating a total of 10,000,000 years of data, which is sufficient to resolve the hazard accurately for return periods of up to 10,000 years. Each simulation samples the logic tree of the SSC model. Then, the ground motion for each event is estimated using the logic tree for the GMC model and "scattered" according to the sigma value, with the lognormal aleatory uncertainty randomly sampled. Following Strasser et al. (2008), we did not truncate the distribution representing the aleatory uncertainty of ground motions. 67% of the synthetic events have epsilon of between -1 and 1; the extreme values are between -4 and -5 (< 0.2% of the simulated events), and between 5 and 6 (around 1% of the simulated data).

Figure 33 shows (N ≥ 3.0 Mw)/yr computed from the catalogue data above the minimum magnitude used in the hazard calculations (i.e. 4.0 Mw) for the individual source zones together with (N ≥ 3.0 Mw)/yr for 100,000 simulated catalogues and provides a check on the implementation of the SSC model in the hazard calculations. It shows that the seismicity simulated using the FMD is being done correctly.

7.1 MINIMUM MAGNITUDE

The minimum magnitude (Mmin) in a hazard calculation is conventionally deemed to be the smallest earthquake of engineering significance. A value of 4.0 Mw is used in this study, which is lower than the value used by MS07 (4.5 Mw). However, we consider 4.0 Mw to be more appropriate because the Folkestone earthquake of 2007, which was relatively small (measured Mw 4.0 ± 0.1 Mw, Ottemöller et al. 2009; 4.0 Mw if converted using Grünthal et al., 2009), caused significant non-structural damage but also some light structural damage in a very few locations (Sargeant et al., 2008). The impact of this earthquake, therefore, demonstrates that earthquakes of this size should be considered in an assessment of hazard for the UK.

The effect of the choice of minimum magnitude on the results is investigated in the sensitivity analysis in section 7.2.

7.2 SENSITIVITY ANALYSIS

The sensitivity analysis is an important tool to show the effect of individual branches of the logic tree and different decisions taken to develop the SSC and GMC models on the seismic hazard. However, there are a number of ways that this could be done. Here, we performed the sensitivity analysis for four sites across the UK: London, Edinburgh, Dover and Cardiff (see Figure 38 for the locations). We tested the effect on the hazard results of using a minimum magnitude of 4.5 Mw (rather than 4.0), the maximum magnitude distribution used by MS07, the assessment of catalogue completeness by MS07, and the SSC model of MS07 (but with a minimum magnitude of 4.0 Mw rather than 4.5). The GMC model of Tromans et al. (2019) was used for each of these tests. We also tested the effect of excluding the Vs-κ_0 adjustments and of using the GMPEs in the GMC model individually.

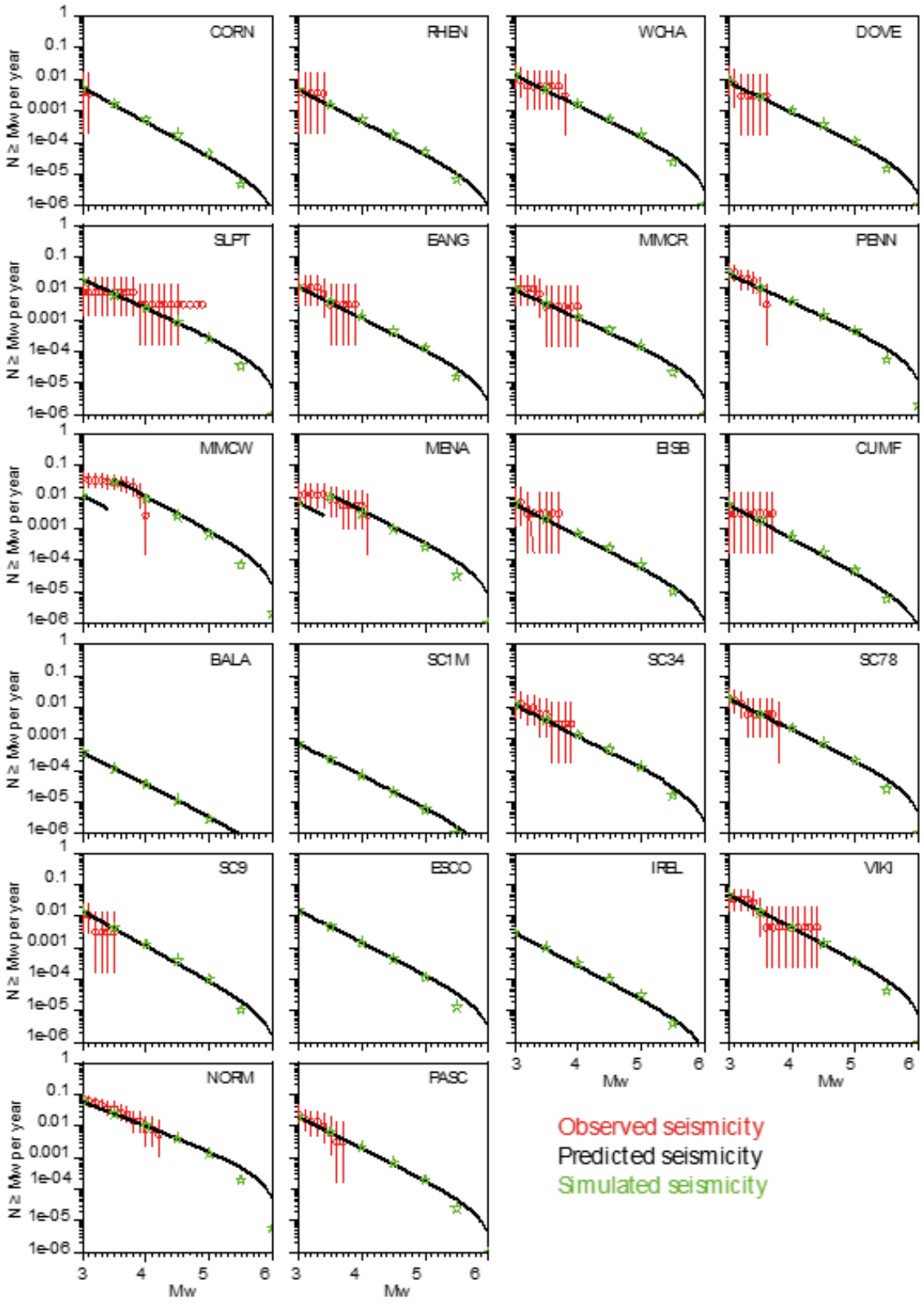

Figure 33: Comparison of the observed FMD (red circles) with the FMD determined from the simulated catalogues (green stars) for the individual source zones of the seismic model. The black line shows the best-fitting Gutenberg-Richter relationship for the observed data.

Figures 34 and 35 show the results in terms of the percentage difference between the values of PGA, 0.2 s and 1.0 s SA hazard for the individual tests and the values in Subsection 7.4 at return periods of 475 yr and 2475 yr, respectively. A percentage difference less than ±5% corresponds to a hazard variation between -0.001 and 0.001 g; whereas a percentage difference < ±20% results in a variation in the hazard between -0.02 and 0.02 g.

For 475 yr (Figure 34) increasing Mmin to 4.5 Mw results in a decrease in PGA and 0.2 s SA hazard (up to 29%) for the sites at Dover, Edinburgh and London. The reduction in PGA and 0.2 s SA for Cardiff and in 1.0 s SA hazard for the four sites is less than 3% because the hazard is dominated by earthquakes of > 4.5 Mw and therefore using a minimum magnitude of 4.0 or 4.5 Mw does not produce any significant difference.

Using the Mmax distribution of MS07 results in an overall decrease in the hazard at all the sites. This reduction is more pronounced for 1.0 s SA because large earthquakes dominate the hazard for long periods. Using the assessment of catalogue completeness by MS07 results in a relatively small (< 14%) reduction in the hazard for PGA, 0.2 s and 1.0 s SA at the four sites. If the SSC model of MS07 is used, there is a significant decrease (50%) in the hazard for London and Dover due to the addition of the source zones NORM and PASC in the 2020 SSC model. There is also a decrease in the hazard for Edinburgh because of differences in the SSC model in Eastern Scotland and offshore. If we exclude the Vs-κ adjustments for the GMPEs in the GMC model, it results in a reduction of the hazard (by up to 20%) for all the sites. Finally, when we use the individual GMPEs in the GMC model, the variation of the hazard is between -50% and 20% with the largest variation associated with Atkinson and Boore (2006) and Rietbrock et al. (2013). These two GMPEs have the lowest weight in the GMC model (see Section 6).
For the 2475 yr return period (Figure 35), the pattern of the observations above is similar although with slightly different variations in the hazard. The largest (> ±20%) variations are for: 1) 1.0 s SA for the four sites using the 2007 Mmax distribution and the 2007 SSC model; 2) PGA and 0.2 s SA for Edinburgh using the 2007 SSC model; 3) PGA, 0.2 s and 1.0 s SA for the four sites using the GMPE of Rietbrock et al. (2013) only; and 4) PGA, 0.2 s and 1.0 s SA for Cardiff and Dover using the GMPE of Atkinson and Boore (2006) only.

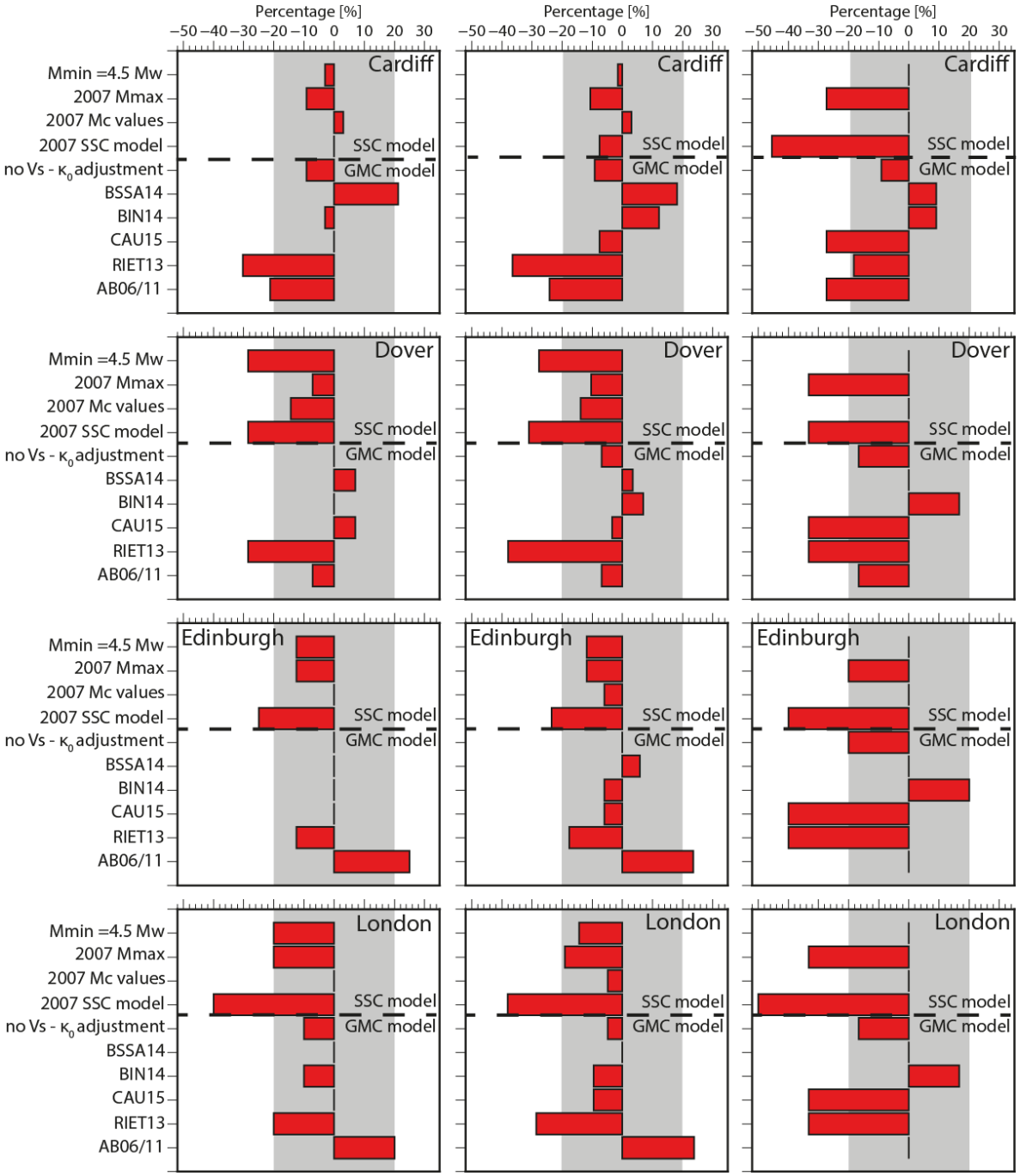

Figure 34: Results of the sensitivity analysis for four sites expressed as the percentage difference between the results computed using the hazard model and the modified model used for each test. Results are for 475 yr return period and three ground motion measures: PGA (left), 0.2 s SA (centre) and 1.0 s SA (right). The grey area describes the variation in hazard of less than ±20%.

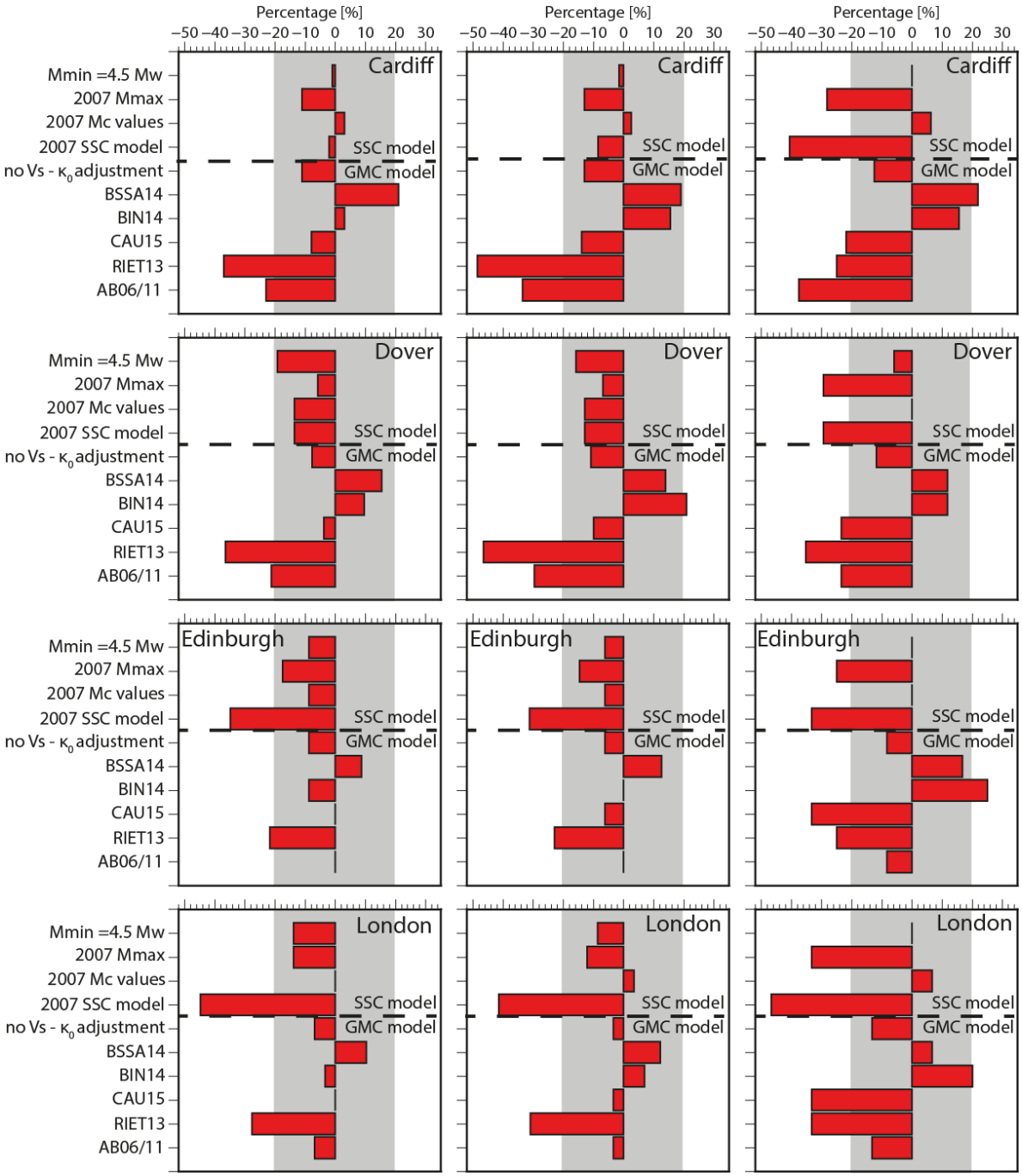

Figure 35: Results of the sensitivity analysis for four sites expressed as the percentage difference between the results computed using the hazard model and the modified model used for each test. Results are for 2475 yr return period and three ground motion measures: PGA (left), 0.2 s SA (centre) and 1.0 s SA (right). The grey area describes the variation in hazard of less than ±20%.

7.3 HAZARD MAPS

The hazard maps cover the region between 49°N - 61°N and 8.5°W - 2°E and the hazard has been calculated for a grid of 4141 points that are spaced 0.125° in latitude and 0.25° in longitude (this is the same grid spacing used by MS07). This corresponds to a spacing of approximately 12 km in both directions. We have estimated the hazard for PGA and spectral acceleration at 0.2 s and 1.0 s for 5% damping on rock (Vs30 = 800 m/s) and for return periods of 475 years (Figure 36) and 2475 years (Figure 37). The seismic hazard maps for return periods of 95 and 1100 years are shown in Appendix 2.

For 475 years, PGA is less than 0.04 g for most of the UK, with the exception of North Wales and the English-Wales border region where the hazard reaches around 0.09 g and 0.05 g, respectively (left panel of Figure 36). A similar spatial variation is observed at 0.2 s but the effects are more pronounced (central panel of Figure 36). These areas of relatively higher hazard are due to source zones with higher levels of seismic activity (i.e. MMCW, MMCR and NORM). At 1.0 s, accelerations are smaller than 0.02 g (right panel of Figure 36) but show less variation across the UK.

For a return period of 2475 years, the Channel Islands, North Wales, the English-Wales border region through to North Central England, the Lake District and NW Scotland are the areas of highest hazard for PGA and 0.2 s (Figure 37). The highest hazard values (0.25 g for PGA and 0.47 g for 0.2 s SA) are observed around the region of Snowdonia, in North Wales.

7.4 RESULTS FOR EXAMPLE SITES

We have also computed the hazard for four sites (Cardiff, Dover, Edinburgh and London) that are located in regions of different levels of hazard. The hazard curves for PGA, 0.2 s SA and 1.0 s SA are shown in Figure 38 and the uniform hazard spectra for 475 yr and 2475 yr are shown in Figure 39. Note that these results should not be considered to be substitutes for site-specific assessments of the hazard in these locations and are only intended to illustrate how the hazard varies across the UK.

We have also disaggregated the results for these sites by magnitude, distance, and epsilon ε (the number of standard deviations above or below the median ground motion prediction), and by zone. The disaggregation analysis aims to identify the earthquakes that control the hazard for the key return periods and can either be done analytically (McGuire, 1995) or empirically (Musson, 1999). The latter is straightforward using the Monte Carlo approach and follows on from the simulations used to compute the hazard. One just searches the synthetic catalogues to find those events that resulted in the design acceleration (plus or minus a small tolerance factor, we use 0.001g here), and then observes their distribution in terms of magnitude, distance, and epsilon. One can also disaggregate the results by zone.

The results are shown in Table 12 and Figures 40-43 for PGA and in Appendix 3 for 0.2 s SA and 1.0 s SA.

Disaggregating by zone for the Cardiff site shows that the hazard is dominated by MMCW2 at 475 yr and 2475 yr for PGA with other zones contributing very little to the hazard. This is the zone that accounts for a second population of earthquakes of 4.5-7.1 Mw in this region. Zones in south-eastern Britain/northern France region control the hazard at the Dover site with by far the biggest contribution coming from zone DOVE. For the Edinburgh site, the largest contributions to the hazard are from zones SC34, SC78 and PENN. Finally, for the London site, zones in southern Britain dominate as would be expected although zone MMCW2 also makes a relatively large contribution.

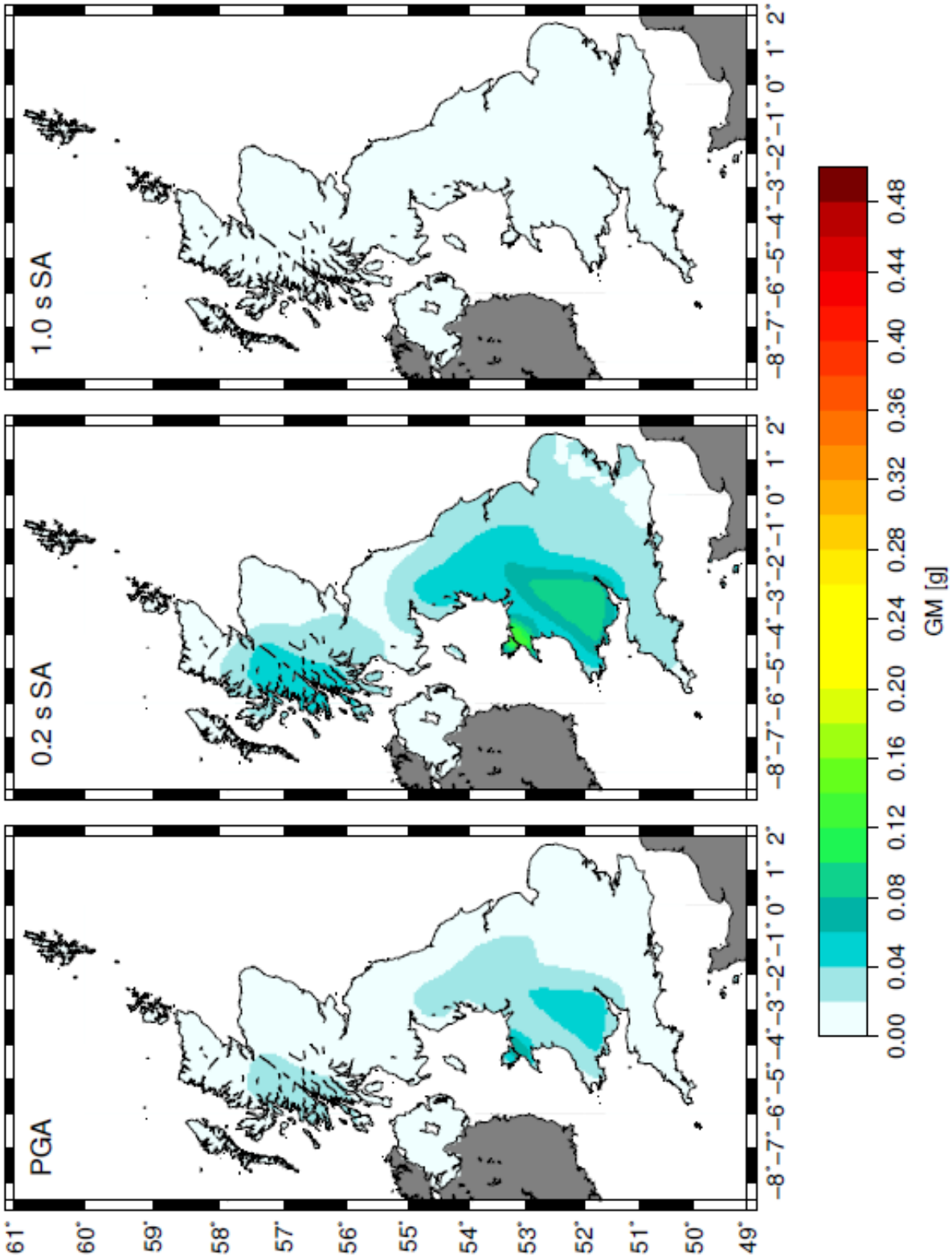

Figure 36: Hazard map for PGA, 0.2 s SA, and 1.0 s SA at the 475 year return period.

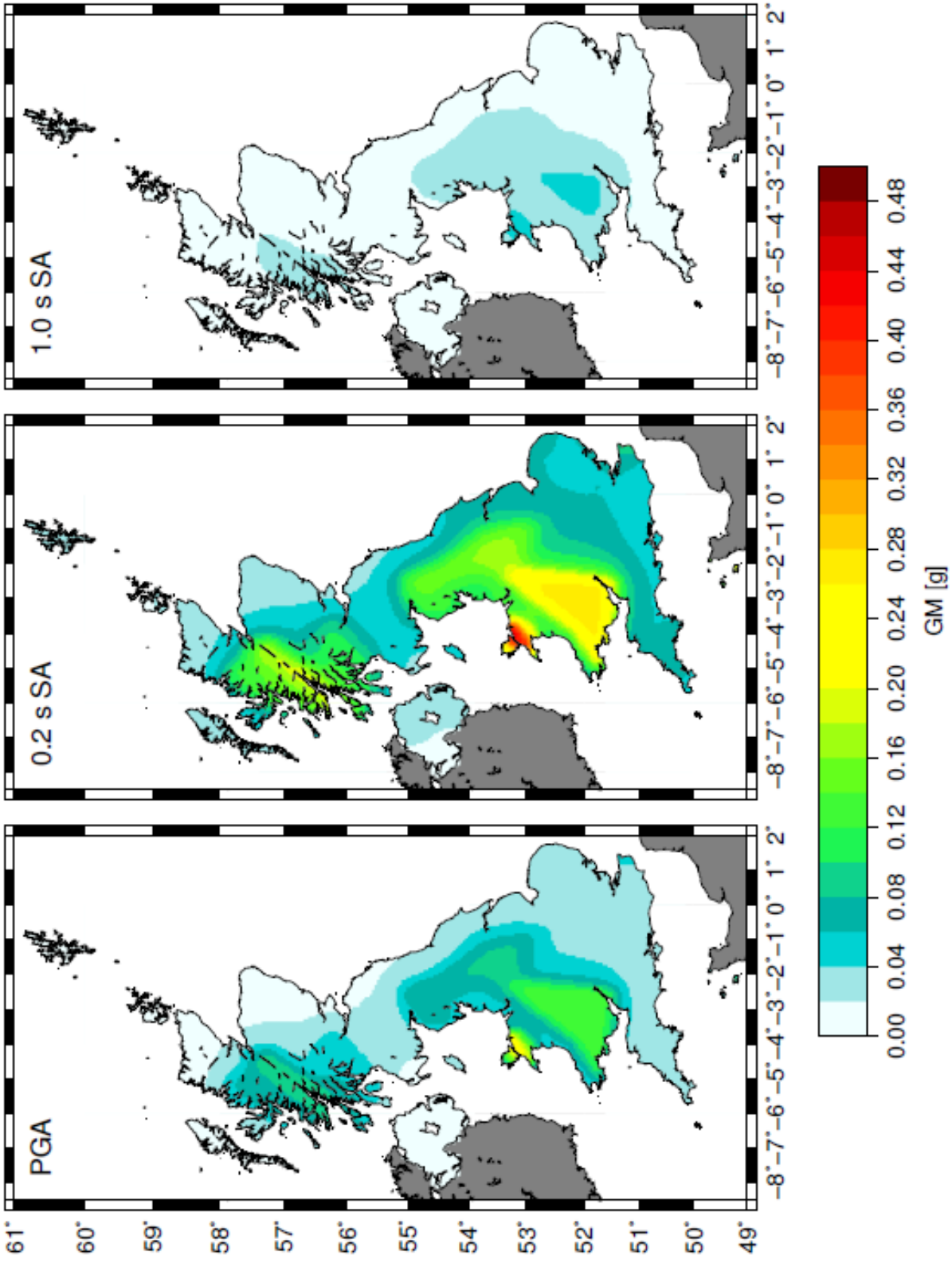

Figure 37: Hazard map for PGA, 0.2 s SA, and 1.0 s SA at the 2475 year return period.

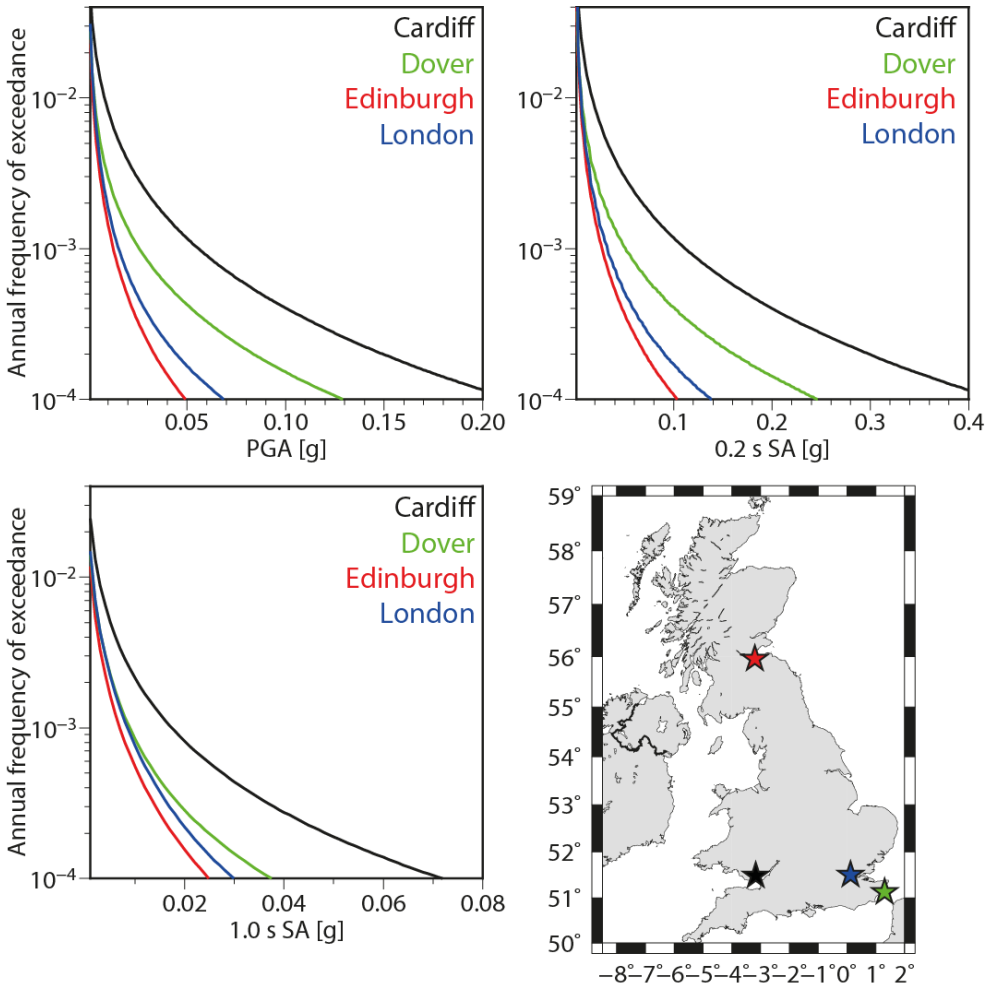

Figure 38: PGA, 0.2 s SA and 1.0 s SA hazard curves for sites in Cardiff (black star), Dover (green star), Edinburgh (red star) and London (blue star).

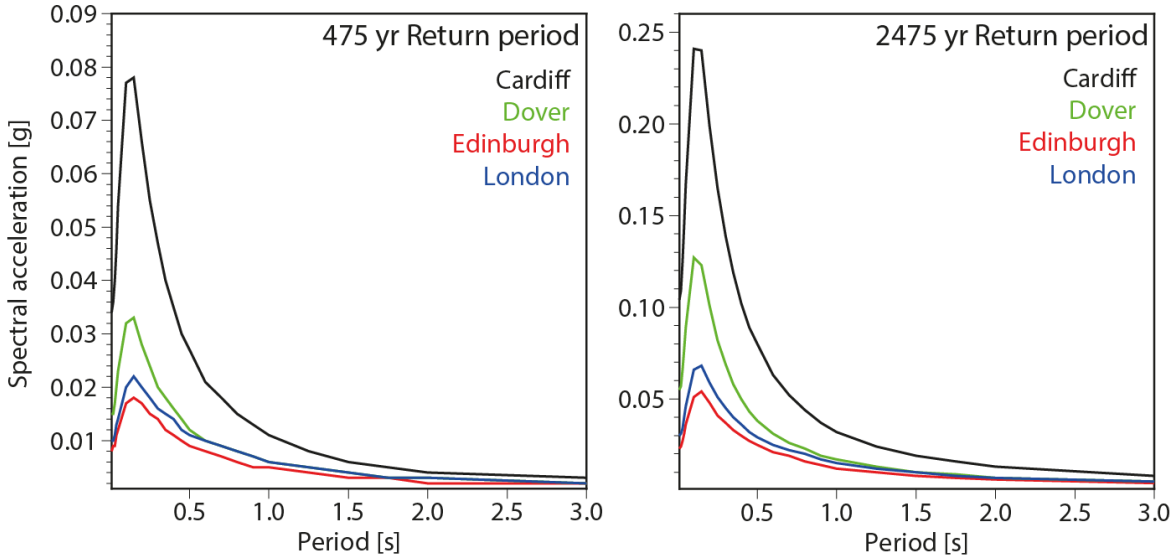

Figure 39: UHS for return periods of 475 yr and 2475 yr for the sites shown in Figure 38.

Disaggregating the hazard by magnitude, distance and ε for the Cardiff site (Figure 40), we observe that at both 475 yr and 2475 yr for PGA, the greatest contribution to the hazard comes from relatively small earthquakes of around 4.5-4.7 Mw and at relatively short distances (< 20 km). The dominance of zone DOVE is evident when the hazard for the Dover site is disaggregated in terms of magnitude, distance and ε (Figures 41). For PGA, there is a single pronounced peak at 4.0-4.1 Mw and distances of 5-15 km for 475 yr and 2475 yr. For the Edinburgh site (Figures 42), a broader range of earthquakes contributes to the PGA hazard (distances of 0-150 km and magnitudes of 5-6 Mw) although there is a peak at 4.3-4.5 Mw and 35-45 km for 475 yr and 4.5-4.7 Mw and 15-25 km for 2475 yr. The hazard at the London site is also dominated by relatively small earthquakes (4.3-4.5 Mw) at short distances less than 40 km) for PGA (Figure 43).

Contribution to hazard [%] for PGA								
	Cardiff		*Dover*		*Edinburgh*		*London*	
Zone	*475 yr*	*2475 yr*	*475 yr*	*2475 yr*	*475 yr*	*2475 yr*	*475 yr*	*2475 yr*
CORN	0.5	0.1	0.0	0.0	0.0	0.0	0.0	0.0
RHEN	3.6	3.0	4.7	4.4	0.0	0.0	5.6	5.2
WCHA	0.2	0.0	5.0	2.0	0.0	0.0	5.2	3.8
DOVE	0.0	0.0	46.9	71.4	0.0	0.0	9.9	7.9
SLPT	0.0	0.0	1.2	0.0	0.3	0.1	2.3	0.8
EANG	0.0	0.0	11.1	8.5	0.3	0.1	16.1	15.0
MMCE	1.0	0.1	6.1	3.3	0.0	0.0	31.5	57.6
PENN	0.1	0.0	0.3	0.0	13.5	10.0	3.7	1.4
MMCW1	7.3	5.3	0.0	0.0	0.0	0.0	0.0	0.0
MMCW2	86.4	91.3	0.8	0.0	0.1	0.0	15.9	4.7
MENA2	0.5	0.1	0.0	0.0	0.3	0.1	0.0	0.0
CUMF	0.0	0.0	0.0	0.0	6.2	4.3	0.0	0.0
BALA	0.0	0.1	0.0	0.0	0.0	0.0	0.0	0.0
SC1M	0.0	0.0	0.0	0.0	10.0	19.3	0.0	0.0
SC34	0.0	0.0	0.0	0.0	37.3	43.5	0.0	0.0
SC78	0.0	0.0	0.0	0.0	17.2	11.4	0.0	0.0
SC9	0.0	0.0	0.0	0.0	6.6	2.7	0.0	0.0
ESCO	0.0	0.0	0.0	0.0	8.0	8.6	0.0	0.0
IREL	0.0	0.0	0.0	0.0	0.2	0.1	0.0	0.0
NORM	0.2	0.0	2.4	0.4	0.0	0.0	4.7	1.4
PASC	0.0	0.0	21.4	10.0	0.0	0.0	5.0	2.1

Table 12: Disaggregation results (by zone) for four sites across the UK and for PGA at 475 and 2475 years.

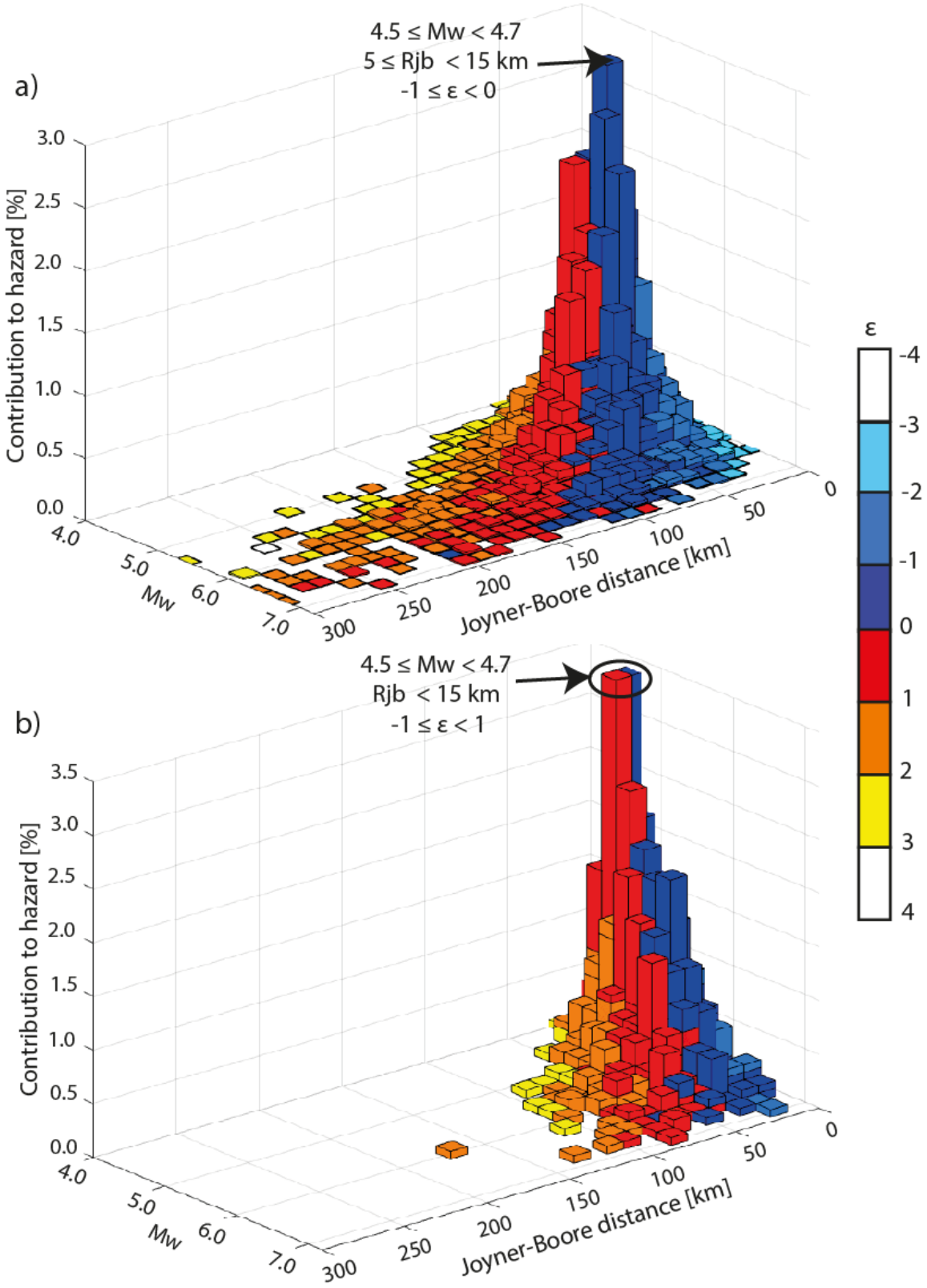

Figure 40: Disaggregation of the PGA hazard for the Cardiff site by magnitude (Mw), Joyner-Boore distance and epsilon(ε) for (a) 475 yr (0.033 g) and (b) 2475 yr (0.100 g). Numbers in brackets are the design values used for the disaggregation.

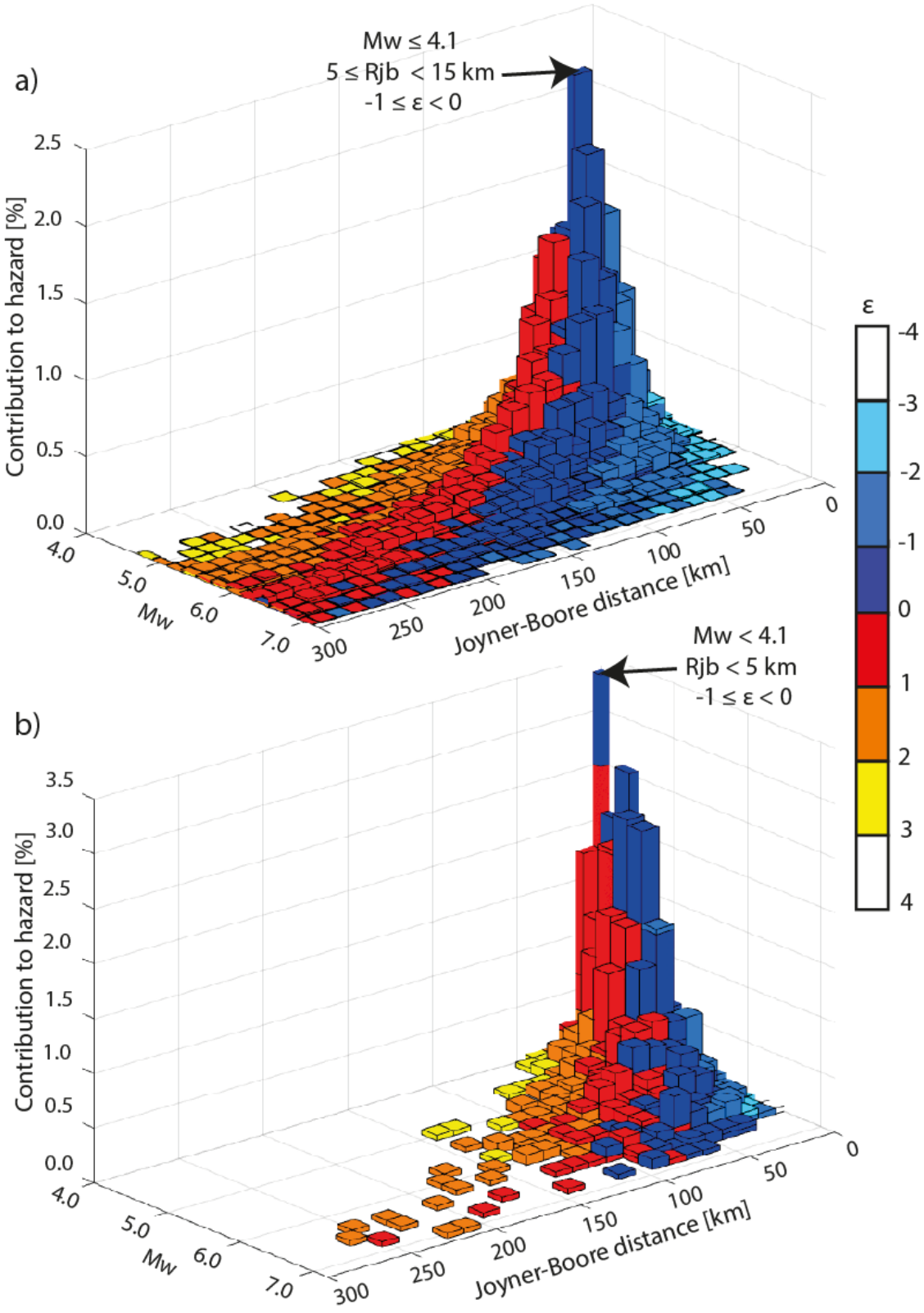

Figure 41: Disaggregation of the PGA hazard for the Dover site by magnitude (Mw), Joyner-Boore distance and epsilon (ε) for (a) 475 yr (0.014 g) and (b) 2475 yr (0.052 g). Numbers in brackets are the design values used for the disaggregation.

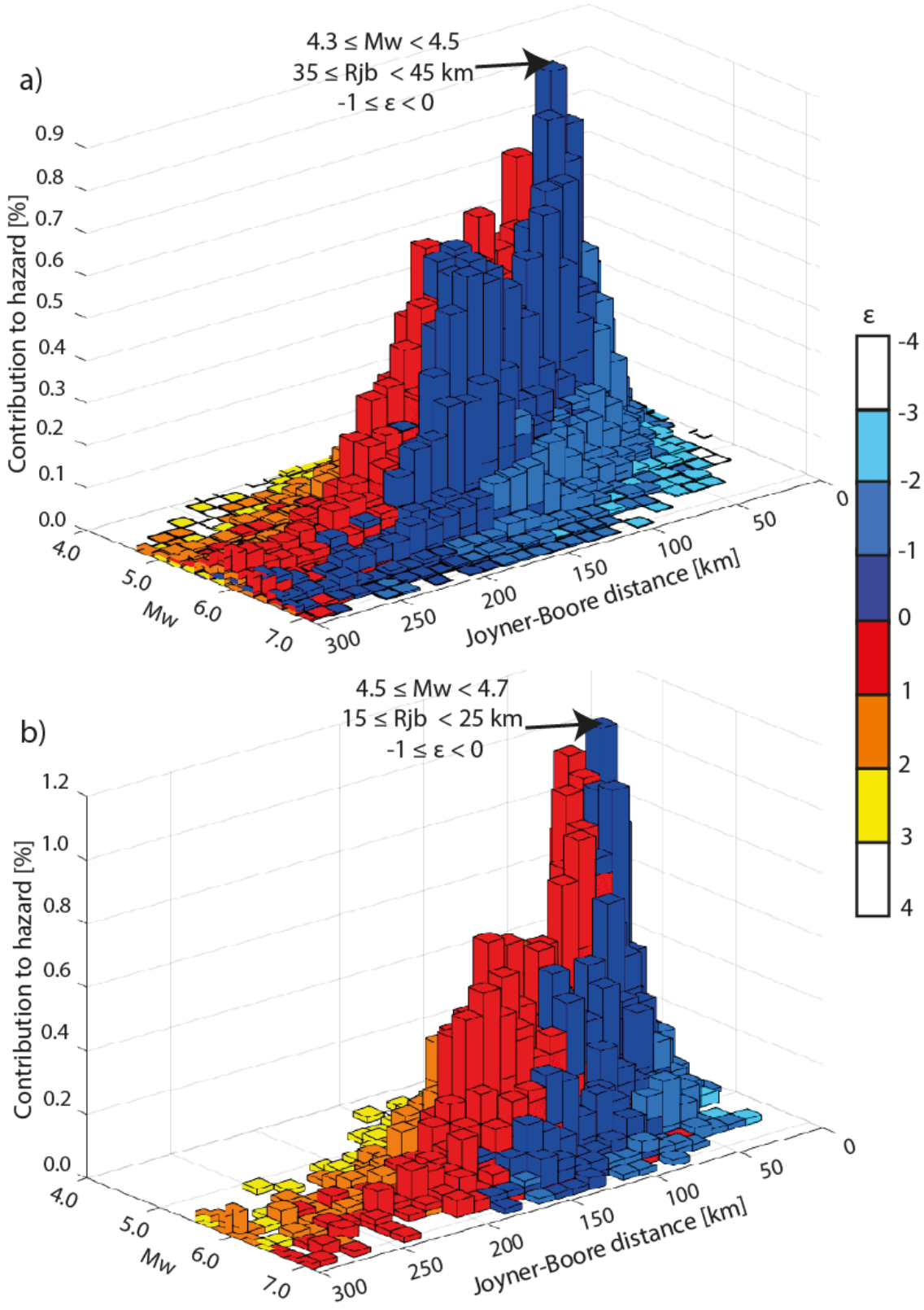

Figure 42: Disaggregation of the PGA hazard for the Edinburgh site by magnitude (Mw), Joyner-Boore distance and epsilon (ε) for (a) 475 yr (0.008 g) and (b) 2475 yr (0.023 g). Numbers in brackets are the design values used for the disaggregation.

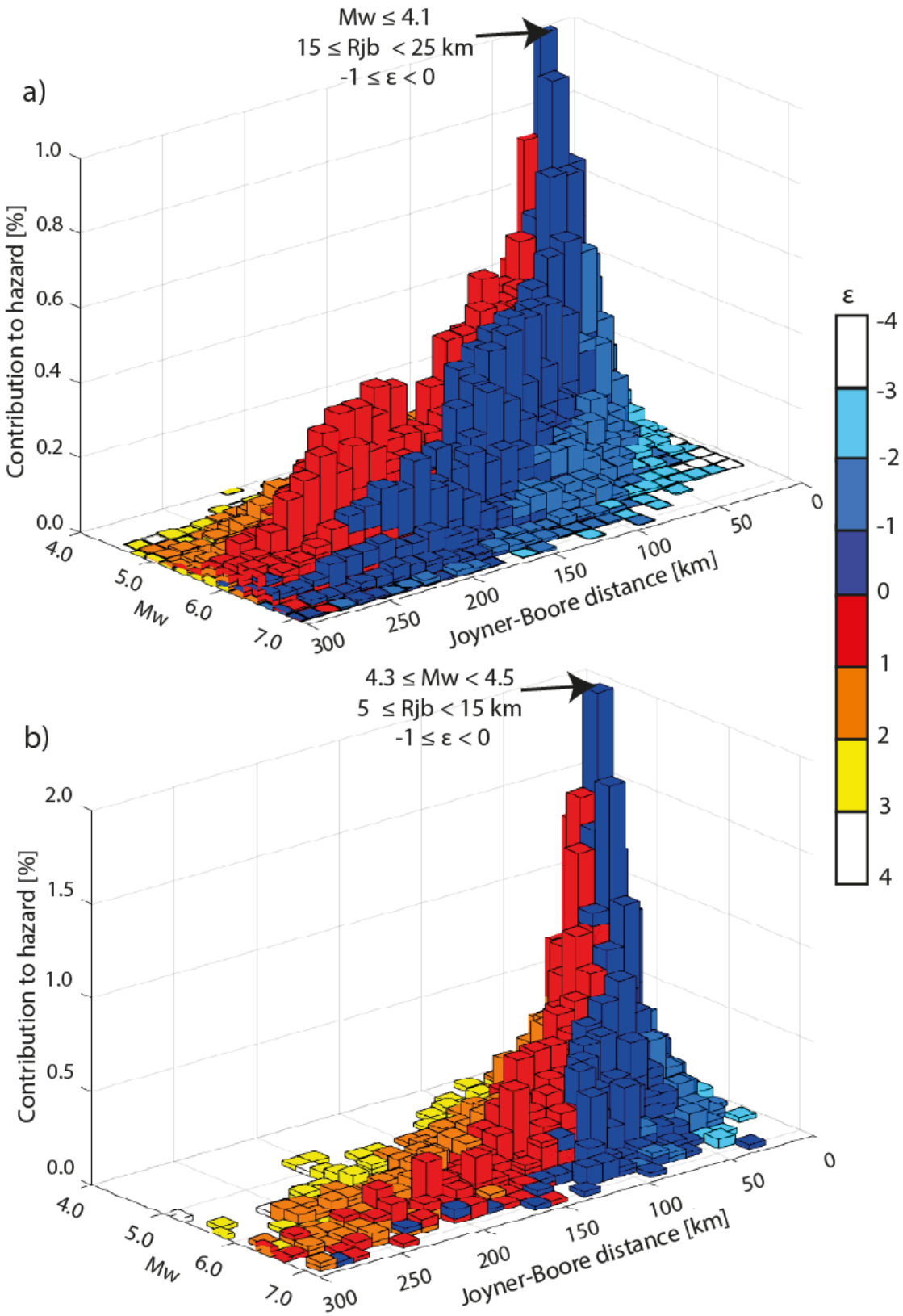

Figure 43: Disaggregation of the PGA hazard for the London site by magnitude (Mw), Joyner-Boore distance and epsilon (ε) for (a) 475 yr (0.010 g) and (b) 2475 yr (0.029 g). Numbers in brackets are the design values used for the disaggregation.

8 Discussion

8.1 COMPARISON WITH PREVIOUS STUDIES

Here, we compare the hazard maps produced in this study with the maps developed by MS07 and Woessner et al. (2015). To aid this comparison, we have calculated the absolute difference between the PGA values at each point for which the maps have been calculated.

8.1.1 Musson and Sargeant (2007)

Both this study and MS07 find that the hazard in the UK is relatively low compared to more active regions. Although many aspects of the models are similar, there are some differences between the results of the two studies. These are shown for PGA at 475 yr and 2475 yr in Figure 44 (we have assumed that the results for 2475 yr and 2500 yr will be practically the same for this comparison). In general, the differences between the maps is not large. For 475 yr, it is between -0.03 and 0.02 g with the more recent study giving slightly lower values in south Wales and the Midlands. The current study produces higher values in mid to north-Wales, along North Central England and in north-west Scotland. Differences follow a similar spatial distribution for 2475 yr although they are larger (-0.07 and 0.10 g).

At 475 years, the hazard in the Great Glen region is slightly higher for this study (0.02-0.04 g). This is probably due to a number of factors relating to the catalogue and completeness analysis rather than zone geometry, which is the same in the two models. The hazard in most of Wales and North Central England that has been computed in this study is also slightly higher, which is probably due to the change in the geometry of the source zones in this region. Note also that MS07 used the magnitude conversion equations of Grünthal and Wahlström (2003), which produce slightly lower estimates of Mw than the equations of Grünthal et al. (2009) that are used here.

For 2475 years, we observe larger differences between MS07 (for 2500 years) and the maps developed in this study. The most noticeable difference is that there is no longer a ‘bull’s eye’ over Comrie in central Scotland. This is because the small source zone SC4H used by MS07 to account for intense earthquake swarms in this area in the past (1795-1801 and 1839-1846) is not included in our model and the seismicity is now accounted for in the larger zone SC34. Around Comrie, the hazard is now lower (0.05 g). Around Snowdonia, the hazard is found to be higher in this study (0.29 g compared to 0.18 g in MS07). There is also a prominent area of relatively higher hazard in South Wales on the MS07 2500 yr map, which does not appear on ours. This is because the seismicity here is no longer modelled as separate zone and is amalgamated into a larger zone (MMCW). This is also the reason that the hazard across Wales is slightly higher in the current study than in MS07. Furthermore, in MS07, the zone for South Wales (V1H in MS07) accounted for a second population of earthquakes of 4.5-7.1 Mw.

One important difference between the model used in this study and that of MS07 is the inclusion of zones NORM and PASC to account for seismicity in northern France and Belgium (see Figure 16). Although the zones have little influence on the hazard in southern England, they do result in higher hazard for the Channel Islands compared to MS07. For Jersey, the PGA values obtained by MS07 are around 0.03 g and 0.07 g for 475 and 2500 years, respectively. In this study, we find that the PGA hazard for Jersey is approximately 0.03 g and 0.10 g for 475 and 2475 years, respectively. We suspect that one reason for this slight increase is the use of the French catalogue for this area, which is probably more complete than the UK catalogue for these two zones and therefore recurrence statistics (and particularly the activity rates) will be more accurately estimated. Furthermore, ML estimates in the French catalogue tend to be higher than estimates from

other agencies for ML < 4.65 (Grünthal et al., 2009), which may have an impact on our results.

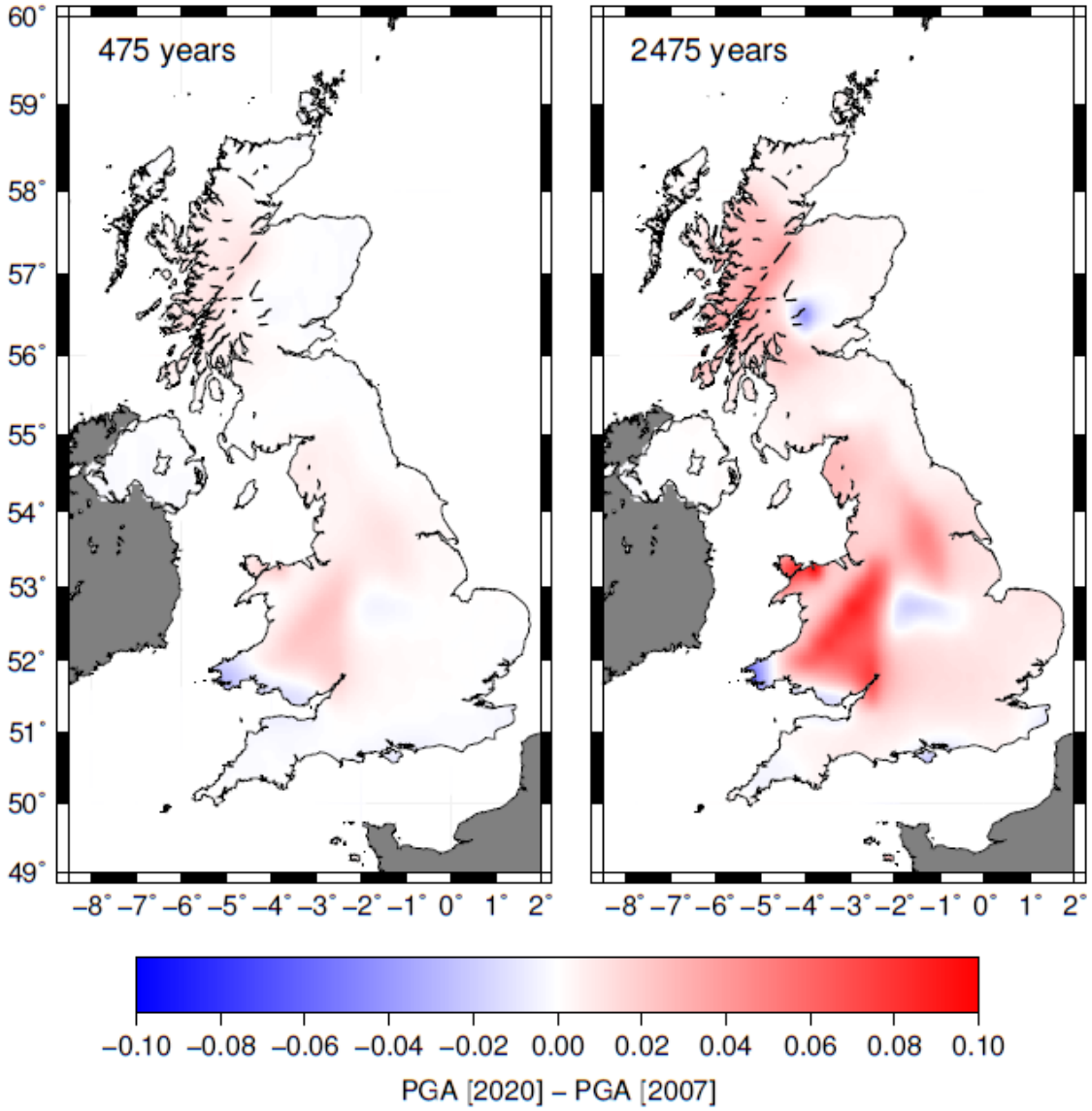

Figure 44: Maps showing the difference between the results of this study (PGA[2020]) and MS07 (PGA[2007]) for return periods of 475 and 2475 yr.

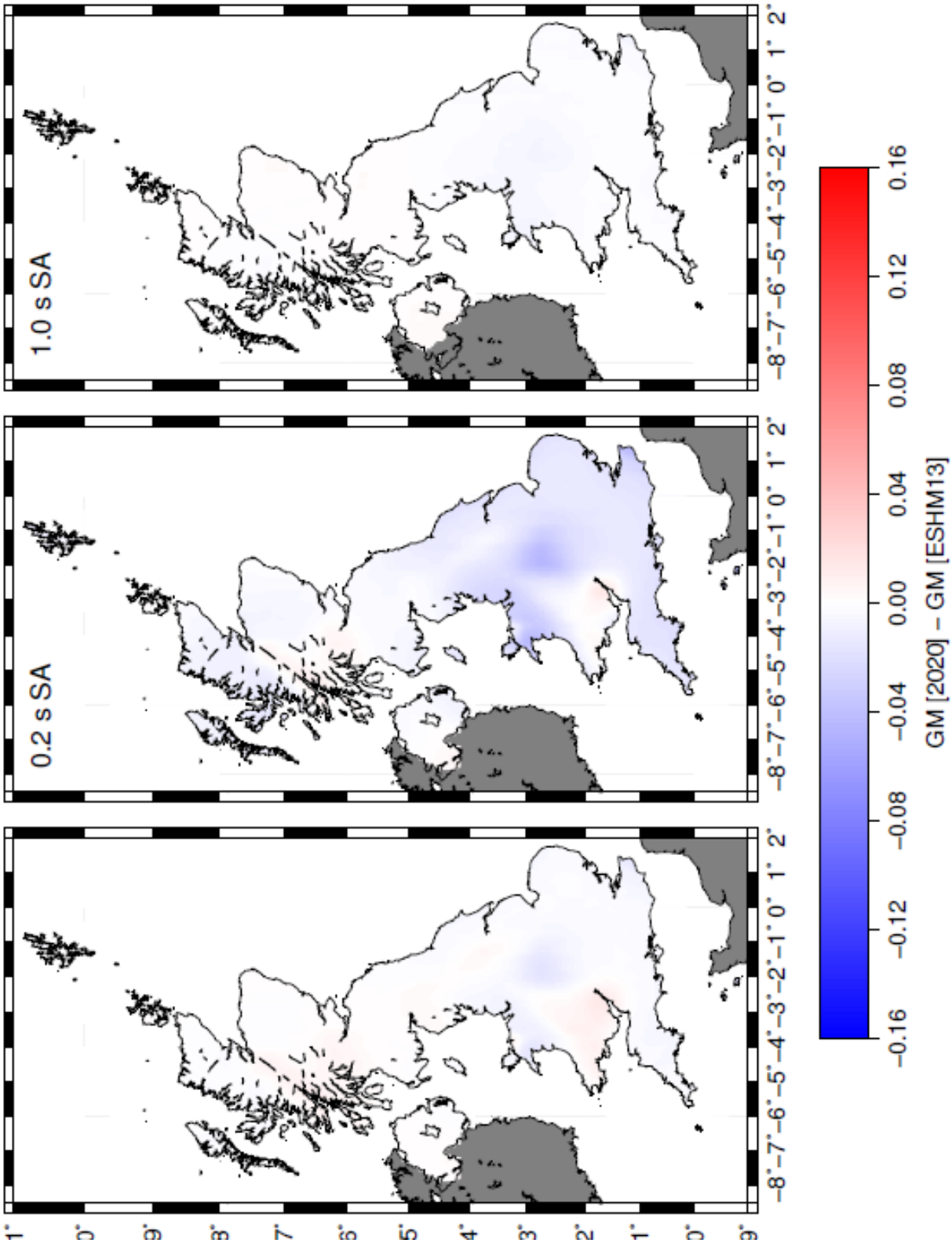

Figure 45: Maps showing the difference between the results of this study (PGA[2020]) and Woessner et al. (2015) (PGA[ESHM13]) for PGA, 0.2 s SA and 1.0 s SA (and a return period of 475 yr).

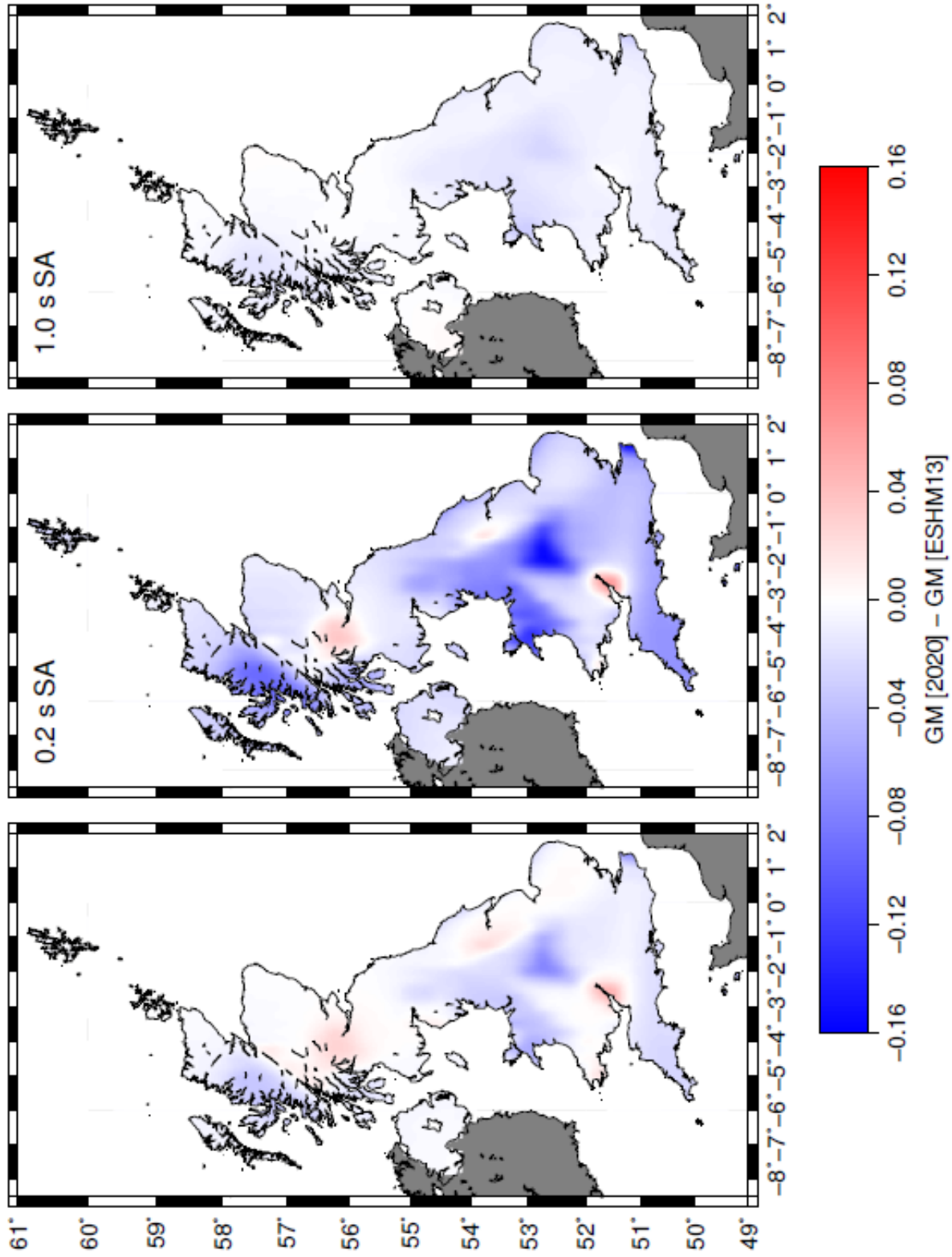

Figure 46: Maps showing the difference between the results of this study (GM[2020]) and Woessner et al. (2015) (GM[ESHM13]) for PGA, 0.2 s SA and 1.0 s SA and a return period of 2475 yr.

8.1.2 2013 European Seismic Hazard Model (Woessner et al., 2015)

The ESHM13 maps developed by the SHARE project (Woessner et al., 2015) cover exceedance probabilities of 1-50% in 50 years and a range of periods for ground acceleration (PGA to 10 s). The results are considered by Woessner et al. (2015) to be an improvement on previous attempts to model seismic hazard in this region because of updated and harmonised databases, standardised procedures, opinions of a large group of European experts from multiple disciplines, and treatment of epistemic uncertainties (Woessner et al., 2015).

The maps in Figures 45 and 46 show the difference in the results of this study and ESHM13 for 475 yr and 2475 yr, respectively. For 475 yr, the differences between the results of the two studies are relatively small for PGA and slightly higher at a spectral period of 0.2 s. The greatest differences are in the English Midlands (-0.02 g for PGA and -0.05 g for 0.2 s SA) and around the Menai Strait (-0.02 g for PGA and -0.05 for 0.2 s SA). For 0.2 s SA, there a general tendency across England for ESHM13 to give higher values (up to 0.02 g higher). At 1.0 s spectral period, the two maps are very similar with only very small differences (less than 0.01 g) between the two maps. For 2475 yr, the ESHM13 results are generally higher than this study and follow a similar spatial distribution to the differences at 475 yr. However, the magnitude of the differences is higher - the ESHM13 results are up to 0.14 g, 0.16 g and 0.06 g higher for PGA, 0.2 s and 1.0 s, respectively. However, there are also areas where the hazard results from this study are higher than the ESHM13 results for PGA and 0.2 s: central Scotland, south-east Yorkshire and at the head of the Bristol Channel (up to about 0.02 g). The difference between the maps is not surprising given that most elements of the models used in the hazard assessments are different.

8.2 LIMITATIONS OF THE PRESENT STUDY

In any study, the resources available limit the extent to which certain aspects of the model or the data on which it is based can be explored. Therefore, our approach has been to try to balance what is necessary to produce the new maps in as rigorous a way as possible with what is achievable with a small team over a relatively short time period. However, there are some important limitations relating to different aspects of the model, which are outlined below.

8.2.1 Catalogue

There are some differences between the BGS and FCAT-17 earthquake catalogues that become apparent when they are merged. First, for common events that appear in both catalogues, the Mw determination in FCAT-17 is generally higher than the Mw calculated for the same event from the ML determination in the BGS catalogue (e.g. the earthquake in the Channel Islands on 23 April 1773 has a magnitude of 4.1 Mw in the BGS catalogue and 5.2 Mw in FCAT-17; an earthquake in Brittany on 2 January 1959 has a magnitude of 5.1 Mw in the BGS catalogue and 5.4 Mw in FCAT-17). Furthermore, FCAT-17 contains a surprisingly high number of earthquakes of 3.0-5.0 Mw (234 events from 842 to 1992) in northern France.

The completeness analysis of FCAT-17 by Drouet et al. (2020) suggests that we may be including a small part of the incomplete portion of this catalogue in the computation of the recurrence statistics. If the data from FCAT-17 are excluded and source zones PASC and NORM are removed from the model, very little changes with respect to the hazard on the south coast of England (Figure 47). Unfortunately, by doing this, the Channel Islands are excluded from the national hazard model. For this reason, we decided to include data from FCAT-17, together with zones PASC and NORM but we recognise that further work is necessary to address these issues if the BGS and FCAT-17 catalogues are used together in future studies.

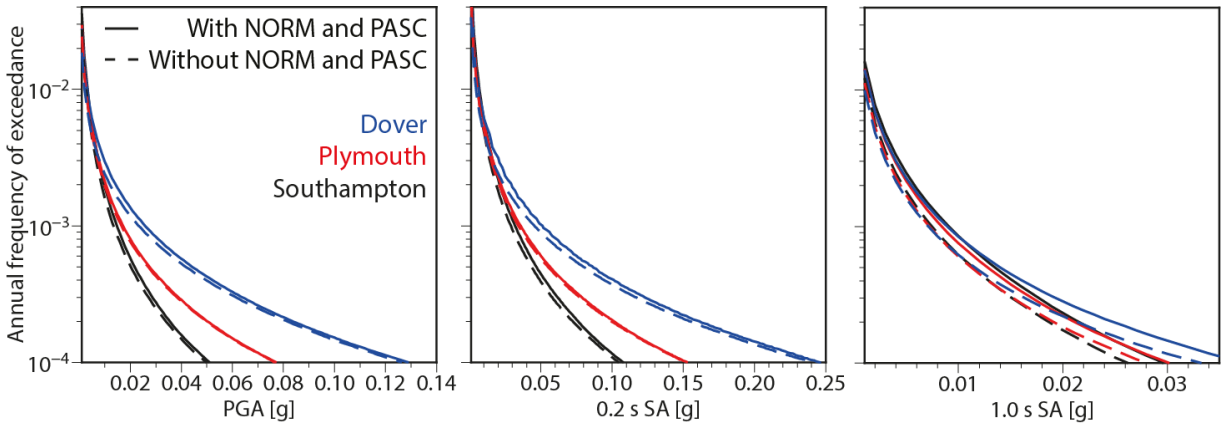

Figure 47: Hazard curves for PGA, 0.2 s SA and 1.0 s SA for sites in Southampton, Plymouth and Dover using the whole seismic source model (see Section 5.1) but excluding the source zones NORM and PASC.

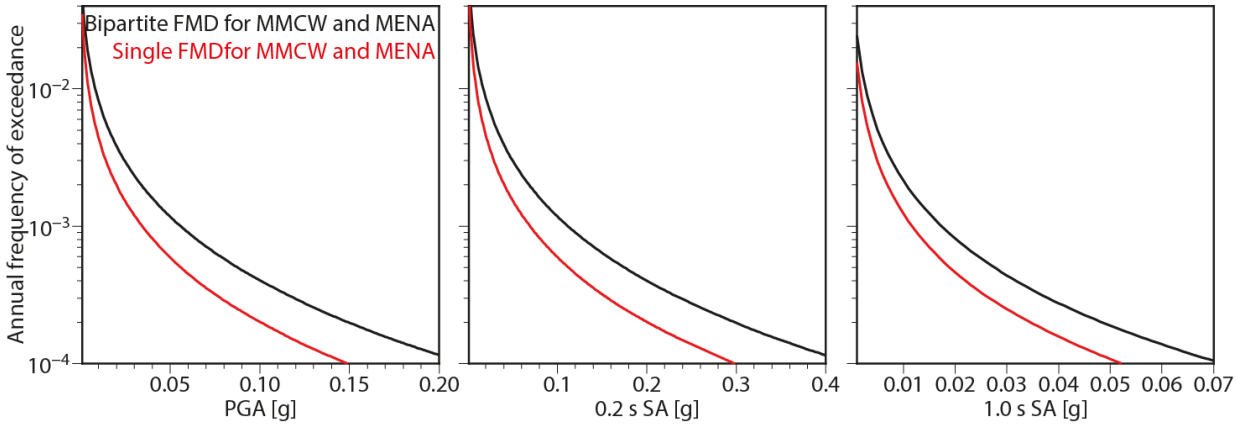

Figure 48: Hazard curves for PGA, 0.2 s SA and 1.0 s SA for the Cardiff site using the bipartite FMD and the single FMD for the source zones MENA and MMCW (see Section 5.3).

A further limitation is that the uncertainty in Mw has not been included when estimating the FMD. This uncertainty consists of two terms: the first is the uncertainty from the original magnitude determination (ML in most cases but also a few mb values for the earthquakes from the ISC database); and the second accounts for the conversion from the original magnitude to Mw. The uncertainty in ML is not assessed throughout the BGS earthquake catalogue. Especially for historical events, this is not straightforward because the ML values for the historical earthquakes result from the conversion of macroseismic intensity data and therefore a third term due to the conversion from intensity into ML should be accounted in the overall Mw uncertainty. The original magnitude in the ISC database does not have an associated uncertainty. Musson (2012b) demonstrates that careful considerations should be taken when the magnitude uncertainties are accounted for in the recurrence statistics, especially when the earthquake catalogue merges many sources and contains more than one original magnitude scale, to avoid over- or underestimation of the activity rate and therefore of the seismic hazard. We recognise that a robust and homogeneous assessment of the magnitude uncertainty in the UK earthquake catalogue must be undertaken in the future.

The model developed in this study is based on a relatively short catalogue, certainly compared to geological time scales (e.g. Stein et al., 2012) and provides only a partial indication of the nature of the seismotectonic environment here. However, although it is possible (and perhaps probable) that the largest earthquake that could occur in the UK does not appear in the catalogue, the maximum magnitude distribution should account for what could potentially happen. A bigger issue is the uncertainty associated with the recurrence statistics. The impact of the limited amount of data and the lack of observations of large (Mw ≥ 6.0) earthquakes is illustrated in Sections 5.2 and 5.3. The 368 year length of the seismic record is significantly shorter than the recurrence interval for the potentially largest earthquakes and is associated with a large uncertainty.

A further limitation is that the locations and magnitudes of historical earthquakes in the UK catalogue are associated with significant uncertainties, particularly for poorly reported events. This is a particularly important issue in zones MMCW, MENA and SC78 where there have been significant historical earthquakes but relatively little recorded seismicity since (see Section 4.2). This has implications for the decision to model the seismicity in MMCW and MENA using the bipartite FMD. The aim of using the bipartite FMD is to better model the available observations of moderate earthquakes in these zones. However, there are significant uncertainties associated with this decision because the locations and magnitudes of the reported earthquakes will be poorly constrained and the length of the catalogue is relatively short. If we use a single FMD rather than the bipartite FMD for MMCW and MENA, the hazard for sites within these zones is lower (Figure 48) because the activity rate is underestimated for earthquakes Mw ≥ 4.5 (Figure 16). Therefore, we decided it was more conservative to use the bipartite FMD rather than underestimate the hazard in this region (i.e. Wales), which is one of the most active areas of the UK.

8.2.2 SSC model

There is considerable epistemic uncertainty associated with our understanding of the seismotectonics of the UK region and the location and character of the structures on which observed seismicity occurs. The model used in this study is an attempt to combine current understanding of the structure of the Crust, mapped structures, large scale deformation, the regional stress field along with observed seismicity. However, this remains a single interpretation of the available information and other possible explanations undoubtedly exist. As a result, our single SSC model may not capture the full extent of the epistemic uncertainty. The inclusion of a zoneless model or alternative zonation models would go some way to better capturing the epistemic uncertainty (see Section 5.1) and we suggest that this should be explored in future. However, true progress in this area is likely to require significant advances in our understanding of the driving forces of deformation and how this interacts with crustal faulting on different scales.

One could argue that the extent of the study area is too small for the effects of distant large earthquakes to be accounted for in the hazard at longer spectral periods (i.e. 1.0 s or more). However, for the return periods here, these events are unlikely to make a significant contribution to the hazard, which is generally dominated by earthquakes around 4-5 Mw at relatively short distances, as shown by the disaggregation results.

We also note that the uncertainty in the fault parameters is not incorporated in the modelling. The orientation of the faults on which the simulated ruptures occur is fixed to be either north-south or east-west strike-slip faulting (equally weighted) but this is consistent with many focal mechanisms that have been determined for UK earthquakes although applying it across the study area (including the Viking Graben and north-western Scotland) is probably an oversimplification of the situation. Furthermore, uncertainty in the computed rupture parameters is not accounted for in the calculations. Both points should be addressed in future. However, we do not expect this to have a significant impact on

the results presented here because most of the simulated earthquakes are relatively small.

8.2.3 GMC model

The GMC model has a number of significant limitations. Besides the uncertainties associated with magnitudes and locations in the catalogue, there is also significant epistemic uncertainty regarding the nature of earthquake ruptures for UK earthquakes and presumably a high degree of aleatory variability if the wide range of stress drop estimates determined for UK earthquakes is an indication. This will have an effect on ground motion and is not accounted for in this study. The lack of ground motion observations for UK earthquakes also presents a serious challenge. It results in uncertainty in the selection of GMPEs and limits which methodologies can be implemented. Had more strong ground motion data and stress drop estimates been available for the UK region, implementation of a backbone approach might have been an option for this study.

For the Vs – κ_0 adjustments to the GMPEs in the GMC model, we use a single generic shear wave velocity profile for the UK target. However, it is possible that multiple profiles with the same Vs30 of 800 m/s could lead to different amplification functions. Further work is needed to better assess the suitability of our generic target profile. This has a rather gradual increase in Vs as a function of depth, whereas existing velocity models for the UK have profiles that are much rougher and lack resolution in the near-surface, so are unlikely to capture the actual variation in shallow shear wave velocities. The general UK velocity model for earthquake location (Booth et al, 2001) and used by Rietbrock et al. (2013) was derived for Central Scotland using data from the lithospheric seismic profile in Britain (LISPB), a north–south profile through Scotland and northern England (Bamford et al. 1978). Velocity models (see Figure 49) have also been developed for other parts of the UK using data from refraction experiments (Bott et al, 1985; Edwards and Blundell, 1984) and passive seismic data (Hardwick, 2008; Booth, 2010; Luckett and Baptie, 2015). We suggest that further work is needed to examine variability in Vs in the near-surface to better understand how this could affect the results and provide better constrained models.

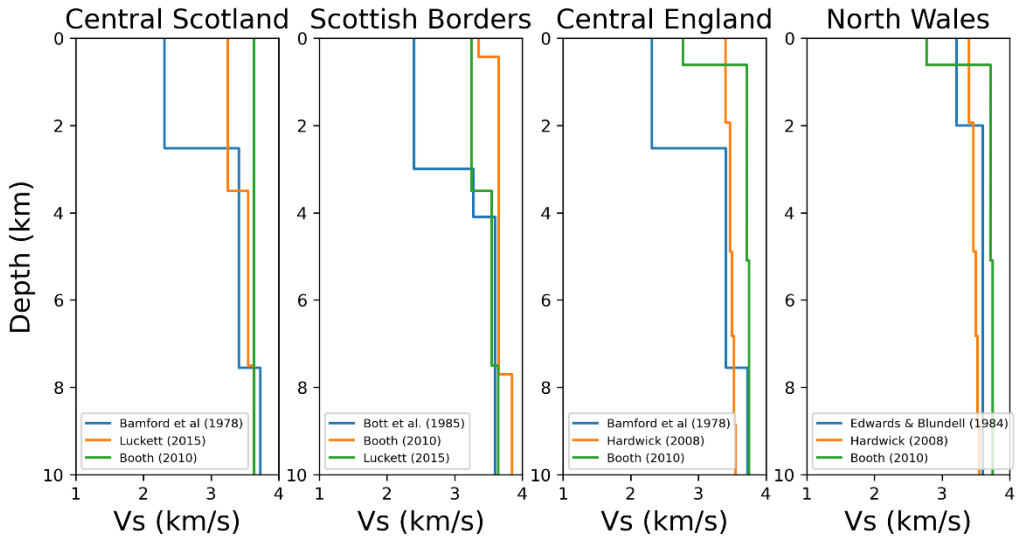

Figure 49. Velocity models derived for Central Scotland, the Scottish Borders, Central England and North Wales using either refraction experiments or passive seismic data.

Finally, we calculate average adjustment factors for a range of different scenarios selected from disaggregation analysis. The results for different scenarios suggest some dependence of the adjustment factors with magnitude and distance. Zandieh et al. (2016) also find that estimates of κ calculated for a wide range of magnitudes using IRVT from the NGA (Next Generation Attenuation) – West 2 ground motion models show magnitude dependence. However, Stafford et al. (2017) suggest that this apparent magnitude dependence results from compensation for the fact that the generic scenario-independent linear site response in the ground motion models will typically overestimate the amplification at small magnitudes and underestimate amplification at larger magnitudes.

8.2.4 Hazard Computations

These computations have not been checked with software besides M3C. However, M3C has been compared with other codes and produces the same results given the same input (Musson, 2012a; Mosca, 2019).

The implementation of the individual GMPEs in M3C has been checked against the ground motion library implemented in the software OpenQuake (Pagani et al., 2014).

9 Conclusions

Revised seismic hazard maps for the UK have been developed using a Monte Carlo approach. This study incorporates updated datasets and some of the advances made in seismic hazard methodology and ground motion modelling since 2007. The results show that seismic hazard in the UK is generally relatively low, consistent with what MS07 found. The work has identified important areas for further research, which would help to better understand and characterise the significant epistemic uncertainties associated with the model on which the maps are based. This includes the questions raised by trying to integrate the BGS and FCAT-17 catalogues and the need for further work to better understand the connection between the spatial distribution of the seismicity and what is known about the tectonics of the UK.

We stress that the new hazard maps provide a general indication of the relative levels of seismic hazard across the UK only and are not a substitute for a site-specific assessment if one is required. When assessing hazard for a specific site, modelling decisions are made with respect to that site and no other. For a map, the SSC model has to serve an entire country; it is common that a decision made one way raises the hazard at site A with respect to site B, and made the other way has the reverse effect – see the discussion in MS07 and also Reiter (1990).

All of the input data and elements of the model described in this report will be freely available from www.earthquakes.bgs.ac.uk as will the output files. The computer code can be made available on request to ukeqs@bgs.ac.uk.

References

British Geological Survey holds most of the references listed below, and copies may be obtained via the library service subject to copyright legislation (contact libuser@bgs.ac.uk for details). The library catalogue is available at: https://envirolib.apps.nerc.ac.uk/olibcgi.

ABRAHAMSON NA, SILVA WJ, and KAMAI, R. 2014. Summary of the ASK14 ground-motion relation for active crustal regions, *Earthquake Spectra*, VOL. 30(3), 1025–1055.

AKKAR S, SANDIKKAYA MA, and BOMMER JJ. 2014a. Empirical ground motion models for point- and extended-source crustal earthquake scenarios in Europe and the Middle East, *Bulletin of Earthquake Engineering,* Vol. 12**,** 359-387.

AKKAR S, SANDIKKAYA MA, S¸ ENYURT M, SISI AA, AY BÖ , TRAVERSA P, DOUGLAS J, COTTON F, LUZI L, HERNANDEZ B, and GODEY S. 2014b. Reference database for seismic ground-motion in Europe (RESORCE), *Bulletin of Earthquake Engineering*, Vol. 12(1), 311–339.

AL ATIK, L, KOTTKE, A, ABRAHAMSON, N, and HOLLENBACK, J. 2014. Kappa (κ) scaling of ground-motion prediction equations using an inverse random vibration theory approach, *Bulletin of the Seismological Society of America*, Vol. 104(1), 336–346.

ALLEN, TI, ADAMS, J, ROGERS, GC, and HALCHUK, S. 2015. 5th generation seismic hazard model for north-western Canada, *11th Canadian Conference on Earthquake Engineering*, Victoria, Canada, Paper 93782.

AMANTE, C, AND EAKINS, B. 2009. ETOPO1 1Arc-Minute Global Relief Model: Procedures, data resources and analysis, *NOAA (NOAA Technical Memorandum NESDIS NGDC-24.*

ANDERSON, JG, and HOUGH, SE. 1984. A model for the shape of the Fourier amplitude spectrum of acceleration at high frequencies, *Bulletin of the Seismological Society of America*, Vol. 74(5), 1969–1993.

ANELL, I., THYBO, H., and ARTEMIEVA, I. 2009. Cenozoic uplift and subsidence in the North Atlantic region: geological evidence revisited, *Tectonophysics*, Vol. 474, 78–105.

ARROWSMITH, SJ, KENDALL, M, WHITE, N, VANDECAR, J, and BOOTH, DC. 2005. Seismic imaging of a hot upwelling beneath the British Isles, *Geology,* Vol. 33 (5), 345–348.

ASSATOURIANS, K, and ATKINSON, GM. 2013. EqHaz - An open-source probabilistic seismic hazard code based on the Monte Carlo simulation approach, *Seismological Research Letters*, Vol. 84, DOI: 101785/0220120102.

ASSUMPÇÃO, M. 1981. The NW Scotland earthquake swarm of 1974, *Geophysical Journal of the Royal Astronomical Society*, Vol. 67(3), 577–586.

ATKINSON, GM, and BOORE, DM. 2006. Earthquake ground motion prediction equations for eastern North America, *Bulletin of the Seismological Society of America,* Vol. 96(6), 2181–2205.

ATKINSON, GM, and BOORE, DM. 2011. Modifications to existing ground-motion prediction equations in light of new data, *Bulletin of the Seismological Society of America,* Vol. 10(3), 1121–1135.

ATKINSON GM, BOMMER JJ, and ABRAHAMSON NA. 2014. Alternative approaches to modelling epistemic uncertainty in ground motions in probabilistic seismic-hazard analysis, *Seismological Research Letters,* Vol. 85(6), 1141–1144.

BAMFORD, D, NUNN, K, PRODEHL, C, and JACOB, B. 1978. LISPB-IV. Crustal structure of northern Britain, *Geophysical Journal of the Royal Astronomical Society*, Vol. 54, 43-60.

BAPTIE, B. 2010. State of stress in the UK from observations of local seismicity, *Tectonophysics*, Vol. 482, 150-159.

BAPTIE, B. 2012. UK earthquake monitoring 2011/2012: Twenty-third Annual Report, *British Geological Survey Commissioned Report,* OR/12/092.

BAPTIE, B, OTTEMÖLLER, L, SARGEANT, S, FORD, G, and O'MONGAIN, A. 2005. The Dudley earthquake of 2002: A moderate sized earthquake in the UK, *Tectonophysics*, Vol. 401(1–2), 1–22.

BAPTIE, B, SEGOU, M, ELLEN, R, and MONAGHAN, A. 2016. Unconventional oil and gas development: Understanding and monitoring induced seismic activity, *British Geological Survey Open Report,* OR/16/042.

BAPTIE, B, FORD, G, and GALLOWAY, D. 2017. The Moidart earthquakes of 4 August 2017, *British Geological Survey Report,* OR/17/062.

BAPTIE, B, FORD, G, and GALLOWAY, D. 2018. The South Wales earthquake of 17 February 2018, *British Geological Survey Commissioned Report,* OR/18/019.

BEAUVAL C, SCOTTI O, BONILLA F. 2006. The role of seismicity models in probabilistic seismic hazard estimation: comparison of a zoning and a smoothing approach, *Geophysical Journal International*, Vol. 165(2):584–595.

BEYER, B, and BOMMER, JJ. 2006. Relationships between median values and between aleatory variabilities for different definitions of the horizontal component of motion, *Bulletin of the Seismological Society of America*, Vol. 96(4A), 1512–1522.

BIJWAARD, H., and SPAKMAN, W. 1999. Tomographic evidence for a narrow whole mantle plume below Iceland, *Earth and Planetary Science Letters*, Vol. 166, 121 – 126

BINDI D, MASSA M, LUZI L, AMERI G, PACOR F, PUGLIA R, and AUGIERA P. 2014. Pan-European ground-motion prediction equations for the average horizontal component of PGA, PGV, and 5%-damped PSA at spectral periods up to 3.0 s using the RESORCE dataset, *Bulletin of Earthquake Engineering,* DOI:10.1007/s10518-013-9525-5

BIS. 2013. Nuclear industrial strategy: government and industry in partnership - The UK's nuclear future, *BIS/13/627*, Department for Business, Innovation and Skills, London, United Kingdom.

BISHOP, I, STYLES, P, and ALLEN, M. 1994. Mining Induced Seismicity in the Nottinghamshire Coalfield, *Quarterly Journal of Engineering Geology*, Vol. 26 (4), 253-279.

BLUCK, BJ, GIBBONS, W, and INGHAM, J.K. 1992. Terranes. In: COPE, JC, INGHAM, JK, RAWSON, PF (Editors), Atlas of Palaeogeography and Lithofacies, *Geological Society London*, Memoirs, Vol. 13, 1–4.

BOMMER, JJ, STAFFORD, PJ, ALARCÓN, JE, and AKKAR, S. 2007. The influence of magnitude range on empirical ground-motion prediction, *Bulletin of the Seismological Society of America*, Vol. 97, 2152-2170.

BOMMER, JJ, and SCHERBAUM, F. 2008. The use and misuse of logic trees in probabilistic seismic hazard analysis, *Earthquake Spectra,* Vol. 24(4), 997-1009.

BOMMER, JJ, DOUGLAS, J, SCHERBAUM, F, COTTON F, BUNGUM, H, and FÄH, D. 2010. On the selection of ground-motion prediction equations for seismic hazard analysis, *Seismological Research Letters,* Vol. 81, 783-793.

BOORE, DM. 2003. Simulation of ground motion using the stochastic method, *Pure and Applied Geophysics*, Vol. 160, 635–676.

BOORE, DM. 2005. SMSIM- FORTRAN programs for simulating ground motions from earthquakes: version 2.3 - a revision of OFR 96-80-A, *U.S. Geological Survey Open-File Report*.

BOORE, DM, and JOYNER, WB. 1997. Site amplifications for Generic Rock Sites, *Bulletin of the Seismological Society of America*, Vol. 87, 327–341.

BOORE, D, STEWART, J, SEYHAN, E, and ATKINSON, G. 2014. NGA-West2 equations for predicting PGA, PGV, and 5% damped PSA for shallow crustal earthquakes, *Earthquake Spectra,* Vol. 30, 1057-1085.

BOOTH, DC, BOTT, JDJ, and O'MONGAIN, AM. 2001. The UK Seismic velocity model for earthquake location – a baseline review, *British Geological Survey Internal Report*, IR/01/188.

BOOTH, DC. 2010. UK 1-D regional velocity models by analysis of variance of P-wave travel times from local earthquakes, *Journal of Seismology*, Vol. 14(2), 197–207.

BOTT, MHP, LONG, RE, GREEN, ASP, LEWIS, AHJ, SINHA, MC, and STEVENSON DL. 1985. Crustal structure south of the Iapetus Suture beneath northern England, *Nature*, Vol. 314, 724-727.

BOTT, MHP, and BOTT, JDJ. 2004. The Cenozoic uplift and earthquake belt of mainland Britain as a response to an underlying hot, low-density upper mantle, *Journal of Geological Society of London*, Vol. 161, 19–29.

BRODIE J. and WHITE N. 1994. Sedimentary basin inversion caused by igneous underplating: Northwest European continental shelf*, Geology*, Vol. 22, 147-150.

BUDNITZ, RJ, APOSTOLAKIS, G, BOORE, DM, CLU, LS, COPPERSMITH, KJ, CORNELL, CA, and MORRIS, PA. 1997. Recommendations for probabilistic seismic hazard analysis: Guidance on uncertainty and use of experts. *NUREG/CR-6372, Volume 1,* US Nuclear Regulatory Commission, Washington, DC.

BURKHARD M, and GRÜNTHAL G. 2009. Seismic source zone characterization for the seismic hazard assessment project PEGASOS by the Expert Group 2 (EG1b*), Swiss Journal of Geosciences*, Vol. 102, 149–188.

BURTON, PW, and NEILSON, G. 1980. Annual catalogues of British earthquakes recorded on LOWNET (1967-1978), *Seismological Bulletin No. 7*, Institute of Geological Sciences, HMSO.

CAMELBEECK, T, VANNESTE, K, ALEXANDRE, P, VERBEECK, K, PETERMANS, T, ROSSET, P, EVERAERTS, M, WARNANT, R, and VAN CAMP, M. 2007. Relevance of active faulting and seismicity studies to assessments of long-term earthquake activity and maximum magnitude in intraplate northwest Europe, between the Lower Rhine Embayment and the North Sea, *Geological Society of America,* 425**,** 193–224.

CAO, AM, and GAO, SS. 2002. Temporal variation of seismic *b*-values beneath northeastern Japan island arc, *Geophysical Research Letters,* Vol. 29**(**9), doi 10.1029/2001GL013775.

CAMPBELL, KW. 2003. Prediction of strong ground motion using the hybrid empirical method and its use in the development of ground motion (attenuation) relations in eastern North America, *Bulletin of the Seismological Society of America*, Vol. 93, 1012–1033.

CAMPBELL, KW and BOZORGNIA, Y. 2006. Campbell-Bozorgnia NGA empirical ground motion model for the average horizontal component of PGA, PGV and SA at selected spectral periods ranging from 0.01-10.0 seconds, *Interim Report for USGS Review*.

CAMPBELL, KW, and BOZORGNIA, Y. 2014. NGA-West 2 ground motion model for the average horizontal components of PGA, PGV, and 5%-damped linear acceleration response spectra, *Earthquake Spectra*, Vol. 30(3), 1087–1115.

CARTWRIGHT, D, and LONGUET-HIGGINS, M. 1956. The statistical distribution of the maxima of a random function, *Proceedings of the Royal Society, London*: *Mathematical and Physical Sciences*, Vol. 237(1209), 212–232.

CAUZZI, C, FACCIOLI, E, VANINI, M, and BIANCHINI, A. 2015. Updated predictive equations for broadband (0.01–10s) horizontal response spectra and peak ground motions, based on a global dataset of digital acceleration records, *Bulletin of Earthquake Engineering,* Vol. 13, 1587-1612.

CEN. 2004. Eurocode 8: Design of structures for earthquake resistance part 1: general rules, seismic actions and rules for buildings, *European Norm. European Committee for Standardization*, Brussels, Belgium.

CHADWICK, R.A., PHARAOH, T.C., WILLIAMSON, J.P., and MUSSON, R.M.W. 1996. Seismotectonics of the UK, *British Geological Survey Technical Report,* WA/96/3C.

CHIOU, B, and YOUNGS, RR. 2014. Update of the Chiou and Youngs NGA model for the average horizontal component of peak ground motion and response spectra, *Earthquake Spectra,* Vol. 30, 1117-1153.

COOPER, M.R., ANDERSON, H., WALSH, J.J., VANDAM, C.L., YOUNG, M.E., EARLS, G. AND WALKER, A. 2012. Palaeogene Alpine tectonics and Icelandic plume-related magmatism and deformation in Northern Ireland, *Journal of the Geological Society*, London, Vol. 169, 29–36.

COPPERSMITH, K and BOMMER, J. 2012. Use of the SSHAC methodology within regulated environments: cost-effective application for seismic characterization at multiple sites, *Nuclear Engineering Design*, Vol. 245, 233–240.

CORNELL,C.A. and VANMARCKE,E.H. 1969. The Major Influences on Seismic Risk, *Proceedings of the Fourth World Conference on Earthquake Engineering*, Santiago, Chile.

CORNELL, CA. 1968. Engineering Seismic Risk Analysis. *Bulletin of the Seismological Society of America*, Vol. 58, 1583-1606.

COTTON, F, SCHERBAUM, F, BOMMER, JJ, and BUNGUM, H. 2006. Criteria for Selecting and Adjusting Ground-Motion Models for Specific Target Regions: Application to Central Europe and Rock Sites, *Journal of Seismology,* Vol. 10, 137-156.

CRAMPIN, S, JACOB, AWB, MILLER, A, and NEILSON, G. 1970. The LOWNET radio-linked seismometer network in Scotland, *Geophysical Journal of the Royal Astronomical Society,* Vol. 21, 207–216.

DAVISON, C. 1924. History of British Earthquakes (Cambridge: University Press).

DAVIS, JC. 1986. *Statistics and data analysis in geology* (New York: Wiley).

DELAVAUD E, SCHERBAUM F, KÜHN N, and ALLEN T. 2012. Testing the global applicability of ground motion prediction equations for active shallow crustal regions, *Bulletin of the Seismological Society of America*, Vol. 102(2), 707-721.

DOUGLAS, J. 2018. Capturing geographically-varying uncertainty in earthquake ground-motion models or what we think we know may change, In *Recent Advances in Earthquake Engineering in Europe, Geotechnical, Geological and Earthquake Engineering*, PITILAKIS K (Editor), Vol. 46, 153-181.

DOUGLAS, J, and EDWARDS, B. 2016. Recent and future developments in earthquake ground motion estimation, *Earth-Science Reviews*, Vol. 160, 203-219.

DROUET, S, AMERI, G, LE DORTZ, K, SECANELL, R, and SENFAUTE, G. 2020. A probabilistic seismic hazard map for the metropolitan France, *Bulletin of Earthquake Engineering*, doi.org/10.1007/s10518-020-900790-7.

EDWARDS B., RIETBROCK, A., BOMMER, J.J., and BAPTIE, B. 2008. The acquisition of source, path, and site effects from Microearthquake recordings using Q tomography: Application to the United Kingdom, *Bulletin of the Seismological Society of America,* Vol. 98, 1915–1935.

EDWARDS, B, CAUZZI, C, DANCIU, L, and FÄH, D. 2016. Region-specific assessment, adjustment, and weighting of ground-motion prediction models: Application to the 2015 Swiss seismic-hazard maps, *Bulletin of the Seismological Society of America*, Vol. 106(4), 1840–1857.

EDWARDS, JWF, and BLUNDELL, DJ. 1984. Summary of Seismic Refraction experiments in the English Channel, Celtic Sea and St George's Channel, *British Geological Survey Marine Geophysics Report* 144.

EN1990. 2002. Eurocode – Basis of structural design, *European Union Per Regulation 305/2011, Directive 98/34/EC, Directive 2004/18/EC*, Brussels, Belgium.

FÄH, D, GIARDINI, D, KÄSTLI, P, DEICHMANN, N, GISLER, M, SCHWARZ-ZANETTI, G, ALVAREZ-RUBIO, S, SELLAMI, S, EDWARDS, B, ALLMANN, B, BETHMANN, F, WÖSSNER, J, GASSNER-STAMM, G, FRITSCHE, S and EBERHARD, D. 2011. ECOS-09 Earthquake Catalogue of Switzerland Release 2011 Report and Database, *Report SED/RISK/R/001/20110417*.

FOULGER, G.R.2002. Plumes, or plate tectonic processes?, *Astronomy & Geophysics*, Vol. 43, 6.19-6.23.

FRANKEL, A.1995. Mapping seismic hazard in the Central and Eastern United States, *Seismological Research Letters,* Vol. 66(4), 8-21.

GALLOWAY, D, BUKITS, J, and FORD, G. 2013. Bulletin of British Earthquakes 2012, *British Geological Survey Seismological Report, OR/13/54.*

GALLOWAY, I. 2019. Bulletin of British Earthquakes 2018, *British Geological Survey Internal Report,* OR/19/002.

GARCÍA-MORENO, D, VERBEECK, K, CAMELBEECK, T, DE BATIST, M, OGGIONI, F, ZURITA HURTADO, O, VERSTEEG, W, JOMARD, H, COLLIER, JS, GUPTA, S, TRENTESAUX, A, and VANNESTE, K. 2015. Fault activity in the epicentral area of the 1580 Dover Strait (Pas-de-Calais) earthquake (northwestern Europe), *Geophysical Journal International,* Vol. 201, 2, 528–542.

GASPARINI, DA, and VANMARCKE, EH. 1976. Simulated Earthquake Motions Compatible with Prescribed Response Spectra, *Massachusetts Institute of Technology*, Cambridge, Massachusetts.

GOES, S, GOVERS, R, and VACHER, P. 2000. Shallow mantle temperatures under Europe from P and S wave tomography, *Journal of Geophysical Research: Solid Earth*, Vol. 105(B5), 11153–11169.

GÖLKE, M, and COBLENTZ, D. 1996. Origins of the European regional stress field*, Tectonophysics*, Vol. 266(1–4), 11–24.

GOULET CA, BOZORGNIA Y, KUEHN N, AL ATIK L, YOUNGS RR, GRAVES RW, and ATKINSON GM. 2017. NGA-East ground-motion models for the U.S. Geological Survey National Seismic Hazard Maps, *PEER Report 2017/03,* Pacific Earthquake Engineering Research Center, University of California, Berkeley, US.

GRÜNTHAL, G 1985. The up-dated earthquake catalogue for the German Democratic Republic and adjacent areas - statistical data characteristics and conclusions for hazard assessment. *3rd International Symposium on the Analysis of Seismicity and Seismic Risk*, Liblice, Czechoslovakia, 17–22 June 1985, Proceedings Vol. I, 19–25.

GRÜNTHAL, G, BOSSE, C, SELLAMI, S, MAYER-ROSA, D, and GIARDINI, D.1999. Compilation of the GSHAP regional seismic hazard for Europe, Africa, and the Middle East, *Annali di Geofisica*, Vol. 42(6), 1215-1223.

GRÜNTHAL, G, and WAHLSTRÖM, R. 2003. An Mw based earthquake catalogue for central, northern and northwestern Europe using a hierarchy of magnitude conversions, *Journal of Seismology*, Vol. 7, 507-531.

GRÜNTHAL, G, WAHLSTRÖM, E, and STROMEYER, D. 2009. The unified catalogue of earthquakes in central, northern, and northwestern Europe (CENEC)—updated and expanded to the last millennium, *Journal of Seismology*, Vol. 13, 517-541.

GRÜNTHAL, G, STROMEYER, D, BOSSE, C, COTTON, F, and BINDI, D. 2018. The probabilistic seismic hazard assessment of Germany—version 2016, considering the range of epistemic uncertainties and aleatory variability, *Bulletin of Earthquake Engineering,* Vol. 16(10)**,** 4339-4395.

GUTENBERG, B, and RICHTER, C. 1954. *Seismicity of the Earth and Associated Phenomena*. (New Jersey: Princeton University Press).

HARDWICK, A. 2008. New insights into the crustal structure of the England, Wales and Irish Seas areas from local earthquake tomography and associated seismological studies. *PhD thesis*, University of Leicester.

HEIDBACH, O, RAJABI, M, REITER, K, ZIEGLER, M, and the WSM Team. 2016. World Stress Map Database Release 2016, *GFZ Data Services*.

HEYBURN, R, BOWERS, D, SELBY, N, and DOUGLAS, A. 2005. How deep was the Dudley (UK) earthquake of 22 September 2002?, *Journal of Seismology*, Vol. 9(1), 61–71.

HILLIS, RR, HOLFORD, SP, GREEN, PF, DORÉ, AG, GATLIFF, RW, STOKER, MS, THOMSON, K, TURNER, JP, UNDERHILL, JR, and WILLIAMS, GA. 2008. Cenozoic exhumation of the southern British Isles, *Geology*, Vol. 36, 371-374.

HOLSCHNEIDER, M, ZÖLLER, G, and HAINZL, S. 2011. Estimation of the maximum possible magnitude in the framework of a doubly truncated Gutenberg-Richter model, *Bulletin of the Seismological Society of America*, Vol. 101(4), 1649–1659.

HOLSCHNEIDER, M, ZÖLLER, G, CLEMENTS, R, and SCHORLEMMER, D. 2014. Can we test for the maximum possible earthquake magnitude?, *Journal of Geophysical Research - Solid Earth*, Vol. 119, 2019–2028.

HONG, HP, and GODA, K. (2006). A comparison of seismic-hazard and risk deaggregation, *Bulletin of the Seismological Society of America*, Vol. 96, 2021–2039.

HOUGH, S.E. and PAGE, M. 2011. Toward a consistent model for strain accrual and release for the New Madrid Seismic Zone, central United States, *Journal of Geophysical Research*, Vol. 116(B03311), doi:10.1029/2010JB007783.

JOHNSTON, A.C. 1996. Seismic moment assessment of earthquakes in stable continental regions—III. New Madrid 1811–1812, Charleston 1886 and Lisbon 1755, *Geophysical Journal International*, Vol. 126(2), 314–344.

JOHNSTON, AC, COPPERSMITH, KJ, KANTER, LR, and CORNELL, CA. 1994. The earthquakes of stable continental regions, *EPRI Report*, Electric Power Research Institute, Palo Alto, California.

JOHNSTON, AC, and SCHWEIG, ES. 1996. The enigma of the New Madrid earthquakes of 1811–1812, *Annual Review of Earth and Planetary Sciences*, Vol. 24, 339-384.

KALE, Ö, and AKKAR, S. 2013. A new procedure for selecting and ranking ground-motion prediction equations (GMPEs): the Euclidean distance-based ranking (EDR) method, *Bulletin of Seismological Society of America,* Vol. 103(2A), 1069–1084.

KING, G. 1980. A fault plane solution for the Carlisle earthquake, 26 December 1979, *Nature*, Vol. 286(5769), 142–143.

KIRSTEIN, LA, and TIMMERMAN, MJ. 2000. Evidence of the proto-Iceland plume in northwestern Ireland at 42 Ma from helium isotopes, *Journal of Geological Society of London*, Vol. 157(5), 923–928.

KOTHA, SR, BINDI, D, and COTTON, F. 2016. Partially non-ergodic region specific GMPE for Europe and Middle East, *Bulletin of Earthquake Engineering,* Vol. 14, 1245-1263.

KOTTKE, AR, and RATHJE, EM. 2008. Technical manual for Strata, *Report 2008/10, Pacific Earthquake Engineering Research (PEER) Center*, Berkeley, California.

KOTTKE, A. 2020. PYRVT, https://zenodo.org/badge/latestdoi/5086299.

KULKARNI, RB, YOUNGS, RR, and COPPERSMITH, KJ. 1984. Assessment of confidence intervals for results of seismic hazard analysis, *Proceedings of the Eighth World Conference on Earthquake Engineering*, San Francisco, pp 263–270.

LAGARDE, JL, AMORESE, D, FONT, M, LAVILLE, E, and DUGUÉ, O. 2003. The structural evolution of the English Channel area, *Journal of Quaternary Science*, Vol. 18(3-4), 201–213.

LAMBECK, K. 1993. Glacial rebound of the British-Isles - 1. Preliminary model results, *Geophysical Journal International*, Vol. 115(3), 941–959.

LEONARD, M. 2014. Self-consistent earthquake fault-scaling relations: update and extension to stable continental strike-slip faults, *Bulletin of the Seismological Society of America*, Vol. 104(6), 2953-2965.

LUCKETT, R, and BAPTIE, B. 2015. Local earthquake tomography of Scotland, *Geophysical Journal International*, Vol. 200(3), 1538–1554.

LUEN, B, AND STARK, P B. 2012. Poisson tests for declustered catalogues, *Geophysical Journal International*, Vol. 189, 691-700.

MAIN, ID, IRVING, D, MUSSON, RMW, and READING, A. 1999. Constraints on the frequency-magnitude relation and maximum magnitudes in the UK from observed seismicity and glacio-isostatic recovery rates, *Geophysical Journal International,* Vol 137(2), 535–550.

MANCHUEL, K, TRAVERSA, P, BAUMONT, D, CARA, M, NAYMAN, E, and DUROUCHOUX, C, 2018. The French seismic CATalogue (FCAT-17), *Bulletin of Earthquake Engineering*, Vol. 16, 2227-2251.

MARROW, PC, and WALKER, AB. 1988. LLeyn earthquake of 1984 July 19: Aftershock sequence and focal mechanism, *Geophysical Journal International,* Vol 92, 487–493.

MARZOCCHI, W, and TARONI, M. 2014. Some thoughts on declustering in probabilistic seismic-hazard analysis. Bulletin of the Seismological Society of America, Vol. 104(4), 1838–1845.

MCGUIRE, RK. 1995. Probabilistic seismic hazard analysis and design earthquakes: closing the loop. *Bulletin of the Seismological Society of America*, Vol. 85, 1275-1284.

MCGUIRE, RK. 2004. *Seismic Hazard and Risk Analysis*. (Oakland CA: Earthquake Engineering Research Institute).

MELETTI, C, D'AMICO, V, and MARTINELLI, F. 2009. Homogeneous determination of maximum magnitude, *SHARE* Deliverable 3.3.

MELVILLE, CP, LEVRET, A, ALEXANDRE, P, LAMBERT, J, and VOGT, J. 1996. Historical seismicity of the Strait of Dover/Pas de Calais, *Terra Nova*, Vol. 8, 626–647.

MILLER AC, and RICE TR. 1983. Discrete approximations of probability distributions, *Management Science*, Vol 29(3), 352–362.

MUIR-WOOD, R. 2000. Deglaciation seismotectonics: A principal influence on intraplate seismogenesis at high latitudes, *Quaternary Science Reviews*, Vol. 19(14–15), 1399–1411.

MOSCA, I. 2019. Comparing seismic hazard software: M3C vs. OpenQuake, *British Geological Survey Open Report, OR/19/038*.

MUSSON, RMW. 1989. Accuracy of historical earthquake locations in Britain, *Geological Magazine*, Vol. 126, 685-689.

MUSSON, RMW. 1994. A catalogue of British earthquakes, *British Geological Survey Global Seismology Report*, WL/94/04

MUSSON, RMW. 1999. Determination of design earthquakes in seismic hazard analysis through Monte Carlo simulation, *Journal of Earthquake Engineering*, Vol. 3, 463-474.

MUSSON, RMW. 2000. The use of Monte Carlo simulations for seismic hazard assessment in the UK, *Annali di Geofisica*, Vol. 43, 1-9.

MUSSON, RMW. 2007. British earthquakes, *Proceedings of the Geologists' Association*, Vol. 118, 305-337.

MUSSON, RMW. 2011. Activity rates for seismic sources. *SHARE* Deliverable 3.7b.

MUSSON, RMW. 2012a. PSHA validated by quasi observational means, *Seismological Research Letters*, Vol. 83, 130-134.

MUSSON, RMW. 2012b. The effect of magnitude uncertainty on earthquake activity rates, *Bulletin of the Seismological Society of America*, Vol. 102(6), 2771–2775.

MUSSON, RMW. 2012c. Interpreting intraplate tectonics for seismic hazard: A UK historical perspective, *Journal of Seismology*, Vol. 16, 261–273.

MUSSON RWM. 2015. What was the largest British earthquake?, *SECED 2015 Conference*, Cambridge, United Kingdom.

MUSSON, RMW, CHADWICK, RA, PHARAOH, TC, HENNI, PHO, WILD, B, and CARNEY, JN. (2001). Seismic hazard assessment for Wylfa, *British Geological Survey Technical Report*, CR/01/253.

MUSSON, RMW, and SARGEANT, S. 2007. Eurocode 8 seismic hazard zoning maps for the UK, *British Geological Survey Report, CR/07/125.*

MUSSON, RMW, and WINTER, PW. 2012. Objective assessment of source models for seismic hazard studies: with a worked example from UK data, *Bulletin of Earthquake Engineering*, Vol. 10, 367-378.

NADIN, P., KUSZNIR, N., and TOTH, J. 1995. Transient regional uplift in the Early Tertiary of the northern North Sea and the development of the Iceland Plume, *Journal of Geological Society*, Vol. 152, 953–958.

NADIN, P., KUSZNIR, N., and CHEADLE, M. 1997. Early Tertiary plume uplift of the North Sea and Faeroe-Shetland basins, *Earth and Planetary Science Letters*, Vol. 148, 109–127, 1997.

NEILSON, G, MUSSON, RMW, and BURTON, PW. 1984. Macroseismic reports on historical British earthquakes V: The South and South West of England, *British Geological Survey Global Seismology Report*, 231.

ONR EXPERT PANEL ON NATURAL HAZARDS, 2018. NS-TAST-GD-013 Annex 1 Reference Paper: Analysis of Seismic Hazards for Nuclear Sites, Expert Panel Paper No: GEN-SH-EP-2016-1.

OTTEMÖLLER, L, and THOMAS, CW. 2007. Highland Boundary Fault Zone: Tectonic implications of the Aberfoyle earthquake sequence of 2003, *Tectonophysics,* Vol. 430(1–4), 83–95.

OTTEMÖLLER, L, BAPTIE, B, and SMITH, NJ P. 2009. Source parameters for the 28 April 2007 Mw 4.0 earthquake in Folkestone, United Kingdom, *Bulletin of the Seismological Society of America*, Vol. 99(3), 1853-1867.

OTTEMÖLLER, L, and SARGEANT, S. 2010. Ground-motion difference between two moderate-size intraplate earthquakes in the United Kingdom, *Bulletin of the Seismological Society of America*, Vol. 100, 1823–1829.

PACIFIC NORTHWEST NATIONAL LABORATORY (PNNL). 2014. Hanford Sitewide Probabilistic Seismic Hazard Analysis, prepared for the *U.S. Department of Energy under contract DE-AC06076RL01830 and Energy Northwest*.

PHARAOH, TC. 2018. The Anglo-Brabant Massif: persistent but enigmatic palaeo-relief at the heart of Western Europe, *Proceedings of the Geologists' Association*, Vol. 129(3), 278-328.

PHARAOH, TC. 2019. The complex tectonic evolution of the Malvern region: crustal accretion followed by multiple extensional and compressional reactivation, *Proceedings of the Open University Geological Society*.

PHARAOH, TC, MORRIS, JH, LONG, CB, and RYAN, PD. 1996. *Tectonic Map of Britain, Ireland and adjacent areas, sheet 1, scale 1:1500000*. Keyworth: British Geological Survey.

PONDRELLI, S, SALIMBENI, S, MORELLI, A, EKSTRÖM, G, POSTPISCHL, L, VANNUCCI, G, and BOSCHI, E. 2011. European-Mediterranean Regional Centroid Moment Tensor Catalog: solutions for 2005-2008, *Physics of the Earth and Planetary Interiors*, Vol. 185(3), 74-81, 2011.

POWER, M, CHIOU, B, ABRAHAMSON, NA, BOZORGNIA, Y, SHANTZ, T, and ROBLEE, C. 2008. An overview of the NGA project, *Earthquake Spectra,* Vol. 24, 3-22.

REDMAYNE, DW. 1988. Mining-induced seismicity in UK coalfields identified on the BGS National Seismograph Network, in Engineering Geology of Underground Movements, *Engineering Geology Special Publicat*ion, Geological Society of London, Vol. 5, 405-413

REITER, L. 1990. *Earthquake Hazard Analysis* (New York: Columbia University Press).

RESTREPO-VELEZ, LF, and BOMMER J J. 2003. An exploration of the nature of the scatter in ground-motion prediction equations and the implications for seismic hazard assessment, *Journal of Earthquake Engineering*, Vol. 7(SI1), 171–199.

RICHARDSON, M. 1975. *Seismicity of Ireland*, Electricity Supply Board, Dublin.

RIETBROCK, A, STRASSER, FO, and EDWARDS, B. 2013. A stochastic earthquake ground motion prediction model for the United Kingdom, *Bulletin of the Seismological Society of America*, Vol. 103(1), 57-77.

RIETBROCK, A, and EDWARDS, B. 2019. Update of the UK stochastic ground motion model using a decade of broadband data, *SECED 2019 Conference*, Greenwich, United Kingdom.

RITCHIE, MEA, MUSSON, RMW, and WOODCOCK, NH. 1990. The Bishop's Castle (UK) Earthquake of 2 April 1990, *Terra Nova*, Vol. 2(4), 390–400.

ROBERTS, NS, BELL, AF, and MAIN, I. 2015. Are volcanic seismic *b*-value high, and if so when?, *Journal of Volcanology and Geothermal Research,* Vol. 308, 127-141.

RYDELEK, PA, and SACKS, IS. 1989. Testing the completeness of earthquake catalogs and the hypothesis of self-similarity, *Nature*, Vol. 337, 251–253.

SARGEANT, S. L., STAFFORD, P. J., LAWLEY, R., WEATHERILL, G., WESTON, A.-J., S., BOMMER, J.J., BURTON, P. W., FREE, M.,, MUSSON, R. M. W., KUUYUOR, T., AND ROSSETTO, T., 2008. Observations from the Folkestone, UK, earthquake of 28 April 2007, *Seismological Research Letters*, 79 (5), 672-687.

SARGEANT, S, and OTTEMÖLLER, L. 2009. Lg wave attenuation in Britain, *Geophysical Journal International*, Vol. 179(3), 1593–1606.

SCHERBAUM, F, DELAVAUD, W, and RIGGELSEN, C. 2009. Model selection in seismic hazard analysis: An information–theoretic perspective, *Bulletin of the Seismological Society of America*, Vol. 99(6), 3234–3247.

SHENNAN, I, BRADLEY, S, MILNE, G, BROOKS, A, BASSETT, S, and HAMILTON, S.2006. Relative sea-level changes, glacial isostatic modelling and ice-sheet reconstructions from the British Isles since the Last Glacial Maximum, *Journal of Quaternary Science*, Vol. 21(6), 585–599.

SHWP. 1993. Report on Seismic Hazard Assessment Volume 3J – A Review of the Seismotectonics of Britain in the Context of NW Europe, *Report by the Seismic Hazard Working Party*.

STEIN, S, and WYSESSION, M. 2003. *An Introduction to Seismology, Earthquakes, and Earth Structure* (Oxford: Wiley-Blackwell Publishing).

STEIN, S, GELLER, RJ, and LIU, M. 2012. Why earthquake hazard maps often fail and what to do about it?, *Tectonophysics,* Vol. 562/553, 1-25.

STAFFORD, PJ. 2014. Source-Scaling Relationships for the Simulation of Rupture Geometry within Probabilistic Seismic-Hazard Analysis, *Bulletin of the Seismological Society of America*, Vol. 104, 1620-1635.

STAFFORD, PJ, RODRIGUEZ-MAREK, A, EDWARDS, B, KRUIVER, PP, and BOMMER, JJ. 2017. Scenario Dependence of Linear Site-Effect Factors for Short-Period Response Spectral Ordinates, *Bulletin of the Seismological Society of America*, Vol. 107(6), 2859–2872.

STRASSER, FO, ABRAHAMSON, N A, and BOMMER JJ. 2008. Truncation of the distribution of ground motion residuals, *Journal of Seismology*, Vol. 12, 79–105.

TRODD, H, WARBURTON, P, and POOLEY, CI. 1985. The Great British Earthquake of 1984 seen from afar*, Geophysical Journal of Royal Astronomical Society*, Vol. 83, 809–812.

TROMANS, IJ, ALDAMA-BUSTOS, G, DOUGLAS, J, LESSI-CHEIMARIOU, A, HUNT, S, DAVI, M, MUSSON, RMW, GARRARD, G, STRASSER, FO, and ROBERTSON, C. 2019. Probabilistic seismic hazard assessment for a new-build nuclear power plant site in the UK. *Bulletin of Earthquake Engineering*, Vol. 17(1), 1-36.

TURBITT, T, BARKER, EJ, BROWITT, CWA, HOWELLS, M, MARROW, PC, MUSSON, RMW, NEWMARK, RH, REDMAYNE, DW, WALKER, AB, JACOB, AWB, RYAN, E, andWARD, V. 1985. The North-Wales Earthquake of 19 July 1984, *Journal of Geological Society of London,* Vol. 142, 567–571.

USNRC. 2012. Practical implementation guidelines for SSHAC level 3 and 4 hazard studies, *U.S. Nuclear Regulatory Commission,* NUREG-2117, Rev. 1.

VAN HOUTTE, C, DROUET, S, and COTTON, F. 2011. Analysis of the origins of κ (Kappa) to compute hard rock to rock adjustment factors for GMPEs, *Bulletin of the Seismological Society of America*, Vol. 101(6), 2926–2941.

VERDON, JP, KENDALL, J-M, BUTCHER, A, LUCKETT, R, and BAPTIE, BJ 2018. Seismicity induced by longwall coal mining at the Thoresby Colliery, Nottinghamshire, U.K., *Geophysical Journal International*, Vol. 212(3), 942–954.

VILLANI M, POLIDORO B, ADER T, MCCULLY R, LUBKOWSKI Z, COURTNEY TJ, and WALSH M. 2019. A selection of GMPEs for the UK based on ground motion and macroseismic datasets, *Bulletin of the Seismological Society of America*, Vol. 109(4), 1378–1400.

VILLANI, M, LUBKOWSKI, Z, FREE, M, MUSSON, RWM, POLIDORO B, MCCULLY R, KOSKOSIDI, A, OAKMAN, C, COURTNEY TJ, and WALSH M. 2020a. A probabilistic seismic hazard assessment for Wylfa Newydd, a new nuclear site in the United Kingdom, Bulletin of Earthquake Engineering, DOI: 10.1007/s10518-020-00862-8.

VILLANI, M, POLIDORO, B, LUBKOWSKI, Z, and WALSH, M. 2020b. Application of the kernel method for the seismic hazard assessment of a new nuclear site in the UK, Wylfa Newydd. *17th World Conference on Earthquake Engineering*, Sendai, Japan, 13-18 September 2020, Paper N° C000125.

WEICHERT, D.H. 1980. Estimation of the Earthquake Recurrence Parameters for Unequal Observation Periods for Different Magnitudes, *Bulletin of the Seismological Society of America*, Vol. 70(4), 1337-1346.

WESTBROOK, GK, KUSZNIR, NJ, BROWITT, CWA, and HOLDSWORTH, BK. 1980. Seismicity induced by coal mining in Stoke-on-Trent (U.K.), *Engineering Geology*, Vol. 16, 225-241.

WIEMER, S, and WYSS, M. 2000. Minimum magnitude of complete reporting in earthquake catalogs: examples from Alaska, the Western United States, and Japan, *Bulletin of the Seismological Society of America*, Vol. 90**,** 859–869.

WIEMER, S, DANCIU, L, EDWARDS, B, MARTI, M, FÄH, D, HIEMER, S, WÖSSNER, J, CAUZZI, C, KÄSTLI, P, and KREMER, K. 2016. Seismic Hazard Model 2015 for Switzerland (SUIhaz2015). *Swiss Seismological Service*, Zurich, Switzerland.

WILSON, M.P., DAVIES, R.J., FOULGER, G.R., JULIAN, B.R., STYLES, P., GLUYAS, J.G. AND ALMOND, S. 2015. Anthropogenic earthquakes in the UK: a national baseline prior to shale exploitation, *Marine and Petroleum Geology*, Vol. 68, 1–17

WHEELER, RL. 2009. Methods of Mmax Estimation East of the Rocky Mountains*, U.S. Geological Survey Open-File Report 2009–1018*.

WOESSNER, J, and WIEMER, S. 2005. Assessing the Quality of Earthquake Catalogues: Estimating the Magnitude of Completeness and Its Uncertainty, *Bulletin of the Seismological Society of America*, Vol. 95, No. 2, 684–698.

WOESSNER, J, DANCIU, L, GIARDINI, D., CROWLEY, H, COTTON, F, GRÜNTHAL, G, VALENSISE, G, ARVIDSSON, R, BASILI, R, BETÜL DEMIRCIOGLU, M, HIEMER, S, MELETTI, C, MUSSON, RWM, ROVIDA, AN, SESETYAN, K, STUCCHI, and THE SHARE CONSORTIUM. 2015. THE 2013 EUROPEAN seismic hazard model: key components and results, *Bulletin of Earthquake Engineering,* doi.org/10.1007/s10518-015-9795-1.

WOODCOCK, N, and STRACHAN, R. 2012. *Geological History of Britain and Ireland*. (Oxford: Blackwell Publishing).

WORTHINGTON, RP, and WALSH, JJ. 2011. Structure of Lower Carboniferous basins of NW Ireland, and its implications for structural inheritance and Cenozoic faulting, *Journal of Structural Geology*, Vol. 33, 1285–99.

ZANDIEH, A, CAMPBELL, K W, and PEZESHK, S. 2016. Estimation of κ0 Implied by the High-Frequency Shape of the NGA-West2 Ground-Motion Prediction Equations. *Bulletin of the Seismological Society of America*, Vol. 106(3), 1342–1356.

ZECHAR JD, and JORDAN TH. 2010. Simple smoothed seismicity earthquake forecasts for Italy, *Annali di Geofisica*, Vol. 53(3), 99–105.

ZIEGLER, PA. 1990. *Geological Atlas of Western and Central Europe*. (Amsterdam: Geological Society London and Elsevier).

Appendix 1

We visually compared the set of GMPEs in the GMC model (Table 7) and the UK ground motion dataset for 0.2 s (Figure 50) and 1.0 s SA (Figure 51). The ground motion curves were computed for a rock site (Vs30= 800 m/s), a strike-slip faulting mechanism and a hypocentral depth of 10 km. The GMPEs for ASCR seem to under estimate the UK data, and the GMPE of Atkinson and Boore (2006, 2011) over predicts the data. There are no recordings around 4.5 Mw for the comparison with the 4.5 Mw ground motion curves for 0.2 s and 1.0 s SA.

The results of the residual analysis (Equation 4) are shown in Figures 52 and 53 for 0.2 s and 1.0 s SA, respectively. As observed for PGA in Figure 25, all of the GMPEs tend to underestimate the UK data, except for the model of Atkinson and Boore (2006, 2011) that overestimates the ground motion.

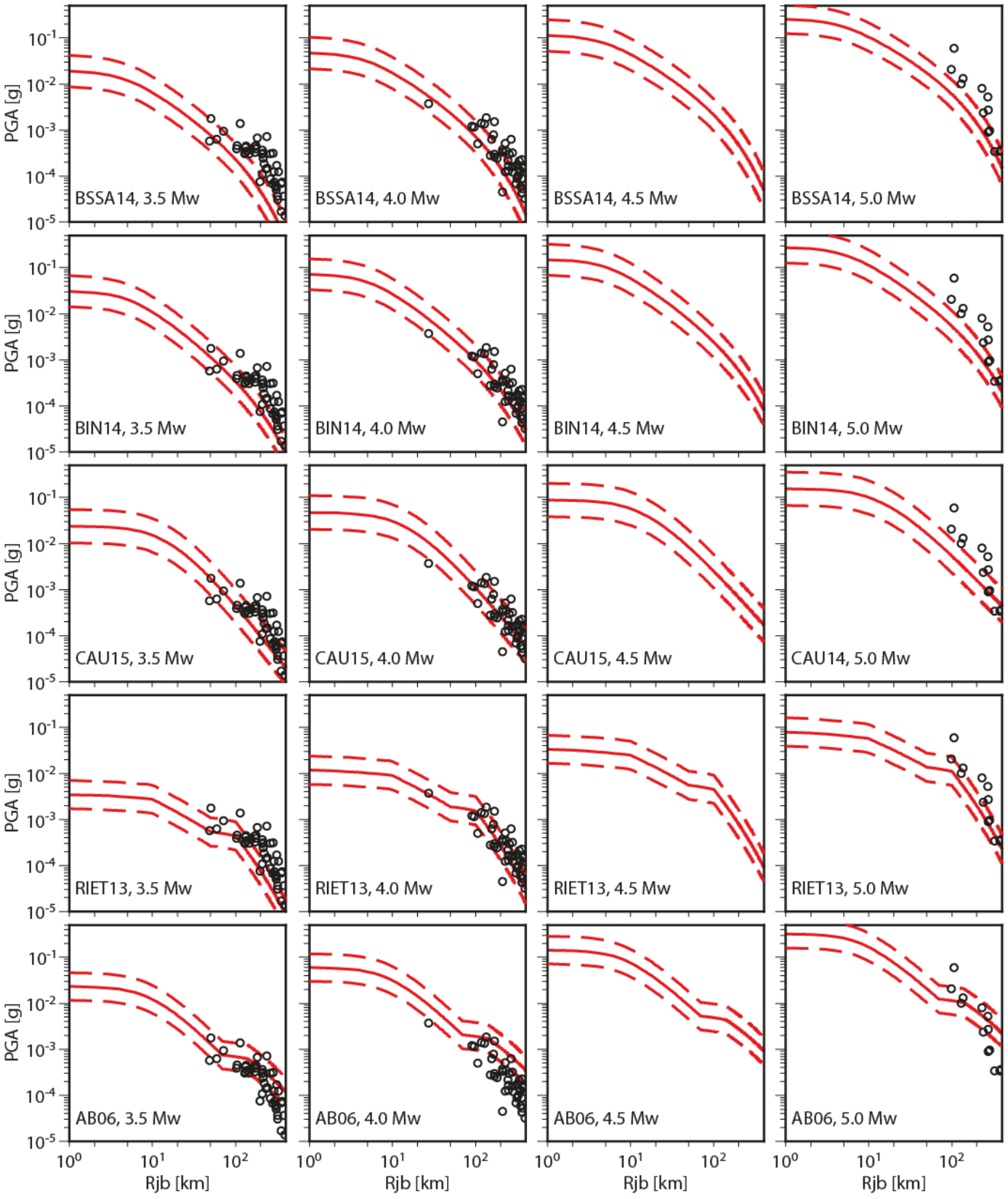

Figure 50: Comparison of the ground motion curves from a set of GMPEs and the UK strong motion data for 0.2 s SA. The solid red lines describe the median prediction of the GMPEs; and the dashed red lines describes the median prediction ± one sigma.

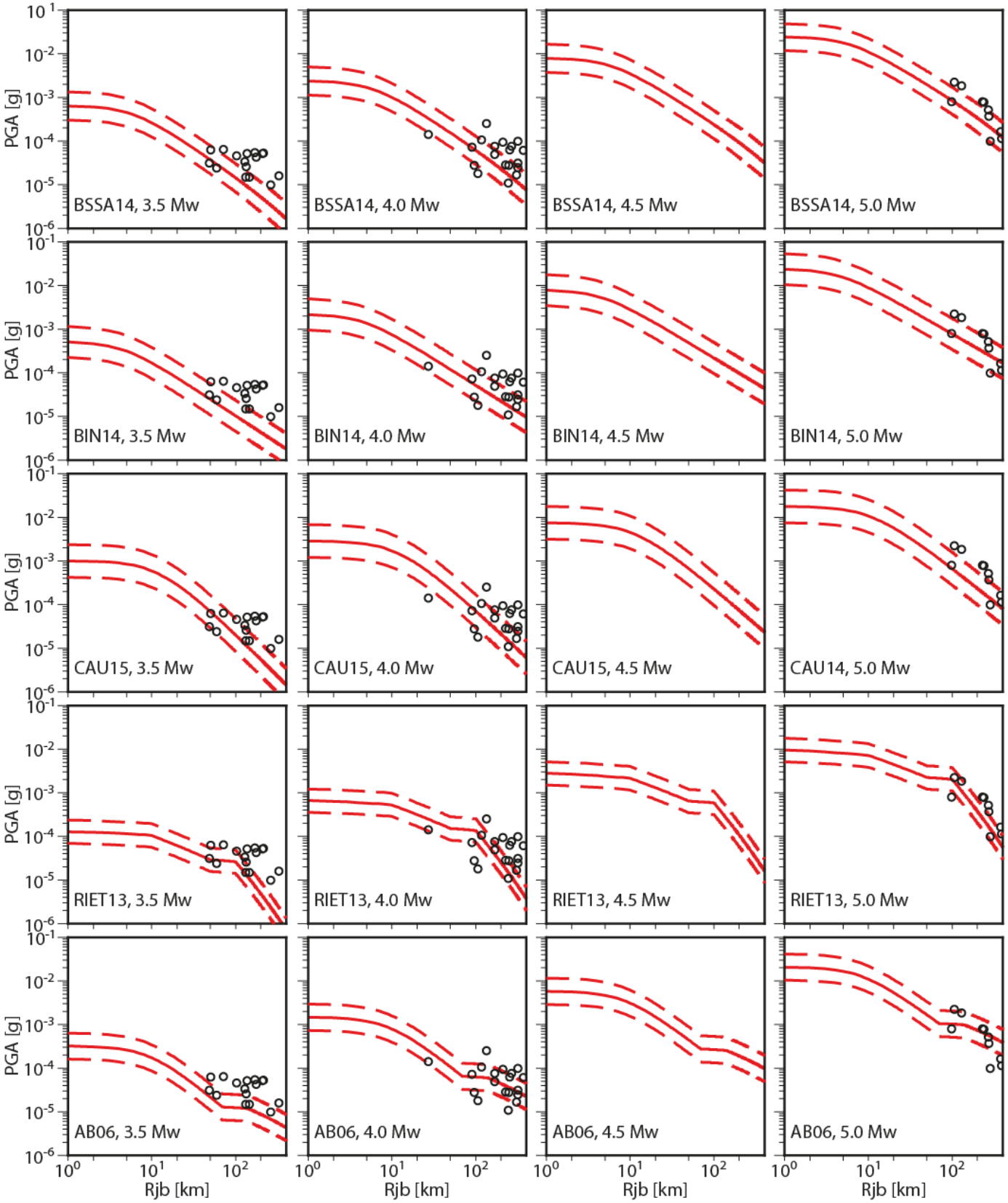

Figure 51: Comparison of the ground motion curves from a set of GMPEs and the UK strong motion data for 1.0 s SA. The solid red lines describe the median prediction of the GMPEs; and the dashed red lines describes the median prediction ± one sigma.

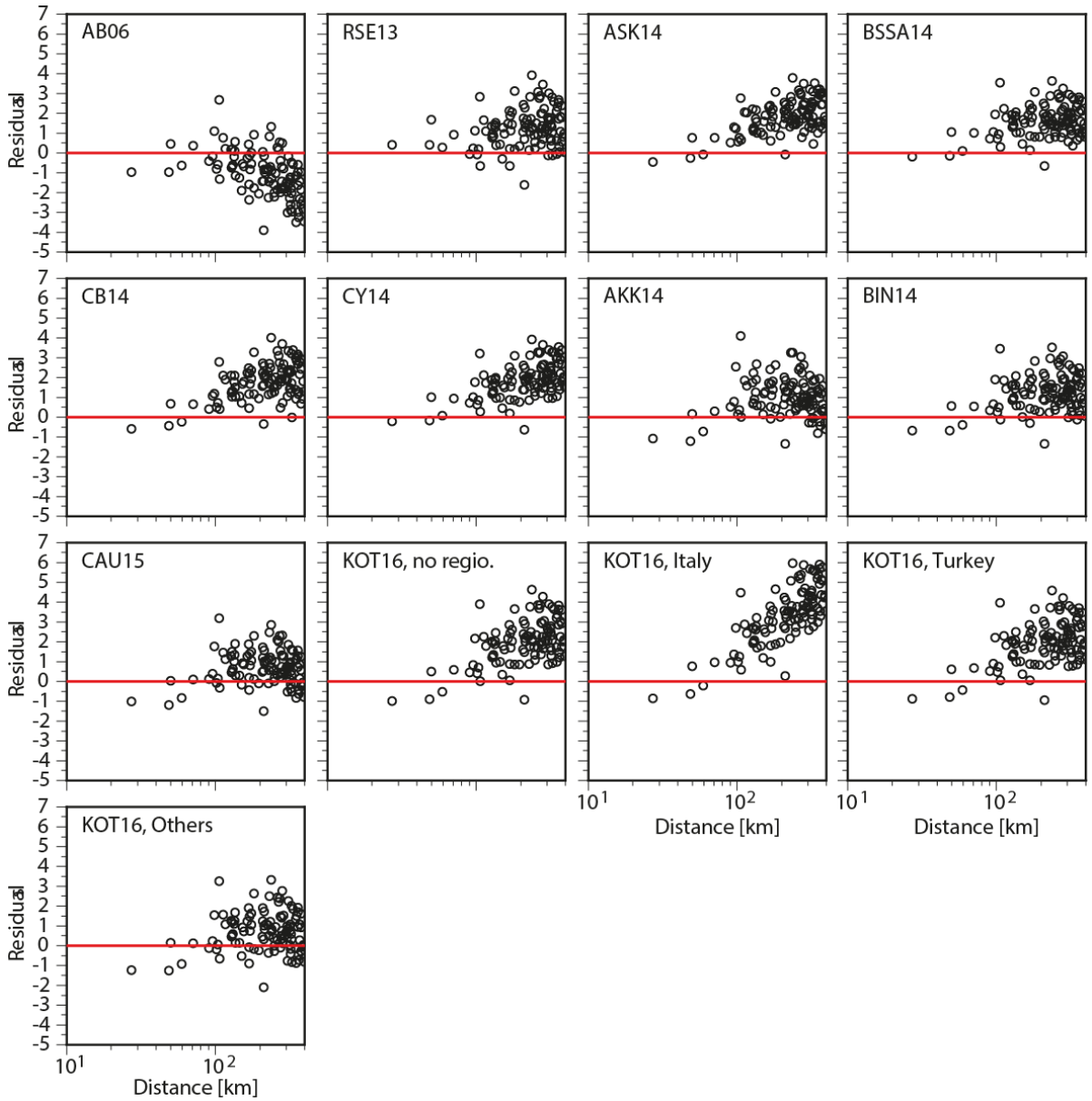

Figure 52: Model residuals between the UK strong motion data and the predictions for a set of GMPEs for 0.2 s SA. The red line describes the ideal case, i.e. when the residuals are zero.

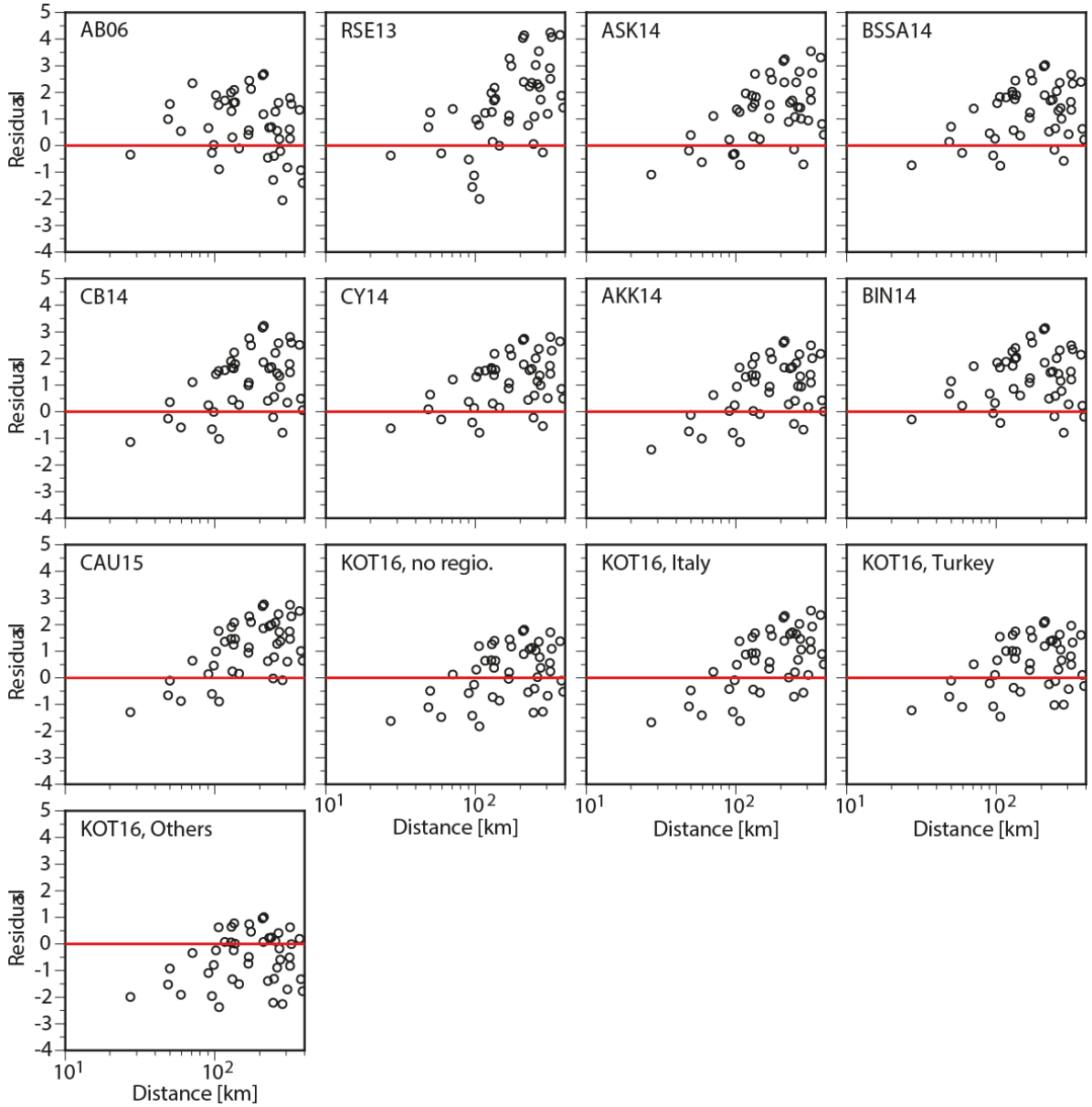

Figure 53: Model residuals between the UK strong motion data and the predictions for a set of GMPEs for 1.0 s SA. The red line describes the ideal case, i.e. when the residuals are zero.

Appendix 2 Hazard Maps

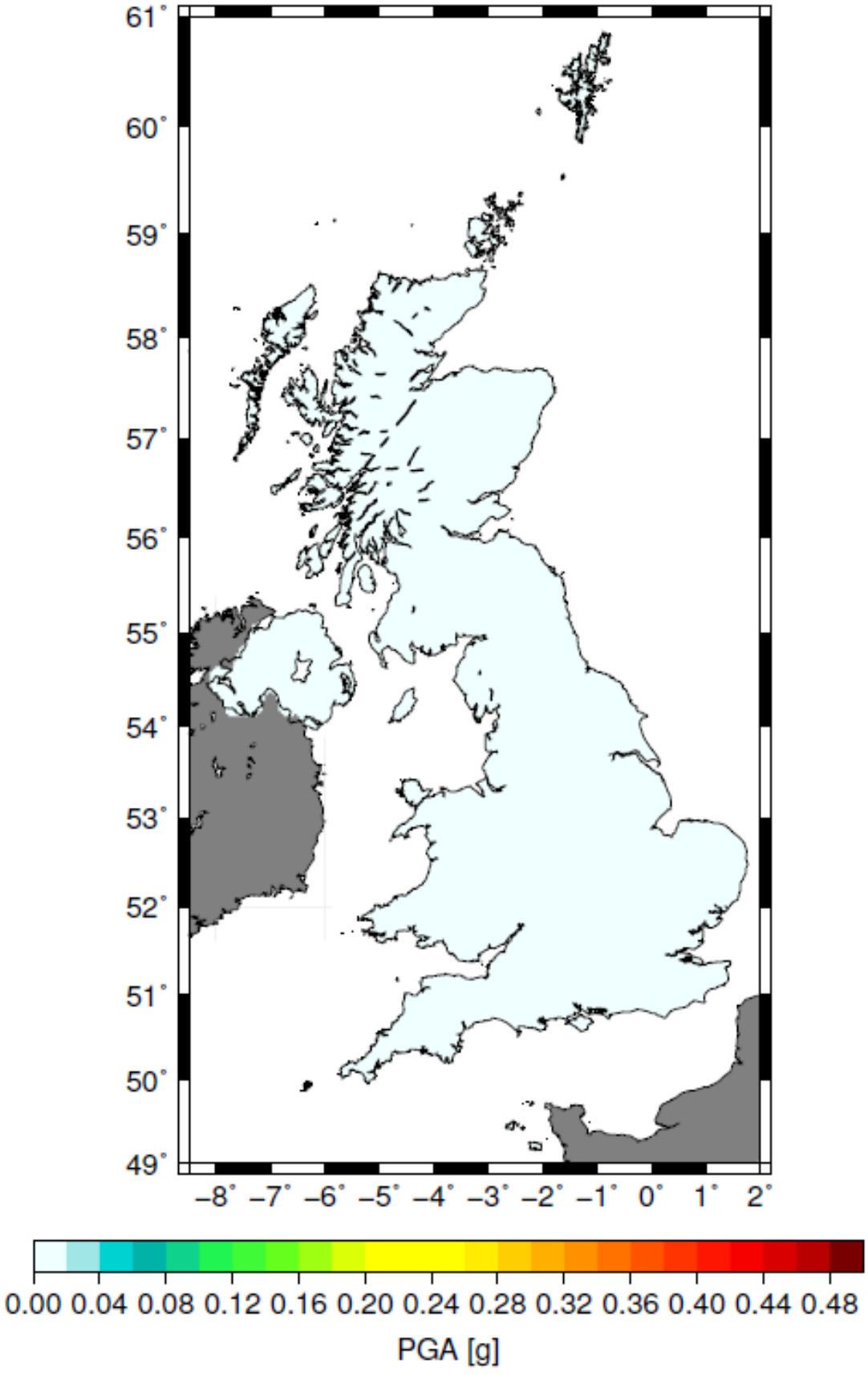

Figure 54: Hazard map for PGA for a 95 year return period.

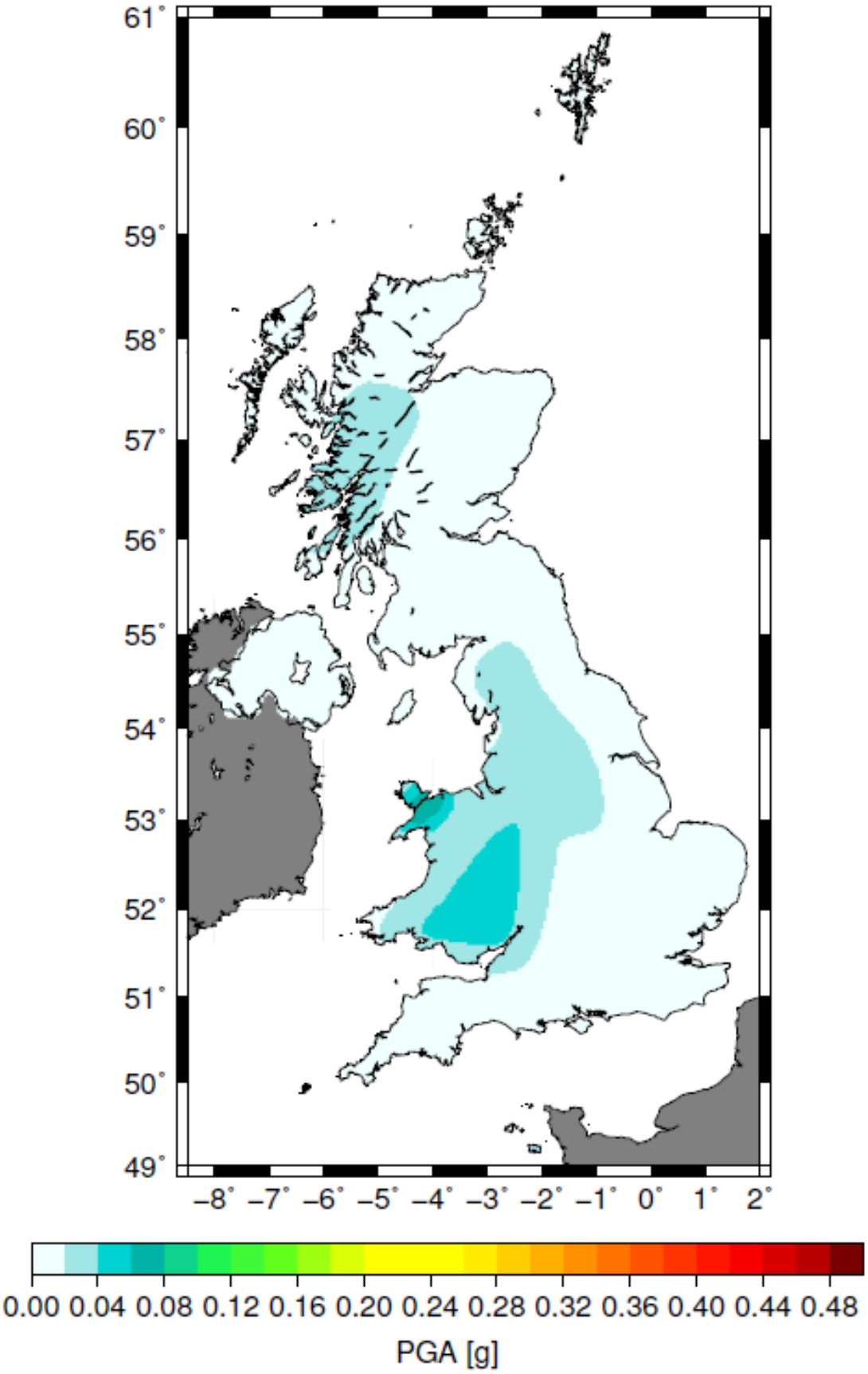

Figure 55: Hazard map for PGA for a 475 year return period.

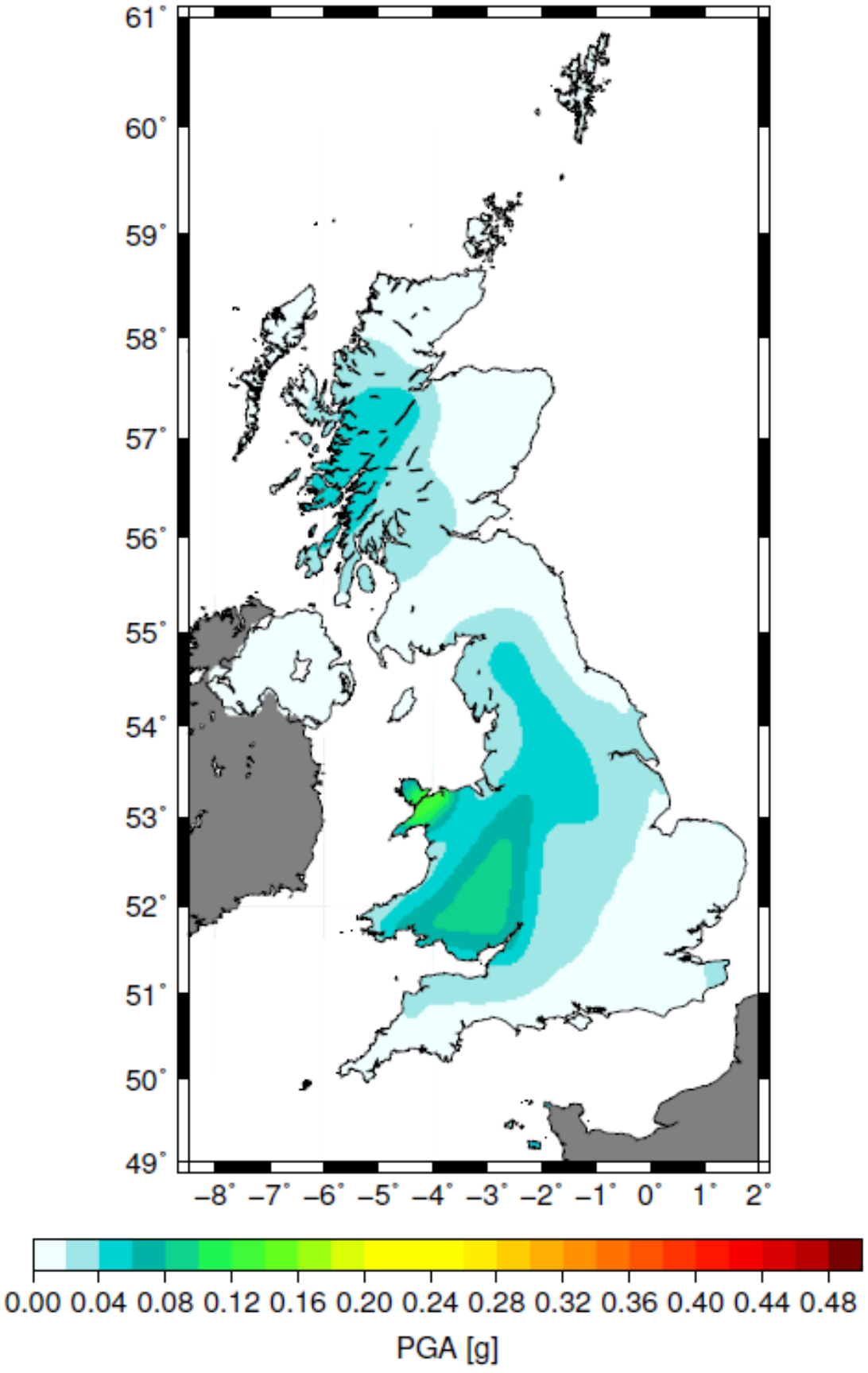

Figure 56: Hazard map for PGA for a 1100 year return period.

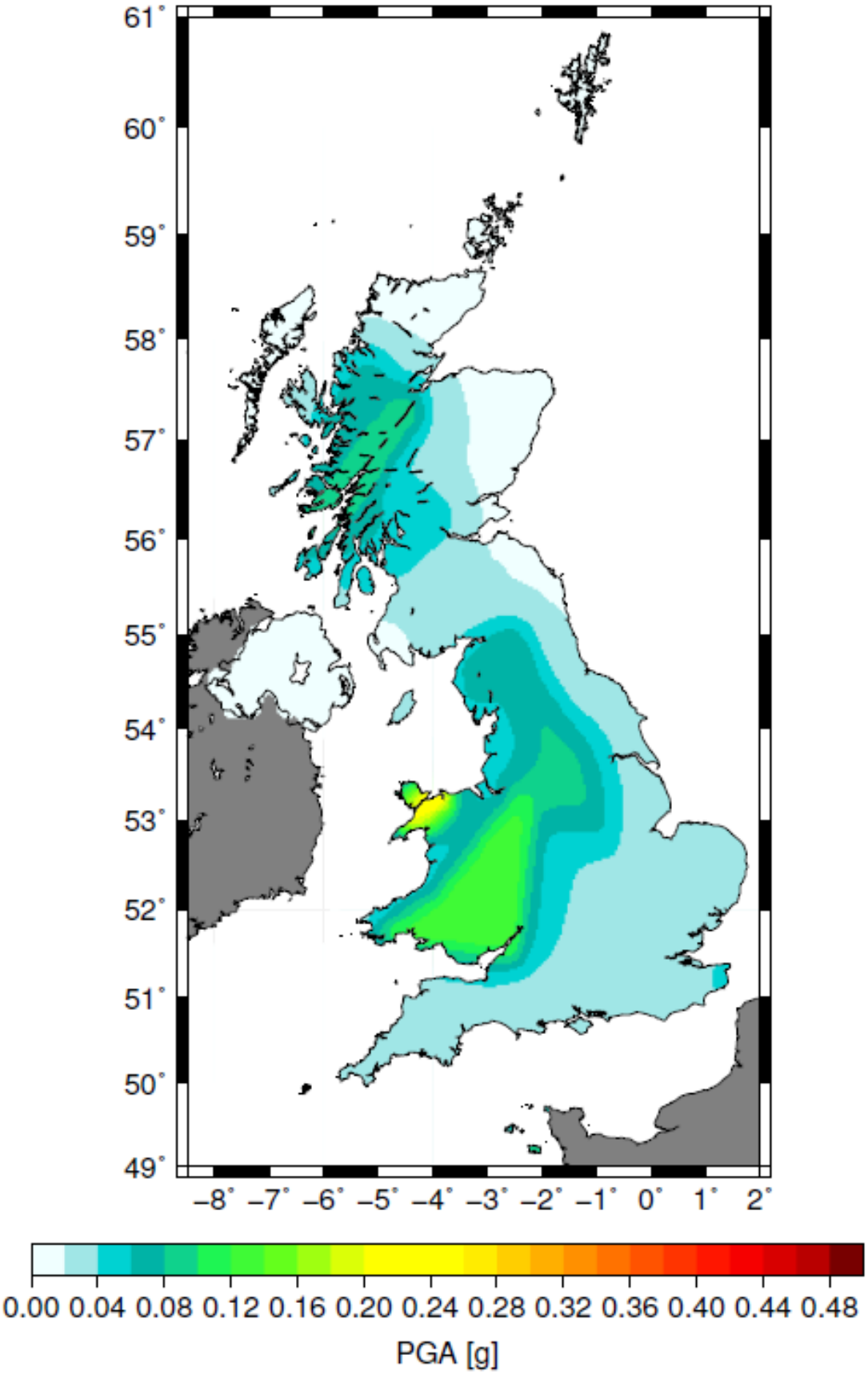

Figure 57: Hazard map for PGA for a 2475 year return period.

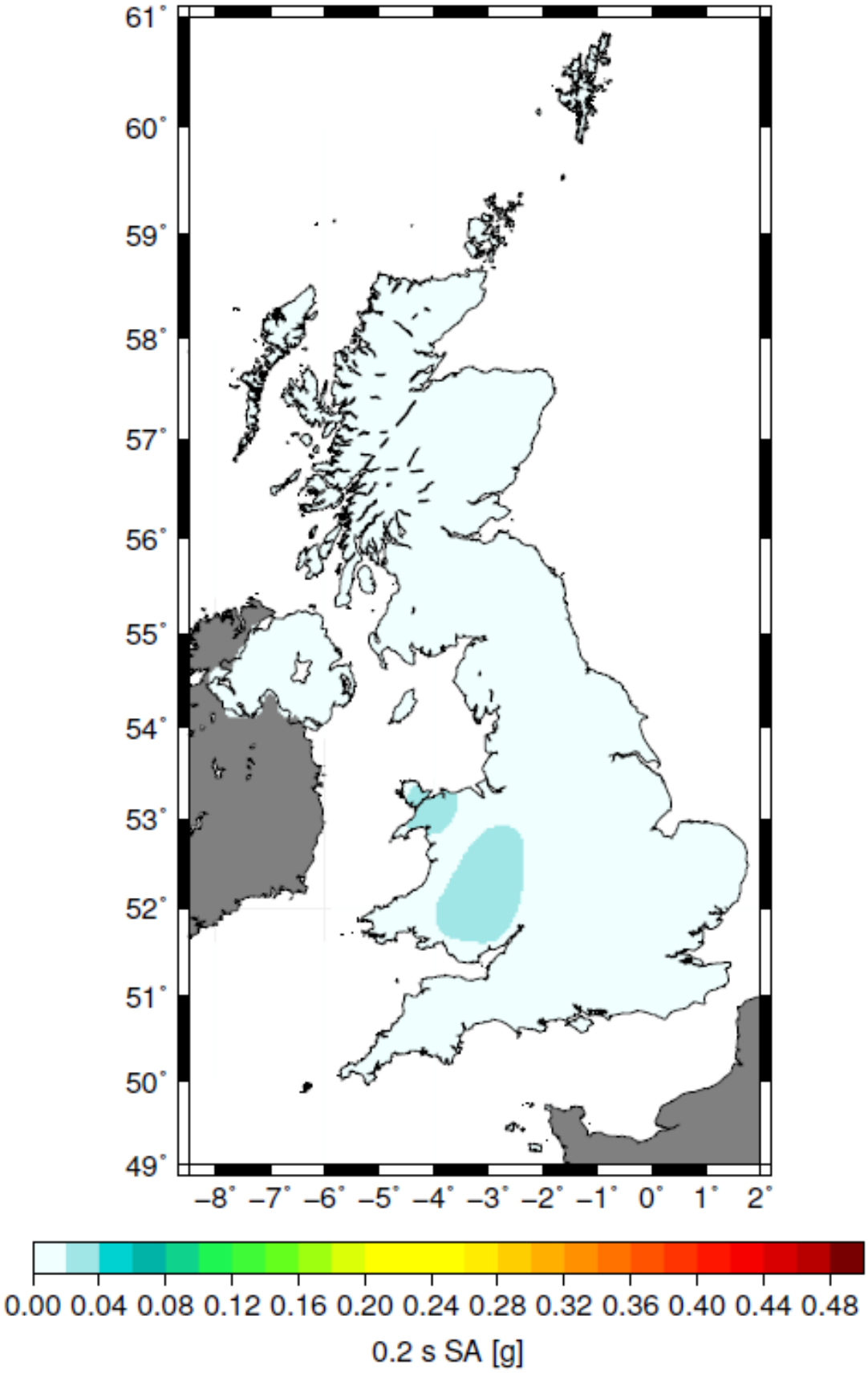

Figure 58: Hazard map for 0.2 s SA for a 95 year return period.

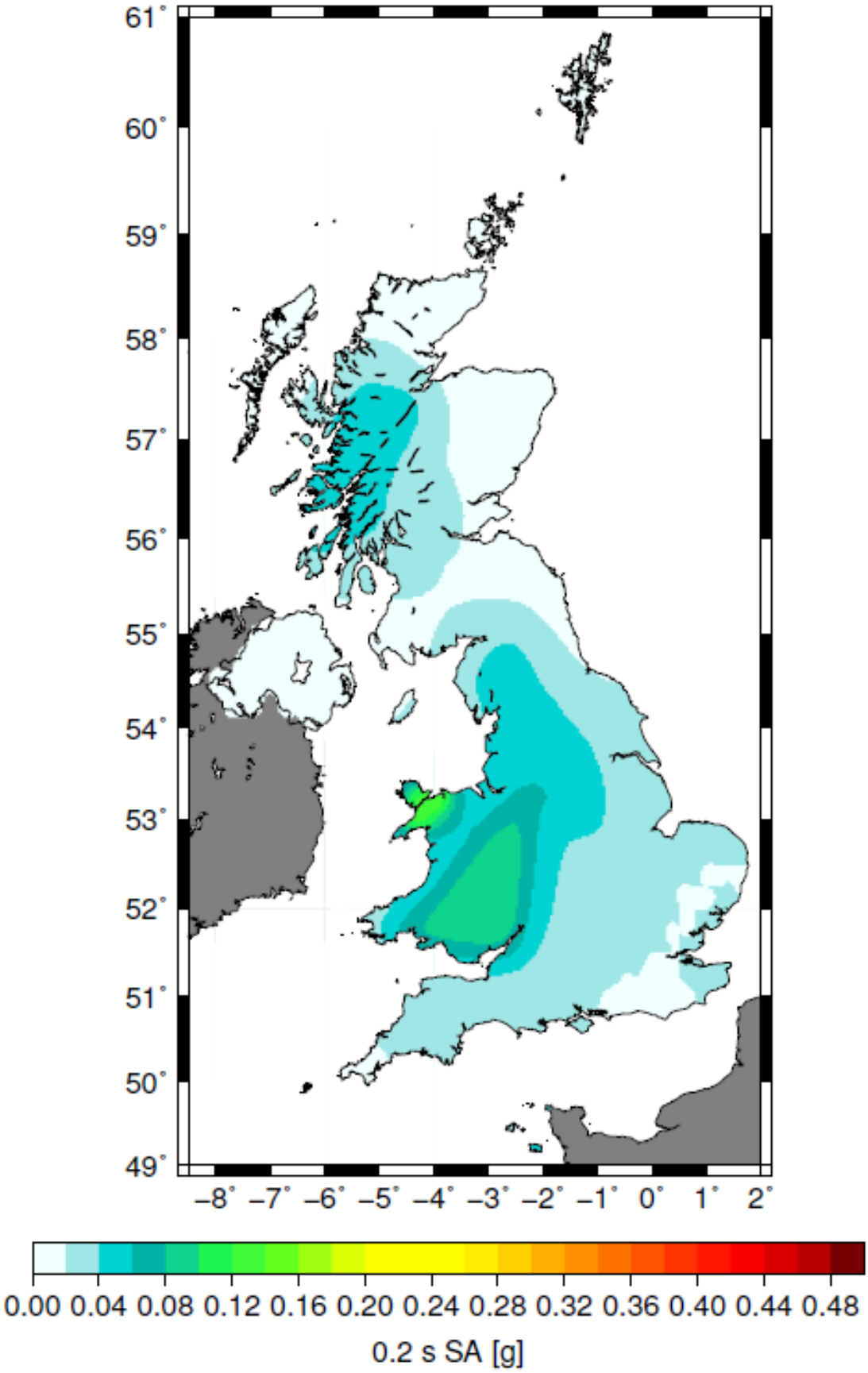

Figure 59: Hazard map for 0.2 s SA at the 475 year return period.

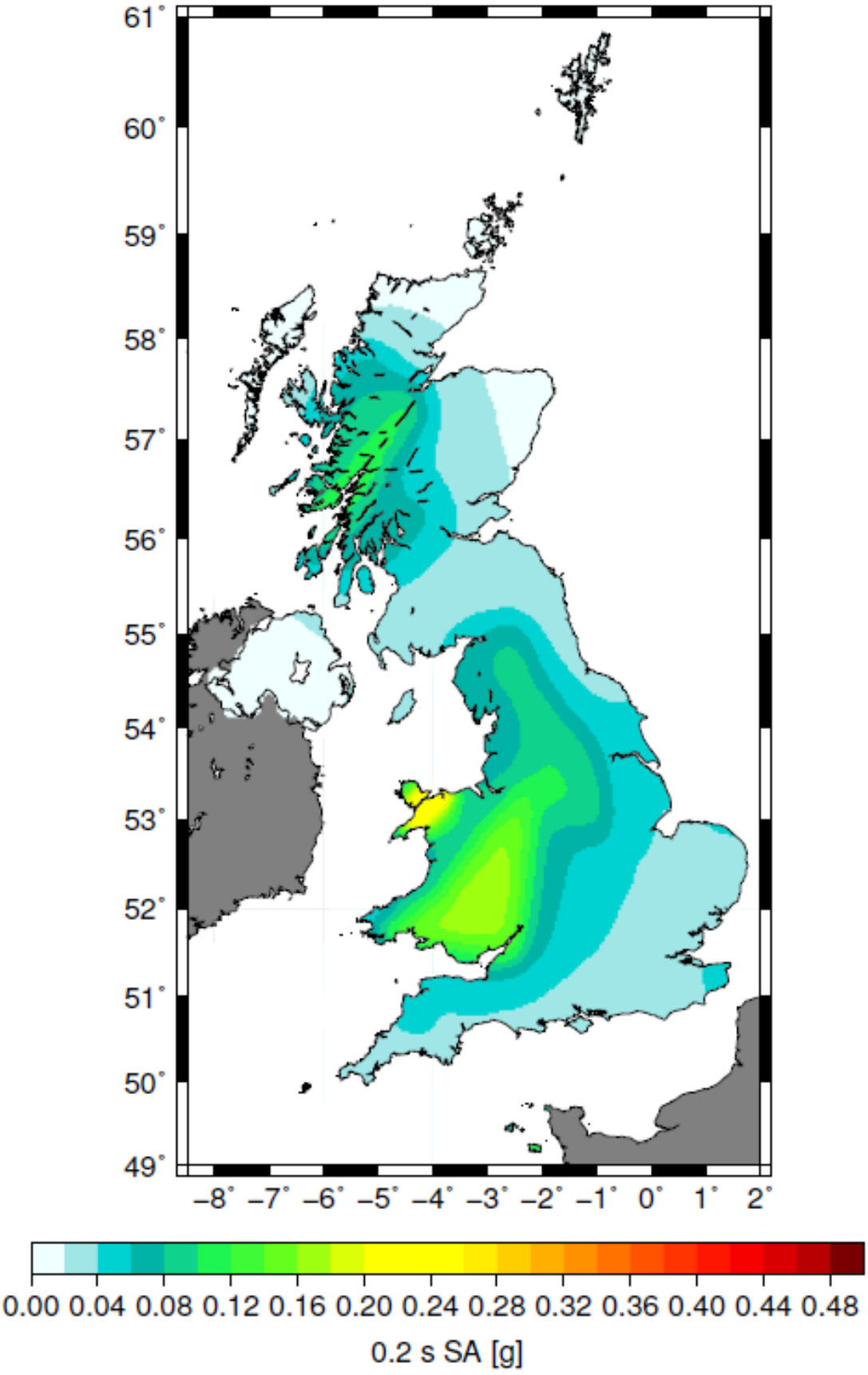

Figure 60: Hazard map for 0.2 s SA for a 1100 year return period.

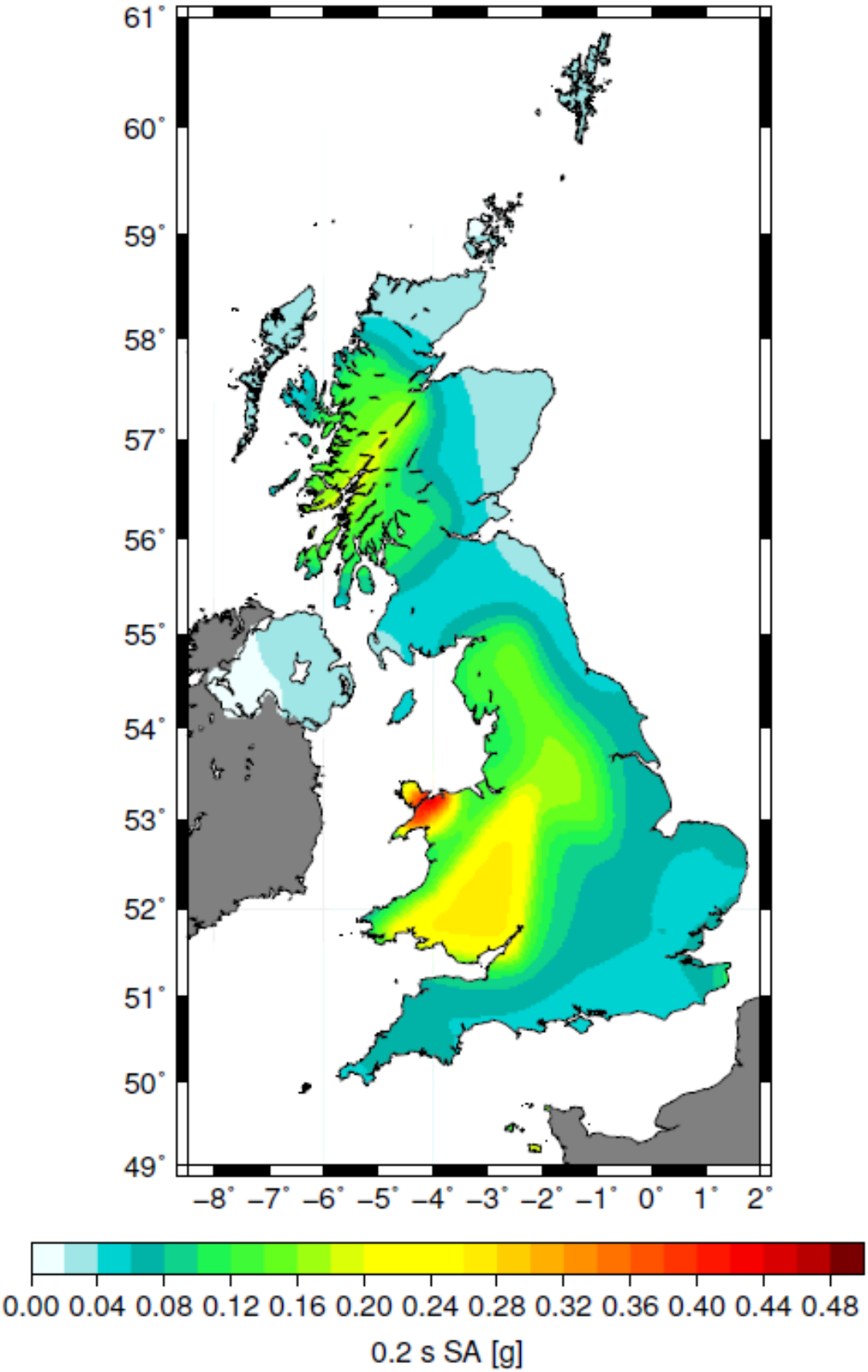

Figure 61: Hazard map for 0.2 s SA for a 2475 year return period.

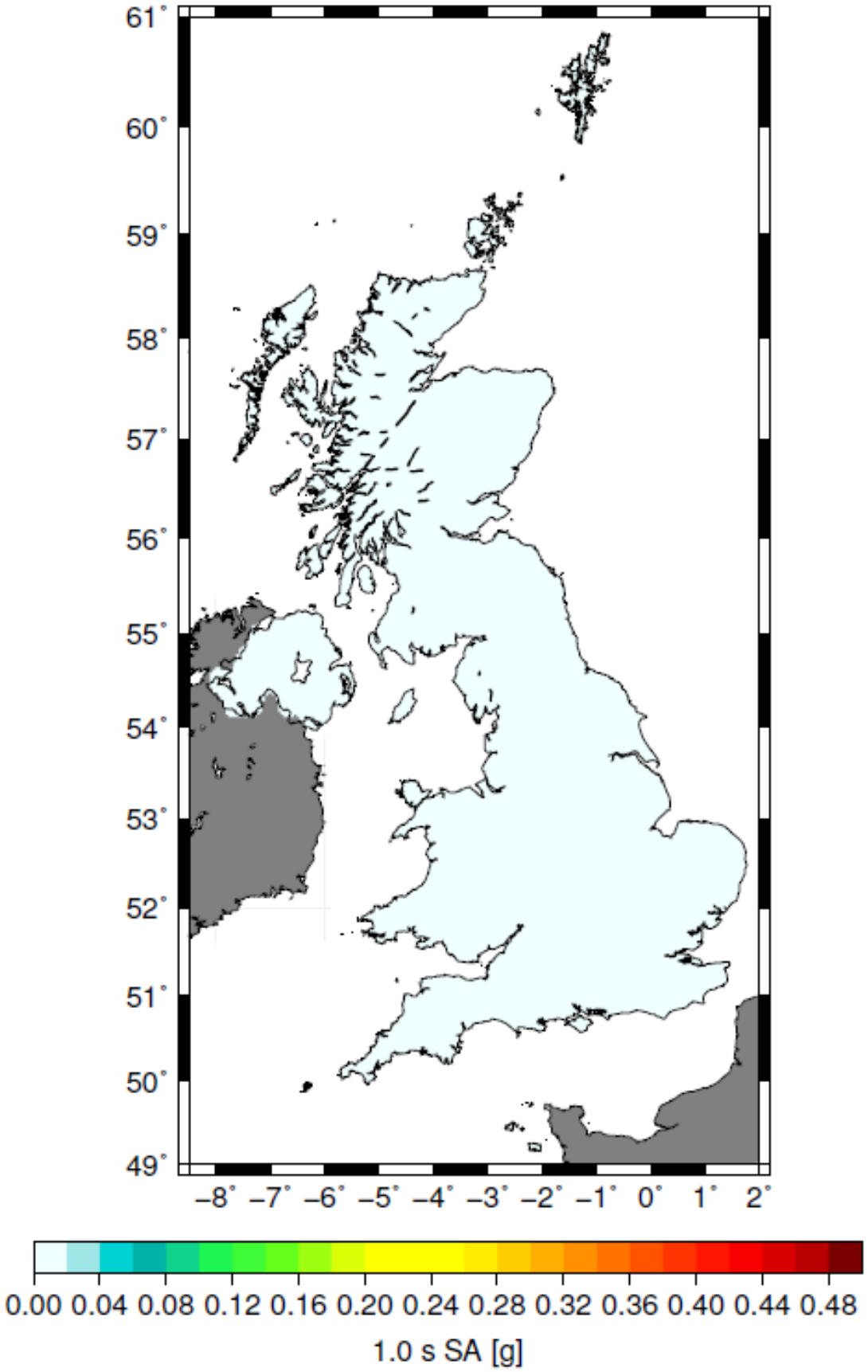

Figure 62: Hazard map for 1.0 s SA for a 95 year return period.

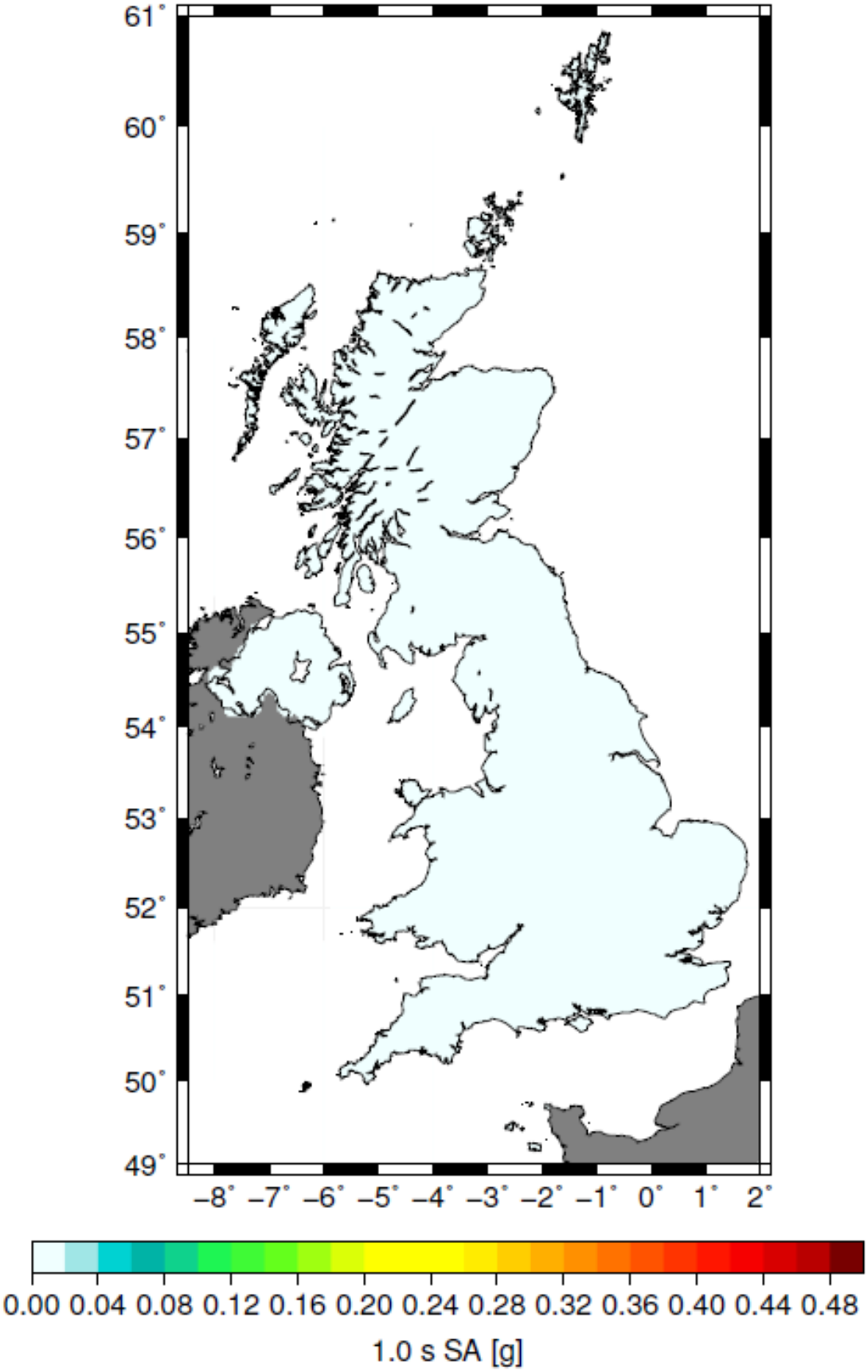

Figure 63: Hazard map for 1.0 s SA for a 475 year return period.

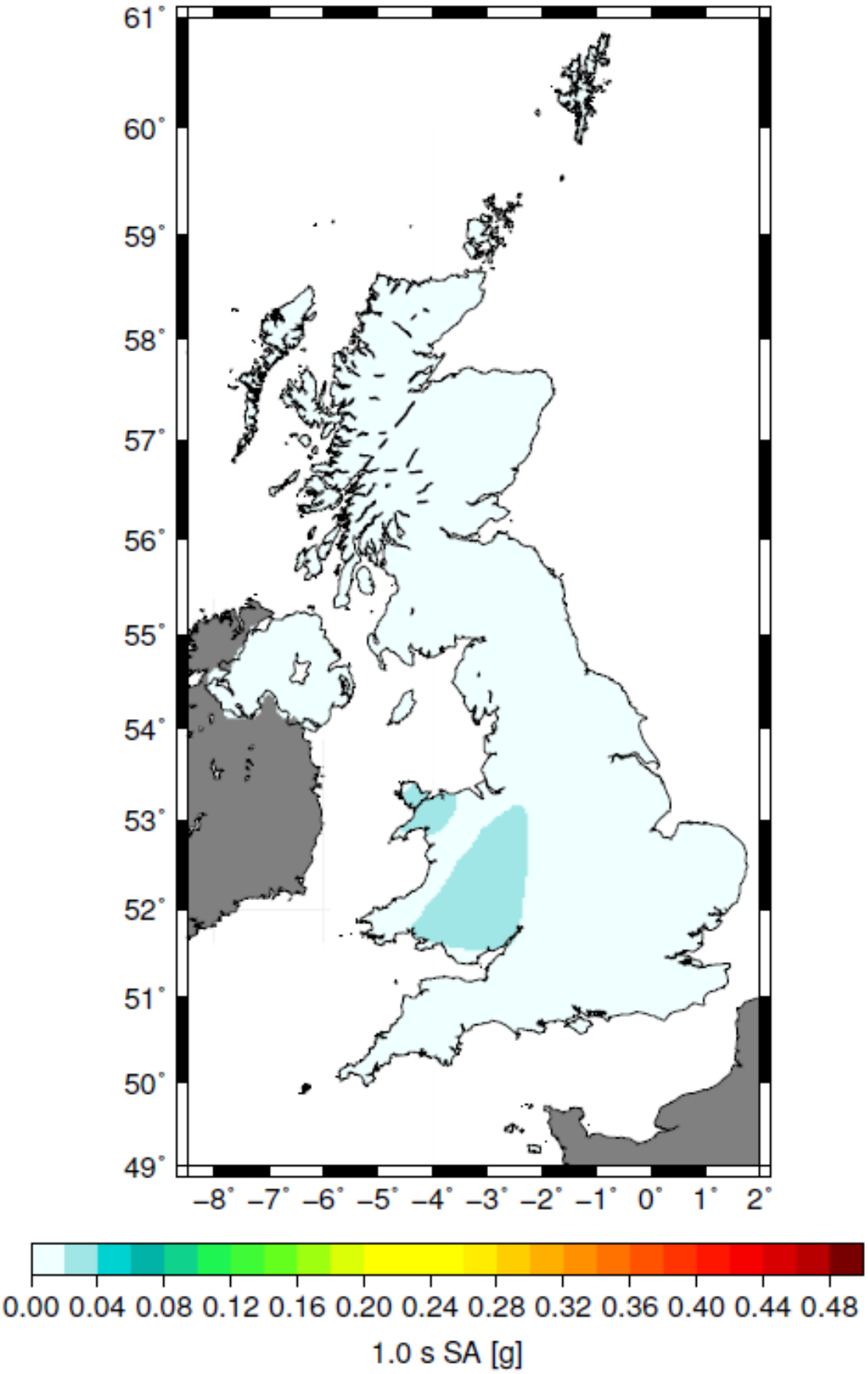

Figure 64: Hazard map for 1.0 s SA for a 1100 year return period.

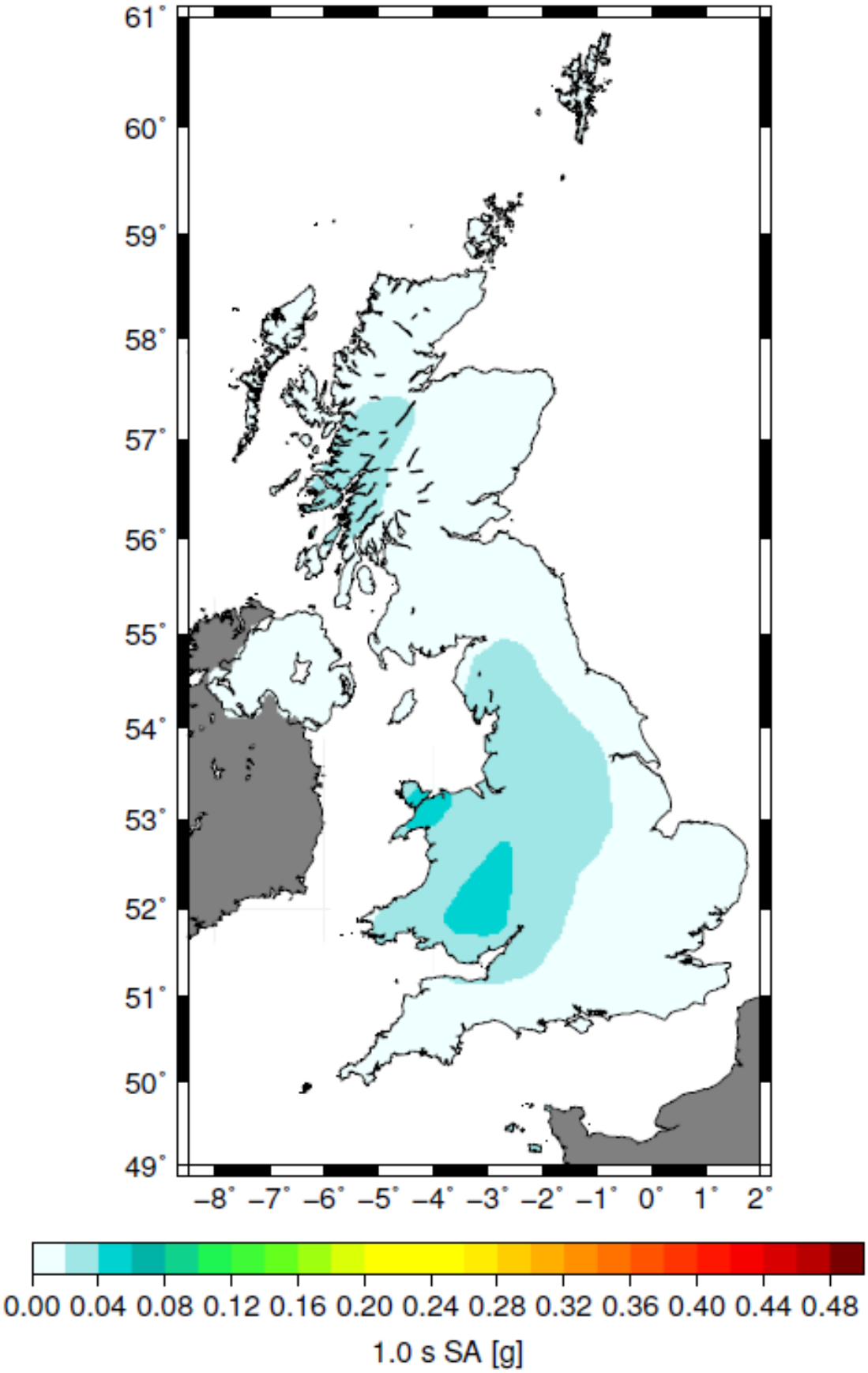

Figure 65: Hazard map for 1.0 s SA for a 2475 year return period.

Appendix 3

The results of the disaggregation analysis for 0.2 s SA and 1.0 s SA are shown in Tables 13-14 and Figures 66-73 for PGA.

As observed for PGA in Table 12, the hazard for 0.2 s and 1.0 s SA is dominated by MMCW2 at 475 yr and 2475 yr for the Cardiff site with other zones contributing very little to the hazard. Zones in south-eastern Britain/northern France region control the hazard at the Dover site and the largest contribution is from zone DOVE. For the Edinburgh site, the largest contributions to the hazard are from zones SC34, SC78 and PENN. Finally, for the London site, zones in southern Britain dominate although zone MMCW2 also makes a significant contribution.

Disaggregating the hazard by magnitude, distance and ε for the Cardiff site, we observe that at both 475 yr and 2475 yr for 0.2 s SA, the greatest contribution to the hazard comes from relatively small earthquakes of around 4.5-4.7 Mw and at relatively short distances (< 20 km; Figure 66). For 1.0 s SA, slightly larger earthquakes (4.7-5.1 Mw) at relatively short distances (< 20 km) make the biggest contribution to the hazard (Figure 67). The dominance of zone DOVE is evident when the hazard for the Dover site is disaggregated in terms of magnitude, distance and ε (Figures 68-69). For 0.2 s SA and 1.0 s SA, there is a single pronounced peak at 4.0-4.1 Mw and distances of 5-15 km for 475 yr and 2475 yr although larger earthquakes (4.6-5.0 Mw) make a great contribution. For the Edinburgh site, a broad range of earthquakes contributes to the 0.2 s SA hazard (distances of 0-150 km and magnitudes of 5-6 Mw) although there is a peak at 4.5-4.7 Mw and 45-55 km distances making the biggest contribution to the hazard for 475 yr and at 4.7-4.9 Mw and 35-45 km distances for 2475 yr (Figure 70). For a 1.0 s period, larger earthquakes at longer distances contribute more to the hazard (5.7-5.9 Mw at distances of 145-155 km for 475 yr and 5.7-6.1 Mw at 125-165 km for 2475 yr; Figure 71). The hazard at the London site is also dominated by relatively small earthquakes (4.3-4.5 Mw) at short distances less than 40 km) for 0.2 s SA (Figure 72). For 1.0 s SA, larger events (5.9-6.1 Mw) at longer distances (> 200 km) do become dominant (Figure 73).

Contribution to hazard [%] for 0.2 s SA								
	Cardiff		*Dover*		*Edinburgh*		*London*	
Zone	*475 yr*	*2475 yr*	*475 yr*	*2475 yr*	*475 yr*	*2475 yr*	*475 yr*	*2475 yr*
CORN	0.5	0.0	0.0	0.0	0.0	0.0	0.1	0.0
RHEN	3.4	1.8	4.5	4.5	0.0	0.0	5.6	5.8
WCHA	0.3	0.0	5.3	2.9	0.0	0.0	5.1	4.1
DOVE	0.0	0.0	45.6	68.0	0.0	0.0	9.8	8.3
SLPT	0.0	0.0	1.2	0.1	0.4	0.1	2.6	0.8
EANG	0.0	0.0	10.9	8.5	0.2	0.1	15.9	15.5
MMCE	1.1	0.6	6.6	2.6	0.0	0.0	29.7	52.3
PENN	0.2	0.0	0.3	0.0	13.3	10.8	3.9	1.7
MMCW1	6.9	4.6	0.0	0.0	0.0	0.0	0.0	0.0
MMCW2	86.7	93.1	1.0	0.3	0.1	0.0	17.0	7.4
MENA2	0.7	0.0	0.0	0.0	0.3	0.1	0.0	0.0
CUMF	0.0	0.0	0.0	0.0	6.4	4.7	0.0	0.0
BALA	0.0	0.1	0.0	0.0	0.0	0.0	0.0	0.0
SC1M	0.0	0.0	0.0	0.0	10.2	18.0	0.0	0.0
SC34	0.0	0.0	0.0	0.0	37.2	41.2	0.0	0.0

SC78	0.0	0.0	0.0	0.0	17.0	12.2	0.0	0.0
SC9	0.0	0.0	0.0	0.0	6.9	3.7	0.0	0.0
ESCO	0.0	0.0	0.0	0.0	7.8	8.9	0.0	0.0
IREL	0.0	0.0	0.0	0.0	0.2	0.0	0.0	0.0
NORM	0.2	0.0	2.8	0.7	0.0	0.0	5.0	1.6
PASC	0.0	0.0	21.8	12.4	0.0	0.0	5.3	2.4

Table 13: Disaggregation results (by zone) for four sites across the UK and for 0.2 s SA at 475 and 2475 years.

Contribution to hazard [%] for 1.0 s SA								
	Cardiff		*Dover*		*Edinburgh*		*London*	
Zone	*475 yr*	*2475 yr*	*475 yr*	*2475 yr*	*475 yr*	*2475 yr*	*475 yr*	*2475 yr*
CORN	1.6	1.2	0.0	0.0	0.0	0.0	0.1	0.1
RHEN	3.1	3.1	3.7	3.7	0.0	0.0	3.6	4.4
WCHA	1.9	1.3	5.8	5.0	0.0	0.0	4.8	4.6
DOVE	0.0	0.0	28.5	37.7	0.0	0.0	6.0	7.0
SLPT	0.0	0.0	4.9	3.0	1.2	0.9	5.4	4.4
EANG	0.5	0.3	9.3	9.8	0.9	0.7	9.5	10.9
MMCE	2.6	1.9	6.9	6.7	0.0	0.0	16.1	22.1
PENN	2.6	1.0	2.1	1.2	18.3	17.8	6.8	5.9
MMCW1	1.4	0.2	0.0	0.0	0.0	0.0	0.0	0.0
MMCW2	77.3	86.4	6.0	3.8	0.3	0.3	29.4	23.9
MENA2	5.0	2.8	0.0	0.0	1.3	1.2	0.0	0.0
CUMF	0.0	0.0	0.0	0.0	6.6	6.9	0.0	0.0
BALA	0.1	0.1	0.0	0.0	0.0	0.0	0.1	0.0
SC1M	0.0	0.0	0.0	0.0	7.1	8.4	0.0	0.0
SC34	0.0	0.0	0.0	0.0	25.3	26.9	0.0	0.0
SC78	0.0	0.0	0.0	0.0	19.9	20.1	0.0	0.0
SC9	0.0	0.0	0.0	0.0	11.2	9.2	0.0	0.0
ESCO	0.0	0.0	0.1	0.0	7.3	7.2	0.0	0.0
IREL	0.1	0.0	0.0	0.0	0.5	0.4	0.0	0.0
NORM	3.8	1.8	13.7	9.0	0.0	0.0	11.9	10.8
PASC	0.0	0.0	19.1	20.1	0.0	0.0	6.3	5.7

Table 14: Disaggregation results (by zone) for four sites across the UK and for 1.0 s SA at 475 and 2475 years.

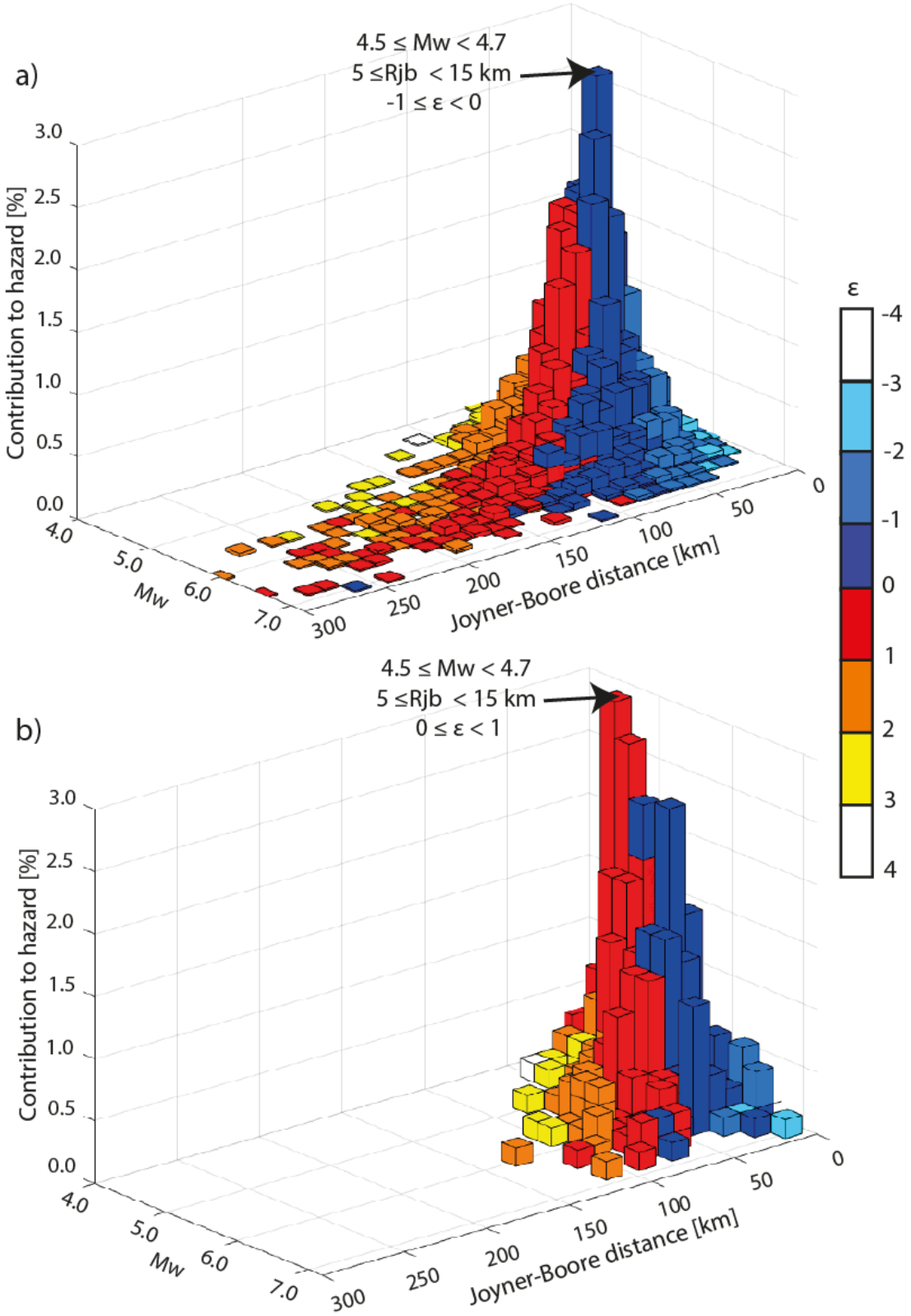

Figure 66: Disaggregation of the 0.2s SA hazard for the Cardiff site by magnitude (Mw), Joyner-Boore distance and epsilon(ε) for (a) 475 yr (0.066 g) and (b) 2475 yr (0.200 g). Numbers in brackets are the design values used for the disaggregation.

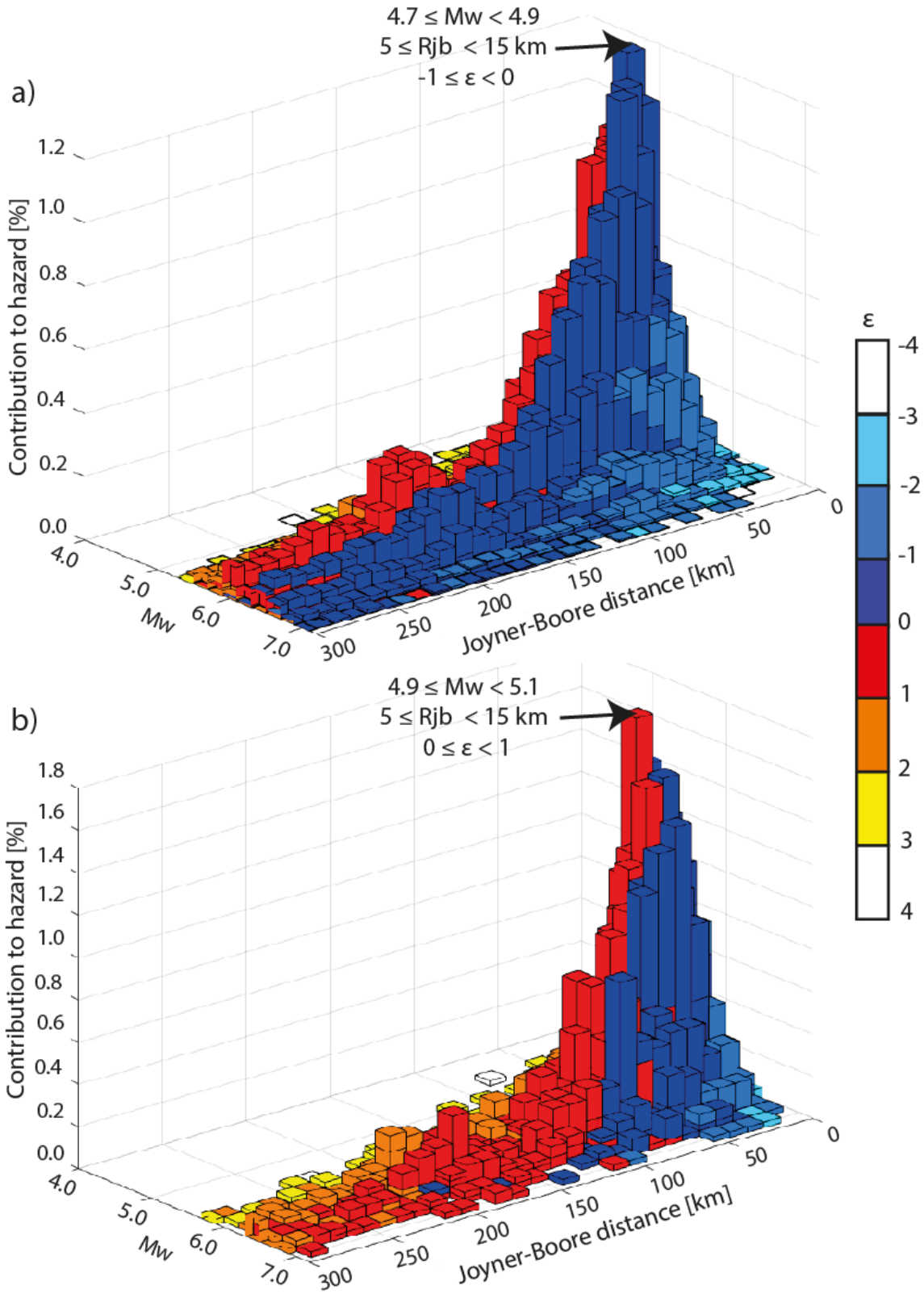

Figure 67: Disaggregation of the 1.0 s SA hazard for the Cardiff site by magnitude (Mw), Joyner-Boore distance and epsilon (ε) for (a) 475 yr (0.011 g) and (b) 2475 yr (0.032 g). Numbers in brackets are the design values used for the disaggregation.

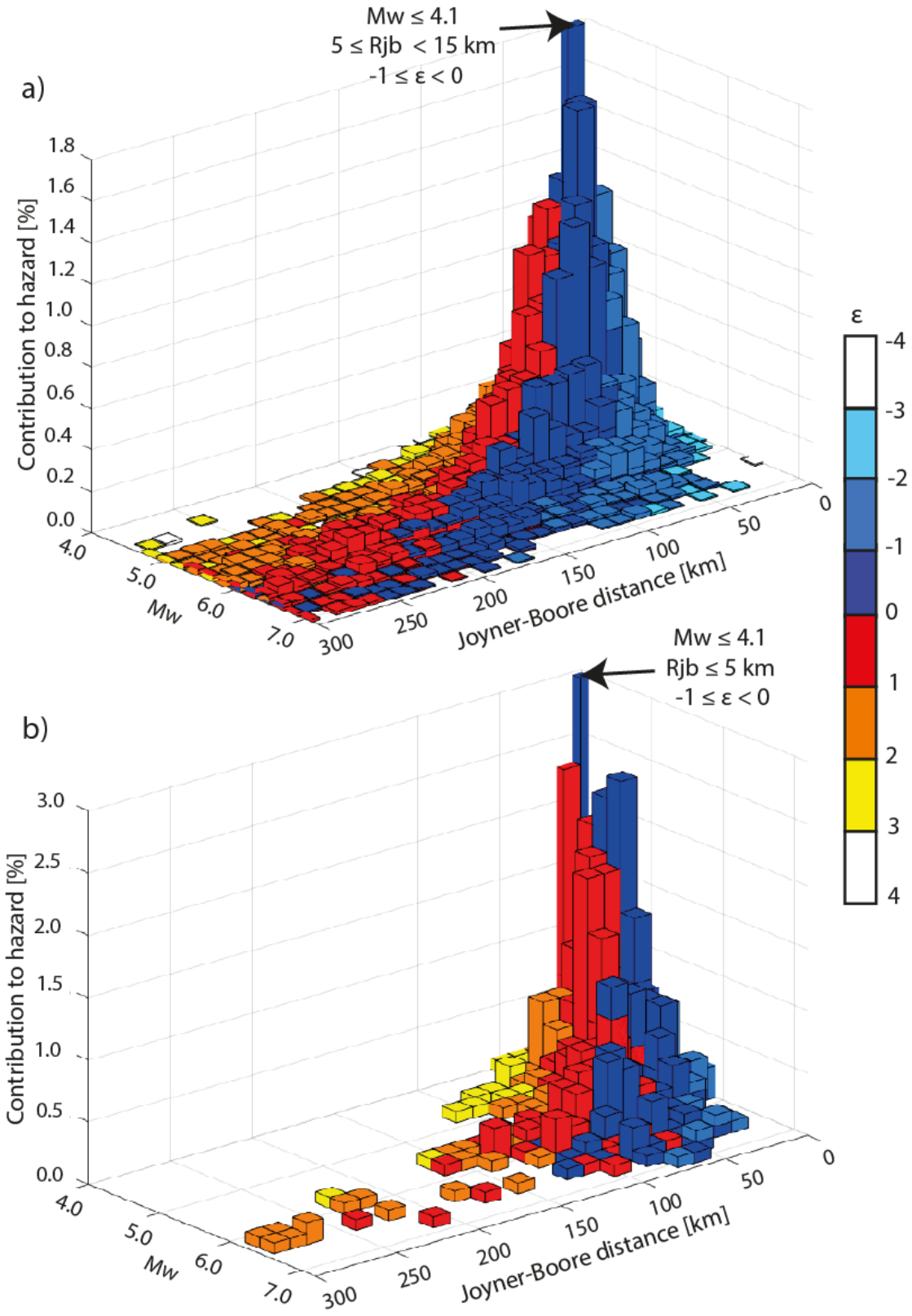

Figure 68: Disaggregation of the 0.2s SA hazard for the Dover site by magnitude (Mw), Joyner-Boore distance and epsilon (ε) for (a) 475 yr (0.029 g) and (b) 2475 yr (0.101 g). Numbers in brackets are the design values used for the disaggregation.

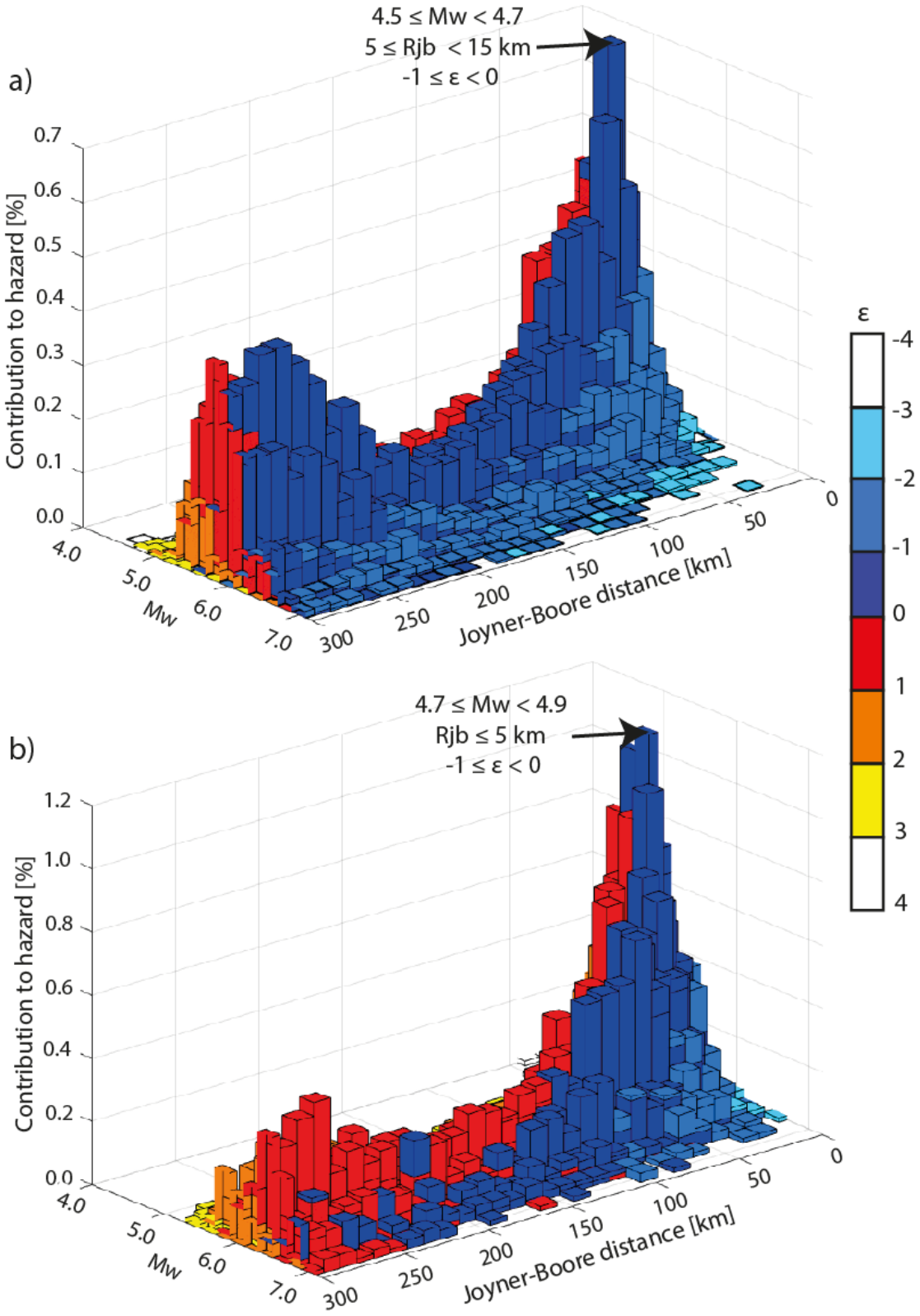

Figure 69: Disaggregation of the 1.0 s SA hazard for the Dover site by magnitude (Mw), Joyner-Boore distance and epsilon (ε) for (a) 475 yr (0.006 g) and (b) 2475 yr (0.017 g). Numbers in brackets are the design values used for the disaggregation.

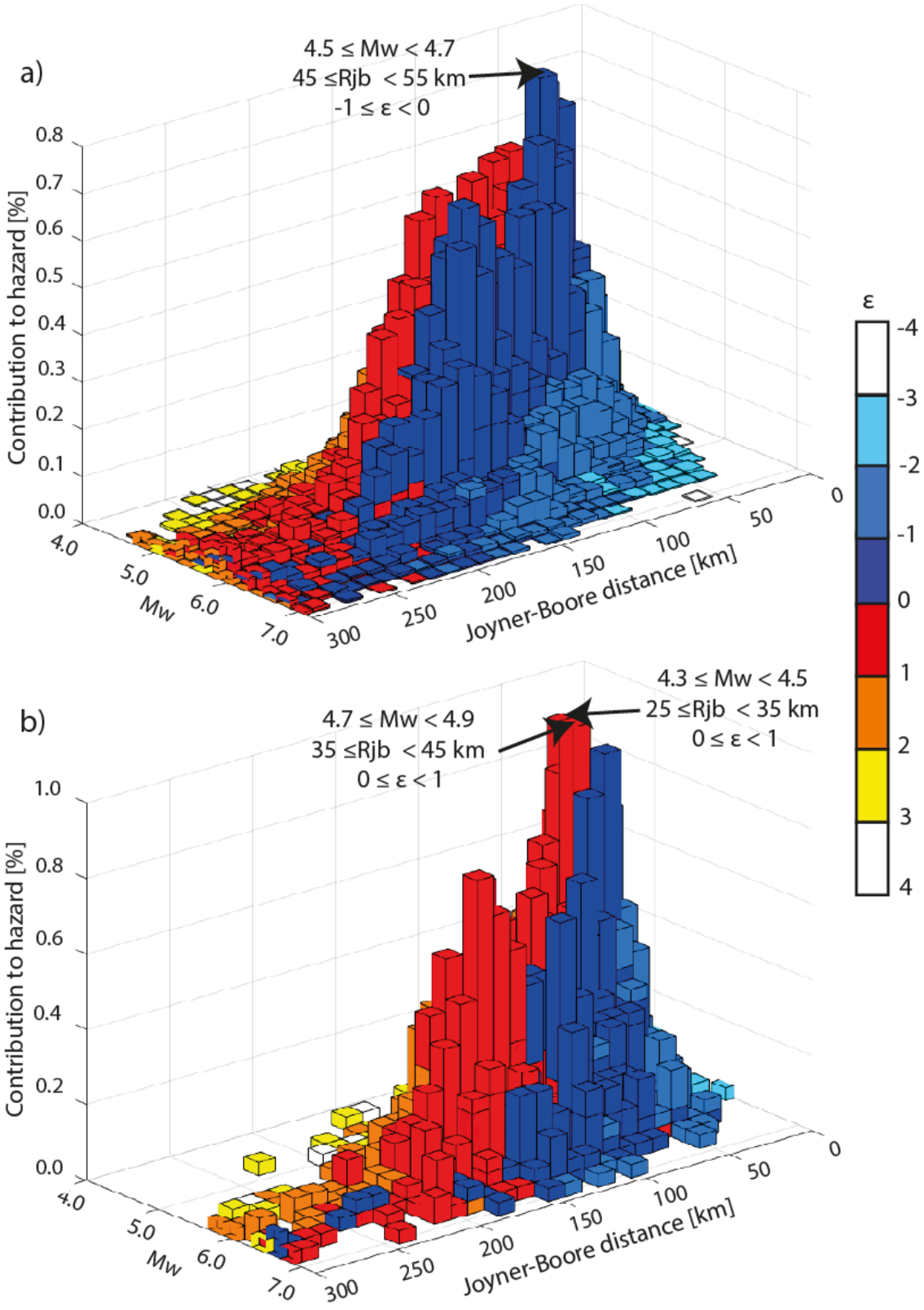

Figure 70: Disaggregation of the 0.2s SA hazard for the Edinburgh site by magnitude (Mw), Joyner-Boore distance and epsilon (ε) for (a) 475 yr (0.017 g) and (b) 2475 yr (0.048 g). Numbers in brackets are the design values used for the disaggregation.

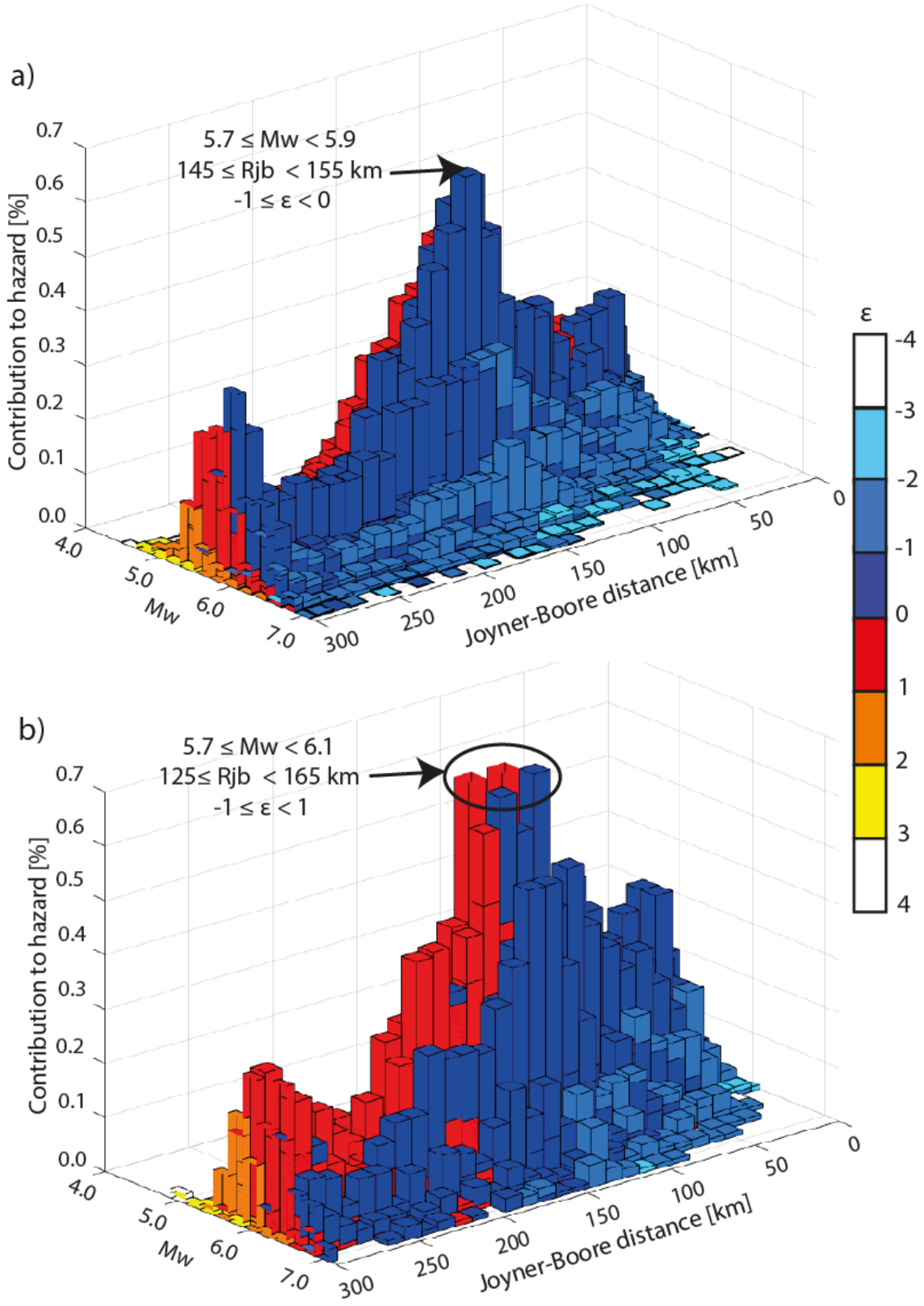

Figure 71: Disaggregation of the 1.0 s SA hazard for the Edinburgh site by magnitude (Mw), Joyner-Boore distance and epsilon (ε) for (a) 475 yr (0.005 g) and (b) 2475 yr (0.012 g). Numbers in brackets are the design values used for the disaggregation.

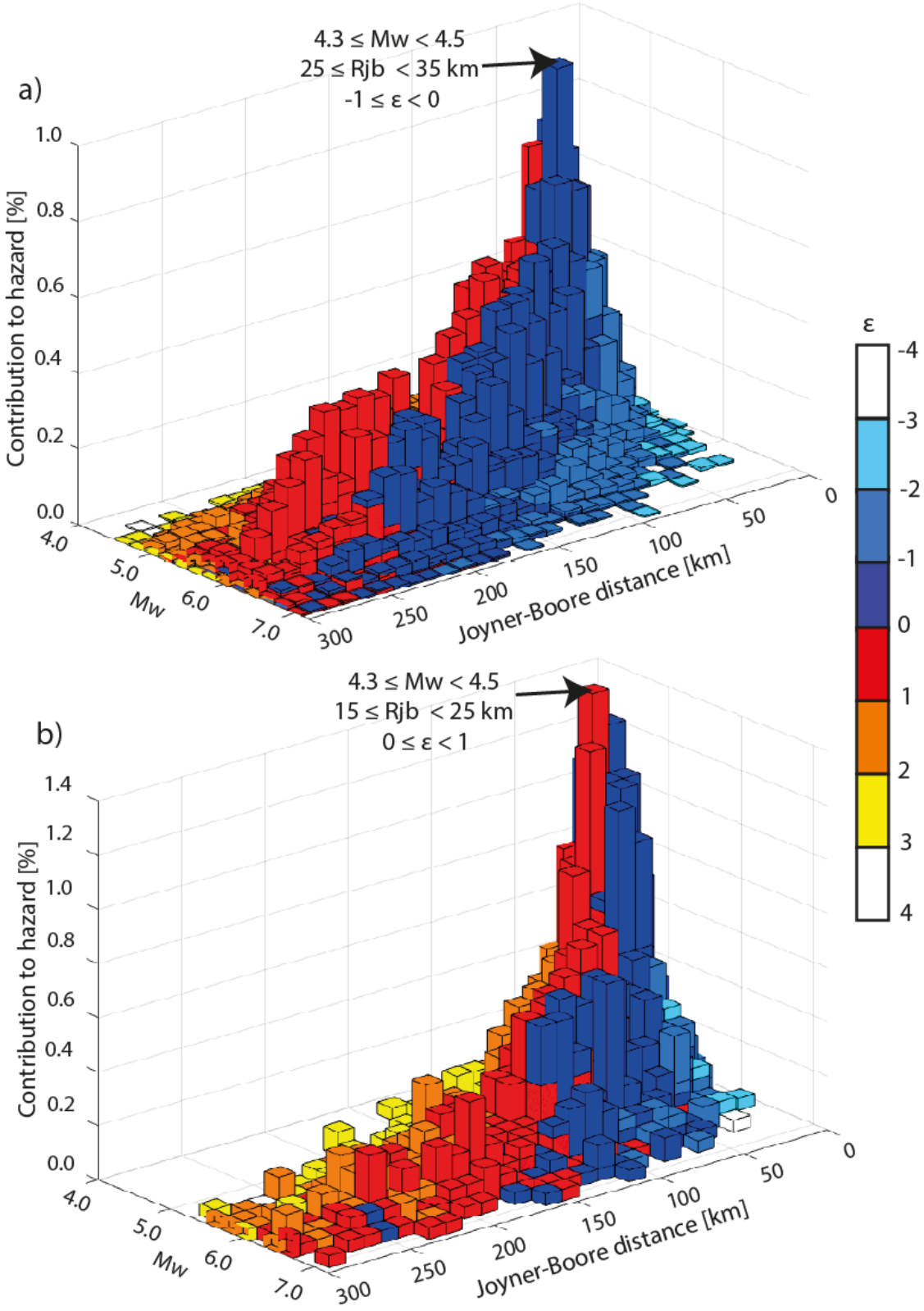

Figure 72: Disaggregation of the 0.2s SA hazard for the London site by magnitude (Mw), Joyner-Boore distance and epsilon (ε) for (a) 475 yr (0.021 g) and (b) 2475 yr (0.058 g). Numbers in brackets are the design values used for the disaggregation.

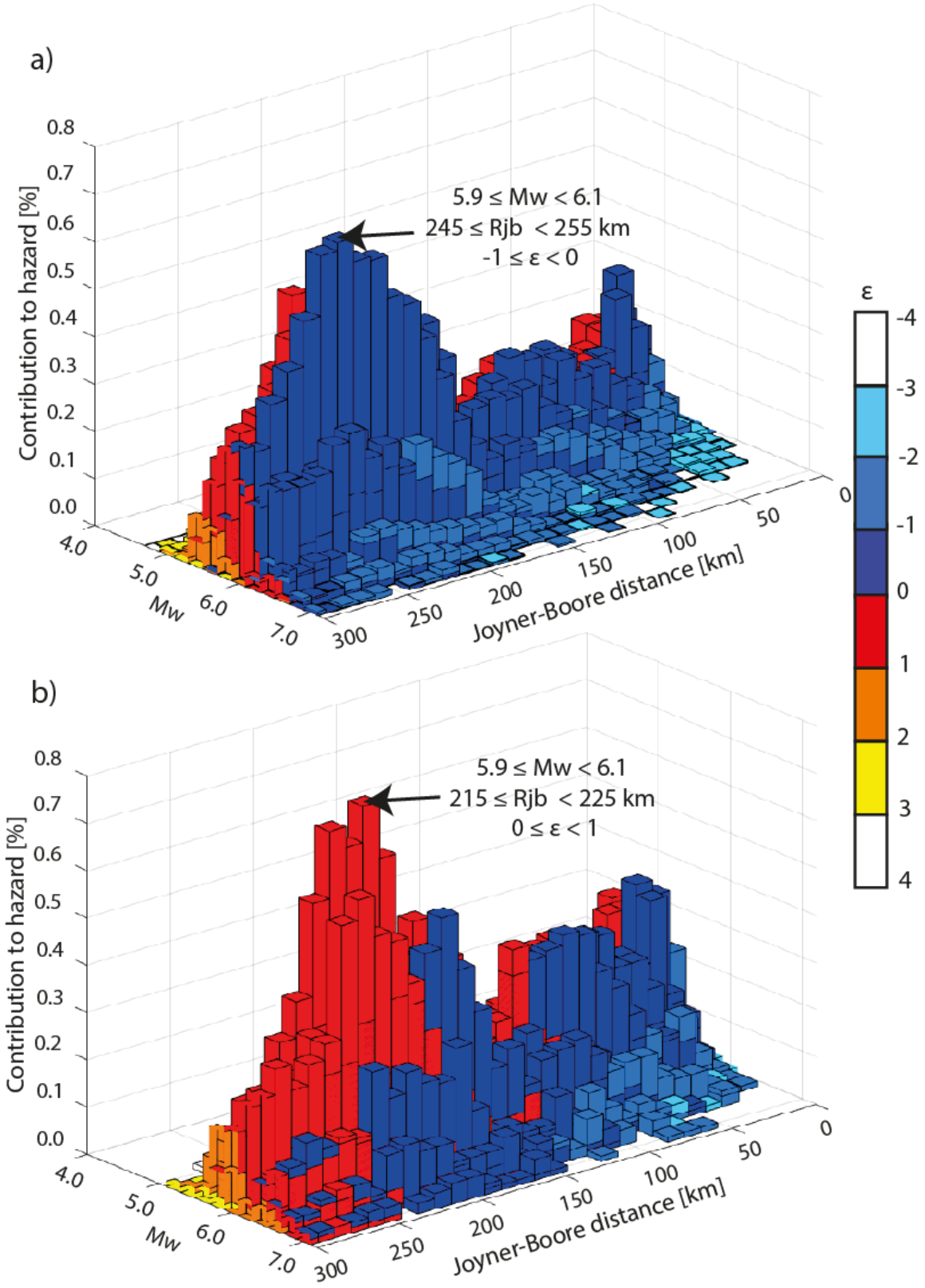

Figure 73: Disaggregation of the 1.0 s SA hazard for the London site by magnitude (Mw), Joyner-Boore distance and epsilon (ε) for (a) 475 yr (0.006 g) and (b) 2475 yr (0.015 g). Numbers in brackets are the design values used for the disaggregation.

Glossary

The definitions included in this section are taken directly from various sources: Reiter (1990), Budnitz et al. (1997), Stein and Wysession (2003), McGuire (2004), and PNNL (2014).

Activity rate: The logarithm of the number of earthquakes of magnitude zero or greater expected to occur in a specific period of time, such as a year.

b-value: The slope of a straight line describing the Gutenberg-Richter recurrence frequency-magnitude law. It expresses the proportion of large earthquakes to small earthquakes.

Declustering: A statistical approach that removes foreshocks and aftershocks to produce a catalogue of independent mainshocks consistent with the requirements of a PSHA model.

Disaggregation: Statistical decomposition of the hazard to show the relative contribution by magnitude, distance, and ground motion deviation.

Earthquake: Phenomenon of fault rupture releasing stored strain in the Earth's crust and propagating from the source through vibratory waves in all directions.

Epicentre: The point of the earthquake on the Earth's surface.

Fault: A fracture surface or zone in the earth across which there has been relative displacement.

Focal Mechanism: A geometrical representation of earthquake faulting expressed in terms of the strike and dip of the fault plane and the rake angle of the slip vector with respect to the fault plane.

Ground motion characterisation model: Description of the expected level of ground shaking for a specific site of interest considering soil conditions and building environments.

Ground motion prediction equation (GMPE): An empirical model that relates a ground motion measure (e.g., peak ground acceleration and spectral acceleration) to a set of independent variables, such as distance, magnitude, source and path parameters. The GMPE predicts a lognormal distribution of values for the ground motion measure described by a median prediction and the standard deviation (sigma).

Gutenberg-Richter (recurrence) frequency-magnitude law: The relationship between magnitude and number of earthquakes in a given region and time period.

Hypocentre: The point in the earth at which an earthquake is initiated.

Joyner-Boore distance (Rjb): The shortest distance from a site to the surface projection of the rupture surface of the earthquake.

Local (or Richter) magnitude (ML): Common logarithm of the trace amplitude of a standard Wood-Anderson seismograph located on the firm ground 100 km from the epicentre.

Logic Tree: A series of branches to describe alternative models and parameter values. The weights, which must sum to unity at each node, are assigned to each branch using expert judgement that reflects the relative confidence in the models and parameters.

Magnitude: The size of the earthquake measured from the amplitude of the motion recorded on seismograms and expressed as logarithm with base 10.

Maximum magnitude (Mmax): The largest earthquake magnitude that a seismic source is capable of generating.

Moment magnitude: Magnitude derived from the scalar seismic moment.

Poisson seismic model: The assumption that earthquakes have no memory, i.e. each earthquake occurs independently of any other earthquake.

Probabilistic seismic hazard analysis (PSHA): A methodology to quantify the frequency of exceeding various ground motion levels at a site given all possible earthquakes in a probabilistic framework.

Peak ground acceleration (PGA): Maximum value of acceleration displayed on an accelerogram.

Return period: The mean (average) time between occurrences of a seismic hazard. It is the reciprocal of the annual frequency of exceeding a particular ground motion level.

Seismic hazard: Potential for dangerous, earthquake-related natural phenomena such as ground shaking, fault rupture, or soil liquefaction.

Seismic source: Region or volume (zone or fault) where the seismic activity is considered to be of homogeneous earthquake potential.

Seismic hazard curve: A graphical curve depicting the frequency (the number of events per unit time, usually a year) with which selected values of a ground motion measure are expected to be exceeded.

Seismic hazard map: Seismic hazard is the hazard associated with potential earthquakes in a particular area, and shows the relative hazards in different areas.

Seismic source characterisation model: Mathematical representation of the spatial and temporal distribution of expected earthquakes within a magnitude range in a specific region.

Seismic Source zone: Area where the seismic activity is considered to be of homogeneous earthquake potential, and earthquakes have an equal chance of occurring at any point in the zone.

Spectral acceleration (SA): Pseudo-absolute response spectral acceleration, given as a function of period or frequency and damping ratio (typically 5%). It is equal to the peak relative displacement of a linear oscillator of frequency f attached to the ground, times the quantity $(2\pi f)^2$. It is expressed in g or cm/s^2.

Vs30: Time-averaged shear wave velocity for the top 30 m.

Uncertainty: In seismic hazard analysis there are two types of uncertainties: aleatory and epistemic uncertainty*. The aleatory uncertainty* is inherent in a random phenomenon and cannot be reduced by acquiring additional data or information. The future earthquake locations and magnitudes have aleatory uncertainty. The *epistemic uncertainty* is due to our lack of knowledge regarding the earthquake process and it can be reduced by the accumulation of additional information. The geometry of the seismic source model and the maximum magnitude have epistemic uncertainty.